Object Oriented Control System in Humanoid Robots for Transport Tasks

by

Juan Miguel García Haro

A dissertation submitted by in partial fulfillment of the requirements for the degree of Doctor of Philosophy in

Electrical Engineering, Electronics and Automation

Universidad Carlos III de Madrid

Advisors:

Dr. Santiago Martínez de la Casa Díaz
Prof. Carlos Balaguer Bernaldo de Quiros

Tutor:

Dr. Santiago Martínez de la Casa Díaz

December 2019

A mi familia

"It has been scientifically established that the bumblebee can not fly. Its head is too big and its wings too small to hold its body. According to the aerodynamic laws, it simply can not fly. But no one has told the bumblebee. So it flies."

— Paulina Readi Jofré

Acknowledgements

This moment is the occasion to show my appreciation for those who have helped me in the pursuit of my academic goals and the elaboration of this doctoral thesis.

My greatest thanks are to my family. Specifically, my parents and my sister. They are entitled to one of the greatest and deserved recognition. They are the ones who have offered their wholeheartedly help and unconditional support for the end of my studies, whether for any kind of moral, material, economic or didactic support. For being the leading inspiration, for trusting and believing in me.

The doctorate is usually an arduous and extensive work for any student, that last step. In many times, the students rely on various professionals who can advise us on the subject. Therefore, these people should have their respective thanks.

To **Santiago Martinez de la Casa**. For being my PhD advisor. If I did another Doctoral Thesis, I would choose you without any doubt. Thank you with all my heart for all the dedicated effort. I consider you not only a great tutor but also a wonderful friend.

To Professor **Carlos Balaguer**. I must also thank him specially and sincerely for accepting me to do this Doctoral Thesis as director. Your support, confidence in my work and ability to guide my ideas have been an invaluable contribution to the development of this thesis.

To Professor **Christian Ott**. For accepting me and giving me the opportunity of being part of his research group in the DLR. For everything that I have learned from him. For his wisdom and knowledge.

Likewise, I would like to thank all the people who participated in this process, either directly or indirectly, that today is reflected in the culmination of this thesis. Thank you for the infinite patience and guidance of **Juan H., Sonia, Edu, Angela and Fernando**; and to my colleagues in the **Robotics Lab**. Also, I want to dedicate this thesis to my closest friends: **Ivan, Javi, Mario, Oscar, Marta and Bea**; that thanks to their moral support they allowed me to continue with commitment, dedication and affection. And in general to all those who do their bit to achieve this goal selflessly successfully. Thank you infinitely, for all your goodwill.

Published Content and Contributions

Journal Publications (5)

1. **Garcia-Haro, J.M.**, Martinez, S., Monje, C.A. & Balaguer, C. Development of Applications for Humanoid Robots using Multiple Platforms, Tools, and Cloud Data Sharing. *International Journal of Humanoid Robotics (IJHR)*. 2019. Q4. [accepted, pending publication]

    - This journal is not included in the Thesis. The material from this source is not singled out.

2. Oña E.D., **Garcia-Haro, J.M.**, Jardón, A., & Balaguer C., (2019). Robotics in Health Care: Perspectives of Robot-aided Interventions in Clinical Practice for Rehabilitation of Upper Limbs. *Applied Sciences*, 9 (13), 2586, 2019. DOI: 10.3390/app9132586.

    - This journal is partly included in the Thesis in the chapter 2. The material from this source is not singled out.

3. Hernandez-Vicen, J., Martinez, S., **Garcia-Haro, J. M.**, & Balaguer (2018), C. Correction of Visual Perception Based on Neuro-Fuzzy Learning for the Humanoid Robot TEO. *Sensors*, 18(4), 972, 2018. DOI: 10.3390/s18040972

    - This journal is wholly included in the Thesis in the chapters 3, 5 and 7. The material from this source is singled out.

4. Martinez, S., **Garcia-Haro, J. M.**, Victores, J., Jardón, A., & Balaguer (2018), C. Experimental Robot Model Adjustments Based on Force-Torque Sensor Information. *Sensors*, 18(3), 836, 2018. DOI: 10.3390/s18030836

    - This journal is wholly included in the Thesis in the chapters 3, 4 and 7. The material from this source is singled out.

5. Pérula-Martínez, R., **Garcia-Haro, J. M.**, Balaguer, C., & Salichs, M. A. (2016). Developing Educational Printable Robots to Motivate University Students Using Open Source Technologies. *Journal of Intelligent & Robotic Systems*,81(1), 25–39. DOI: 10.1007/s10846-015-0205-3

    - This journal is partly included in the Thesis in the chapter 2. The material from this source is not singled out.

Conference Publications (10)

1. **Garcia-Haro, J.M.**, Oña, E.D., Martinez, S., Victores, J.G., & Balaguer C. (2019). Whole-Body Postural Control Approach Based on Multiple ZMP Evaluation in Humanoid Robots. *2019 IEEE/RSJ International Conference on Intelligent Robots and Systems (IROS)*. 2019-11-5, Macau, China. [accepted 2018-8-10, pending publication]

    - This journal is wholly included in the Thesis in the chapters 3, 6 and 7. The material from this source is singled out.

2. **Garcia-Haro, J.M.**, Henze, B., Mesesan, G., Martinez, S., Ott, C. (2019). Integration of Dual-Arm Manipulation in a Passivity Based Whole-Body Controller for Torque-Controlled Humanoid Robots. In *Humanoid robots, 2019 IEEE-RAS International Conference on*. IEEE. 2019-10-15, Toronto, Canada. 2019. [accepted 2018-8-26, pending publication]

    - This journal is wholly included in the Thesis in the chapters 6 and 7. The material from this source is singled out.

3. **Garcia-Haro, J. M.**, Martinez, S., & Balaguer, C. (2018). Balance Computation of Objects Transported on a Tray by a Humanoid Robot Based on 3D Dynamic Slopes. In 2018 IEEE-RAS *18th International Conference on Humanoid Robots (Humanoids)* (pp. 704–709). IEEE. DOI: 10.1109/HUMANOIDS.2018.8624920

    - This journal is wholly included in the Thesis in the chapters 4 and 7. The material from this source is not singled out.

4. **Garcia-Haro, J. M.**, Daniel Ona, E., Martinez, S., Hernandez-Vicen, J., & Balaguer, C. (2018). Waiter Robot Application: Balance Control for Transporting Objects. In 2018 IEEE/RSJ *International Conference on Intelligent Robots and Systems (IROS)* (p.5036). Madrid, Spain: IEEE. DOI: 10.1109/iros.2018.8593760

- This journal is partly included in the Thesis in the chapter 6. The material from this source is not singled out.

5. **Garcia-Haro, J. M.**, Martinez, S., & Balaguer, C. (2018). Detección de la Orientación mediante Visión Artificial para el Control de Equilibrio en Robots Humanoides. *XXXIX Jornadas de Automática* (pp. 951–957). Badajoz, Spain: CEA-IFAC. ISBN 978-84-09-04460-3

   - This journal is not included in the Thesis. The material from this source is not singled out.

6. **Garcia-Haro, J. M.**, Martinez, S., & Balaguer, C. (2018). Humanoid Balance Control based on Force/Torque and Visual Information. In U. de Valladolid (Ed.), *Jornadas Nacionales de Robótica 2018*. Valladolid, Spain: CEA-IFAC. ISBN 978-84-09-02877-1

   - This journal is partly included in the Thesis in the chapter 5. The material from this source is not singled out.

7. **Garcia-Haro, J. M.**, Martinez, S., Pinel, M. D., & Balaguer, C. (2017). Experimental Error Compensation of the Linear Inverted Pendulum Model for humanoid robot TEO. In IEEE (Ed.), *2017 IEEE/RSJ International Conference on Intelligent Robots and Systems (IROS)* (p. 5489). ISBN 9781538626818

   - This journal is partly included in the Thesis in the chapter 4. The material from this source is not singled out.

8. Hernandez-Vicen, J., **Garcia-Haro, J. M.**, Martinez, S., & Balaguer, C. (2017). Control of Robotic Arm for Transporting Objects based on Neuro-Fuzzy Learning Visual Information. *XXXVIII Jornadas de Automática* (pp. 760–765). Oviedo, Spain: CEA-IFAC. ISBN 978-84-16664-74-0

   - This journal is partly included in the Thesis in the chapters 3 and 5. The material from this source is not singled out.

9. Lorente, J., **Garcia-Haro, J. M.**, Martinez, S., Hernandez, J., & Balaguer, C. (2016). Waiter Robot: Advances in Humanoid Robot Research at UC3M. *RoboCity16 Open Conference on Future Trends in Robotics* (pp. 195–202). CSIC. ISBN: 978-84-608-8452-1

   - This journal is partly included in the Thesis in the chapter 3. The material from this source is not singled out.

10. Hernandez-Vicen, J., **Garcia-Haro, J. M.**, Martinez, S., Lorente, J., & Balaguer, C. (2016). Manipulation Balance Control System by Computer Vision Tools. *RoboCity16 Open Conference on Future Trends in Robotics* (pp. 203–210). CSIC. ISBN: 978-84-608-8452-1

    - This journal is partly included in the Thesis in the chapter 5. The material from this source is not singled out.

Other Research Merits

In this section, I have included all the Master and Bachelor thesis, in which I have participated as a Director. These works are part of my doctoral dissertation. Therefore this is the reason why I have incorporated them here.

- María Dolores Pinel del Valle. (2016) Balance Control of Humanoid Robot TEO using Force/Torque Sensors. Master's Degree in Robotics and Automation. University Carlos III of Madrid.
  - This work is partly included in the Thesis. It has used in the chapters 3 and 4. The material from this source is not singled out.
- Juan Lorente Monzó. (2016) Equilibrium Control of Humanoid Robot TEO by Inertial Perception. Master's Degree in Robotics and Automation. University Carlos III of Madrid.
  - This work is partly included in the Thesis. It has used in the chapters 3 and 4. The material from this source is not singled out.
- Juan Hernández Vicén. (2017) Control of a Robotic Arm for Transporting Objects based on Neuro-Fuzzy Learning Visual Information. Master's Degree in Robotics and Automation. University Carlos III of Madrid.
  - This work is partly included in the Thesis. It has used in the chapters 3 and 5. The material from this source is not singled out.
- Álvaro Martínez Robledo. (2017) Methodology for Task Development in Humanoid Robots Using ArmarX Framework. Bachelor's Degree in Industrial Technologies Engineering. University Carlos III of Madrid.
  - This work is partly included in the Thesis. It has used in the chapters 3. The material from this source is not singled out.

Abstract

Humanoid robot research is one of the most challenging topics in robotics. The research in this field has been inspired by the fact that these machines replicate the human shape and, in the end, human behaviour. Many humanoid robots have been presented in the last decades, but their behaviour is far from human performance. Therefore, the improvement of humanoid performance is one of the main goals in the field, mimicking as much as possible human tasks.

This Thesis has been focused on the development of one of these behaviours and the study of open questions related to its performance. Concretely, the main goal of this thesis is to integrate a waiter behaviour in the humanoid robot TEO from the Carlos III University of Madrid. This behaviour consists of transporting objects on a tray, imitating the human task of a waiter, but this research must face different problems.

The first problem to deal with is the balance of the robot. One of the essential characteristics of a humanoid robot is its capacity of upright stance and walking. Humanoid robot balance has been one of the main problems studied from the beginning of the development of this kind of robots. Keeping balance is still a matter of study in humanoid robotics, and it is crucial to develop tasks. Due to the complexity of this problem, its study is favoured using simple representations of the humanoid balance behaviour, such as the simple inverted pendulum. This kind of simplifications makes the study of the balance problem computationally easier, but it does not solve all questions related to balance. This Thesis has dealt with balance problem because it should be a key feature for a waiter robot. A new simplified model has been proposed as an improvement of the classic Linear Inverted Pendulum Model (LIPM). Its development is based on an experimental procedure that allows tackling many inherent problems of humanoid mechanics, electronics, computing, and more at the same time. The results show that this improvement reduces the control effort need for keeping balance during the waiter task.

The second problem faced in this Thesis is related to manipulation that is another essential characteristic defining the human being: the capacity of manipulating objects. In this Thesis has been treated a specific case of manipulation. In the waiter task performance, usually the objects are transported on a tray, and no gripping force is applied to them. Then another problem arises: to transport the objects keeping their equilibrium or balance. Thanks to the use of exoceptive perceptions of the robot (vision, force, etc.) are possible to interpret the balance status of the objects transported. This sensorial information and its application with a simple inverted pendulum model enable the balance control of the object.

Finally, the results obtained from the study of the two main problems exposed have been integrated into a Whole-Body Postural Control architecture. It accomplishes with all the requirements needed for performing the waiter task.

Resumen

La investigación en robots humanoides es uno de los temas más desafiantes en robótica. La investigación en este campo se ha inspirado en el hecho de que estas máquinas reproducen la forma humana y, por ende, el comportamiento humano. Muchos robots humanoides han sido presentado en las últimas décadas, pero su comportamiento está lejos de ser humano. Por lo tanto, la mejora el rendimiento en humanoides es uno de los objetivos principales en este campo, imitando la mayor cantidad posible de tareas humanas.

Esta tesis se ha centrado en el desarrollo de uno de estos comportamientos y el estudio de preguntas aun sin resolver relacionadas con su desempeño. Concretamente, el objetivo principal de esta tesis es integrar el comportamiento de un camarero en el robot humanoide TEO de la Universidad Carlos III de Madrid. Este comportamiento consiste en transportar objetos en una bandeja, imitando la tarea humana de un camarero, pero esta investigación debe enfrentar diferentes problemas.

El primer problema a lidiar es el equilibrio del robot. Una de las características esenciales de un robot humanoide es su capacidad de mantenerse erguido o caminar. El equilibrio de humanoides ha sido uno de los principales problemas estudiados desde que se comenzó a desarrollar estos robots. Mantener el equilibrio sigue siendo una tema de estudio en robótica humanoide, y es crucial para desarrollar tareas. Debido a la complejidad de este problema, este estudio se ve favorecido por el uso de representaciones simples del comportamiento del equilibrio humanoide, como el péndulo invertido simple. Este tipo de simplificaciones hace que el estudio del problema del equilibrio sea computacionalmente más fácil, pero no resuelve todas las preguntas relacionadas con éste. Esta tesis ha tratado el problema porque debería ser una característica clave para un robot camarero. Se ha propuesto un nuevo modelo simplificado como una mejora del clásico modelo de péndulo invertido lineal (LIPM). Su desarrollo se basa en un procedimiento experimental que permite abordar muchos problemas inherentes de la mecánica humanoide, la electrónica, la informática y más al mismo tiempo. Los resultados muestran que esta mejora reduce el esfuerzo de control necesario para mantener el equilibrio durante la tarea del camarero.

El segundo problema enfrentado en esta Tesis está relacionado con la manipulación, que es otra característica esencial que define al ser humano: la capacidad de manipular objetos. En esta Tesis se ha tratado un caso específico de manipulación. En el desempeño de la tarea del camarero, generalmente los objetos se transportan en una bandeja y no se les aplica fuerza de agarre, pero entonces surge otro problema: transportar los objetos manteniendo su equilibrio o equilibrio. Gracias al uso de percepciones exoceptivas del robot (visión, fuerza, etc.) es posible interpretar el estado de equilibrio de los objetos transportados. Esta información sensorial y su aplicación con un modelo de péndulo invertido simple permiten el control del equilibrio del objeto.

Finalmente, los resultados obtenidos del estudio de los dos problemas principales expuestos se han integrado en una arquitectura de control postural de cuerpo entero, la cual, cumple con todos los requisitos necesarios para realizar la tarea de camarero.

Abbreviations

Nomenclature

TEO Task Environment Operator

TORO TOrque-controlled humanoid RObot

WBPC Whole-Body Postural Control

BiM Bi-Manipulation

WB-M Whole-Body Manipulation

UBC Upper-Body Controller

LBC Lower-Body Controller

OBP Object Balance Perception

OBE Object Balance Execution

BBP Body Balance Perception

BBE Body Balance Execution

IMU Inertial Measurement Unit

F-T Force - Torque

LIPM Linear Inverted Pendulum Model

D-LIPM Dynamic - Linear Inverted Pendulum Model

CT Cart-Table

TCP Tool Centre Point

Contents

List of Tables

List of Figures

List of Algorithms

Part I

Introduction and Overview

Chapter 1

Introduction

"Hello, my name is TERMINATOR, and I'll be your server today."

Diners might soon be feeling this greeting, with Optimus Prime in the kitchen and Wall-E then sending your order to C-3PO.

In our daily lives, a version of that future is already showing up. Robotics companies are designing robots to handle tasks, including serving, cooking and food preparation.

1.1 Motivation

The statistics are very evident. Taking the IFR (Internacional Federation of Robotics) global robotic report (Robotics, 2017): "sales in robotics increased by 16% to 294,312 units in 2016. This is a new peak for the fourth year in a row. The main driver of the growth in 2016 was once more the electronics/electrical industry (41%). In the automotive manufacturing, the sales grow at a rather modest rate (by 6%) after substantial advancement from 2010 to 2014. The automotive industry is still the primary customer of industrial robots with a share of 35% of the total supply in 2016. The electronics/electrical industry has been catching up, especially in 2015, reaching a share of 31% of the final supply in 2016. The electronics/electrical industry has become the most critical customer in almost all essential Asian markets, e.g. Republic of Korea, Japan, China. The market for industrial robots has accelerated considerably since 2010, due to the continuing trend toward automation and continued innovative technical improvements in industrial robots. From 2011 to 2016, the average robot sales increment was at 12% per year. The number of robot installations had never increased so massively before. From 2005 to 2008, the average annual number of robots sold was about 115,000 units".

"Also, in 2010, robot investments, which had been restrained in 2009, were the main driver of the significant increase . From 2011 to 2016, the average annual supply rose to about 212,000 units. This one is an expansion of about 84% compared to the average annual supply between 2005 and 2008 and clear evidence of the considerable rise in demand for manufactured robots worldwide in the next years" (Fig. 1.1).

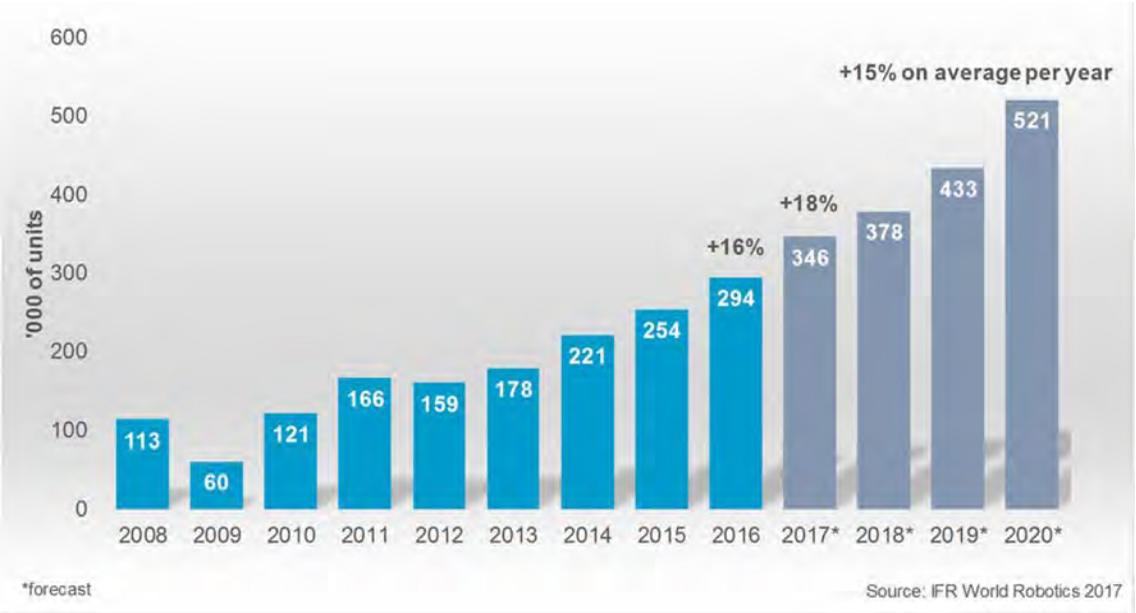

Figure 1.1: *Estimated annual worldwide supply of industrial robots 2008-2016 and 2017-2020 (Robotics, 2017)*

On the other hand, by the Bureau of Labor Statistics (part of the U.S. Department of Labor) (United States of America, 2017) reported that: "more than 3.4 million people work in serving in places such as cafeterias, fast-food restaurants and food preparation, with a median wage of $9.44 per hour. More than 4.7 million people are working as waitresses and waiters, receiving a median wage of $9.61 per hour. Also, there are approximately 2.3 million cooks who earn a median salary of $10.99 per hour". The catering industry is a significant sector where many companies are investing much money. Therefore, in a few years, this industry will have an explosion of production and investment in the robotics field, and it will follow the grown development in agricultural-related robotics. It seems that it will be a logical next topic for robotics, with a vast market (Flyppy, 2017).

In fact, robots are being put to work out front in the restaurant industry as well (Fig.1.2). In some countries (for examples, China and Pakistan), restaurants are using robots to serve food and take orders (Pontaza, 2017, Nguyen, 2016). Pizza Hut has used Pepper robots, made by Japanese company SoftBank, to restaurants in Asia (Curtis, 2016, Yap, 2016, Puerto, 2015, Asenador, 2016).

However, robot waiters have not been a hit in all facets of food-service. Chinese restaurant chain Hewelai found out the difficult way after spending in robot waitstaff for three restaurants, at the cost of more than $7,000 per unit. There were problems from the beginning. The robotics platforms regularly broke down and were unable to complete basic tasks such as pouring drinks, taking orders, or carrying bowls of soup. Two of the restaurants closed (Rob Price, 2016, Coffrini, 2016).

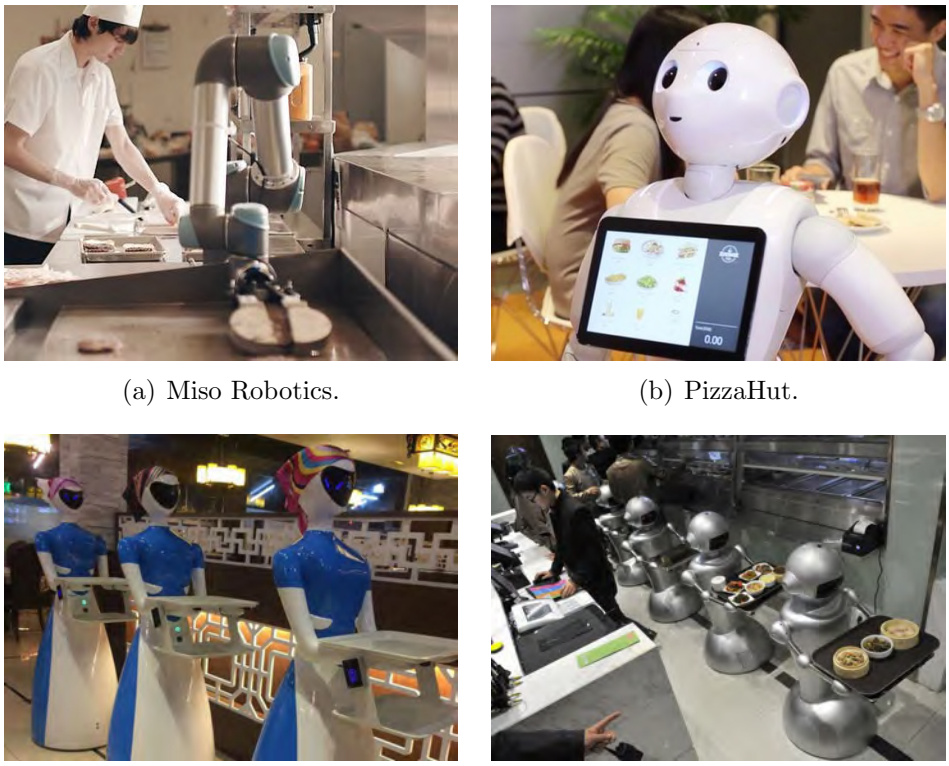

(a) Miso Robotics. (b) PizzaHut.

(c) CH Premiere Restaurant. (d) Hefei restaurant.

Figure 1.2: *Different examples of service robots working in a restaurant or in a kitchen nowadays. (a) Chef robot from MISO ROBOTICS. (b) Robot Pepper in a PizzaHut restaurant. (c) Robot Collection from CH Premiere Restaurant (Malaysia). (d) Robot platoon from Hefei restaurant (China).*

1.2 Open Challenges

As stated in the previous section, there are still too many problems to solve in the latest robotic restaurant projects. It is evident that this new line of research has yet to mature. Before us, a wide range of possibilities for improving opens. Then, we deal with two purposes: the tasks of a waiter robot and the versatility of a humanoid robot.

On the one hand, a waiter robot needs enough skills and abilities to develop multiple tasks. Actually, an assistant waiter robot should be able to work with food and drinks, preparing the food for cooking or plate meals, cleaning dishes for an excellent presentation, transport plate meals, moving across the restaurant, avoiding people, chairs or tables, going up or downstairs.

Moreover, waiter robots present unique challenges for robots. They have to be created to work with human beings in tight spaces. There is also grease, smoke, water, heat and steam to contend with. The most critical challenge is what the robots are working with. Food and drink over a tray are clearly unpredictable when they have to be served to a customer. The instability of these when the robot is moving makes the task even more difficult.

On the other hand, humanoids are robots with their body shape built to resemble the human being body. The design might be for functional purposes, such as the locomotion studies, such as interacting with environments and human tools, for experimental purposes, or other purposes. The fundamental difference between humanoid robots and other mobile platforms is the movement. Humanoids walk like human beings. They use their legs with a biped gait. Considering human behaviour and its minimum energy consumption, humanoid robots replicate the step planner while walking. Therefore, researches on control or dynamics of humanoid platforms have frequently turn into more critical. We consider the problem of stabilisation of a biped robot while walking very important. We could choose to provide a stable position as a challenge and an aim of control. The idea could be keeping the CoM of the robot inside the support polygon generated by the feet.

Figure 1.3: *Figure that shows the main idea of what a future waiter robot could be.*

The possibilities of a humanoid robot are numerous. The ability to socialise with humans and their environments make this robot very useful. They push the boundaries of engineering, cognitive science and biology, producing a mountain of scientific papers in many areas related to humanoid robotics, including A.I., perception, robotic navigation, cognitive robotics, computational neuroscience, compliant grasping and manipulation, speech recognition, and the integration of these fantastic technologies within total humanoids.

If we mix the waiter's tasks with the capabilities of a humanoid robot, the challenges intensify. One of the most difficult would be a waiter humanoid robot transporting a drink on a tray in its hand. During this task, the robot should be able to maintain its stability while trying to keep the balance of the drink on the tray (Fig.1.3).

1.3 Objectives of this Thesis

It's evident that robotics applied to the catering industry is something still very new, and this field has not been deeply investigated yet. The opportunities that it has to offer are numerous, and this thesis tries to take advantage of it researching in waiter robots.

There are already some examples of robots that take orders or transport trays, in a very simple way, or with straightforward robotic platforms. These examples are easy to implement but are very limited regarding their tasks.

However, a humanoid robot is a more complex robotic platform that could execute more than one task or be useful for other purposes.

This one is the principal idea of this thesis. The main goal is to study how a humanoid waiter robot should be, and more specifically, how it should transport objects on a tray.

More technically, the doctoral thesis is focused on the study of Whole-Body Postural Control of the humanoid robot, focused on the task of transporting non-grasping objects. As it is shown in the central part of Figure 1.4, the final objective of the transport task is based on the transported object control through a bi-manipulator robot. The waiter humanoid robot should be able to control both arms to guarantee the transport of the object while the robot is walking or maintaining its own balance.

For this purpose, there are four blocks in which we have divided the main objective. Each one of them is a fundamental part and has been investigated individually in order to be able to integrate them in a final Whole-Body Postural Control architecture. In this case, these groups are Body Balance (section 4), Manipulation (section 5), Bi-Manipulation (section 5) and Whole-Body Manipulation (section 6). We have considered these parts as sub-objectives needed to achieve the final purpose:

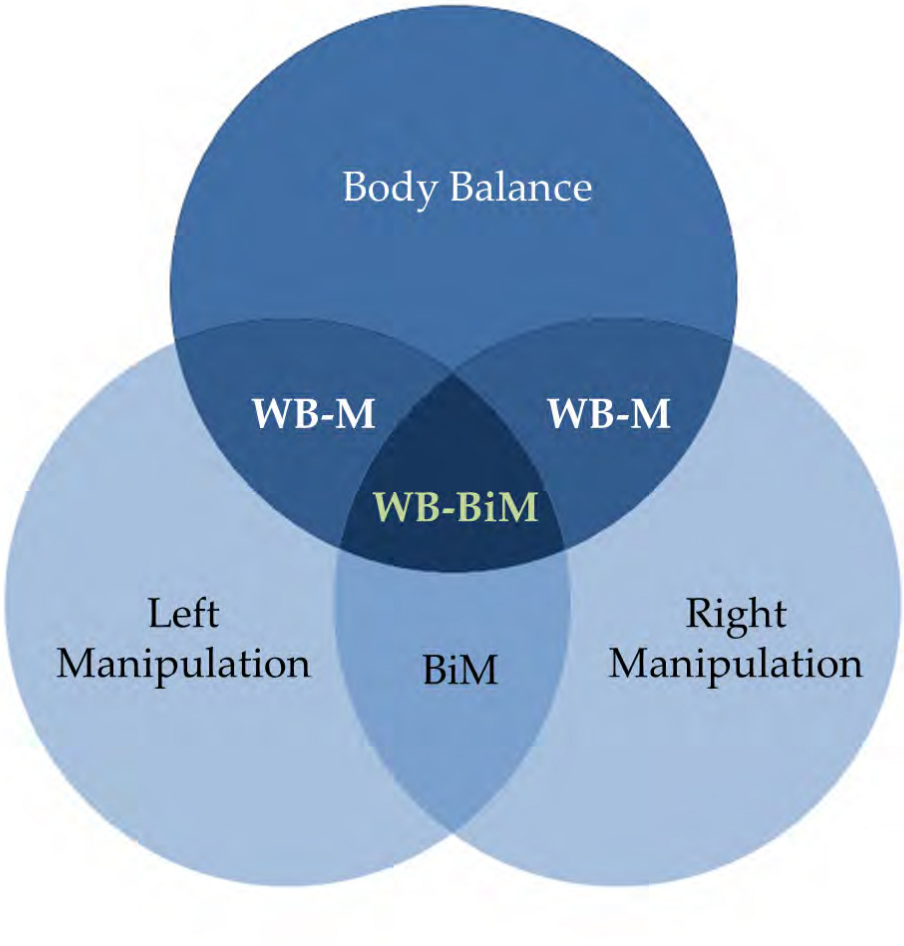

Figure 1.4: *Representation of the global vision of the thesis.*

- The content "Body Balance" is focused on the study of the stability of the robot based on simplified models. These models ease the computation of the stability grade, but the linearisation introduces errors. In this block, a proposed method is explained to adjust the parameters of the model for the multiple working points of the robot balance controller dynamically.
- The content "Manipulation" describes the investigation of the stability of the object during transport. This section explains the inherent difficulties of the object, which is not physically attached to the tray, and how we can use multiple systems of perception, combining its information to compute the stability of the transported object.

- The content "Bi-Manipulation" (BiM) is an improvement of the previous block where everything learned in it is adapted and applied to a new bi-manipulated object controller. The use of two arms for transporting objects unlocks the advantages of the previous block and also allows the transportation of heavier objects by dividing the weight between both arms.

- The content "Whole-Body Manipulation" (WB-M) is the junction between the blocks Body Balance and M, where we are executing both controllers of the body and object stability at the same time. This block introduces the Whole-Body Postural Control architecture and explains how both controllers disturb each other.

Such Whole-Body Postural Control architecture is focused on the use of the perception systems of the humanoid robot. In this case, the perception systems used are the vision, inertial and F-T systems. Each perception system is applied to the different blocks explained previously, and these blocks adapt according to the complexity of the task or the strategy used: the use of a big or small tray, transport of the order, or just keeping the balance.

1.4 Organization of the Document

The document is ordered as follows:

- Chapter 2 introduces the state of the art of service robots, explaining the economic progression of this sector and classifying them according to their application (professional or personal). Also, a new type of robot is introduced to which to add to the classification: catering robots (robochefs and waiter-bots). This chapter details how these robots should be, what tasks they should accomplish, and how they should behave to achieve it.

- Chapter 3 addresses several issues specifically related to the robot waiter. In this chapter, we find the definition of the robotic platform TEO used, the specific description of the purpose of the waiter robot and its most essential complements, the presentation of the perception systems used and an evaluation of the different tools necessary for balance control (models simplified, stability criteria, Push-Recovery).

- Chapter 4 describes the problems introduced both by the robot's mechatronics itself and by the use of simplified models on stability control. This chapter also describes a new and improved model to solve this, and deals with these errors by adjusting their parameters dynamically. This model will be used later for the Whole-Body integration. The experimental methodology applied in this process is also applied to other models for validation.

- Chapter 5 introduces the problems associated with the transport of objects without gripping and presents a method to achieve this task using balance control and sensory fusion tools. Taking advantage of all the tools described in Chapter 3, Chapter 5 describes the evaluation of stability and its control architecture. Finally, applying the same concepts, the problem is extrapolated to bi-manipulation tasks.

- Chapter 6 describes the entire process of unification of the previous two chapters. This chapter presents the WB postural control architecture where both body and object stability controllers are integrated to work at the same time. Besides, this research applies to a new robotic compliance platform. By implementing a new dynamic model of the TORO DLR robot, bi-manipulation is integrated into a Whole-Body compliance controller.

- Chapter 7 compiles all the experiments performed associated with chapters 4, 5 and 6. In this chapter, the progress of the task of the waiter robot can be observed sequentially.

- Chapter 8 contains the concluding remarks, key contributions and recommendations for future improvements of this work.

Chapter 2

Service and Waiter Robots

2.1 Introduction

Automatic, self-aware automata are not new. They can look like human beings and can do the monotonous and tiresome daily tasks for us. They have always been present in our society; depicted as whimsical or fictional roles, as can be shown in Figure 2.1(a) and now we use simply the name "robots" to call them.

Nowadays, they have been improved to "service robots". They are quite functional and real. However, our imagination can produce invented designs of their "new and improved" updates. An example can be shown in Figure 2.1(b).

(a) Robot Bender.

(b) Robot TARS.

Figure 2.1: *Different examples of TV robots that have appeared in films or series. (a) Bender. The foul-mouthed Futurama robot. And (b) The multi-functional Robot TARS from the Interstellar film.*

If we focus on the universe of service robots, this one is growing continuously. Also, applications and diversity are maturing all years. However, service robots do not have an accepted definition, due to this very changing market behaviour, the multitude of structures and application areas or the multitude of structures.

The International Federation of Robotics (IFR) has done an introductory definition. Among other things, it aims at distinguishing this kind of robots from other devices: "A service robot is a robot that works semi or completely autonomously to perform useful services for the well-being of humans and equipment, excluding manufacturing operations" (Litzenberger, 2018).

IFR also declares that: "service robots may or may not be equipped with an arm structure as is the industrial robot. Manipulating industrial robots could also be considered as service robots, conforming to the above-stated definition, provided they are installed in a non-manufacturing environment".

IFR mentions that: "the vast majority of the current service robots are mobile, but this is not a strict defining characteristic since they can also be fixed. In some cases, service robots consist of a mobile platform which has attached one or several arms that can be controlled in a similar model to the control of an industrial robot".

Since 2007 the International Organization for Standardization is reviewing the ISO 8373 (currently 8373:2012) since 2007. They work on: "the definition of the terms used in relation to robots and robotic devices that operate in industrial and non-industrial environments, for the standard inclusion of an official definition of service robots" (International Organization for Standardization, 2012).

2.2 Service Robots Statistics

Delving into the IFR global robotics report (Robotics, 2017): "in 2016, the total number of professional service robots sold in increased considerably by 24% to 59,706 units, compared to 48,018 in 2015. If we summarise some statistics of the main topics, about 25,400 logistic systems (manufacturing scenarios), they were installed in 2016, 34% more than in 2015 (19,000), representing 43% of total units and 21% of total sales (in value) of professional service robots. Service robots in defence applications, with 11,100 units, consider for 19% of the total number of professional service robots sold in 2016. In 2016, a total of approximately 5,300 milking robots were sold compared to 5,860 units in 2015, which represents a 10% decrease. Milk producers suffered financially. As a result, investments were advanced, and acquisitions were postponed. (Figure 2.2). Sales of medical robots increased by 23% compared to 2015 to 1,600 units in 2016, accounting for a share of 2.7% of the total unit sales of professional service robots. The most critical applications are robot-assisted surgery or therapy. Sales of powered human exoskeletons were up from 4,970 units in 2015 to 6,018 units in 2016. These are successfully used for rehabilitation and ergonomic support for reducing loads and have high growth potential".

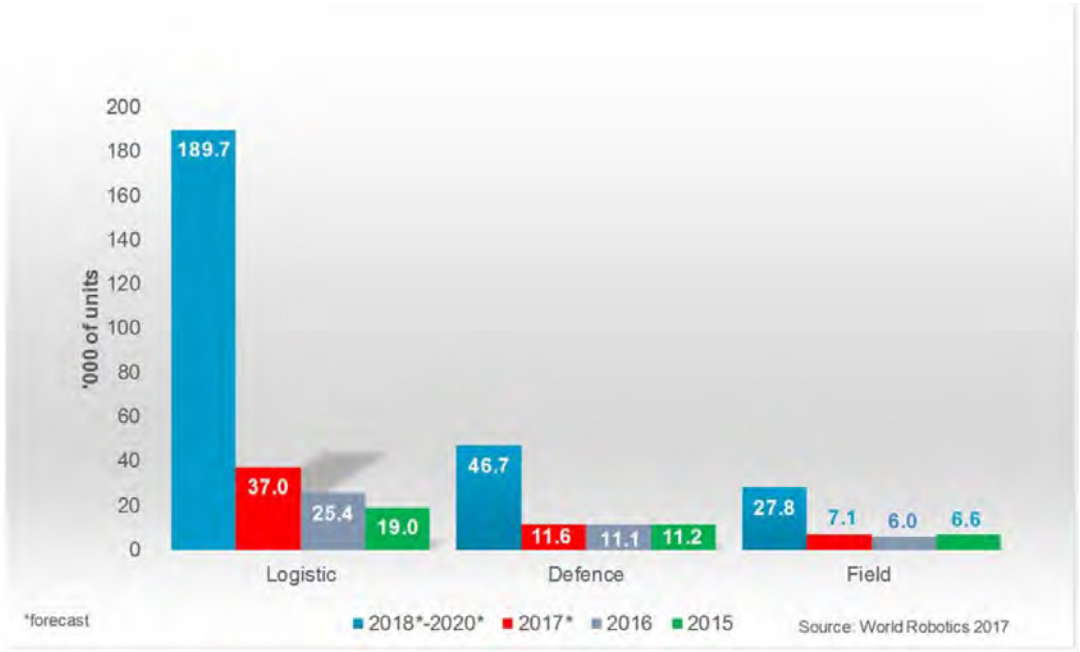

Figure 2.2: *Unit sales 2015 and 2016, forecast 2017* and 2018*- 2020* of professional service robots in more applications (first part)(Robotics, 2017).*

Figure 2.3: *Unit sales 2015 and 2016, forecast 2017* and 2018*- 2020* of professional service robots in more applications (second part)(Robotics, 2017).*

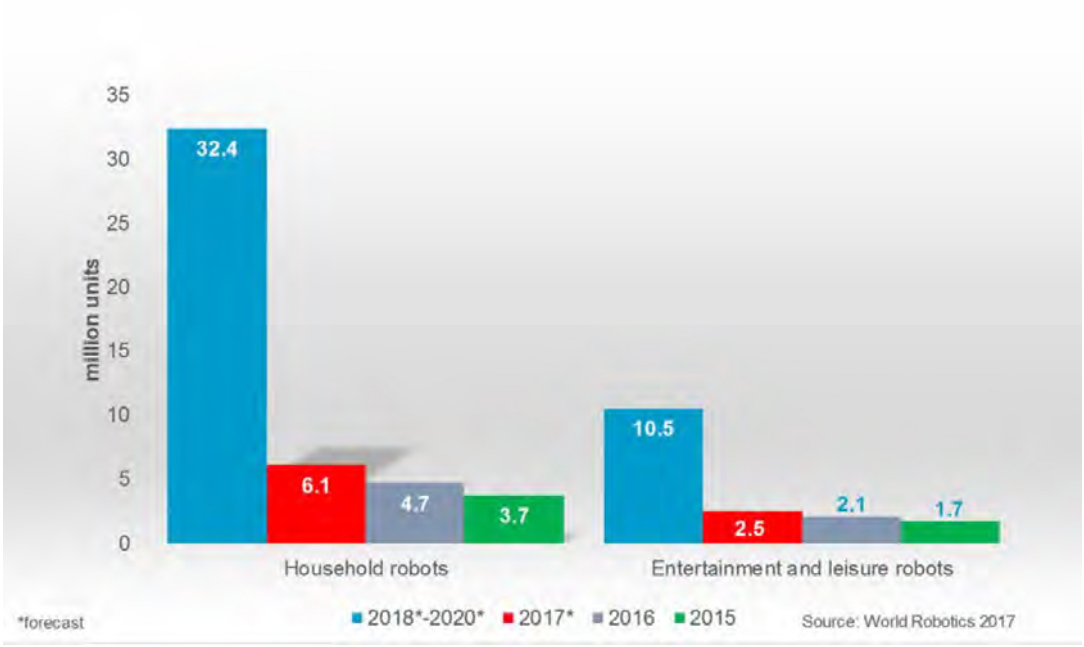

Figure 2.4: *Unit sales 2015 and 2016, forecast 2017* and 2018*- 2020* of personal or domestic service robots (Robotics, 2017).*

"Another strong growing sector (crucial for this thesis) is *public relation robots*. Almost 7,500 units were sold in 2016, 133% more than in 2015. Most of these robots were telepresence robots, robots for mobile guidance and information with a sales volume of 7,200 units in 2016 up from 3,100 units in 2015" (Figure 2.3).

"Service robots for domestic and personal use are registered separately since their unit value is generally only a fraction of many types of service robots for professional use. They are also produced for a mass-market with completely different pricing and marketing channels. Until now, service robots for personal and domestic use are mainly in the areas of domestic robots, which include cleaning vacuum cleaners and floors, lawn mowing robots and entertainment and leisure robots, including toy robots, hobby systems, education and research" (Figure 2.4).

2.3 Classification of Service Robots

They come in all forms and heights and most of the time and are mobile and autonomous. Depending on the usability, we can separate them into two big levels: "professional service robots" and "personal/domestic service robots". Some of the latest robots designed are detailed inside this section. We can consider them representative for each class (Figure 2.5).

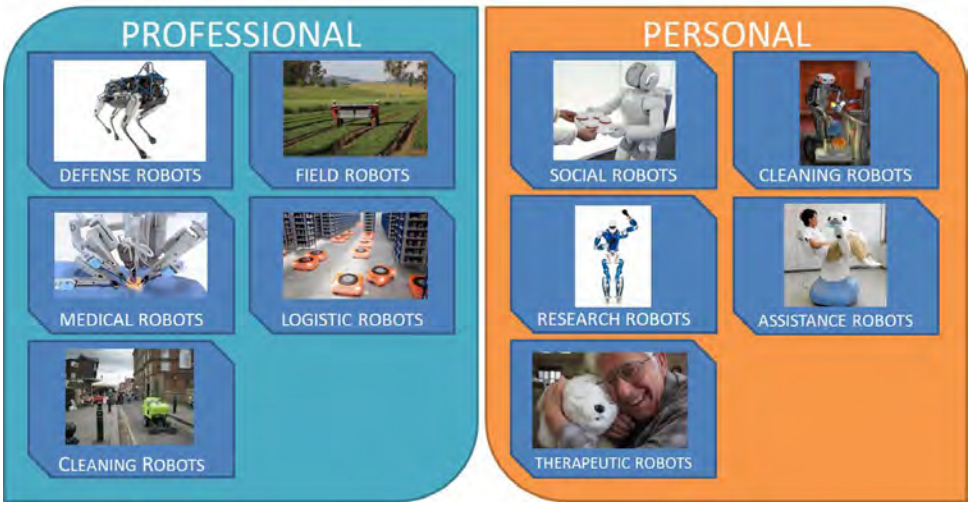

Figure 2.5: *Classification of different service robots (Ciupe and Maniu, 2014).*

2.3.1 Professional Service Robots

For the private sector, *"professional service robots"* are still fascinating. Either in the number of units sold or in the new fields in which the robotics are becoming indispensable.

Defence Robots

Based on the previous idea, *"defence robots"* have the most significant share of professional robots domain. In units manufactured and in market value. These have a short-lived because they work in hostile scenarios. Inside this robotic class, three main divisions emerge: the unmanned aerial vehicles (UAV), unmanned ground vehicles (UGV) and unmanned underwater vehicle (UUV) (Table 2.1).

The "Black Hornet" nano copter from ProxDynamics is one of the most interesting surveillance UAV on the market (Figure 2.6(a)), which British soldiers have been utilizing to look over walls and around corners in Afghanistan since 2013. It is a small (200 mm long) device equipped with, and it can float up to 25 minutes with a charge from its battery, and the digital data link to its terminal has a range of up to one mile (1.6 kilometres). The company augmented the Black Hornet, in 2014, with night-vision and infra-red (Fregene, 2012).

Spot, the quadruped robot from Boston Dynamics, is used by ground forces as supporting device. Its dynamic planner permits to follow soldiers anywhere they need (Figure 2.6(b)). The spot is a UGV four-legged robot designed for outdoor and indoor operation. It also lay the ground for a new approach to dynamic robot control that brings genuine autonomy within reach. It operates for 45 minutes on a battery charge and carries a 23 kg payload (Zhang et al., 2017).

Table 2.1: *Classification of defence robot according to the application environment.*

TYPE	DESCRIPTION
UAV	They are used from the air. Sometimes they are known as drones. UAVs look like model aeroplanes and vary in size from small planes to full-size planes.
UGV	They are robots that work in contact with the ground. Usually, UGVs are employed for jobs where it may be inconvenient, dangerous, or the presence of a human is impossible.
UUV	These marvels have capabilities to operate underwater. The UUVs were designed to contribute to the following mission areas: Mine Warfare, Intelligence, Surveillance, and Reconnaissance and Mapping undersea environmental.

(a) Black Hornet. (b) Spot. (c) MAARS.

Figure 2.6: *Three different examples of defence robots. (a) Black Hornet. A nanocopter from Prox Dynamics. (b) Spot. A dynamic robot developed on Boston Dynamics. And (c) MAARS. A wheeled combat-ready robot by Qinetiq.*

Another impressive UGV design in this field is Qinetiq's MAARS (Figure 2.6(c)). Powerful, modular and combat-ready, MAARS is a UGV created particularly for target acquisition, surveillance and reconnaissance purposes. It increases the security of employees staffing forward locations. MAARS could be placed in isolated regions where employees are currently incapable of controlling their security or bringing a fire weapon (Martinic, 2014).

Field Robots

The other primary domain is *"field robots"*. In this class, milking robots are the most widely spread. The multi-box system GEA's MIone is one of the most intricate and novel milking robot (Figure 2.7). When the cow goes into the milking post, the robot checks the dimensions of the cow with a depth camera. The MIone system is perfect for herds of 120 cows and more.

From a central control station, we could verify and monitors all tasks fast and efficiently. We can attend with basic and adjusted functions cows with particular requirements, while the MIone system is milking the rest of the cattle automatically (Barrett, 2014).

Figure 2.7: *Example of field robots. MIone is a robotic milking system by GEA.*

Medical Robots

Moreover, one of the most important fields of professional service robots is *"medical robots"*. Its market value is very high. Due to a wide testing of the robots, an extensive range of accessories and a high complexity, the costs usually exceed 1 million US dollars per unit. There are three main categories within the field of medicine: Delivery, Rehabilitation, Surgical (Table 2.2)

Table 2.2: *Classification of medical robot according to the application environment.*

TYPE	DESCRIPTION
Delivery	These robots aim to carry meds, lab specimens, sterile supplies, linens, trash, medical waste, patient meals and even carry patients.
Rehabilitation	Rehabilitation robotics is based on assisting different sensorimotor functions, development of different schemes of assisting therapeutic training, or assessment of the sensorimotor performance of the patient.
Surgical	The purpose of this kind of robots is to give enhanced diagnostic capabilities, a less invasive and comfier experience for the patient, or the capability to perform more accurate interventions.

The "CyberKnife" surgical device from CyberKnife Accuray is a good example in this field (Figure 2.8(a)). CyberKnife is another non-invasive alternative to surgery for the treatment of cancerous and non-cancerous tumours in the whole body. The CyberKnife treatment involves no cutting, although its name may conjure images of scalpels and surgery. The CyberKnife System is the only radiosurgery and the world's first robotic system designed to treat tumours throughout the body non-invasively (without cutting) (Kilby et al., 2010).

Instead of surgery, there are other essential medical categories like injury rehabilitation robots or the handicap assistance. Hocoma, a robotic gait orthosis from LocomatPro, is a fascinating example (Figure 2.8(b)). The Hocoma orthosis is focused on the automation of walking therapies and the improvement of the routine training efficiently. The robot is equipped with an augmented performance feedback device, pre-programmed routines and the body-weight support. Related to the pre-programmed physiological gait pattern, the routine guides the legs of the patient (Neckel et al., 2006).

(a) CyberKnife. (b) LocomatPro.

Figure 2.8: *Two different examples of medical robots. (a) CyberKnife. A robotic platform designed to treat tumours by CyberKnife Accuray. And (b) LocomatPro. The driven gait orthosis from Hocoma.*

Logistic Robotic Systems

In the *"logistic robotic systems"*, 75% of current warehouses are manually operated, and they have no supported automation at all. These warehouses deal with demands for increased productivity and throughput. Existing workers with good layout design and mobile material handling equipment are supporting this increased demand. In this scenario, logistic service robots have their place with a good market value. The atypical working places that require fast and tedious work is not a problem for them.

For the robotic logistics category, the Kiva robot from Automated Material Handling Systems is a good candidate (Figure 2.9(a)). Kiva uses game-changing automation technology for distribution centres. Trying to grow strategic flexibility, Kiva simplifies processes and decreases costs, supporting companies. Based on advanced control software and a crowd of autonomous mobile robots, Kiva fulfilment system enables speedy cycle times with reduced labour requirements, from receiving to picking to shipping (Andrea and Wurman, 2008).

Building or construction robots are emerging in the industry slowly. However, demolition robots are more popular. The Brokk 400 demolition robot is a representative sample (Figure 2.9(b)). With demolition plans, this robot is created and produced particularly. It has been improved for this kind of work. Also, it does it better than any other equipment available. Its weight is 5100kg without attachment, and also It can manipulate tools of up to 600kg. These features make this robot better than most demolition robots (Derlukiewicz and Cieślak, 2017).

(a) Kiva. (b) Brokk 400.

Figure 2.9: *Two different examples of logistic robotic systems. (a) Kiva. A mobile-robotic fulfilment system for inventory distribution centres by Kiva System. And (b) Brokk 400. The demolition robot from Brokk.*

Cleaning Robots

The first robots to gain acceptance in the world (cleaning the windows or the floor) were the *"Professional cleaning robots"*. And moreover, novel professional robotic cleaners approaches are emerging: inspection robots or solar panel cleaners.

One of the newest and most complex robots of solar panel cleaners is E4, developed by Ecoppia (Figure 2.10(a)). The E4 is a waterless cleaning system. Its main advantages are two. The avoidance of the cost of water. And the cost of infrastructure that carries it. For example, tank trucks, storage containers, hoses and pipes. The E4 eliminates almost 100% of soiling daily. Its unique microfiber cleans dirt smoothly, controlling airflow over the panel surface. That way, it guarantees trash moves down and out of the panel rows (Shen et al., 2016).

The robotic inspection systems are becoming too important. They are able to come to inaccessible scenarios like pipes for the inspection and cleaning. One of them is Versatrax 450 (Figure 2.10(b)) built by Inuktun. Inuktun created Versatrax 450, particularly for dangerous scenarios. It is excellently readjusted for an extended variety of applications. These are related to remote handling or inspection tasks. This embedded robot could be built in a few minutes. Therefore, this allows a safety inspection, capturing dangerous substances from any site faster than any conventional device. (Choi et al., 2015).

(a) E4 solar panel robot. (b) Versatrax 450.

Figure 2.10: *Two different examples of cleaner systems. (a) E4 solar panel robot. Designed to clean windows by Ecoppia. And (b) Versatrax 450. A modular robotic inspection system from Inuktun.*

2.3.2 Personal Service Robots

"Personal or domestic service robots" had a huge increment in variety and units sold in the last few years. Nevertheless, its low market value is not comparable with respect to professional service robots.

Social Robots

In this case, *"social robots"* are used as a personal service robot. These robots are designed to work surrounded by people safely and efficiently, and to increase people's lives value by helping, caring, teaching and entertaining.

The robot Maggie is a robotic platform aimed for study Human-Robot Interaction (HRI) designed and built by Carlos III University of Madrid (Figure 2.11(a)). They are focused on the adjustment the potential of Maggie and provide to human users novel method of operating, learning or stimulating.

Maggie is a girl-like doll robot. Its height is 1.35 meters, and its mobile platform is provided with 12 bumpers. It uses them to detect objects around. The upper body includes interaction devices: different touch sensors are found on the surface of the carcase. A touch screen is placed in the front. It provides bi-directional interaction between the user and the robot. Two DoF (Degrees of Freedom) arms are attached to both sides of the body. On top of the platform is located a two DoF robot head, which presents an attractive design. Maggie has 4 DoF (Degrees of Freedom). Two for its arms moving the shoulders, and two for its head to affirm or deny. Its design is very attractive for the users. To sum up, Maggie is a massive variety of sensors to help more efficiently for humans (Salichs et al., 2009).

(a) Maggie. (b) Reem.

Figure 2.11: *Two different examples of social robots. (a) Maggie. An interactive social robot from UC3M. And (b) Reem. A multi-functional platform designed by Pal Robotics.*

REEM by PALRobotics is another example of humanoid service robot (Figure 2.11(b)). This interactive "waiter" robot has multiples purposes with characteristics like: face or sound detection, user-friendly interface and autonomous system for the navigation. The entertainment in public environments or helping people are the typical uses for REEM, However, it can offer others possibilities like video-conferencing assistance, multimedia information or transport of small packages. REEM weighs 100 kg. Its height is 1.70 m. It is equipped with 8 hours of autonomy and 22 DoF (Ferro and Marchionni, 2014).

Cleaning Robots

"Domestic cleaning robots" are the most widespread personal service robots, and their goal is related to household cleaning tasks in the house. Over personal cleaning robots, two central classes rise according to the scene where they work: indoor robots and outdoor robots (Table 2.3).

Table 2.3: *Classification of personal cleaning robots according to the scenario.*

TYPE	DESCRIPTION
INDOOR	This type of robot performs household cleaning tasks inside the house. Nowadays, we can find numerous and different tasks that have been automated and replaced by robots. In fact, in the market, we can find robots that sweep and scrub the floor, robots that clean the windows of difficult access or robots that clean the air.
OUTDOOR	These robots perform their tasks outside the house. On this side, we can find other tasks that robots can also perform. For example, we can find robots that cut the grass, robots that clean the pool or robots that unblock pipes.

iRobot is an important company in the cleaning department. It is well known by its vacuum cleaners. But also, iRobot are developing gutter cleaning robots, like Looj (Figure 2.12(a)). It has two clean modes to work: automatic and manual. In both, the Looj robot goes through the gutter. First, it goes forward while cleaning, and then it goes back at the insertion point to recovery. Also, it is able to monitor and adapt itself for perfect cleaning. It can be used in manual or automatic clean mode. The cleaner moves down the gutter on its own (forward for cleaning and backward for retrieval at insertion point). Also, it senses and adapts to debris to produce efficient cleaning. The robotics can vacuum in less than 50min a gutter section of 10m (Keller, 2008).

Cleaning the water of swimming pools is another horrible and hard work related to the household. In this case, this task fits better for a robot, and the Solar-Breeze from Eco Pool Technologies is one of the most current platforms (Figure 2.12(b)). The Solar-Breeze revolutionises pool cleaning in an intelligent way, sustainable and straightforward way. The pools accumulate leaves, dust, pollen and other debris throughout the day. Generally, before decomposing and sinking down, debris floats for 3-4 hours. After this time, the bacteria would have reproduced favouring the growth of algae in its pool. Solar-Breeze effectively removes dirt and debris from the water while navigating the pool. The reduction of sink and bacteria on the pool is appreciable (Gualotuña and LLinín, 2011).

(a) Looj. (b) Solar-Breeze.

Figure 2.12: *Two different examples of cleaning robots. (a) Looj. A guttle cleaning robot by iRobot. And (b) Solar-Breeze. The pools' cleaner from Eco Pool Technologies.*

Research/Educational/Competition Robots

"Robot platforms for research" is an vital approach in the personal service robots domain. Many institutions and companies are developing their version of robots and use them for teaching (Alonso-Martín et al., 2010, Pérula-Martínez et al., 2016). Also, these research centres are participating in robotics competitions to encourage and motivate new generations like the 1st SciRoc Challenge (EuRobotics, 2019).

One of the most advanced platforms of this type is the KIT's Armar III robot (Figure 2.13(b)). The main goal of this humanoid is to mimic the sensorimotor and sensory capabilities of human beings closely. The robot can deal with household scenarios. But also, it can deal with the objects and tasks found in it. Armar III is a fully integrated autonomous humanoid system. The total number of joints is 43 and is equipped with force-torque, velocity and position sensors. Focused on the modularity and the lightweight, they developed the upper part with comparable shape and size as a human being. For the navigation, a platform with wheels is used to permit omnidirectional mobility in the application area. The Armar's head holds two cameras per eye. They have a wide-angle lens for peripheral vision. But also, Armar has a narrow-angle lens for foveal vision. It has 7 DoF, six microphones and an inertial sensor (Asfour et al., 2006).

Another advanced robotics platform is the humanoid robot TORO (Figure 2.13(a)) from the Institute of Robotics and Mechatronics (DLR). The humanoid walking robot TORO (TOrque-controlled humanoid RObot) is a research platform for scientific purpose. It mainly deals with locomotion and dynamics. This one incorporates researches like dynamic walking or multi-contact environments. The two arms are equipped with articulated hands for interaction with the environment. These hands have limited dexterous manipulation but allow for robust interaction with the environment. For environment perception, the system is equipped by an actuated head with a Kinect sensor, IMU and stereo cameras. TORO has a height of about 160 cm and a weight of 75 kg (Englsberger et al., 2015).

(a) Armar III.

(b) TORO.

(c) TIAGo.

Figure 2.13: *Two different examples of robots used for research. (a) Armar III. The robotic platform from KIT. (b) TORO. The whole-body humanoid robot from the DLR. And (c) TIAGo. The autonomous mobile robot from PAL Robotics.*

Assistance Robots

We cannot ignore another personal service category like *"assistance robots"*. And we have to pay attention especially in both researchers and companies for this robotic class (Fernández-Caballero et al., 2012, Castro-González et al., 2016). This group covers the aspects of robotics in the healthcare process. The main role of these robotic systems is to assist hospitals and specialized centres. This assistance can be provided with both the carers and to the patient directly. For better classification, the different assistance robots are grouped according to the place of their application environment (Table 2.4).

Table 2.4: *Classification of assistance robot according to the application environment.*

TYPE	DESCRIPTION
At hospital	The operation of a hospital or health centre comprises a complex system of tasks. These tasks are not only limited to medical care but also require a combination of logistics, administration and organization tasks.
At home	The demand for home care services is growing. The Ambient Intelligent systems provide their service in a sensitive and receptive manner and are discrete in our environment. Also, supervision systems are used to monitor users in their homes.

A good example is the manipulator Asibot with 5 DoF, 1.3 m of reach, about 10 kg of weight and 2 kg of payload (Figure 2.14(a)). When it was designed and built, it was one of the few robots with an on-board control system. As a particularity, 24 Volts are needed to supply power for all the robot. This trait is the reason why Asibot is portable. Even it can be transported as a handbag on an aeroplane. Its small size and weight enable to move it everywhere.

Taking more detailed information from (Jardón et al., 2008a): "Asibot has a symmetrical construction and is fitted out with special conical connectors on each tip. This configuration makes it able to climb between static and very simple docking stations situated in the kitchen. This ability of the Asibot transforms it into a mobile robot able to move in domestic and office structural environments. The robot applications are oriented to domestic assistive tasks for elderly and disabled people. The robot has a three-finger (with 8 flanges) gripper inside of each tip conical connector to handle different tools or objects. The applications are eating, making-up, teeth brushing, drinking, shaving, makeup, teeth brushing, and they have been tested with real patients and in real environments".

Therapeutic Robots

Alongside the assistance robots, another category emerges: the *"therapeutic robots"*. This scope covers post-operative or post-injury care. Here, the direct physical interaction of a robotic system helps improve recovery or acts as a replacement for the lost function. The contribution of robotics in this field can be classified according to how the robotic system is fitted to the user's body in three groups (Table 2.5). Prostheses, orthoses and rehabilitation aids.

Table 2.5: *Classification of therapeutic robots according to how it is fitted.*

TYPE	DESCRIPTION
Prostheses	Prostheses are defined as external devices that partial or totally replace a limb. This definition includes any device placed within the body for structural or functional purposes.
Orthoses	Orthoses are an external device that is used to modify the structural and functional characteristics of the neuromuscular and skeletal system. It does not replace a member or organ but replaces or reinforces its functionality.
Rehabilitation Aids	This Rehabilitation Aid systems or treatments (therapies) help to recover motor functionality through training. This training is based on physical or cognitive exercises, and the therapy is adapted to the patient.

A good example is Mini from the Carlos III University of Madrid (Figure 2.14(b)), an advanced interactive robot that assists elders suffering Alzheimer's disease, or other causes of cognitive impairment, and also their caregivers in environments like hospitals and extended care facilities. Its characteristics are posture sensors, audition, light and tactile. Besides Mini can learn and behave in a path that the patient desires.

The design and construction of Mini are based on the results obtained from a series of meetings of a team of subject-matter experts. In those meetings, the functionalities of the robot were discussed, obtaining a list of usage scenarios classified in the areas of Safety, Personal Assistance, Entertainment and Stimulation. Those have served as a baseline to obtain the requirements for the construction of Mini.

Mini is approximately 50 cm tall, 30cm wide and weighs 3kg. It is conceived to be situated on top of a table and interact with a person sat in front of it. Mini has five degrees of freedom: one in the torso to rotate it with respect to a vertical axis, two in its head and one in each arm. Underneath its plush skin, Mini has three touch sensors situated right below its shoulders and its belly. Besides, Mini has various luminous devices situated in its eyes, cheeks, mouth and heart (Salichs et al., 2016).

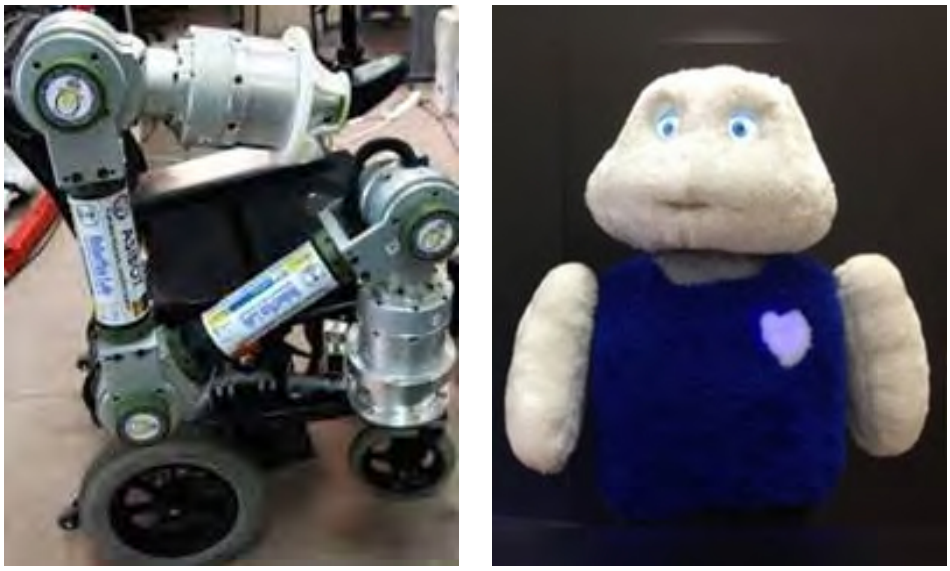

(a) ASIBOT. (b) Mini.

Figure 2.14: *Two different examples of assistance and therapeutic robots. (a) ASIBOT. The manipulator robot. And (b) Mini. A teddy platform for people with cognitive impairments. Both of them developed on the UC3M.*

2.4 Catering Service Robots

In the previous section 2.3, a possible classification of the different existing service robots has been shown. It is undeniable that every year, companies and research centres develop innovative robots. These robots have abilities or capabilities, which they already had, have been updated. From this new situation, robots can develop new tasks that they could not do before.

From this robotics progressive evolution, catering robots arise. Improvements in the algorithms of navigation, perception, artificial intelligence, or mechatronic systems (mechanics, hardware, computing) allow creating more complex tasks in challenging environments. This new group of robots in the field of catering could be included within the private sector, in particular, the group of professional service robots (Ray et al., 2008).

The catering industry is a vast sector that brings much money. Now companies have found the appropriate moment to invest in robots for this new sector. Depending on the interest rate of the company, two types of robot catering have emerged. On the one hand, there are chef robots, and on the other hand, there are waiter robots.

2.4.1 Robochefs

On the one hand, skills of cooking robots are focused on manipulation. Most of them aim to assist human beings with repetitive tasks for food preparation. Also, some robots make cocktails or drinks. Whatever these robots usually have limited mobility, sometimes even null. These robots have complex perception systems and precise and sophisticated grip systems with different interchangeable tools to achieve the task.

(a) MK1. (b) Spyce.

Figure 2.15: *Two different examples of robotchefs. (a) MK1. The robochef from Moley Robotics that cooks with the skill and flair of a master chef. And (b) Spyce. The restaurant with a robotic kitchen.*

The concept of robochef or robotic kitchen can be found all around the world. Spyce, a restaurant opened in Boston, priding itself of dishing out food cooked by a nine-foot-long, 14-foot full robotic kitchen (Spyce, 2018). Moley Robotics, a British company, has built a fully automated cooking robot MK1 (Moley Robotics, 2015). In India, two Bengaluru engineers have showcased Julia, a mechanised cooking pot that can dish out food in twenty minutes (DigitalFoodLab, 2010).

2.4.2 Robowaiters

On the other hand, some examples of waiter robots are the robot Pepper implanted in the PizzaHut restaurants for taking orders and processing payments (Curtis, 2016) or the PR2 robot of Willow Garage trying to serve beers and work together with other robots (Puerto, 2015). These waiter robots have skills focused on interaction with humans and their environment. Those can perform numerous tasks, from serving food and drinks, to taking orders, while they are moving around the restaurant. A restaurant is a continually changing scenario, where there are obstacles, such as tables, chairs, customers or other robots; that the waiter robot must recognise and overcome. Therefore, a waiter robot must have essential skills related to locomotion, manipulation, perception of the environment and social interaction.

(a) Pepper. (b) PR2.

Figure 2.16: *Two different examples of waiter robots. (a) Pepper. The social humanoid robot from SoftBank Robotics. And (b) PR2. The robotic research platform by Willow Garage.*

There is some evidence that the waiter robots are still very simple. However, the foundations to implement and integrate this new type of robots into society are already being established. At this moment, they can barely perform one or two complex tasks. The conditions in which the robot is moving is minimal and controlled, and also the movements are very elementary and pre-defined. Therefore, in the next sections, all the requirements, limitations, characteristics and skills that a future waiter robot should have, according to my point of view, are exposed.

2.5 Challenges for a Waiter Robot

Research in robotics has evolved from quasi-stationary robotic platforms to mobile and autonomous service-oriented robots. From constrained scenarios to real dynamic environments. These mobile robots are almost ready to work and help as service robot due to the novel investigation in fundamental robotics algorithms like mapping, planning, and perception.

Now we have the opportunity to apply this new knowledge in developing more complex tasks, which may serve to help or replace human beings, depending on socio-economical or security purposes.

It is possible to progress in the up-and-coming waiter application area in the area of professional service robots by supporting humans as assistants. These new waiter robots are going to be very similar to personal robots, which have to move around the home (dynamic environments for humans), interacting with humans verbally (HRI) or even physically (manipulation) (Elinas et al., 2003, Maxwell et al., 1999, Chen et al., 2010).

Therefore, robots related to the waiter domain will have very similar characteristics to personal service robots applied to the private sector. Thereby, waiter robots will be able to assist in a restaurant and support human-beings in tasks like serving to customers, cooking food, preparing cocktails, taking orders..., as a chef, a barman or a waiter (Ray et al., 2008).

There is a discussion about trials that robots will have to confront in human environments. Most researchers believe that there are three basic types of challenges. Those are: organising and cleaning a house, preparing and serving food and working with a person collaboratively. Researching in the field of catering can be an excellent opportunity to solve some challenges and achieve new ones. However, what is the real task of a waiter robot during its job in a restaurant?

A useful catering robot needs to perform reasonably, within an acceptable time frame and not being constrained by the environment. For achieving this, a waiter service robot must be provided with different capacities like human-robot interaction, recognition and tracking people, planning, reasoning, object recognition, classification and grasping. Nevertheless, these skills are active and interdisciplinary study areas by themselves.

Thereby, the integrative character of the waiter service robot investigation offers novel challenges. They are focused on accurate and robust abilities. The skills have to be correctly chosen, improved or even generated from scratch for the achievement of these requirements. Some of them are robustness against dynamic scenarios or collaboration with people safely.

2.5.1 Waiter Robot Trends

Throughout the thesis, a search on robot waiters has been carried out. In this search, most of the robotic platforms are autonomous mobile robots. As a purpose, these robots are dedicated to taking orders through a tablet or serving dishes on a large and fixed tray. These tasks are very predetermined, and it is difficult to adapt the robot to new ones. All the information about these robots can be found in the references of the previous chapter.

For that reason, another search has been made focused on the development of more complex and specific tasks. In these investigations, the objective is not to apply programs or algorithms to a waiter robot, but there is the possibility of applying them in the future development of a waiter robot.

For example, in (Srinivasa et al., 2010) HERB is presented as a home exploring robot. This is focused on the development of object manipulation skills. This mobile autonomous manipulator has algorithms of search and recognition of objects, learning of the environment, or planning and execution of grasping tasks.

The PR2 robot by WillowGarage is another whole service robot. It is composed with a dual-arm system for bi-manipulation tasks (Meeussen et al., 2010, Bohren et al., 2011). This assistance robot has skills related to the identification of dynamic obstacles, navigation or execution of grasping tasks.

Another example is the Care-O-bot system, which is already in its 3rd generation. It appears as a friendly butler, explicitly designed for domestic environments. The most special thing about this robot is its 7 DoF light-weight arm with its tactile sensors on the fingers, making possible advanced grips (Reiser et al., 2009).

In the DESIRE platform, the main goal is to give to this robot the skills towards the use of service robots in everyday scenarios. The DESIRE robot is a bi-manipulated research platform focused on manipulation and perception abilities required scenarios with human beings Plöger et al., 2008).

In (Beetz et al., 2010), it is presented a robot which can perform everyday manipulation tasks incorporating knowledge from various sources. The idea is to emphasise the importance of a high-level control system, and that methods related to artificial intelligence can help in the development and improvement.

2.5.2 Scenarios for a Waiter

To date, there are many robots capable of manipulating objects and moving around environments satisfactorily. In most cases, this is achieved by testing the robots in virtual simulations, in controlled environments, or operated by humans (LaValle, 2006, Sian et al., 2006).

However, human environments have several challenging features. These generally are beyond the control of robot developers. We have to address with some trials summarised in the next list (Kemp et al., 2007):

- By humans, for humans. The objects and the environment are adapted perfectly to humans and their capabilities.
- Presence of people. The robot can be close to users while they move.
- Other actors. Other robots can collaborate.
- Conditions of the object. The objects can be located in different places at different times, or even change in shape and size.
- Architectural obstacles. The robot can be encountered with doors or stairs.
- Sensory variations. Some examples are changes in brightness, background sounds, or dirty surfaces.
- Dynamic variations. The scenario may change independently of the robot interaction.
- Real-Time Constraints. The robot must know the implicit environment restrictions.
- Use of tools. Some tasks require the use of particular tools.

Besides, due to the exceptionality of the robots, it is really difficult to evaluate them in real and dynamic environments. We can include the lack of a benchmarking methodology or the loss of measures and procedures. An option to perform accepted and feasible benchmarking is by using real scenarios. With this idea, the integration of robots is easier for both economic and development levels. However, it has the disadvantage that robots are limited to simple tasks (Tzou and Su, 2009, Tan et al., 2012, Asif et al., 2015).

It is not very appropriate to assume that the environment through which the robot moves is static. In our case, a waiter robot works in a restaurant which has characteristics that perfectly match the dynamic scenarios previously described. In fact, in a restaurant, it is possible to find both dynamic and static objects. For example, all objects and the environment are custom-made for human beings. Other people and robot waiters can be walking around the restaurant. Objects (such as dishes) can be in the kitchen and then on the guest's table, with or without food. There are architectural elements to consider as tables, doors, stairs, or slopes. The luminosity or noise will not be constant during the workday. Even robots may have to use tools such as a tray or cooking utensils. In Figure 2.17, there are some examples of different situations in a restaurant.

Figure 2.17: *Different and possible scenarios within a restaurant in which a waiter robot should be able to manage. From left to right and from top to bottom, there are some architectural obstacles such as stairs, an area of tables, other waiters and guests, ramps and entrance or exit doors.*

All these changes can happen while the robot fulfils its task or within its trajectory. The waiter robot must identify these changes in the environment, mainly detected by the robot's sensors. It is evident that in a restaurant, the waiter robot must be able to handle dynamic environments.

To see waiter robots working in this type of environment, those must-have features similar to human beings. Waiter robots will need legs and arms like a human being to move anywhere and manipulate anything. Also, they will need some skills to develop complex tasks. All these questions will be discussed in the following section.

2.6 The Approach to Develop a Waiter Robot

During the process of developing a robotic platform, it is essential to consider what the purpose or objective of the robot is. For example, a rover-type robot will move faster and better than a humanoid robot on uneven terrain. An RGB camera will not contribute anything to an underwater robot. Therefore, it is necessary to know what tasks will be developed by the robotic platform, to define the characteristics and skills of this one.

In the case of a waiter robot and this changing environment, the robot should have to do some diverse tasks. A survey of the most important tasks is presented in the following list:

- Take orders from guests like food and drinks
- Deliver orders to the correct customer.
- Welcome clients at the entrance.
- Guide customers to their seats.
- Cheer clients up by recognising their mood.
- Take reservations for the seat.
- Grasp dishes or drinks.
- More duties ...

All these possible tasks to be developed by a waiter in a restaurant or pub are related to different robotic topics. Some of these topics are social interaction with human beings, navigation, manipulation, computer vision, task planner, and others. In the end, taking into account these considerations, requirements, and the workspace environment, it could be possible to define the fundamental skills so that a robot can behave like a waiter. In the case of a waiter robot, there are four main features or skill: Robot Architecture, Human-Robot Interaction, Robot Planning and Plan Execution. These characteristics have been described.

2.6.1 The Architecture for the Waiter Robot

Careful design of the shape of a robot can reduce the use of perception and control systems, neutralise the uncertainty and improve senses. Social scenarios have multiple conditions with respect to industrial environments. The lack of adequate robotic platforms can be a severe obstacle to research. From my point of view, there are three crucial aspects of the architecture definition of a waiter robot: the form, the unknown, and security (Acosta et al., 2006, Gurav et al., 2017, Asif et al., 2015).

- **"On Human Form"**. Human scenarios are usually suitably adapted to the shape of human beings. Sometimes, benefiting of these conditions, humanoid robots are able to make easier handling works. For instance, in the human scenarios, we can find, in most case, different objects over a horizontal surface. In these localisations, a human could reach them adequately. In the same way, a humanoid can recognise and handle these objects more efficiently if its manipulator touch or its sensors point to this horizontal plane. Obviously, all the objects manufactured are conceived to be used by a human hand. So, we will design grippers with a variety of grip ranges to handle multiples and different objects.

A logical method to implement humanoids that emulate the human shape is taking advantage of the features of the scenarios where humans live. In this way, the waiter robot could go upstairs, or open doors locate dishes on the table or kitchen or interact in a friendly way with guests (Fig 2.18) (Hart et al., 2006, Deegan et al., 2006, Katz et al., 2006).

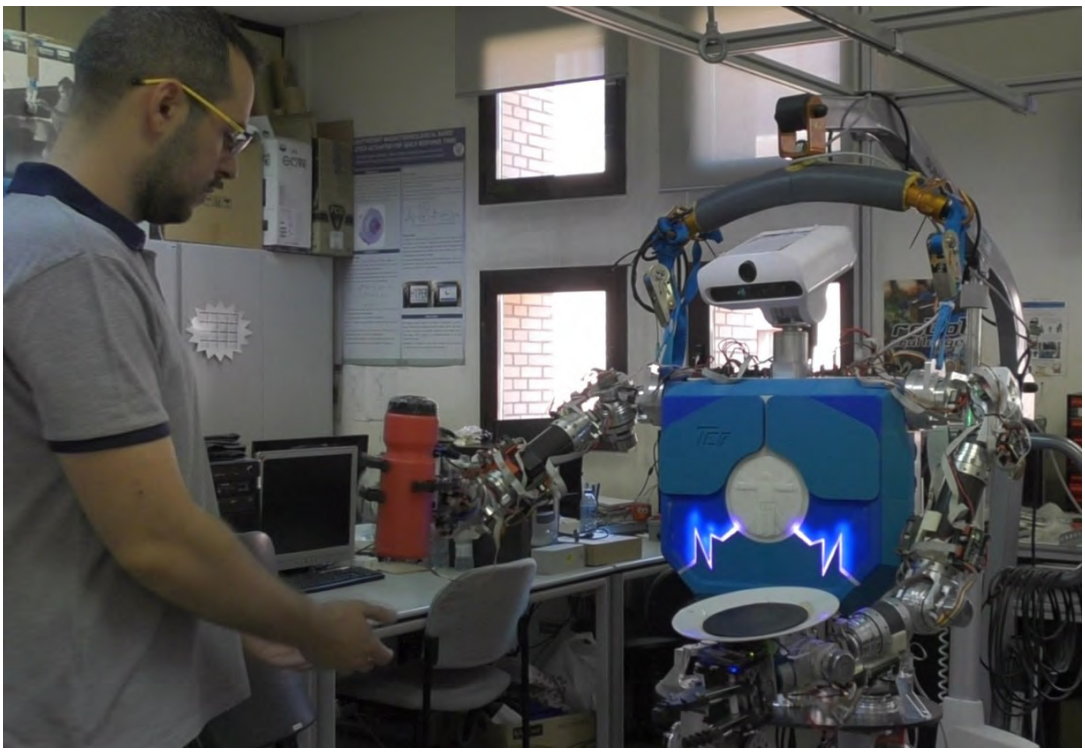

Figure 2.18: *A possible and critical situation with a waiter robot while it is serving drinks.*

- **"Designing for Uncertainty"**. Traditionally, industrial robots have avoided compliance control for the robot at the expense of stiff, precise, and fast operation. This one is a compromise on the design when the state of the job is known. Force and compliance control is more profitable for collaboration with customers safely in human scenarios. It can be applied while examining the environment or coping with uncertainty.

  In the design of a robot hand, a good example could be the optimisation of different parameters. The idea can consist of improving object grasp with uncertain physical properties. We can build a hand out of compliant elements of variable stiffness. We can incorporate position or tactile sensors or include tendons for the actuation. Combining the compliance of the hand and a new versatility, we could make robust grasping. Even it could grasp different objects with sensing uncertainties.

Our humanoid robot developed by the "RoboticsLab" research group uses F-T (Force-Torque) sensors in both wrists of the arms. These sensors offer the possibility to have a compliant control of the tray of the waiter robot. This compliance allows us to work in unknown environments (external disturbance) and to adapt to geometric uncertainty (balance position). On our robot TEO, this compliant control helps to control the stability of the transported object in an unknown scenario where the robot can be disturbed by human's hit, the whole-body controller, or the own balance control of the object (Edsinger and Kemp, 2006, Natale and Torres-Jara, 2006).

- **"Safety"**. Robots have to be safe if they work with people. In the traditional industry, robots with manipulation are hazardous, so it is generally forbidden to enter into the workspace of a robot when working. The damage generally happens during accidental physical contact. Above all, impacts are the most critical, and those depend on the speed, mass and other characteristics of the robot (Zinn et al., 2004).

  There are already companies that are adding some security elements to their robots. Some examples of such companies are Neuronics or KUKA. In the case of Neuronics, the Katana robot has been developed. Its safety methods are based on the use of lightweight materials, low speeds and low power. In the case of KUKA, the IIWA arm is a robot with a compliance controller. The controller is capable of adjusting its compliance using the feedback of its torque sensors.

  Other methods are based on mechanical safety like the Manus robot. This robot has some current limiters in the motors to avoid the forces of impact. In the case of the waiter robot, the ability to adjust the compliance of the body will allow better control of the stability of the robot and the transported object (Vermeulen and Wisse, 2008, Enotiades et al., 2014, Albu-Schäffer et al., 2007).

2.6.2 Interaction between Humans and Robots

It does not make much sense that a waiter robot cannot communicate with the customers. For example, in a restaurant or pub, it is necessary that the waiter robot understands and takes note of the orders of the clients. Therefore, elements or tools are required for interaction with humans.

In this way, several modalities could be used, but not all could be useful. This is going to depend on the task. Pointing to a menu may be less feasible than asking for a drink through speech. Nevertheless, a pointing gesture is more natural and automatic to show the table in which consumers should sit on. (Noor et al., 2012, Pieskä et al., 2012, 2016).

Human-Robot Interaction (HRI) is a multidisciplinary area. It seeks and more natural and active methods of interaction between robots and humans (Jevtic et al., 2012). Mainly, the intentions of humans are expressed through speech, expressions, gestures and sounds. Waiter robots have to be conscious of those expressions and moreover understand them. Below, it is presented the two possible HRI modules equipped in the TEO humanoid robot. Depending on the scenarios, these modules could be combined to improve the robot's communication capacity.

The first HRI system is the camera and the second one is the microphone. These two devices are located at the head of the robot. The reason is that the robot has to see and listen in the best possible way. Therefore, if we intend to interact with a humanoid robot, this is the most logical location. With these sensors, it is possible to develop basic functionality in the robot. Some examples are the detection or tracking of people, the recognition of facial expressions, acoustic localisation, the recognition of specific gestures, and others.

- **"Detection and tracking"**. This method is one of the most important HRI's for interaction with humans. The detection or the tracking of people could be the first approximation for the use of other HRI methods (Scheutz et al., 2005, Castillo et al., 2010).

- **"Facial expression"**. The identification of facial expression allows a waiter robot a natural way of interacting with clients. Robots can use this tool to know if their actions are executed correctly or to express empathy. Nevertheless, we must address some challenges before a waiter robot could fully employ this method of communication.

- **"Acoustic localisation"**. Based on acoustics and for humans, talking is an effortless way to communicate. Therefore, verbal communication is apparently the most intuitive way to communicate with a waiter robot. In this regard, a robot that can listen and talk will develop a robust interaction with humans (Bodiroža et al., 2012).

- **"Pointing gestures"**. This one is another promising and intuitive way of communication (Bodiroža et al., 2013, Murthy and Jadon, 2010). Signalling with a gesticulation can show objects, locations, or the number of orders of the same drink for an application of a waiter robot. But describing the shape of an object or its localisation verbally can be more difficult and less precise than pointing the object (Kahn et al., 2002). However, pointing gestures are not easy to recognise (Eckes et al., 2007). The difficulty lies in a precise 3D detection of the positions of hands or the face in motion of a new client in a non-static environment under unknown and changing lighting conditions. Besides, the identification of a designated point at the appropriate moment is complex when the client is signalling the point.

2.6.3 Robot Motion Planning

Robot Motion Planning is usually responsible for solving the question of "how". There are three problems to discover: "how can the robot move from one place to another?" (trajectory planning), "how can it reach an object?" (planning of movements), or "how can it perform the desired task?" (task planning) (Russel and Norvig, 2012, Kumar et al., 2007).

Mainly, trajectory planning and movement planning are considered in this subsection. For the implementation of the navigation for mobile robots, an essential operation is the route planning. Moreover, there are other important actions like self-location, planning of routes, construction and study of maps (Qing-Xiao et al., 2010, Hertzberg et al., 2014, Tzou and Su, 2009). All these operations are fundamental for a waiter robot inside a restaurant.

- **"Robot location"**. For the question "Where am I in the restaurant?", robot location gives the solution. For the question "how should I get to the table?", The route planning gives the solution. Or even, "where am I going?" In the end, the process of construction and interpretation of the map defines the geometric representation of the scenario of the robot.

  Related to the waiter robot's reference frame, the idea is to describe the position in the restaurant. This operation is necessary to know the position of tables, doors, or even people moving.

- **"Path planning"**. This one can be local or global. On the one hand, the planning of the local route is applied to dynamic scenarios. While the robot is obtaining sensory information and walking, this one is planning. Moreover, a different route is created if the environment has changed.

  On the other hand, the planning of the global trajectory can only be done if the environment is static, without modifications. In this case, the robot knows the scenario correctly.

- **"Motion planning"**. This one is related to the method of selection of movements and their corresponding inputs. At the same time, all restrictions must be met (avoidance of obstacles, avoidance of risks, etc.).

  Motion planning can be described as an algorithm based on a set of computations. These computations provide sub-objectives or set points for robot control. These computations and the resulting plans are based on a proper model of the robot and the environment in which it is moving (Garrido et al., 2008).

2.6.4 Plan Execution

A series of movements is the performance of a planning system. These movements have a symbolic description — for instance, the execution of grasping and delivering an order in a waiter task can be composed by the next movements:

1. Move to a table.
2. Look for a proper workspace.
3. Manipulate food and drinks.
4. Come back and so on.

These movements still have a symbolic description. Such a description is not sufficient for the low-level controller. The planning system cannot understand how the table looks or where the drinks are. Hence, we need understandable instructions for the low-level controller, previously interpreting these movements by a plan execution system (Xu et al., 2009, Lehmann et al., 2014, Neumann et al., 2014). For the description of the plan execution to perform tasks in a waiter's robotics domain to do multiple works, two approaches have been defined.

- **"Pre-programmed capabilities"**. In this procedure, the robotic platform has pre-programmed skills, like navigating to the kitchen, following a person, serve a drink, etc. Related to this strategy and based on commands, the robotic platform could do these works. Nevertheless, at the end, the solution of the performance of more and different intricate works in dynamical environments would be impossible.

- **"Plan execution system"**. The other method is to use a plan execution system. With the composition of different pre-programmed robot capacities, this plan execution system concedes the resolution of intricate tasks. For the domain of the waiter robots, it can be quite complex if all the objects should be modelled within the planning area (tables, chairs, other waiters, dishes, cutlery). This complicated domain can do the planning issue unmanageable.

  A deliberative system supports the translation process (from actions to commands). Here, the plan execution system might request extra data to interpret the responses. For instance, it is possible to claim the deliberative system the position of other waiters or the location of the table where the chips should be served. The plan execution supervises the performance of the task to check if the objective is reached. In the case of a non-repairable failure, it will request the planning system to produce a new plan (Gat, 2007, Ghallab et al., 2004, Sirin et al., 2007).

2.7 Conclusions

Chapter 2 describes service robots, classifying them according to their application and explains the economic progress of this sector. There is a great variety of robots, and the need to automate processes cause this variety. Because of that, new types of robots emerge always. This one is the case of catering robots. In particular, robochefs and waiterbots. These new service robots focus on more professional sectors, such as restaurants.

Nevertheless, existing catering service robots are very basic or perform simple tasks. In the end, we need that those server robots have enough capabilities to perform complex tasks, have a satisfactory performance and work time, and not be limited by the environment. For achieving these features, a waiter service robot must have a wide variety of skills. All these skills are active and interdisciplinary investigation areas by themselves.

Chapter 3

TEO: The Waiter Humanoid Robot

3.1 Introduction

The humanoid service robots will participate in the daily life of people during the next decade and will help to improve their quality of life during work, performing the most complex and tedious tasks. The complexity of the task is based on the integration of various systems at the same time as stability, trajectory planning, human-robot interaction.

Some humanoid robots that help within the industrial sector have already been announced. For example, the Connie robot helps to deliver the tip to the hotel robot. The Hilton hotel company and IBM as a whole have put Connie on their counters to inform guests about local tourist attractions. Therefore, Connie makes gastronomic recommendations and highlights the features and amenities of the hotel (Ivanov et al., 2017).

The HRP-5P is a humanoid robot that can build homes. From the Japan Institute of Industrial Science and Technology, this robot has learned to perform basic construction tasks. These tasks even include the installation of drywall (Kaneko et al., 2019).

Toro aims to work on tasks related to aircraft assembly operations. In cooperation with Airbus, the goal is focused on showing accurate accessibility (namely into areas where wheeled robots cannot be deployed) of humanoid robots in co-located spaces with human workers (Henze et al., 2017).

In our case, we have used the humanoid robot of the Carlos III University of Madrid. The idea is to develop a robot that can behave like a waiter. With this idea, we have used this robot to implement the algorithms, tools, drivers needed to investigate the problems related to the waiter robots. In a specific manner, we have studied the difficulties of balance control of both the robot and the object manipulated the transport task.

(a) Connie.

(b) HRP-5P.

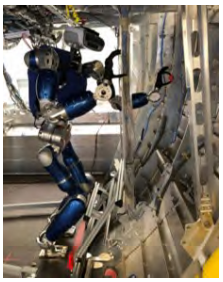

(c) TORO.

Figure 3.1: *Three different examples of defence robots. (a) Connie in a Hilton hotel. (b) Experiments with HRP-5P. (c) TORO in an aircraft assembling task.*

In this chapter, we address several issues such as the definition of the robotic platform used, the description of the purpose of the waiter robot and its most essential complements, the presentation of the perception systems, and an evaluation of the applied balance control system.

3.2 TEO - the Humanoid Robot Platform

In Madrid, at Carlos III University, the humanoid robotics group "RoboticsLab" has been working for more than ten years on the RH-project; a robust and open humanoid platform for researching on biped walking, balancing control, sensor fusion, HRI for a collaborative task, etc (Jardón et al., 2008b, Arbulú et al., 2005, Staroverov et al., 2007). At present, the third version of a humanoid robot is being developed.

RH-1 and the previous version, RH-0, were anthropomorphic robots with 21 degrees of freedom, 145mm height and 50kg weight. Those developments achieved stable walking but needed: improved robustness of the robot's structure, to reach a faster gait, to have reduced joint compliance, and to suffer from less link flexibility.

TEO (Task Environment Operator) is the new version that can walk, sit down on a chair, go up and downstairs, and move in human environments. The height, weight, and link rigidity have been increased using a different approach. Also, hardware and control systems have been critically improved. Thus, more sensor information and complex control algorithms may be managed with a higher computational capability. The main research aims of this humanoid robot have been its stability (Kaynov et al., 2009) and gait generation (Pardos and Balaguer, 2005, Arbulu and Balaguer, 2009).

The humanoid robot TEO (Figure 1) weighs about 62.5kg, has a height of 1.70m, and has 28 Degrees of Freedom (DoF). The DoF is distributed as follows: 6 DoF per leg, 2 DoF in the waist, 6 DoF per arm and 2 DoF in the neck. Also, it has 2 under-actuated hands (Martínez et al., 2012). Although at the moment, we are working to replace the neck with a soft platform.

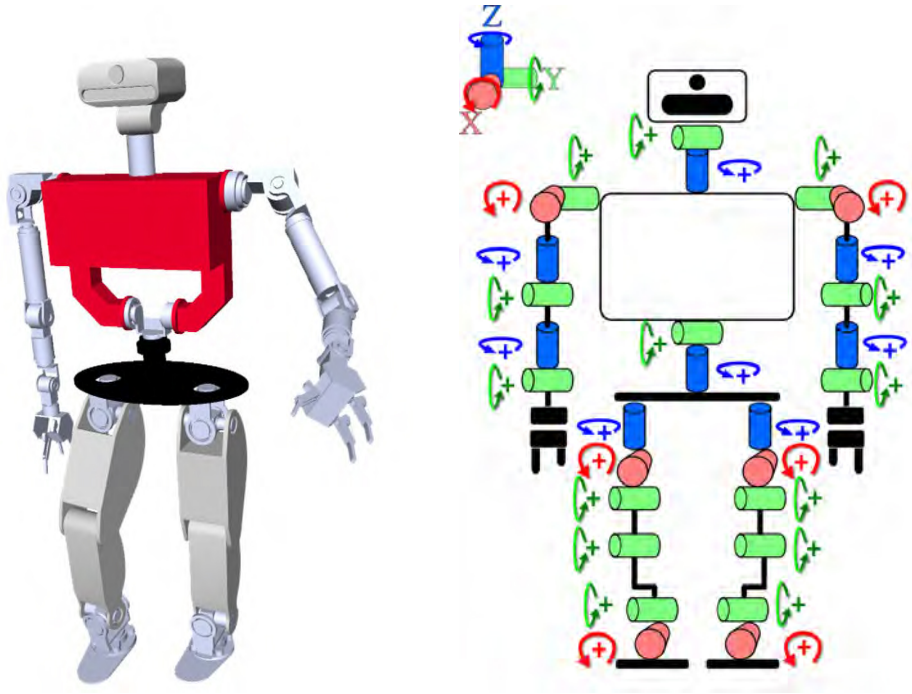

(a) OpenRave TEO model. (b) Motor directions.

Figure 3.2: *The humanoid robot TEO.*

The opportunities and possibilities that TEO can offer are numerous. Its anthropomorphic form along with its 28 DoFs allows guiding the investigations on humanoid robots in different disciplines. Currently, there are four main lines of research. The researchers and students of RoboticsLab are working on applications that allow TEO to reproduce movements and tasks such as ironing (Estevez et al., 2017), painting (Fernandez-Fernandez et al., 2018), bi-manipulating objects, or behaving as a waiter (Hernandez-Vicen et al., 2016, Lorente et al., 2016). All these tasks are plausible because TEO can learn and interact with the environment. In short, TEO can successfully perform tasks in human environments. After all, most humanoid robots have this ultimate purpose.

However, to understand how TEO is capable of performing these complex tasks, it is necessary to describe both hardware and software architectures, and what elements make it up. In this way, the central part of this chapter can be understood much better, and the main idea of the doctoral dissertation will be more precise.

3.2.1 Hardware Architecture

Its modularity mainly characterises the hardware architecture of the TEO robot. An attempt has been made to maintain this concept as much as possible to facilitate assembly, connection (plug and play) and subsequent software integration.

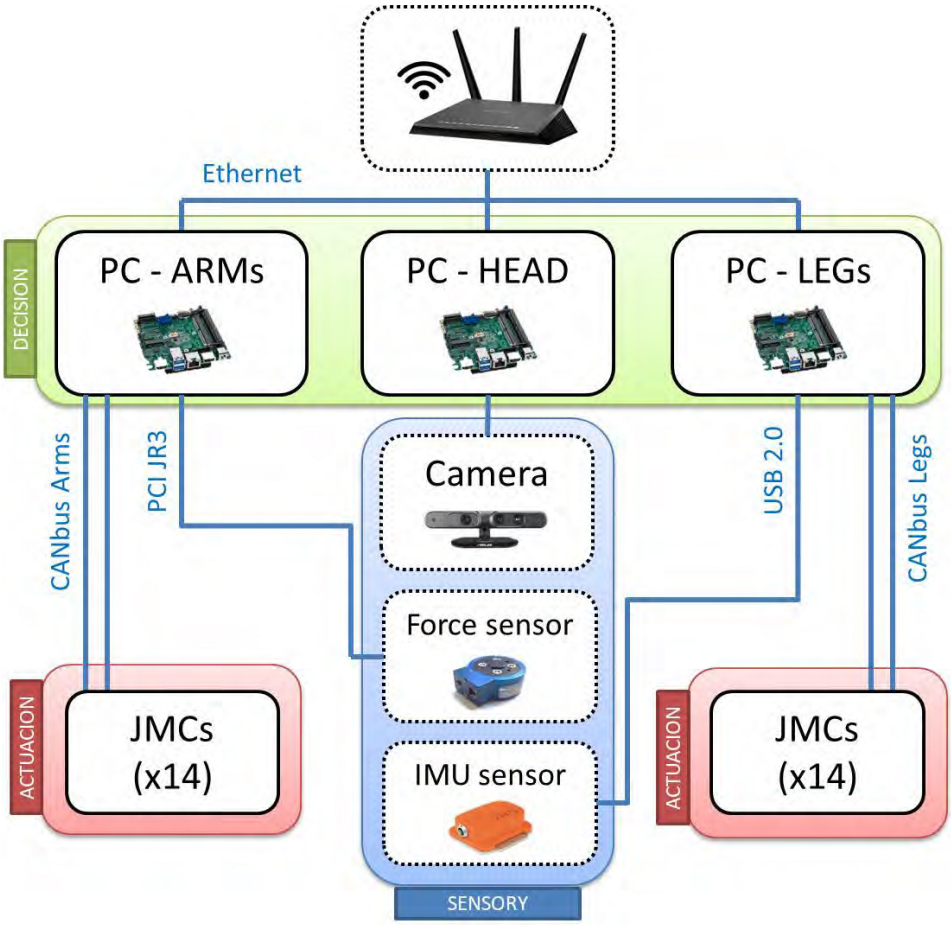

Figure 3.3: *Hardware Architecture implemented in the humanoid robot TEO. The blocks with the discontinuous line are related to components which interact with the outside. The blocks with the continuous line are related to components which process the information.*

- **"Communication system"**. Starting with the description of the TEO hardware communication system, there are two types of networks. The first communication system is a Gigabit Ethernet network (with high speeds beyond 1Gbps). This network connects all high-level hardware systems, even with a remote computer. The second system is a CANbus network (with speeds of approximately 1Mpbs). In total, there are four CANbus networks (one for each limb) that connect high-level systems with joint control systems (low-level).

- **"Decision System"**. Within this system, at the highest level, the TEO humanoid robot has three embedded computers (Intel^{TM}NUC7i5DNHE Core i5). Each of them has a role. The first one is the locomotion computer. This computer is responsible for processing all information related to the control of the legs and waist. On the one hand, it has a Peak-Can^{TM}4 ports mini-pci card to send and receive information on each leg joints. On the other hand, it has connected the inertial sensor, which provides information for the stability and walking of the robot. The second one is the manipulation computer. This one is responsible for processing all information related to the control of the arms and neck. On the one hand, it also has a Peak-Can^{TM}card with the same purpose. On the other hand, the Force-Torque (F-T) sensors are connected via PCI card to this computer, which provides information for stability and walking, as well as for manipulation and grip of objects. The third one is the vision computer. This computer is used exclusively for the computer vision associated to the camera, which is connected to this computer via USB. The reason is that typically, computer-vision programs are the heaviest computationally.

- **"Actuation system"**. There is a dedicated control unit for each joint. This system has the name of the Joint Motor Controller (JMC). Essentially, this device is a driver connected to the CANbus and is composed by the motor and the two absolute and relative encoders.

- **"Sensory system"**. This system is responsible for obtaining the necessary data for the robot through different sensors. In this robot, the three integrated sensors are the camera, the force sensor and the inertial sensor.

  Considering these desirable properties, the camera model chosen for the TEO humanoid robot is the ASUS^{TM}Xtion Pro live camera (Fig 3.4(a)). This low-cost device, linked with external image processing, equips the robot with the ability of self-movement, optical flows or moving objects detection; and applies the resulting visual data for the task of the waiter robot.

  This camera is constituted of two different optical sensor systems. On the one hand, there is the RGB Camera, and on the other side, there is the depth sensor. This second camera is an infrared laser projector combined with a monochrome CMOS sensor. This sensor takes 3D video data under different light conditions. In both cameras, the field of vision is 58ºH 45ºV 70ºD, and the resolution is of 1280*1024. The functioning of the 3D sensor consists of the projection of a structured infrared light that is captured by the monochromatic camera and, therefore, through software processing, reconstructs a 3D scene. Because of the available programming interfaces of open-source applications (APIs), such as Openkinect or OpenNI, it is plausible to perform gesture identification, motion analysis, others.

The mechanical morphology of the robot TEO equips four F-T sensors. Two in the hands and also two in the feet. The JR3^{TM}F-T sensors (Fig 3.4(b)) are monolithic titanium devices that contain analogue and digital electronic systems. The aluminium strain gauges detect the loads supported on the sensor. The voltage meter signals are amplified and filtered to become analogue signals of the force loads in the three axes (Fx, Fy, Fz) and the torques in the three axes (Tx, Ty, Tz). The axes on the standard JR3^{TM}sensors are situated with their X and Y axes in the plane of the sensor body, and the Z-axis perpendicular to this plane. The geometric centre of the sensor is the reference point for all measurement data. Respect to a clockwise frame, the forces and torques are the opposite: anti-clockwise frame.

The Inertial Measurement Unit (IMU) of the company Xsens^{TM} is the inertial sensor that we use in the humanoid robot TEO (Fig 3.4(c)). It is necessary to note that an IMU is not just a typical device. These types of units include 3D accelerometers, gyroscopes, and 3D magnetometers (compass), as sensing components. Besides, they incorporate electronics to prepare and publish the information detected in an appropriate form. If we combine all the output data, we could used to keep the stability of the humanoid robot. The IMU device is able to compute the roll, pitch and yaw in real-time, as well as sending calibrated 3D linear acceleration data, speed of rotation (rotation) and magnetic field. Besides, this IMU sensor implements a sensorial fusion algorithm with the measurement of gravity (using 3D accelerometers) and the magnetic north of the Earth (using 3D magnetometers) and compensates the drift errors of the integration of the speed data (angular velocity of gyroscopes). This inertial measurement allows the evaluation of the movement in a particular point without the necessity of a reference. However, we represent the output quantities in one signal. (Veltink et al., 2001).

(a) ASUS Xtion Pro Live. (b) 85M35A JR3. (c) MTi-28A53G35 IMU.

Figure 3.4: *Sensory systems equipped into the humanoid robot TEO. (a) ASUS^{TM}Xtion Pro Live camera equipped in the head. (b) JR3^{TM}model 85M35A F-T sensor for the ankles and the wrists. (c) MTi-28A53G35 IMU sensor from Xsens^{TM}situated in the CoM estimated in the trunk.*

The hardware architecture of TEO will influence the development methodology for the waiter robot application. Because TEO has two computers that control the limbs of the robot, the solution to the waiter robot problem will also be divided into two main parts.

3.2.2 Software Architecture

The software architecture of the humanoid robot TEO is focused on the CBSE (Component-Based Software Engineering) programming approach. This method of programming is a branch of software engineering which focuses on designing and dividing programs into different parts (also known as Separation of Concerns). The final goal is to be able to reuse these parts to define, develop or compose independent components. In this way, the concept of modularity is achieved, which results in programming focused on functionality.

As software support for all programming, the YARP (Yet Another Robot Platform) platform is being used in the humanoid robot TEO. YARP is an open-source middleware written on the C ++ programming language and oriented to robotic control applications. More specifically, YARP is designed for the implementation of any robotic system, in which a set of different modules interconnect and communicate with each other from different computers.

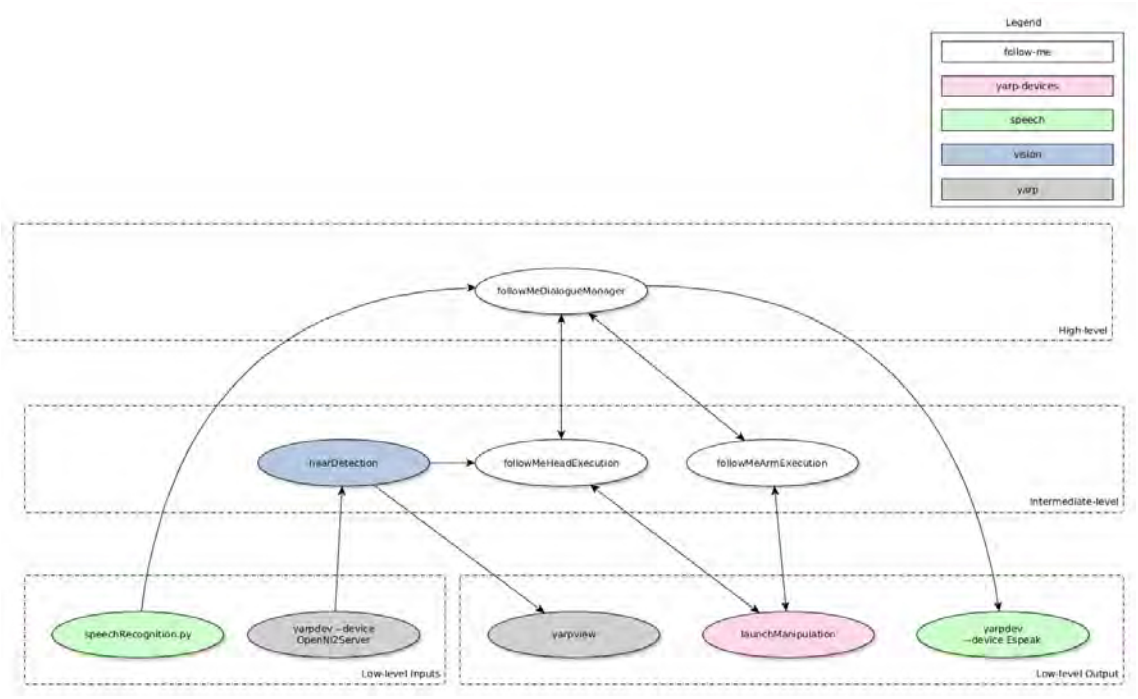

Figure 3.5: *Software Architecture implemented in the humanoid robot TEO. Example of the implementation of the FollowMe application based on the Software Architecture.*

In our case, we are implementing our own loosely coupled program and library infrastructure. The way to interconnect all these processes allows us to perform more complex functionalities (as shown in Figure 3.5). In this example, several independent programs are interconnected in a concrete way to generate, in this case, the functionality of recognising faces and following them (https://github.com/roboticslab-uc3m).

One of the most important libraries developed for TEO is "teoBase". Currently, this plug-in a set of modules at low-level which are related to perception and joint motor control. Therefore, this plug-in is highly essential for the development of any application.

Like hardware architecture, software architecture influences the development methodology for the waiter robot application. Its modular capacity and its approach to the development of software components means that the research is aimed at implementing and improving TEO's medium and high-level processes.

3.3 Whole-Body Postural Control Application

In this thesis, we present a possible approach to a waiter robot. The waiter robot TEO aims to transport objects (drinks or food) on a tray. Therefore, at all times, the robot will have a bottle on a tray. The plate is mechanically attached to the wrist of the robot. However, the transported object will be situated over the tray. This condition implies that there will not be any way of grasping of the object. On the other hand, the robot can be pushed by clients during the transport task. So, it will be essential that the robot is capable of recovering its stability.

Figure 3.6: *Demonstration of a possible situation for the TEO waiter.*

To achieve this approach, TEO must have the following skills. First, the robot should be kept in balance (balance tasks). Also, the robot should transport objects on a tray (without grasp). And finally, it should do both locomotion and manipulation tasks at the same time. In other words, TEO should perform a Whole-Body Postural Control (WBPC), keeping both body and object balance (Figure 3.6).

Therefore, we have considered four essential factors to achieve these skills in TEO. First, the architecture of this WBPC application must be described. The definition of this architecture helps to understand which modules have been used and how they have been implemented, programmed and interconnected with each other.

Second, the mathematical models that describe the behaviour of TEO must be explained. The use of simplified models helps to implement controllers easily because they have fewer degrees of freedom and are even linearised. Therefore, TEO has been modelled to simplify the complexity of the waiter robot task.

Third, the perception systems essential for this application must be described. Because the waiter robot's task is bio-inspired, the selected perception systems have been chosen to improve the efficiency and robustness of this application. In this particular case, not all the accessible systems in TEO have been used.

Finally, the balance control systems necessary for the stability of the robot and the transported object must be defined. On the one hand, the equilibrium criteria allow computing the degree of instability of both the robot and the bottle. The more unstable, the higher the generated action will be. On the other hand, Push-Recovery control strategies allow making different behaviours, which depend on the degree of stability. Both concepts will help both to maintain balance and to absorb possible external disturbances.

3.4 Whole-Body Postural Control Architecture

Figure 3.7 shows an overview of the WBPC architecture, which has three levels. With a programming CBSE approach based on components, we have implemented different and independent modules in this architecture. Each module fulfils a specific functionality. However, together, systems created are capable of developing more modular complex functions, up to the task of the robot waiter.

In this case, the task of the waiter robot is the most complex and is at the highest level. This module is the WBPC. This system is similar to a state machine that allows controlling the stability of both the transported object and the robot. Therefore, the WBPC needs the information of both stabilities to evaluate and decide how to act. The state machine evolves as a function of these stabilities, modifying the control strategy. The balance control of the robot is the main focus of the chosen strategy. This controller is the most critical and the WBPC systems focus more on achieving this sub-task than on transporting the object.

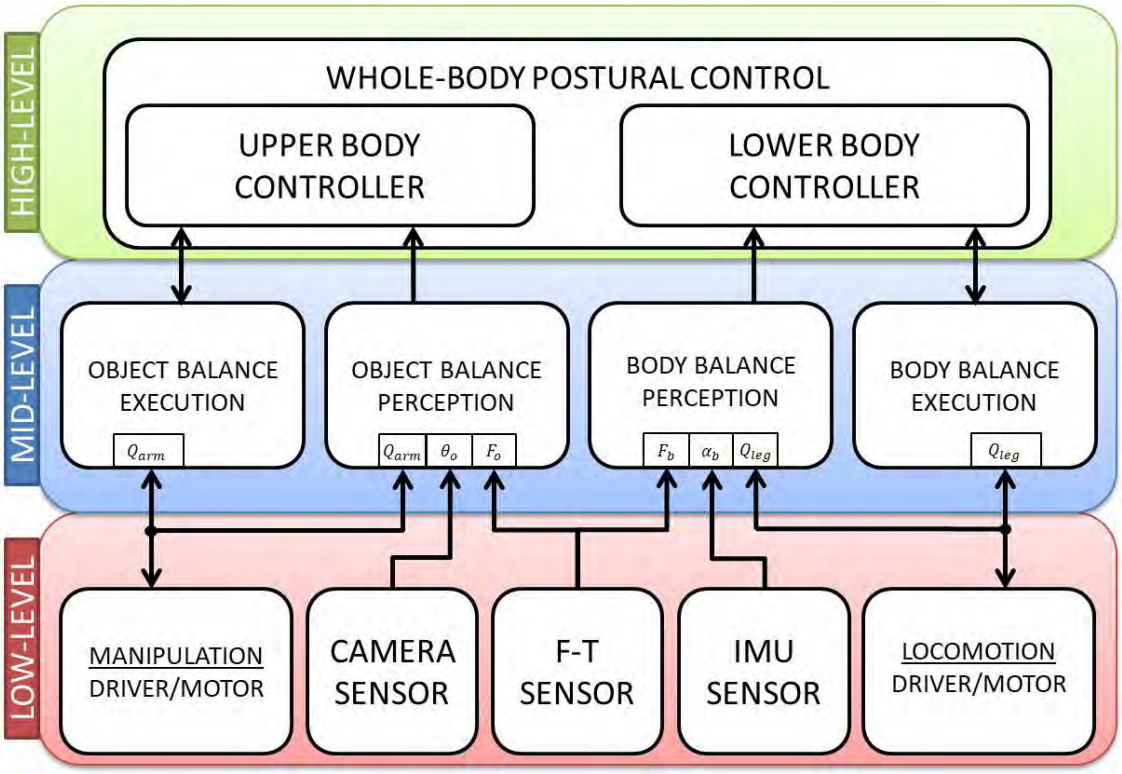

Figure 3.7: *Whole-Body Postural Control Architecture implemented in the TEO.*

It is evident that, in a human being or a humanoid robot, the movements of the upper and lower limbs affect on each other. On the one hand, if a human carries a weight on his outstretched arms, his body swings forward. On the other hand, if he starts or stops walking, the acceleration or deceleration affects the bottle on the tray. Moreover, the effect is more significant because the bottle is not physically attached. One line of research of this thesis studies the effects or influences between the movements of the upper and lower limbs.

For these reasons, the waiter WBPC architecture has two controllers in the high-level. In this application, both upper-body (Upper-Body Controller - UBC) and lower-body (Lower-Body Controller - LBC) controllers have the goals of control the balance of the body and the object, respectively. For better performance, the WBPC process modifies the gains of both controllers depending on if the task is whole-body or is just keeping the body or the object balance.

In the case of manipulation, the UBC process decides the action to follow in the arms according to the Object Balance Perception (OBP) and Object Balance Execution (OBE) processes. Evaluating the balance state of the bottle, the upper-body controller adopts the pose of the tray dynamically.

The UBC process must consider that the object is not grasped. This limitation implies the study of the behaviour of the manipulated object and also the study of the efficiency of a controller based on sensory fusion. The feedback of this UBC process is based on the previous state (applied in the OBE process) and the information on the equilibrium of the object model calculated (in the OBP process).

In the case of locomotion, the LBC process chooses the work to do in the joint's legs depending on Body Balance Perception (BBP) and Body Balance Execution (BBE) processes. Through a new simplified model, the lower-body controller dynamically adjusts itself considering the stability status of the CoM of the robot.

During the implementation of a previous body controller, we found some problems. Errors such as flexibility of the robot, mechanical gaps or noise in the sensors caused instabilities in the controller. For this reason, a dynamically adjustable model has been implemented to eliminate them. We compute the feedback of this LBC process basing on the previous state (applied in the BBE process) and also calculate the information on the equilibrium of the dynamic model (in the BBP process).

At the middle level, there are two types of processes. Some processes take advantage of the postural information of the robot and the sensors, and other processes modify the posture of the robot. For this waiter application, we have developed four processes altogether. The OBP process is responsible for discerning the equilibrium state of the transported object. The object balance is obtained, mixing the data from the camera and the F-T sensor in the wrist.

The BBP process has the objective of calculating the equilibrium state of the body based on the dynamic adjustment of the body model of TEO. The OBE process generates the corresponding action on each of the joints of the arm. Finally, the BBE process controls the joints of both legs.

At the low level, all robot devices that interact directly with the outside are implemented and integrated here. On the one hand, the robot takes advantage of the information from the camera, the F-T and inertial sensors (inputs). Also, on the other hand, the robot acts on the drivers of each joint (motors), both for the lower- and the upper-body. As explained in the software architecture section, all these components have been implemented and previously tested within the "teoBase" library.

We have primarily implemented this WBPC architecture considering the waiter task as a whole-body balance and mono-manipulation controller. The purpose of the architecture is to transport the bottle with one just arm. However, this architecture can be extrapolated to a bi-manipulation control, keeping the object balance by using two arms, while the CoM's robot is balancing.

To validate the WBPC architecture, we have tested it in two different robot platforms. The mono-manipulation controller has been verified with the TEO platform. So the bi-manipulation controller has been tested with the humanoid robots TEO and TORO (Englsberger et al., 2014).

3.5 Simplified Models

To tackle more complex problems like the waiter task, we often describe humanoid robots by using simplified models which allow efficiently implementing drivers. These models define the kinematics and dynamics of the robotic system in action. However, we can propose many approximate models of the robot for each task context considering the different characteristics of the robot, such as the mass, the location of its CoM, the inertia tensors.

3.5.1 Basic Models for Humanoid Robots

Simplified models are used in the control of robots, overall in humanoids. Because of the complexity of a whole dynamic model, it is more complicated to implement a controller for that model. These simplified models have fewer degrees of freedom than their respective full models. It also happens that to be compatible later with the theory of linear control, these models are often linearised.

There are three general aspects of the use of simplified models that must be considered. First, implementing a simplified model means representing the fundamental features of the full dynamic. Secondly, that implementation means deriving numerically or symbolically and also linearising the movement equation of the mechanical system. Also, finally, the development of these models determines the mapping between simplified and full models.

Single Inverted Pendulum Model

In a simplified way, the dynamic model of the humanoid robot TEO can be considered similar to the inverted pendulum model, shown in Figure 3.8. The resemblance is established under the following assumptions (Kajita et al., 2014). The mass of the robot m is fixed at its CoM, which is at a distance l from the floor. The mass of the stiff link is then considered negligible. Moreover, the joint motor controller fixed at the end of the link (floor) produces the torque action T that allows the mass m to move a specific angle θ at speed $\dot{\theta}$ (movement of the CoM during the balance control). This joint motor performs the control action to ensure the equilibrium of the modelled system while balancing.

To define the equation of motion of the pendulum, we identify the forces acting on the CoM. There is a downward gravitational force equal to mg, where g is the acceleration due to gravity. There is also a torque $m\ddot{\theta}$ due to the rotational motion, which is assumed to be proportional to the angular acceleration of the CoM. Using Newton's second law of motion, the equation of motion in the tangential direction can be written as:

$$\tau = -ml^2\ddot{\theta} + mgl\sin\theta \tag{3.1}$$

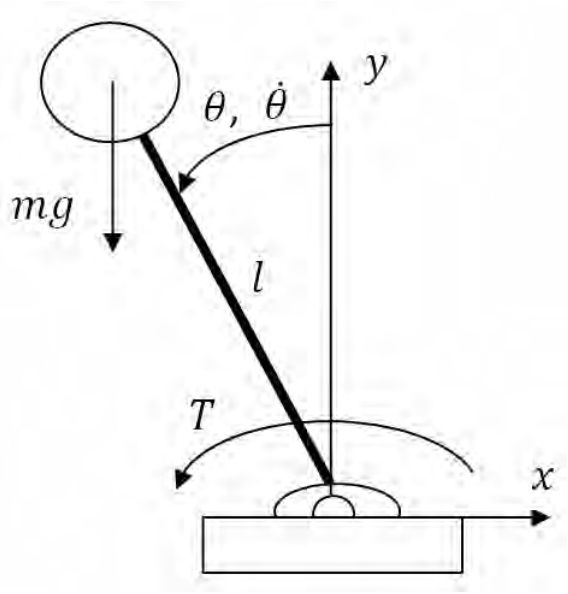

Figure 3.8: *Single inverted pendulum model.*

where τ is the torque generated by the joint motor, θ is angular position and $\ddot{\theta}$ is angular acceleration. For simplification of a control task, it is possible to make a linearization of non-linear differential equations, taking the approximation that perturbations are small enough to consider $\sin\theta = \theta$. It is not defined how small these angles have to be in practice to apply the linearization assumptions, but in this case, it is assumed that $\theta \leq 10^{o}$ Then, equation (3.1) changes to linearised equation (3.2), obtaining the LIPM (Linear Inverted Pendulum Model).

$$\tau = -ml^2\ddot{\theta} + mgl\theta \tag{3.2}$$

Cart-Table Model

The Cart-Table model (shown in Figure 3.9) is based on the ZMP (Zero Moment Point) preview control scheme that obtains the CoM trajectory from a defined ZMP trajectory (Kajita et al., 2003). ZMP is one of the main tools developed for describing the body's equilibrium, and it is explained in detail in Section 3.7.1. Thus, for this model, the relationship between the ZMP trajectory and the CoM trajectory is defined by the following equations (3.3) and (3.4):

$$p_x = x - \frac{z_c}{g}\ddot{x} \tag{3.3}$$

$$p_y = y - \frac{z_c}{g}\ddot{y} \tag{3.4}$$

where p_x, p_y are the coordinates x and y of the ZMP, x, y, z_c are the distance to the CoM in the three axes, $\ddot{x}$, $\ddot{y}$ are the acceleration in X-axis and Y-axis, respectively and g = acceleration of the gravity.

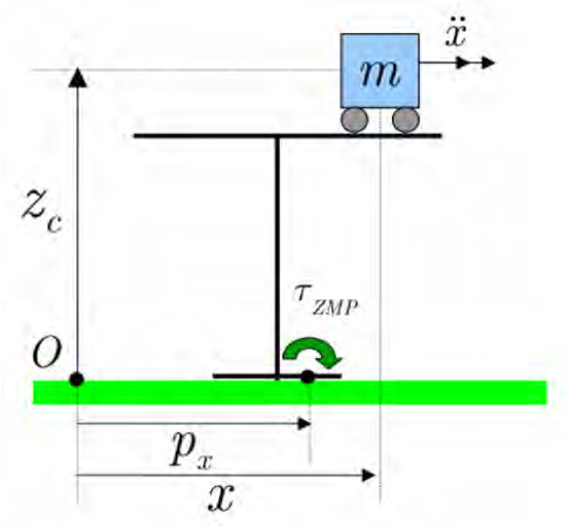

Figure 3.9: *Cart-Table model.*

For the frontal plane, the procedure to define the equation of motion (3.5) is the same as the LIPM model but using the y component of these terms. In the cart-table model, the cart mass corresponds to the CoM of the robot. If the cart accelerates with a proper rate, the table can be upright for a while. At this instant, the ZMP exists because the torque over the px point is not equal to zero.

$$\tau_{ZMP} = -ml(x - p_x) - m\ddot{x}z_c \tag{3.5}$$

3.5.2 Simplified Models for a Waiter Robot

The previously described models are a possible example of simplification of the behaviour of the robot. These possible models can represent better or worse such behaviours, and sometimes it is not necessary or convenient to use such simplified models to compute the movement of the robot. If the robot is very sophisticated and the simplification very large, it could accumulate too many errors, and therefore the development of the controller would be infeasible.

Sometimes, a possible intermediate solution is to use simplified models, and then modify them (increasing their complexity a little). Thereby, we can take into account certain essential and intrinsic aspects of the task while maintaining the simplicity of the model.

Based on Figure 3.6, we have divided the transport task problem into two parts: the lower-body issue and the upper-body issue. Both for locomotion and manipulation, the approach is based on controlling the body or the object using simplified models. Through these models, we calculate the equations of movement and thus can define adequate controllers for both issues. For the waiter task, we have proposed the 3D-LIPM model (Feng and Sun, 2008) to solve both problems. We can apply the same models for both Uni-Manipulation and Bi-Manipulation task because the humanoid robot TEO is rigid. Therefore, a force generated on the body is transmitted to the hand with the same module. With a closed chain in the robot TEO (like in bi-manipulation), we can observe the same behaviour of the forces between the hands and the body.

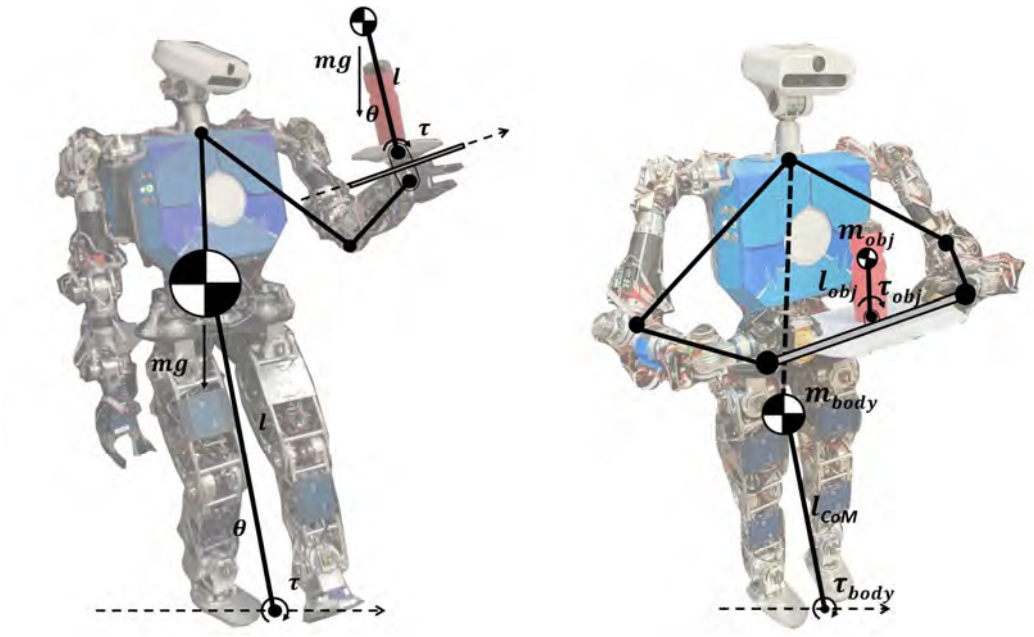

(a) Uni-Manipulation. (b) Bi-Manipulation.

Figure 3.10: *Approach to solve the waiter task using simplified models.*

The 3D-LIPM is an extension of the LIPM in the sagittal and frontal planes. The main advantage of the 3D-LIPM is that the linear equations are quite easy to program on a computer. We usually used this model for balance control or walking pattern generation. Moreover, we can apply this 3D-LIPM in balance control tasks only when the ground reaction (vertical force) and torques in the robot's ankle joint (which correspond with the rotation point of the model) can be measured. In our case, we can achieve this requirement because there are four F-T sensors assembled in both ankles and wrists of TEO.

For us, the model is an excellent option to be able to generate a controller of the transported object or the body of the robot. However, particular challenges require us to modify the model to fit even better to the real behaviour of the waiter robot.

In the case of body balance, the 3D-LIPM model is very appropriate for this type of stability and walking tasks. However, there are many errors that the controller must handle. On the one hand, the use of simplified and linearised models introduces errors. However, on the other hand, the wrong calibration and the noise of the sensors, the flexibility of the robotic structure, or the mechanical losses can accumulate errors for a control. In this case, the 3D-LIPM model is not able to consider all these irregularities. Thus, it is necessary to modify the model by adding a new system that models these errors (cloud).

In the case of the object transport, it is necessary to explain that the bottle is not firmly fixed to the tray. So, it can pivot when the robot or the bottle are disturbed. This behaviour makes the 3D-LIPM model adapt well. Nevertheless, there is a problem. The pendulum is always supported and rotated on a fixed and static point (ground) for the 3D-LIPM model. By contrast, a waiter varies the inclination of his wrist and therefore, the inclination of the tray. In other words, the floor of the model is not static. When the waiter robot tries to control the bottle, the tray is tilting. Therefore, it is necessary to extend the model taking into account the dynamics of the tray.

3.6 Perception Systems for a Waiter Robot

The main features of a waiter robot were described in the previous chapter. Some features are more connected with the mechatronic part of the robot. Other skills are more related to the software part. However, in all these skills, some requirements have been considered to make more efficient the performance of the robot.

In any case, this efficiency depends mainly on the sensory systems of the robot. A proper robotic perception system will allow making more robust these characteristics, and therefore making more accurate the execution of the tasks of the waiter robot.

During this chapter, the idea of a waiter robot has always been based on imitating the characteristics of a human waiter. For this reason, perception systems should also be similar. In the case of humans, perception is constituted with the visual and vestibular systems.

The vestibular system provides complementary information to maintain the balance of the body and is not a auditory section of the inner ear. There are three main goals of this system in humans (Hain and Helminski, 2007): it provides the subjective feeling of movement and orientation of the head, it adjusts the muscular motion and the position of the body, and it stabilises the fixed point of the eyes in space when we move our heads.

In the vision system, the eye has the objective of providing the images that surround it. The stereo vision of human beings not only serves to help instability. Moreover, the foveal ability of human perception helps in detection, recognition, or even manipulation tasks.

In the case of TEO, this humanoid robot is provided with several detection devices that provide and manage the essential information of the perception systems. The raw data originating from the sensors compose the effects on the robotic platform, and this information must be processed to be useful for the performance of the waiter task.

The result of the sensor data depends to a large extent on the performed task. In other words, the resultant perception is not the same if the work performed is, for example, simple grasping or basic locomotion. Therefore, the perceptual system oriented to the task is responsible for filtering the information and using it appropriately. Two premises can be established for the perceptive system of the humanoid robot TEO considering this approach:

- Considering the task performed, the same sensory data can generate a distinct perception. For the waiter case, the same sensors of the hands and feet provide different information due to different tasks.

- Considering the task performed, we can compose the perceptions in diverse sensory sources. In the waiter case, information from several sensors may be necessary to keep the object's balance over a tray. For this purpose, the data is merged and complemented each other.

Once we have defined the central characteristics of the human beings' perception systems, the three comparable systems that read the data in the humanoid robot TEO will be presented. On the one hand, the vision system based on stereo cameras is the sensorial system related to human visual capacity. The vision in humans has many purposes in the performance of tasks. For example, it is used to detect and estimate the distance of objects and their tendency or, also, helps in the control of human equilibrium.

The second sensory system is composed of the force-torque sensors of the ankle and wrist joints. In human beings, this purpose seems to involve sensors inside the muscle tendons. These sensors measure the powers exerted straightaway on the humanoid body due to close synergy.

The third system is composed of an inertial measurement unit (IMU). This sensor is responsible for identifying differences in the speed and acceleration of the robot as the vestibular system behaves. Next, we describe the different devices integrated with the TEO robot as perception systems.

3.6.1 Visual Perception

In humanoid robotics, the vision systems seek to replicate the performance of human vision. We use the information read by the vision sensors to recognise remote objects and their movement properties. Thus, the performance in an artificial system depends on its electromechanical components, including software. One of the most typical applications of vision systems is visual servoing. The aim is to obtain feedback control of the estimated pose/motion of a robot by using vision sensors. This application could be implemented in the waiter robot to help in the task of transporting objects (Thuilot et al., 2002, Cholewiak et al., 2013). In the case of TEO, the objective is to imitate the human vision for the visual perception integration in the control system of catering tasks. For this reason, the selected vision system must fulfil conditions such as mat vision (3D perception), colour vision, minimum viewing ranges (closest to the robot), and the ability to be programmable.

3.6.2 Force-Torque Perception

The F-T sensors are sensory systems employed to detect external forces and torques in humanoid robotics. Although we can consider these sensors as part of proprioceptive system like encoders, they measure external forces. In other words, these sensors compute the effects of gravity. The primary difference between the inertial devices or the vestibular system is the ability to distinguish static forces and torques with the F-T sensor in a humanoid robot.

For the upper-body extremities, we normally place in the wrists the F-T sensors. These sensors estimate the forces and moments generated in the handling of objects. Also, in multi-contact tasks with the environment (Weimin Zhang et al., 2006). For the lower-body extremities, they are placed in the ankle. The reaction forces of the floor are sensed by them (Nishiwaki et al., 2003). Also, the movement of the body itself generates forces on the ankle joint that are sensed too. This is the reason why these sensors are not correlated with a sensory organ in human beings.

Particularly, the F-T sensors attached to the ankles obtain the data generated when the feet come into contact with the floor. They estimate the reaction forces and torques provided during the walking of the robot. With this idea in mind, we can use this data to characterise the locomotion tasks.

The information of the F-T sensors could be evaluated or used for diverse tasks. The stage of walking is the first option to use F-T sensors. Single or double support phases. The second way is the evaluation of the orientation of the feet related to the gravity direction (ground angle). The third way to evaluate the sensation of the F-T sensor is the balance range based on the calculation of ZMP. According to Vukobratovic's stability theory, ensuring movement stability consists essentially of maintaining the ZMP reference point within the adequate support area (Vukobratović and Borovac, 2004).

Moreover, data that is read in the F-T sensors of the wrists is managed mainly for handling operations. In this case, the data from the wrists F-T sensors can also be applied in different ways. For instance, sensory information may be associated to the handling of objects and the forces and torques caused by this interaction. Also, the sensor can be used for stability in multi-contact situations (Henze et al., 2016b).

3.6.3 Inertial Perception

For a humanoid robot, we can correlate the inertial measurement system and the human vestibular system. In our heads, the vestibular perception is placed. It identifies its location, angular inclination and linear acceleration (speed and acceleration). By contrast, the location of the inertial sensor could change between different robot developments.

Nevertheless, they are principally found in the trunk (Buschmann et al., 2009, Gienger et al., 2005, Xia et al., 2008). Its location is linked to simplified robot models or diverse reference points of the robot (the centre of mass or the point zero moment) (Popovic et al., 2005). In this way, the inertia sensor gives the information to provide the calculation of these models and reference points within the closed-loop control.

In a primary inertial sensor, the accelerometer estimates the particular force applied to the mass, which creates its motion. Besides, it senses the acceleration of the body. The gyroscope estimates orientation or angular velocity related to an external reference. We can use a magnetometer to estimates direction of a magnetic field and its intensity, habitually the Earth's magnetosphere (Groves, 2015).

3.6.4 Fusion of Perceptions

For more demanding tasks like the waiter robot, it is necessary to use several sensors at the same time. Each perception system is limited to a single type of sensory information (camera-image, IMU-inertial). However, in our case, we have used the FIS (Fuzzy Inference System) systems to be able to unify the sensory measurements and obtain an exit focused on the purpose of the task.

Bio-inspiration is the reason for using this type of system. By using a humanoid robot and also imitating an application of human beings, it is interesting to use a system similar to the way human beings think. FIS systems can model the qualitative aspects of human knowledge and reasoning processes. The use of Fuzzy systems presents multiple advantages. Some of these advantages are the use of real information of the system to be controlled, its good resistance to the noise, or the low computation effort. Besides, the capability of the Fuzzy filters to come up against non-linear systems is useful. So, it can fit very well with the behaviour of a humanoid robot.

The ANFIS tool (Adaptive-Network-based Fuzzy Inference System) from Matlab is used to train the FIS systems of each of the controllers. Introduced in (Jang, 1993), "the architecture and learning procedure underlying ANFIS is presented as a fuzzy inference system implemented in the framework of adaptive networks. By using a hybrid learning process, the proposed ANFIS can set up an input-output mapping based on both human knowing (in the form of fuzzy *if-then* rules/filters) and stipulated input-output data pairs. The Matlab software can generate a single-output *Sugeno* FIS and tunes the system parameters using the detailed training data. The FIS structure is automatically generated by grid partitioning. By the way, the training algorithm uses a combination of the minimum squares and backward spread gradient descent ways to model the training data set".

Neuro-Fuzzy Learning

For this thesis, the use of the ANFIS tool helps us generate Fuzzy filters applicable to both sensing and control. There are already some examples of the application of FIS systems. In (Qi et al., 2016), Peng Qi implemented a Fuzzy filter to control manipulation applications. In (Kumar et al., 2017), the Fuzzy filter is used as a clustering algorithm to process a high amount of information. In (Precup et al., 2003), a significant problem is the non-linearities of the motor system or its load, and they are solved with the use of FIS systems. The application range of the Fuzzy is extensive. For example, it is applicable on schedulers to find the paths in grids with higher accuracy and convergence velocity (Prado et al., 2012).

In Figure 3.11, we present the evolution diagram for the application of a Fuzzy filter with the ANFIS tool. The Fuzzy filter can only be used online if it has previously been validated offline. However, to validate the filter, we must check that error is less than an established threshold. Moreover, to get a lower error, the FIS system must learn through neural networks. In more detail, the ANFIS tool has to create a multilayer feed-forward network in which each node performs a particular function on incoming signals as well as a set of parameters belonging to this node. The equations of the node functions may vary from node to node, and the choice of each node function depends on the overall input/output function that the adaptive network is required to perform. For the different adaptive capabilities in this ANFIS network architecture, both circle and square nodes should be used. A square node (adaptive node) has parameters while a circle node (fixed node) has none (Gómez Vargas et al., 2010).

We can start supposing a given adaptive network with L layers and a k^{th} layer with $r(k)$ nodes. The node can be denoted in the i^{th} position of the k^{th} layer by (k, i), and its node function (or node output) by O_i^k. Since a node output depends on its incoming signals and its parameter set, then O_i^k can be presented with next Equation (3.6):

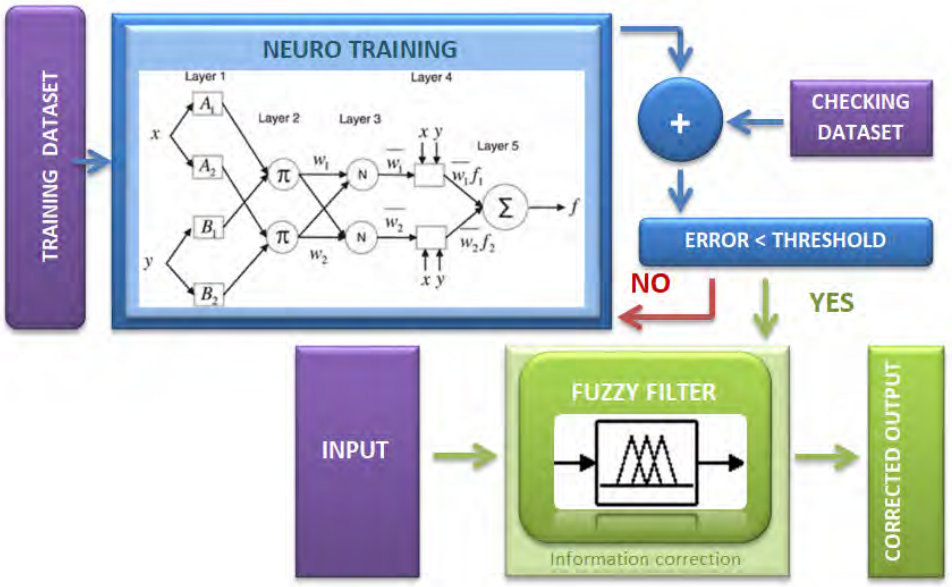

Figure 3.11: *The evolution diagram using ANFIS tool (Hernandez-Vicen et al., 2018).*

$$O_i^k = O_i^k(O_i^{k-1}, ..., O_{r(k-1)}^{k-1}, a, b, c, ...), \tag{3.6}$$

Where $a, b, c, \ ...$ are the parameters belonging to this node. On the assumption that the given training data set has P entries, the error measure can be defined for the p^{th} $(1 \leq p \leq P)$ entry of training data entry as the sum of squared errors, as can be shown in Equation (3.7):

$$E_p = \sum_{m=1}^{r(L)} (T_{m,p} - O_{m,p}^L)^2, \tag{3.7}$$

where $T_{m,p}$ is the m^{th} component of k^{th} target output vector and $O_{m,p}^L$ is the m^{th} component of the actual output vector produced by the presentation of the p^{th} input vector. Accordingly, the update formula (Equation (3.8)) of the training parameters, the generic parameter λ (parameter of the given adaptive network) is:

$$\triangle \lambda = -\eta \frac{\partial E}{\partial \lambda}, \tag{3.8}$$

in which η is a learning rate that can be further expressed as Equation (3.9):

$$\eta = \frac{k}{\sqrt{\sum_\lambda (\frac{\partial E}{\partial \lambda})^2}}. \tag{3.9}$$

Hence, the overall error measure is:

$$E = \sum_{p=1}^{P} E_p. \tag{3.10}$$

The training process ends when the overall error E is less than or equal to a pre-established threshold value ξ at the n^{th} iteration. Otherwise, the neuro training should be performed again, maybe with a higher amount of samples, by choosing ones more representatives or with more accurate information. The result is the set of functions of the output node O_i:

$$if \quad (E \leq \xi)_n \longrightarrow (O_i)_n. \tag{3.11}$$

When the training process has finished, the Fuzzy filter is ready, as shown in Figure **??** (bottom). The Fuzzy filter consists of a set of *if-then* rules in the form of Equation (3.12). The input parameters p_n are compared with the corresponding bounding values (A_n,B_n) that have been established for each parameter. The output of the Fuzzy filter is one value ($\hat{C}$) that accomplishes with all conditions inferred by the rules.

$$if \quad (A_1 < p_1 < B_1) \quad and \quad \cdots \quad (A_n < p_n < B_n), \quad then \quad \hat{C}. \tag{3.12}$$

The output value of the Fuzzy approximation must be less than the training threshold (Equation (3.13)). This should be the maximum error committed by the Fuzzy filter for each input set:

$$\mid C - \hat{C} \mid \leq \xi. \tag{3.13}$$

3.7 Balance Control Systems

This section refers to the study of humanoid robots balance and how the simplified models have supported it. Many tools have been developed to describe the kinematic and dynamic behaviour of a humanoid when it performs tasks. Taking into account that one of the main goals of a humanoid robot is to achieve stable walking behaviours, many researchers have widely studied these tools in this area.

The development of humanoid balance control architecture is mainly related to the study of two specific reference points. The first one is the Centre of Mass (CoM) used to model the humanoid body, as described in the previous subsection. The CoM of a discrete or continuous system is the geometric point that dynamically behaves as if the resultant of the external forces were applied to it. In the case of a single rigid body, the CoM is fixed concerning the body. In the case of a redistribution of separate bodies (the different parts of a robot), the CoM may not correspond to the position of any individual member of the system. However, the CoM does not provide useful information about body balance status.

3.7.1 Stability criteria

Therefore, the second point must produce all the information related to the stability of the transported object or the robot's body. There are significant points related to the stability criteria concept, and we have described three of these.

Centre of Pressure

We take the definition of the Centre of Pressure (CoP) from (Benda et al., 1994) as "the point of application of the ground reaction force vector, in biomechanics. The ground reaction force vector represents the sum of all forces acting related to a physical object and its supporting surface. Analysis of the CoP is standard in studies on human postural control and gait. The CoP is not a static outcome measure. For instance, during human walking, the Centre of Pressure is near the heel at the time of heelstrike and moves anteriorly throughout the step, being located near the toes at toe-off". This concept is useful with F-T sensors, which gathers data about the surface pressures for calculating the CoP (Figure 3.12).

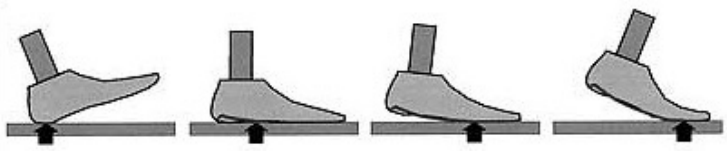

Figure 3.12: *Center of Pressure in a foot's sole while walking.*

Centroidal Moment Pivot

The Centroidal Moment Pivot (CMP) is the point where the ground reaction force would have to act to keep the horizontal component of the angular momentum constant of the entire body. The CMP is equal to the CoP in the case of zero moments about the CoM (Figure 3.13(a)). However, humanoids have a lot of internal joints, particularly the arms and torso, that allow them to apply a torque about the CoM. For a non-zero centroidal moment, the CMP moves beyond the edge of the support polygon (Figure 3.13(b)).

Zero Moment Point

The Zero Moment Point concept introduced by Vukobratovic in (Vukobratović and Borovac, 2004) is the first and the main tool developed for describing the body's equilibrium. The ZMP was defined firstly as the point in the support base; usually, the ground, where the resulting torque caused by all forces exerted over the robot's body is equal to zero. Figure 3.14 illustrates the ZMP location P, and Equation (3.14) defines it mathematically.

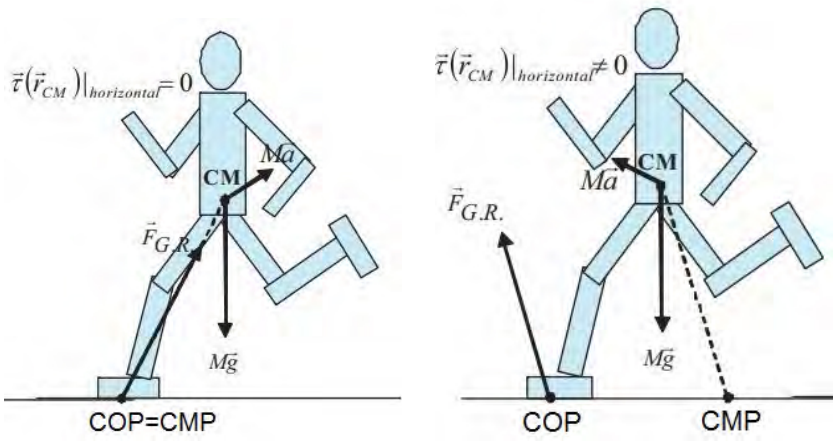

(a) $CMP = CoP$. (b) $CMP \neq CoP$.

Figure 3.13: *Comparative in different situation of the CMP respect to the CoP, (a) CMP with zero moment about the CoM. And (b) CMP with non-zero moment about the CoM.*

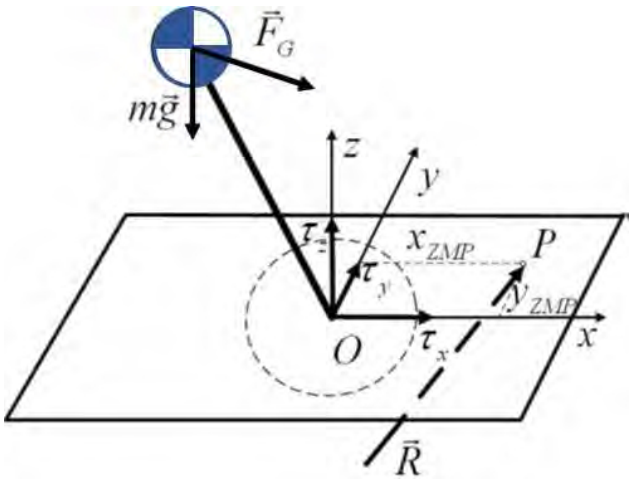

Figure 3.14: *The ZMP location (P).*

$$X_{ZMP} = \frac{\sum_{i=1}^{n} m_i(\ddot{z}_i + g)x_i - \sum_{i=1}^{n} m_i\ddot{x}_i z_i - \sum_{i=1}^{n} I_{iy}\ddot{\theta}_{iy}}{\sum_{i=1}^{n} m_i(\ddot{z}_i + g)} \tag{3.14}$$

where X_{ZMP} is the X coordinates of ZMP. , x_i, $\ddot{x}_i$, z_i, $\ddot{z}_i$ are the position and the acceleration of the robot's parts along the X and Z coordinates, respectively. m_i is the mass of the robot's parts. I_{iy} is the inertial component of the robot's parts around the Y coordinates. $\ddot{\theta}_{iy}$ is the rotational acceleration of the robot's parts. Finally, g is the gravitational acceleration.

In Equation (3.14), for the coordinate X, the sum of the torques produced by the mass of each link of the body due to gravity is divided by the sum of reaction forces. For a static posture, if the value of the ZMP coordinate lies inside the support polygon of the robot, the balance of the robot can be guaranteed. However, when the ZMP is at the edge of the support area, the humanoid body can lose balance and fall.

The computation of the ZMP depends on the posture of the robot and the location of the CoM of each limb. Due to this, ZMP calculations have an advantage in representing the robot body as a simplified model for two main reasons. The first one is the simplicity of the equations used for ZMP computation. The second reason is the possibility of using F-T sensors to measure all the forces and torques needed for ZMP computation. The model applied in this work is the 3D-LIPM modified to match with the TEO robot structure, as can be observed in Figure 3.15.

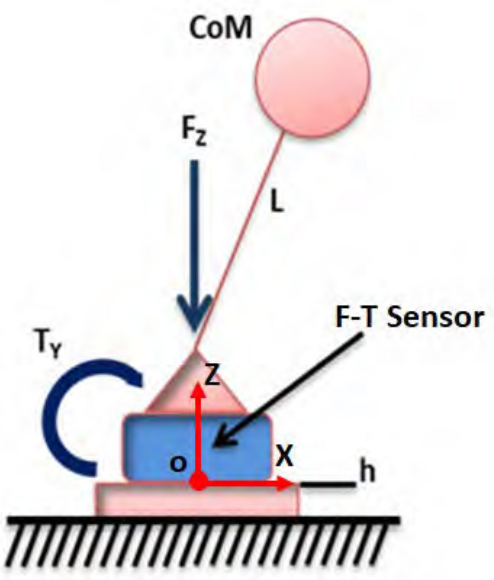

Figure 3.15: *The LIPM model with an F-T sensor between the sole and ankle joint.*

When a biped robot is supporting its body on one foot, the robot ankle is considered the pivot point connected to the robot's CoM through a massless leg. The simplest model only considers the gravitational force exerted on the mechanism, and the pendulum motion is represented by Equation (3.2). According to Kajita in (Kajita et al., 2003) and with some simplification from Equation (3.14), the ZMP equation in the sagittal plane obtained from the 3D-LIPM when the robot is standing on one foot is as follows:

$$X_{ZMP} = -\frac{\tau_y + hF_x}{F_z} \tag{3.15}$$

where τ_y is the torque at the pivot point around the Y-axis, F_x is the measured force in the X direction, and h is the distance from the ground to the location of the sensor (generally the sole height). However, when the robot stands with double support (with both feet flat on the ground), the ZMP obtained from each foot is used to compute the global ZMP (Kajita et al., 2014):

$$X_{ZMP_{DS}} = -\frac{X^R_{ZMP} \cdot F^R_z + X^L_{ZMP} \cdot F^L_z}{F^R_z + F^L_z} \tag{3.16}$$

where the upper index R represents the right foot, and L represents the left one. When the robot is in the double-support phase and two pivot points at the ankle joints exist, the inverted pendulum can be used. If the movement is in the sagittal plane, the robot behaves as a single inverted pendulum because both ankles have the same movement along the *X-Axis*.

3.7.2 Push-Recovery Control

This control aims to develop a reflex dedicated to preventing the fall of the robot, using the information provided by its sensors. The principle is to compensate for the tilt of the robot when a disturbance is applied. If the robot can be stabilised by itself, it will use its joints and motors to prevent the fall.

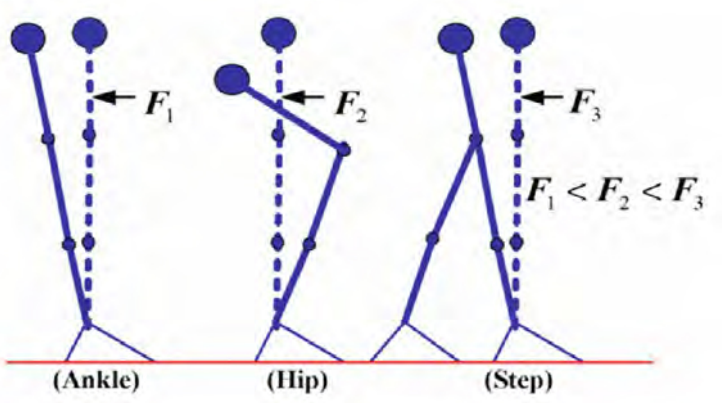

Figure 3.16: *Concept of Push-Recovery on humanoid robots and their three control strategies (Ankle, Hip and Step).*

Researchers have been studying balance in bipedal robots since years ago, and this topic has suffered major development in recent years. Some authors have studied the forces acting on humanoid robots (Sardain and Bessonnet, 2004) and others have even developed balance strategies. The stability control can be designed in different ways. Benjamin Stephens explores different models and strategies used for humanoid balance (Stephens, 2011). Their researches present three basic strategies (Figure 3.16):

- **"CoP Balancing or Ankle Strategy"**
- **"CMP Balancing or Hip Strategy"**
- **"Stepping or Step Strategy"**

In general, we could employ these approaches sequentially from top to bottom. If the selected approach odes not work, we should apply the next strategy. For little perturbation, the application of a moment in the ankle joint using an inverted pendulum model could be more than enough. As the perturbation rises, more joints of the robot must be employed. Swinging its arms or bending its hips produces an extra recovering moment. In the end, for a perturbation quite significant, take a step is the only way to avoid the fall of the robot.

Stephens chooses the CoP and the CMP as the reference points for the equilibrium control. However, other points can be considered for being the reference, such as the Zero Moment Point (Vadakkepat and Goswami, 2008). In fact, in this thesis, we have used the ZMP as the reference stability point. Despite the fact of using another point for control, we have chosen Stephen's strategies.

Ankle Strategy

The most basic strategy for balancing is the ankle strategy. With the rest of joints fixed, torque in the ankle is applied to recover the balance. It consists of an ankle reaction torque proportional to the ZMP (Figure 3.17).

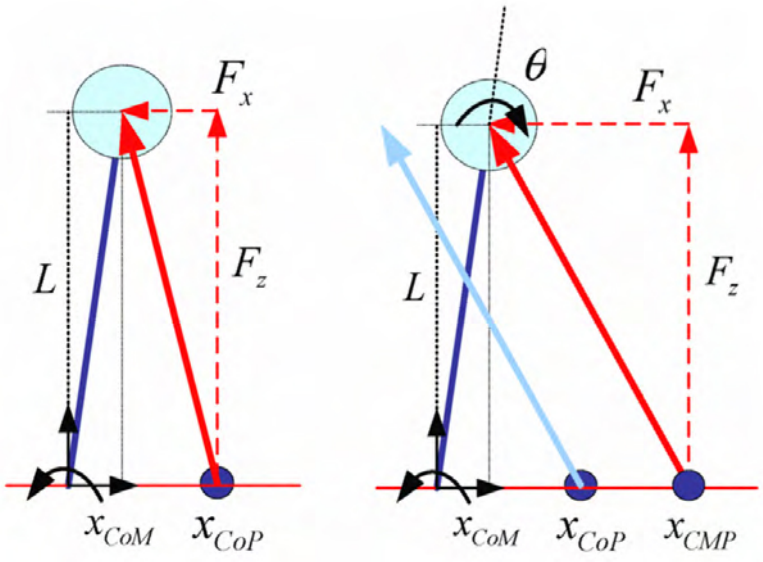

Figure 3.17: *The linear inverted pendulum model when applying Ankle Strategy.*

Stephens in (Stephens, 2011) calls "decision surfaces" to the functions of reference points which predict if a fall is inevitable by the use of a control strategy. These are useful for determining when can we stick to the lower strategy, or we need to jump into more complex ones to make a recovery. The decision surface proposed to check if the Ankle Strategy is viable is the following:

$$\delta^- < \frac{\dot{x}_{CoM}}{\omega} + x_{CoM} < \delta^+ \tag{3.17}$$

where δ^- is the back edge of support polygon. δ^+ is the front edge of support polygon. x_{CoM} is the CoM position. $\dot{x}_{CoM}$ is the CoM's velocity. $\omega = \sqrt{g/Z_{CoM}}$. The constants g and Z_{CoM} refer to the gravitational acceleration and the distance from the origin of coordinates to the CoM in the z-axis, respectively.

The support surface plays an essential role. When the status of the CoM is not within this area, then the ankle strategy is no longer useful. So, other strategies such as the hip must be applied to keep balance against larger perturbations.

Hip Strategy

The disturbance may be stronger. In the case where the perturbation is large enough, the state of the CoM of the humanoid robot would be outside the balance surface (Equation (3.17)). The Ankle Strategy is not enough for restoring the equilibrium, so the Hip Strategy comes into action. This strategy consists in increasing the restoring torque by creating a moment about the CoM using the hip torques. This is to say, not only the ankles will react, creating a restoring torque, but also the hip (Figure 3.18). In the case of the Hip Strategy, the balance surface is:

$$\delta^- - \frac{\tau_{max}}{mg}(e^{\omega T_{max}} - 1)^2 < x_0 + \frac{\dot{x}_0}{\omega} < \delta^+ + \frac{\tau_{max}}{mg}(e^{\omega T_{max}} - 1)^2 \tag{3.18}$$

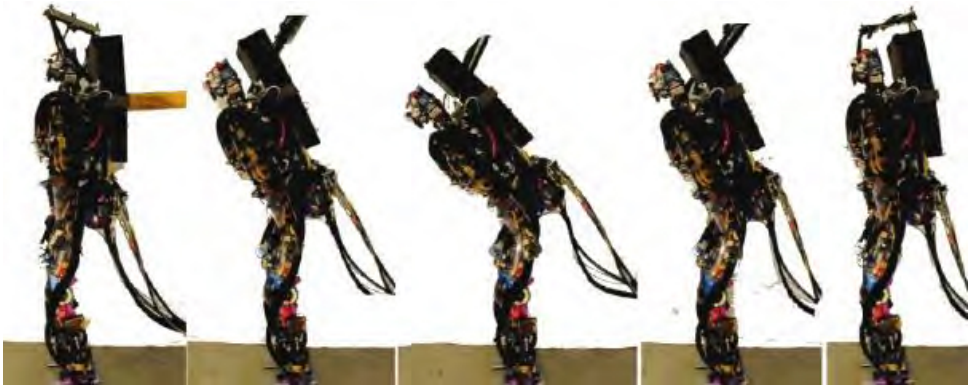

Figure 3.18: *Push recovery using Hip Strategy on the Sarcos Primus humanoid robot.*

Where δ^- is the back edge of support polygon. δ^+ is the front edge of the support polygon. x_{CoM} is the CoM position. $\dot{x}_{CoM}$ is the CoM's velocity. $\omega = \sqrt{g/Z_{CoM}}$. τ_{max} is the maximum torque. T_{max} is the maximum time. The constants m, g and Z_{CoM} refer to the total mass of the robot, the gravitational acceleration and the distance from the origin of coordinates to the CoM in the z-axis, respectively.

Using the hip strategy, the system can only maintain stability if the stability region contains the CoM of the system. Otherwise, in which this region does not contain the CoM, we will have to move on to the step strategy.

Stepping

In the case of even larger perturbations, no reaction of the ankle or hip would make it possible to maintain balance. On this occasion, the step strategy would be the solution. As said previously, this condition can be checked with the balance surface (Equation (3.18)). For this strategy, there are two situations. Single support, where the support foot serves as a support area. Double support, where the area between the heel of the back foot and the tip of the front foot serves as a support area. The stronger the perturbation is, the longer the step needs to be (Figure 3.19).

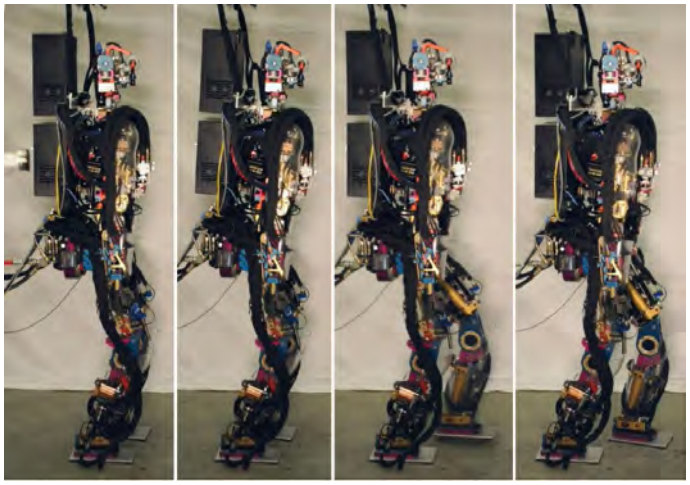

Figure 3.19: *Push recovery using Step Strategy on the Sarcos Primus humanoid robot.*

Stephens also implements a stepping strategy (Stephens and Atkeson, 2010). So also other authors dig deeper into this matter introducing more complex controls, which involve topics such as additional step to place feet side by side, knee bending (Assman, 2012), walking on slippery ground (Hofmann, 2006), and much more. However, this thesis will not focus on these last two strategies.

3.8 Conclusions

Chapter 3 explains the abilities of the waiter robot to do a Whole-Body Postural Control while transporting objects. We have described the TEO humanoid platform, detailing the hardware and software tools available, and explaining the requirements to generate many of the tasks proposed in Chapter 2.

Moreover, we explain in detail the task of transporting objects without grasping. In our case, a bottle on a tray. We focus on controlling the stabilities of the robot and the bottle at the same time. Therefore, we have defined a WBPC architecture that allows generating sub-tasks (such as non-prehensile manipulation, bi-manipulation, body balance control) or the main task as the situation requires. Finally, we introduce the concepts, methods and tools necessary to explain and understand the rest of the chapters.

Part II

Whole-Body Control

Chapter 4

Dynamic Adjustment of the Body Balance

4.1 Introduction

In robotics, the most versatile and sophisticated machines are humanoid robots. Their complex platforms (mechanical, hardware and software requirements) favour the search for simplifications that enable the deployment of multiple tasks. However, the use of these simplifications entails the possibility of other problems arising.

In the case of humanoid robots, a handy tool to simplify these complexities are the simplified mathematical models. As explained previously, the 3D-LIPM model is the one that has been used to model the body of the robot. However, by using this model, we are assuming errors at the mechanical, hardware and software levels. These errors make adequate control of the stability of the robot more difficult.

Therefore, the main objective of this chapter is to explain the new, improved model to deal with these errors. This model (more adjusted to reality) can also be used to tune the CT model associated with the inertial sensor. So in this way, we can apply these models for a Whole-Body controller and improve the task of the waiter robot.

The chapter is organised as follows. Section 4.2 introduces some preliminary work and research on the development of new models or improvements. Section 4.3 explains in detail the problems associated with model-based control and the inaccuracies that appear when using simplified models. Section 4.4 describes the new model implemented for the humanoid robot TEO based on the results of previous Push-Recovery experiments. Section 4.5 presents the tuning of the CT model based on the new LIPM. The purpose is to compute the same stability values of the robot with both models. Finally, in the last section 4.6, some conclusions are summarised.

4.2 Related Works

When a humanoid robot performs tasks and walks through plain, or rough terrains, we have to ensure that the robot does not fall over (Henze et al., 2016b, Morisawa et al., 2014). If there are obstacles placed in the robot environment and path replanning is required (Budiharto et al., 2013, McGill et al., 2012), the usual step pattern must be changed while maintaining stability. Moreover, in the case of the presence of human beings, unexpected disturbances can occur due to intentional or accidental interactions. In this situation, the robot is subject to an external force, and the robot must counteract it to recover its balance status and prevent a fall (Yun et al., 2009, Stephens, 2008). Each one of these situations leads to the use of one particular model of the robot, which takes into account different requirements from the surrounding environment, or the mechanical distribution of the robot itself.

The complex mechanical structure, high number of degrees of freedom, and control requirements of humanoid robots have led to the search for simplified models that enable the deployment of multiple tasks. However, the use of these models leads to the amplification of the inherent inaccuracies of the humanoid robot system. The concept of the "simplified model" implies the assumption of errors to favour other aspects such as computing velocity or controllability. The simplest model of a humanoid robot used in balance control is the inverted pendulum. It represents the location and movement of the centre of mass (CoM) of the robot, which pivots around a support base thanks to a rotating joint. Due to its simplicity, it is easy to state that many inaccuracies are introduced and system features are omitted. For instance, the location at any time of the CoM depends on the posture of the robot. The CoM may coincide with the location represented by a pendulum model with a specific and fixed configuration.

Researchers have developed many improvements and new models. The purpose is to add more information about the robot body or to address the lack of information. For instance, in (Lee and Goswami, 2009), Lee introduces the Reaction Mass Pendulum (RMP) model. This model is used for humanoid robot gait and balance control. The reaction mass ellipsoid represents the spatial inertia of the robot at the CoM, and it is located a the top of the leg (Figure 4.1(a)). In (Yin, 2006), Yin explains the use of a complete robot model for the walking stability of a humanoid robot. The application of the Fictitious Zero-Moment Point (FZMP) in this full model avoids many simplification errors (Figure 4.1(b)). Besides, these new models can represent spatial behaviours or model tasks. In Feng and Sun, 2008), Feng presents the Three-Mass Linear Inverted Pendulum Model (3MLIPM). This model is an extension of the LIPM, and it is divided into the standing leg, the swinging leg and the trunk (the three masses) and is focused on the walking trajectory generation (Figure 4.1(c)). In (González-Fierro et al., 2016), Gonzalez-Fierro describes the Triple Inverted Pendulum (TIPM) Model, which is used for the robot to learn to get up from a chair (Figure 4.1(d)).

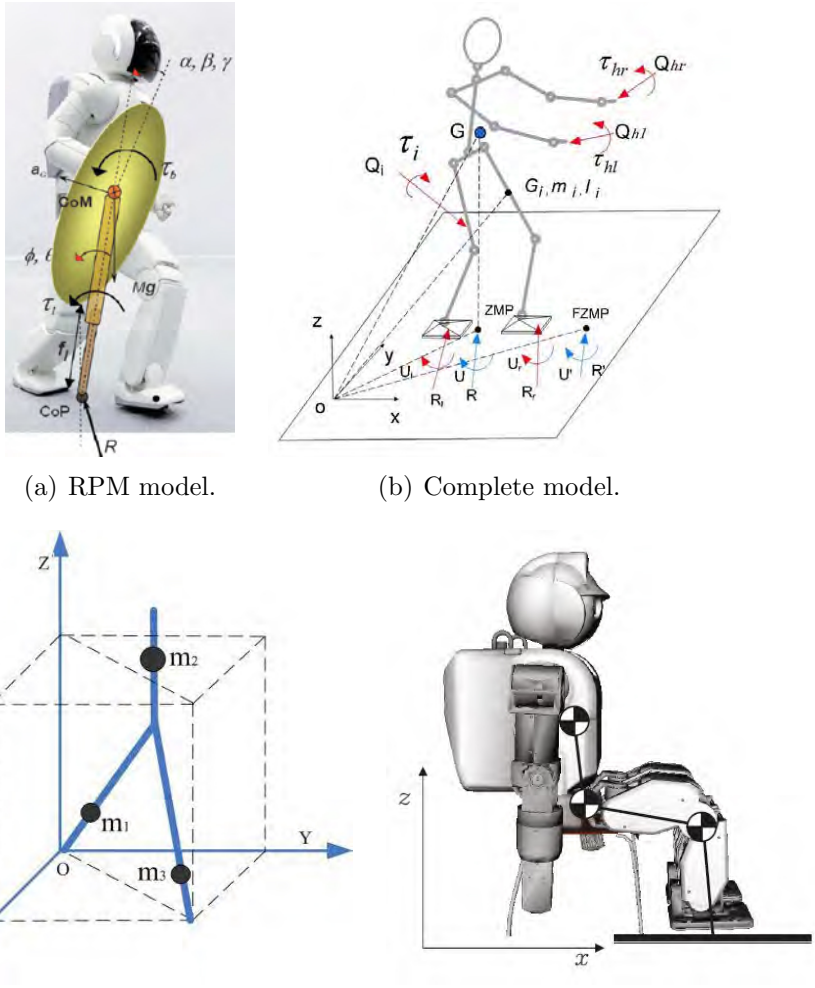

(a) RPM model. (b) Complete model.

(c) 3MLIPM model. (d) TIPM model.

Figure 4.1: *Different examples of robotic simplified models to representing/modelling the behaviour of the robot for a specific task. (a) RPM model for humanoid robot gait. (b) a Complete model for walking stability. (c) 3MLIPM for walking trajectory generation. (d) TIPM for learning to get up.*

4.3 Problem Statement

One of the primary skills that define a human being is the ability to walk upright. This ability is one of the main characteristics that a humanoid robot must achieve. The critical problem is the balance of the upright posture to avoid falls during a walking task or when standing still. The use of simplified body models and tools such as ZMP allows the deployment of stabilisers to maintain balance for the humanoid robot.

Nevertheless, both the balance control of the robot and the use of simplified models do not provide universal and definitive tools for all problems. Both have their limitations which harm the development of the waiter task efficiently and robustly as we introduced in section 3.5.

4.3.1 Classical ZMP controller using Simple Models: LIPM and CT

Balance control with the ankle strategy concept applies both to standing in an upright posture and to walking tasks. In both situations, we can model the robot as an inverted pendulum. If a force disturbance is applied to the CoM of the model, this force can lead the ZMP to be out of the support polygon, and the robot can lose balance (Figure 4.2).

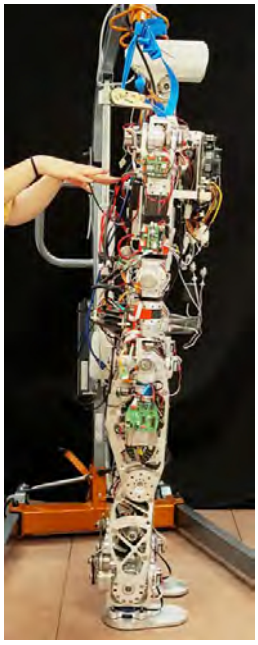

Figure 4.2: *Experiment on applying force to the TEO robot.*

Then, the robot must counteract this disturbance by applying a torque in the ankle joints, trying to maintain ZMP inside the support area. This kind of control is called *ZMP control by ankle torque* (Kim and Oh, 2004, Kaynov et al., 2009). Finally, the ankle's torque is transformed into angle commands $\theta = f(\tau)$, and the joint motors of the robot compute this angle. We have represented this concept by the control architecture depicted in Figure 4.3. This control architecture is not only applicable to the LIPM model. Also, we can extrapolate this architecture to the CT model. In this case, we should change the LIPM model for the CT and the F-T sensors for the inertial sensor to control the ZMP position.

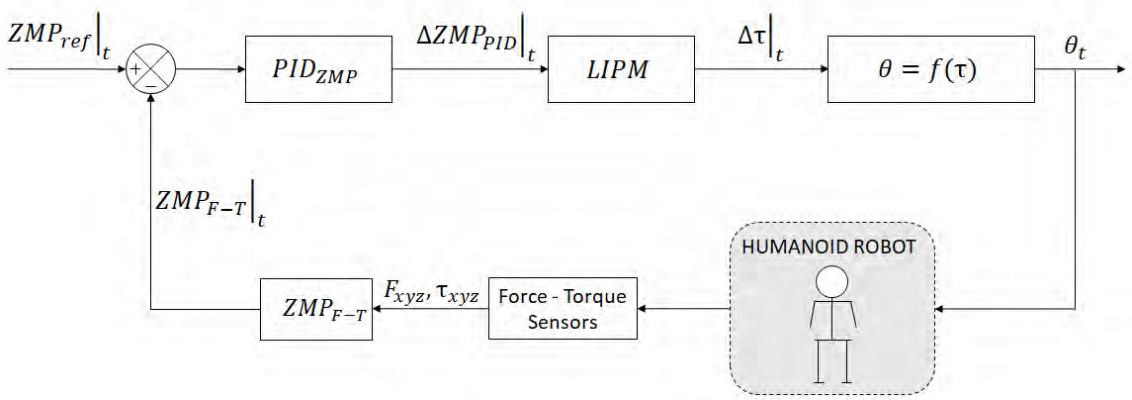

Figure 4.3: *Basic ZMP position controller using the LIPM model.*

However, traditional PID control relies on the proper selection of values to be used for the proportional (P), integral (I), and derivative (D) constants for a linearised working point (Ogata, 2009). If the process is non-linear, the control designer must then continuously evaluate the new working point and tune the constants.

Instead of using PID controllers, model-based controllers are a good option. They can learn how a process responds to changes, and in turn, they can automatically make the tuning adjustments that would traditionally be manual. However, there are other errors related to the use of models and the balance control system must deal with them.

4.3.2 Problems arising from Model-Based Control

Simplified model control approaches always introduce errors. The mathematical pendulum model is not linear, but we can obtain the ZMP equations from a linear pendulum. When the angle of the pendulum is small enough, it is assumed that $\sin\theta = \theta$, which introduces an error to the system. The mass of the centre of gravity (CoG) is also an approximated value of the whole robot mass, and even its location can change. When all these assumptions are added together, errors in the system become remarkable.

Also, there can be measurement deviations in the F-T or the Inertial sensors due to calibration errors, in analogue-to-digital data conversions or other electronic problems. Other systematic errors, such as the flexibility of the structure (due to the height of the robot), looseness between mechanical parts (as transmissions or unions of pieces), and small irregularities in the ground, are usually not considered. All of these errors lead to an increase in the control effort and make the control tuning task more difficult.

This work aims to improve the ZMP control system described in Figure 4.3, and therefore, we have proposed the Dynamic LIPM (DLIPM). This model will include the errors depicted in Figure 4.4 and more. The procedure to model this error is based on push-recovery experiments in which we compute the ZMP with the measures provided by F-T sensors. Then, the real ZMP is compared with the planned ZMP, obtaining the error. Finally, the error is introduced in the model as a fictitious force that modifies the inverted pendulum model behaviour.

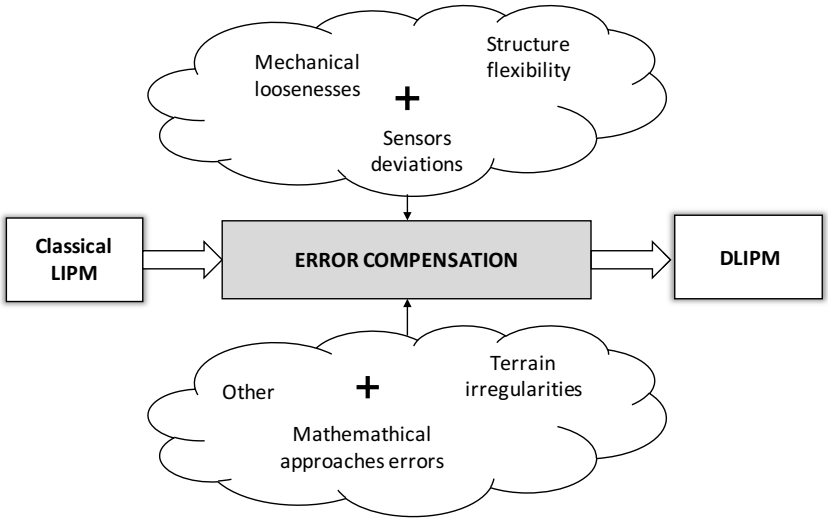

Figure 4.4: *Error compensation diagram. From classical LIPM to new DLIPM.*

From the control point of view, real humanoid mechanisms are slightly flexible (Kim and Oh, 2004). Usually, the flexibility is closely related to the robot height and, although robot designers try to make stiff structures, it is impossible to eliminate the flexibility altogether. Because of this, the humanoid robot exhibits the characteristics of a lightly damped structure. For example, in a static case, when the ankle joint is under position control, an external pushing force can easily excite an oscillation. This oscillation exists even when the position error in every joint is zero. Also, other error sources have an influence on the correlation of the robot with the model (Figure 4.4). However, it is complicated to identify and define these errors mathematically.

The existence of these errors has a significant influence on the ZMP computation and, in consequence on the balance control system. Figure 4.5 illustrates how robotic system inaccuracies and other error sources affect the location of the ZMP. In this example, u denotes the model angle expected caused by the commanded joint torque. We would represent the expected ZMP by x_{exp}. If we consider only the error introduced by the robot flexibility, the ZMP location would be the one represented by x_{err}. Nevertheless, the real ZMP computed using the forces and torques measured is x_{F-T}.

Then, the problem is the mismatch between the expected or planned ZMP and the real ZMP measured with the F-T sensors. For reducing this gap, this work proposes a model improvement to represent real robot behaviour more closely. Furthermore, a ZMP control architecture for keeping balance can be improved as well.

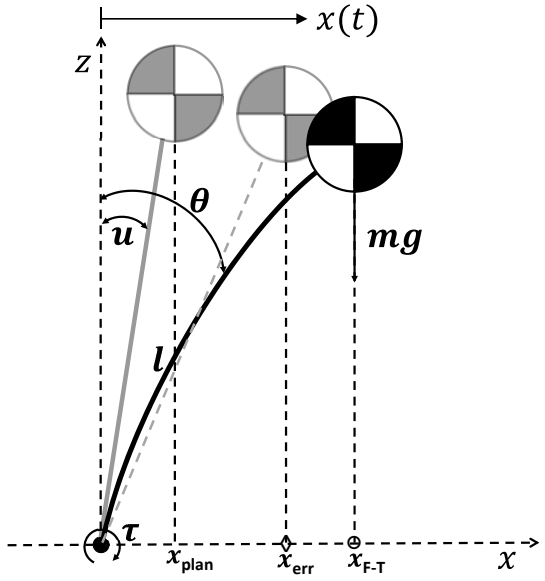

Figure 4.5: *Single inverted pendulum model, including the robot's flexibility (Kim and Oh, 2004).*

4.4 Updating Body Balance Model

The error has been modelled using the information of the F-T sensors installed in the ankles of the robot. All the effects caused by any disturbances are reflected in the forces and torques measured by the sensors. In this way, it is necessary to separate the information related to the inaccuracies and the information related to the expected behaviour. Two assumptions need to be made before performing this procedure. The first one is the need to establish the inverted pendulum model parameters: CoM location and mass. They come from the robot design, but they are not entirely accurate because of the differences between CAD designs and real implementation. The correction of these parameters using the real robot is not possible, so the use of the theoretical values is assumed. The second assumption is related to the planning of the balance control task. Taking into account the established model, the ZMP location can be planned. That is, ZMP location can be pre-planned in order to always remain inside the support polygon. The balance plan should resemble the reality in order to reduce the effort of the control system. This means that lower gains will be needed to adjust the control system.

The method used to develop the new improved model is as follows: based on the open-loop system push-recovery set of experiments, the measurements of the F-T sensors are captured and processed. Then, with this information, the real ZMP x_{F-T} is computed and compared with the expected ZMP x_{exp}. The difference between them is modelled, and one equation describing this error is obtained. The modelled error is included in the original model as a fictitious force that corrects the difference found. Once the new model has been obtained, the new planned ZMP behaviour is close to that of the measured ZMP.

4.4.1 Study of System Response

For the introduction of all the errors mentioned before into the TEO simplified model, the procedure summarised in Figure 4.6 has been followed. This procedure has been divided into three phases: the experimental phase, data analysis, and validation of results. This procedure has allowed obtaining a set of data from the F-T sensors to be used in the generation of the new custom model.

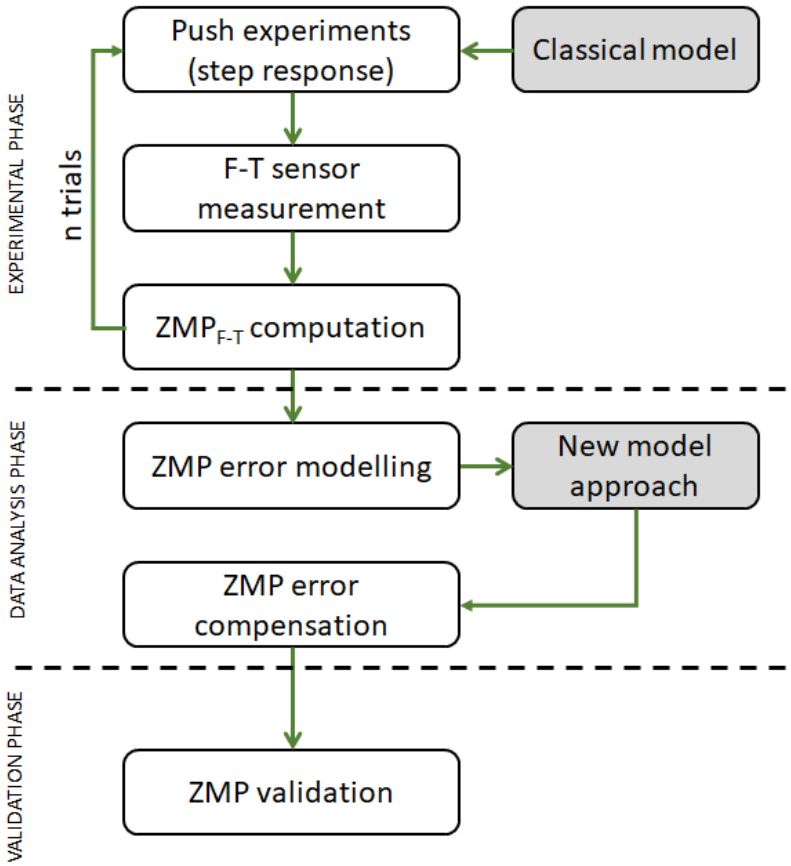

Figure 4.6: *Experimental procedure diagram for the LIPM model.*

The first stage of the procedure is to fix the inverted pendulum model parameters with the characteristics of the TEO humanoid robot. The weight of the is 62.6 kg, and the height from the ground to the CoM is 0.893 m (the pendulum length). Then, the movement of the robot caused by a pushing force was tested. The effect of this force is a variation of the ZMP location depending on its intensity. It is important to remark that the robot does not keep the initial value of the ZMP during each experiment. That is, it does not recover the initial posture. This behaviour is similar to the study of the response of a system with a step angular input in the ankle joint. After a set of trials, the ZMP error has been modelled as the difference between the expected and the measured value. The dynamic behaviour of the ZMP variation has also been studied. The last phase of this procedure consisted of the validation of the new model within the new control architecture.

For the illustration of the method, only the results from the sagittal plane (x-z) of the robot are presented because the experimental methodology for the frontal plane (y-z) is the same and similar results were obtained. This study and methodology is applicable to any other spatial direction. In this way, the experimental set-up is represented in Figure 4.7. The robot is in a flat ground environment with both feet on the ground (double support). Therefore, the support area includes the robot footprints and the common tangents between them.

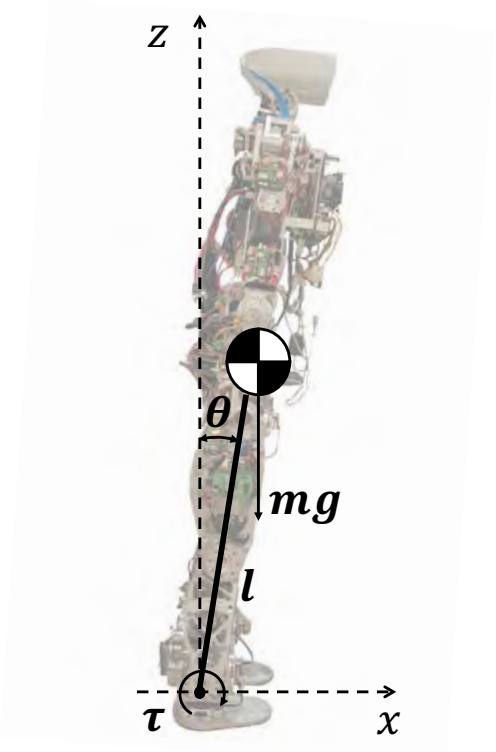

Figure 4.7: *Experimental set-up of the TEO robot.*

The results of a set of trials are shown in Figure 4.8. This figure represents the measured ZMP (the oscillating signals) and the expected ZMP (the step form signals). Each pair of ZMP signals (oscillating step) corresponds to a specific pushing force applied to the robot. If we examine each pair, some conclusions can be extracted. Larger disturbances imply a further location of the ZMP from its origin, making the robot more unstable because the ZMP is closer to the support polygon edge. This means that the angle from the model that is commanded to the robot is larger, and the errors have more influence mainly with respect to robot flexibility and mechanical tolerances. For this reason, the steady-state error is higher as well. Furthermore, the system has a higher initial oscillating response, which is not desirable when the ZMP is located near the edge of the support polygon.

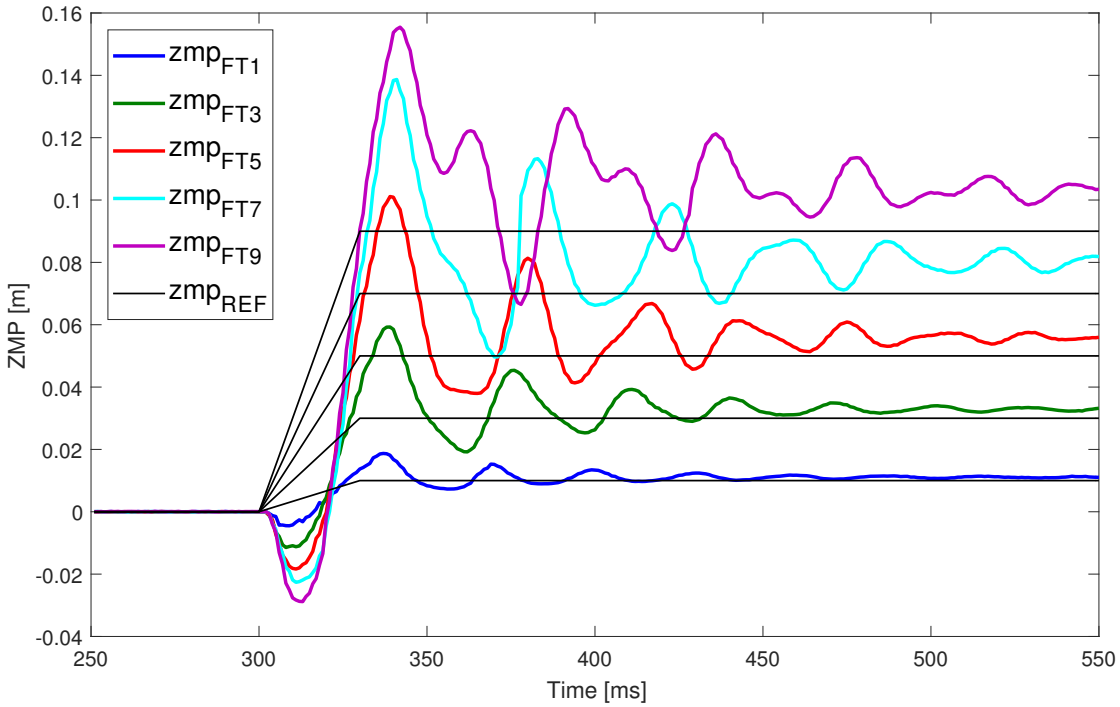

Figure 4.8: *Step response experiments with the F-T sensors.*

This dataset is the basis for developing an improved ZMP control without the necessity for a low-level position or torque controller parameter tuning. The objective of the next steps is to obtain a transfer function modelling the behaviour of the ZMP. The resulting transfer function that models ZMP deviations will be added to the classic LIPM with two main purposes: the elimination of the steady-state error and the reduction of transient oscillation and overshooting.

4.4.2 Improvement of the LIPM Model: Dynamic-LIPM

For the achievement of the ZMP control requirements (settling time and overshoot level), this work proposes an improvement model derived from the classic LIPM. The objective is to modify the initial model, adding a system that represents the errors of the real robot obtained from experimentation. Then, the measured balance parameters will have less of a deviation from planned ones, and the control response can be reduced. Figure 4.9 represents the complete model in which a spring k_a and a damper B_a have been added to the initial inverted pendulum model. These mechanical models try to compensate for the steady-state response (k_a) and the transient response to limit oscillations (B_a).

Then, the equation of motion of the model shown in Figure 4.9 is given by:

$$\tau = -ml\ddot{x}(t) - B_a l\dot{x}(t) - k_a l x(t) + mgx(t) \tag{4.1}$$

where $x(t)$ is the CoM movement, m is the pendulum mass located at the CoM, l is its longitude, k_a is the spring constant, and B_a is the damper constant. The displacement of the CoM is small enough to assume $sin\theta = \theta$. Then, Equation (4.1) becomes:

$$\tau = -ml^2\ddot{\theta}(t) - B_a l\dot{\theta}(t) - k_a l\theta(t) + mgl\theta(t) \tag{4.2}$$

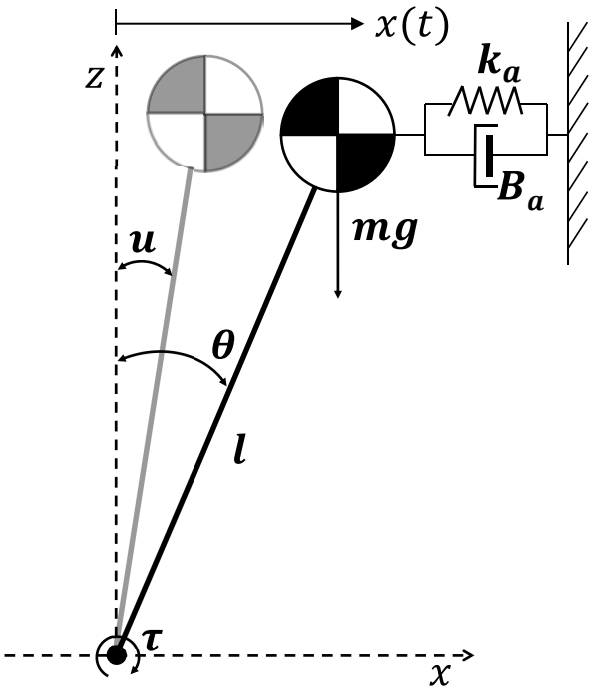

Figure 4.9: *Proposed compensated inverted pendulum model.*

On the other hand, the torque for the ankle can be also obtained from the ZMP measurement as:

$$\tau = -x_{FT} \cdot mg \tag{4.3}$$

where x_{FT} is the measured ZMP from the sensors. Combining Equations (4.2) and (4.3), we obtain:

$$-ml^2\ddot{\theta}(t) - B_a l\dot{\theta}(t) - k_a l\theta(t) + mgl\theta(t) = -x_{FT}(t)mg \tag{4.4}$$

Finally, the transfer function obtained from Equation (4.4) is represented as follow:

$$\frac{\Theta(S)}{X(S)} = \frac{\gamma}{S^2 + \alpha S + \beta} \tag{4.5}$$

where $\gamma = g/l^2$, $\alpha = B_a/ml$, and $\beta = (k_a - g)/l$.

In the steady-state, when time goes to infinity, the DC gain of the system is represented by Equation (4.6), that only depends on the k_a parameter. This one is in charge of eliminating the static error.

$$K_{DC} = \frac{\gamma}{\beta} \tag{4.6}$$

4.4.3 Steady-State ZMP Error Characterization

The next step is to characterise the deviation of the ZMP. Even though the ankle position control succeeds, the ZMP measurement presents deviations. This means that the angular controller of the ankle joint works correctly, but the measured ZMP value has a deviation from the planned or expected value. From the trial dataset depicted in Figure 4.8, the deviation of the ZMP can be determined.

Figure 4.10 represents this deviation of the ZMP_{F-T} (output) from the ZMP_{ref} (input). The relation between the expected ZMP value and the measured one should be linear, but the figure demonstrates that the real values do not match with the expectations.

The deviation in each test point is used for fitting to the second-order polynomial Equation (4.7). This equation represents the real ZMP x_{F-T} measured by the ankle sensors:

$$x_{F-T} = a \cdot x_{ref}^2 + b \cdot x_{ref} + c \tag{4.7}$$

where $a = 0.834$, $b = 1.024$, and $c = -0.0004$.

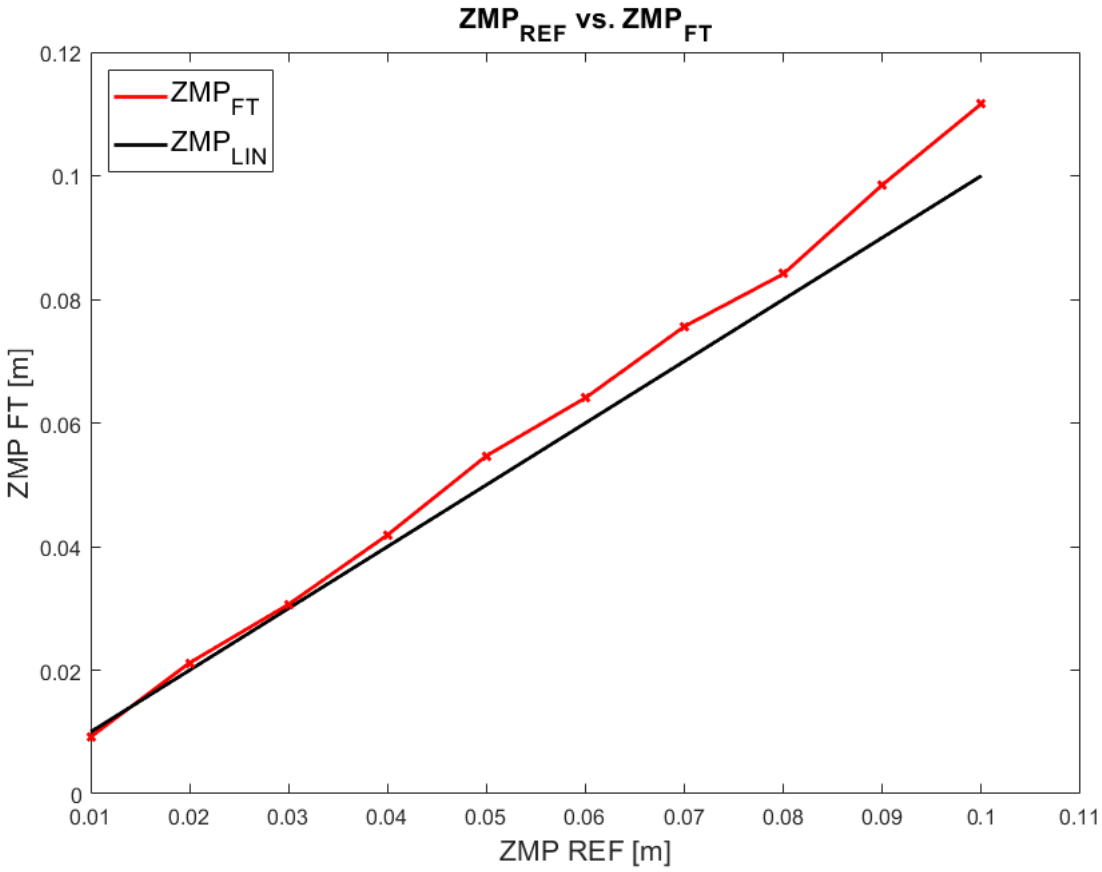

Figure 4.10: *Comparison of experimental $ZMP_{ref} - ZMP_{F-T}$ steady state values.*

This equation represents the steady-state error of the open-loop system for each working point. Equations (4.6) and (4.7) are the basis for planning the evolution of the joint angle and, therefore, ZMP location. Once the static error has been minimised, the transient response must be optimised to reduce the level of oscillations.

4.4.4 ZMP Transient Response Characterization

The linear inverted pendulum is inherently unstable. It is necessary to develop a controller to stabilise it against any kind of disturbance. Meanwhile, the angular response of the inverted pendulum is infinite, and higher-order systems can present stable behaviours. Figure 4.11 shows the comparison of the LIPM vs DLIPM transfer functions in response to a simulated step perturbation. This behaviour also means that the dynamic parameters can be adjusted to higher values in the DLIPM case than in a controller including the LIPM model, with a higher margin of adjustment.

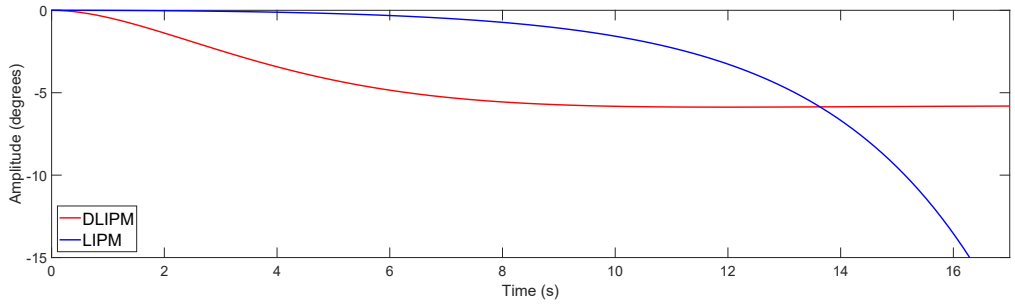

Figure 4.11: *Angular step response for the LIPM and DLIPM.*

The behaviour of the humanoid robot system acting as an inverted pendulum has been demonstrated as an under-damped system. By selecting appropriate gain and dynamic parameters, it is possible to manipulate the overall response of the system, reducing the overshooting and oscillations of the system. The ZMP oscillations have higher values when the location of the ZMP is further from the origin and, additionally, when the input angles have a high variation. This relation between ZMP and ankle angle allows a reduction of the oscillation level by means of angle planning. In Equation (4.5), dynamic parameters can be configured; for example, to limit the overshooting level. These dynamic parameters can be obtained from α that is related to B_a. Figure 4.12 shows the signal obtained from the simulation of a disturbance causing a ZMP variation of 9 cm. The dynamic parameters were designed to obtain an over-damped response ($\xi = 0.8$, $\omega_n = 0.4376$).

Then, selecting the proper parameters, it is possible to modulate the dynamics of the robot and reduce undesired oscillation levels on the robot.

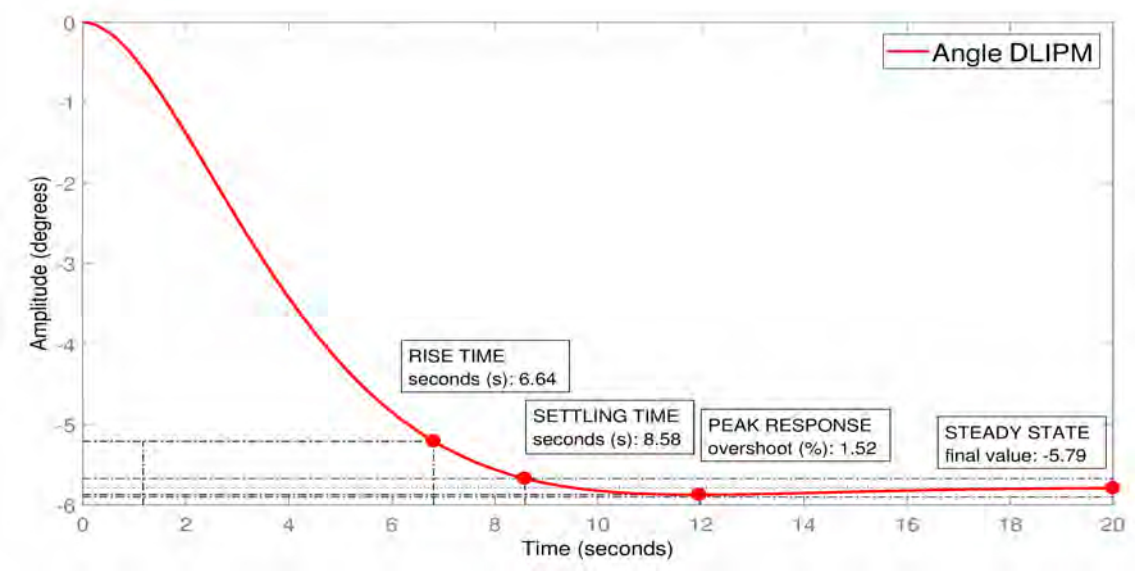

Figure 4.12: *Angular step response of the DLIPM.*

4.4.5 ZMP Control using DLIPM

Classical control architectures, such as the one shown in Figure 4.3, are based linearised controllers around a working point. This means that the controller has almost no error at this working point, and it commits more error as the control target moves further than this point.

In this work, a non-linear solution is proposed based on *gain scheduled matching*. The main goal is to dynamically select the most appropriate parameters for multiple working points of the controller. That is, the dynamics of the DLIPM model depend on the actual behaviour of the robot and not on pre-computed static parameters. In control theory, a gain-scheduled controller is a system control architecture in which its gains are automatically adjusted as a function of time, operating condition, or plant parameters (Kljuno and Williams, 2010).

Gain scheduling is a common strategy for controlling systems in which its dynamics change with such variables. Typically, gain-scheduled controllers are fixed single-loop or multi-loop control structures that use lookup tables to specify gain values as a function of the scheduling variables. For tuning purposes, it is convenient to replace lookup tables with parametric gain surfaces, such as fuzzy surfaces (Safiotti, 1997, Takagi and Sugeno, 1985). A parametric gain surface is a basis function expansion in which its coefficients are tunable. For applications where gains vary smoothly with the scheduling variables, this approach allows for the tuning of a few coefficients rather than many individual lookup-table entries, drastically reducing the number of parameters. This approach also provides explicit formulas for the gains and ensures smooth transitions between operating points.

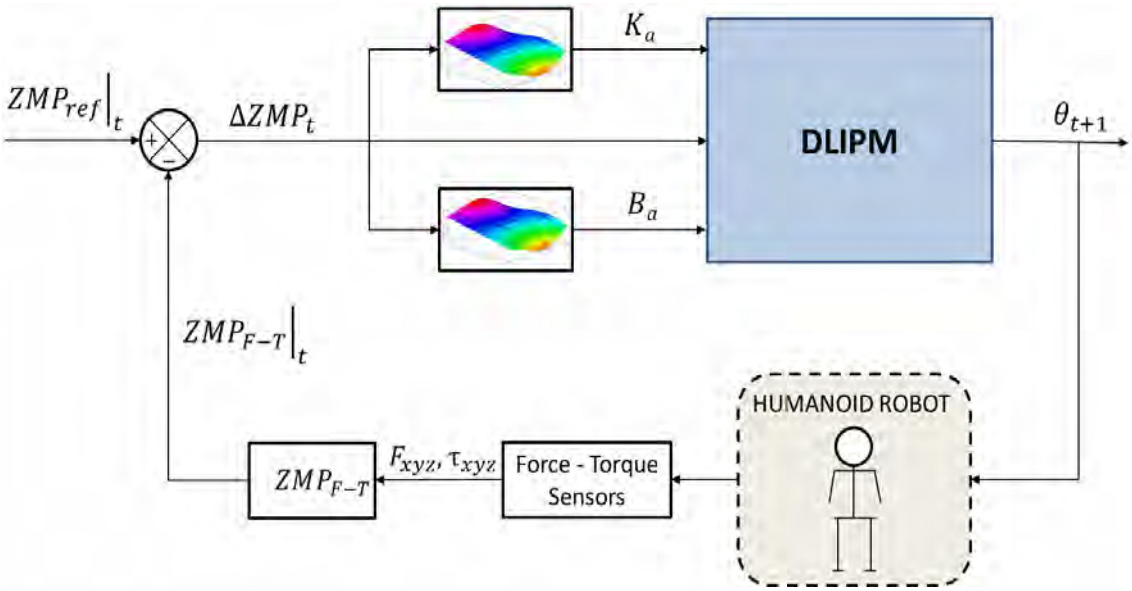

Figure 4.13: *The TEO ZMP controller based on the DLIPM model.*

The control architecture is presented in Figure 4.13, similar to the human-inspired control architecture presented in (Martínez de la Casa Díaz, 2012). In this case, there is a preprocessing module for control parameter planning. Depending on the input ZMP_{error}, the appropriate values for k_a and B_a can be selected. Then, these parameters are used for computing the values of the coefficients of the DLIPM's transfer function. These parameters customise and modify, for each control state, the dynamics of the DLIPM model. Finally, the DLIPM module outputs the ankle angle to be commanded to the robot. The angular transition is, in this cases smoother than that obtained with other approaches.

4.5 Others Models for Body Balance

For this new study, the error has been computed using the information of the IMU sensor (inertial) installed at waist height. In the same way, all the effects caused by any disturbance are reflected in the linear accelerations measured by the sensors. However, it is not necessary to separate the information related to inaccuracies and the expected behaviour. In this case, the characterisation of the model is based on the comparison with the DLIPM model to obtain a similar behaviour.

The obtaining of a correct model based on CT requires to apply an assumption. This one is the need to establish a common ZMP stability value. Since the DLIPM model has been adjusted and contemplates the robot's errors, the CT model should have the same behaviour. For this, we tuned the CT model parameters: CoM location and mass of the robot, which come from the design of the robot. However, CAD designs and real robot implementation are different again. Therefore, correcting these parameters is essential. Because we cannot use the real robot, we will use the ZMP of the DLIPM to calculate the CT parameters.

Now the method used to develop the redesigned CT model is as follows: based again on open-loop system push-recovery sets of experiments, the inertial sensor measurements are captured and processed. After this, the real ZMP_{IMU} of the CT is computed and compared with the ZMP_{F-T} of the DLIPM model. Depending on the difference between both ZMP values, the CT model parameters are adjusted. Once the model is tuned, the new ZMP behaviour associated with the CT is very close to the ZMP of the DLIPM.

4.5.1 Tuning Methodology of the Cart-Table Model

For the introduction of the robot's parameters mentioned before into the TEO cart-table model, the procedure (shown in Figure 4.14) is followed in the same way as in DLIPM model. This procedure is divided into three phases: the experiment, data analysis, and validation of results. This procedure allowed us to obtain a set of data from the IMU sensors to be used in the generation of the tuned CT model.

The first stage of the procedure is to fix the cart-table model parameters with the characteristics of the TEO humanoid robot. Again, the weight of the is 62.6 kg, and the height from the ground to the CoM is 0.893 m (the pendulum length). Next, we test the movement of the robot caused by a pushing force. The effect of this force is a variation of the ZMP location depending on its intensity. It is important to remark that the robot does not keep the initial value of the ZMP during each experiment again. That is, it does not recover the initial posture. As in the DLIPM model, the behaviour is similar to the system response study with a step angular input in the ankle joint. After a set of trials, the ZMP error is computed and compared with the DLIPM value. Later, the CT model parameters are adjusted to compensate for the ZMP error. Besides, we study the dynamic behaviour of the ZMP variation. The last phase of this procedure consists of the validation of the tuned model within the proposed control architecture.

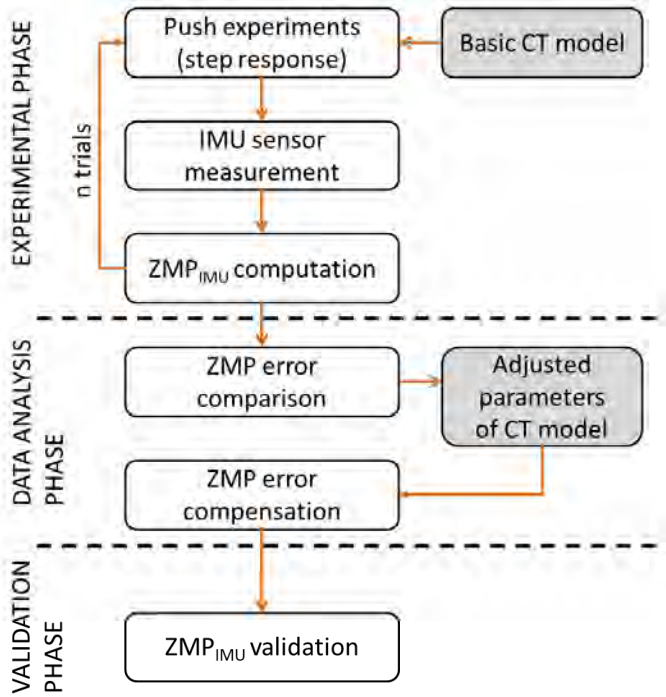

Figure 4.14: *Experimental procedure diagram for the CT model.*

As in DLIPM model, to demonstrate the procedure, only the results from the sagittal plane (x-z) of the robot are presented. The experimental methodology for the frontal plane (y-z) is the same and has similar results. Even this study and methodology can be applied to any other spatial direction. In this way, the experimental set-up is represented in Figure 4.7. Again, the robot is in a flat ground environment with both feet on the ground (double support). Therefore, the support area includes the robot footprints and the common tangents between them.

4.5.2 Comparison of the DLIPM and CT models

Therefore, the first step is associated with the experimental part. We have repeated the same test battery that we did for the DLIPM model. We have applied different intensities of pushing forces to be able to check the inertial sensor measurements and the value of the ZMP related to the CT model for each of the experiments.

The results of a set of trials are shown in Figure 4.8. This figure represents the measured ZMP_{IMU} (the signals with thick and coloured line), the measured ZMP_{F-T} (the signals with thin and coloured line) and the expected ZMP (the black step form signals). Each trio of ZMP signals corresponds to a specific pushing force applied to the robot.

If we examine each trio, we can extract some conclusions. In the same way as in DLIPM model, more significant disturbances imply a further location of the ZMP from its origin, making the robot more unstable because the ZMP is closer to the support polygon edge. This situation means that the angle from the model that is commanded to the robot is more significant, and the errors have more influence mainly concerning robot flexibility and mechanical tolerances. For this reason, the steady-state error is greater as well. However, the system has not a higher initial oscillating response. This behaviour is because the inertial sensor has its own filters that affect the reading behaviour of the sensor.

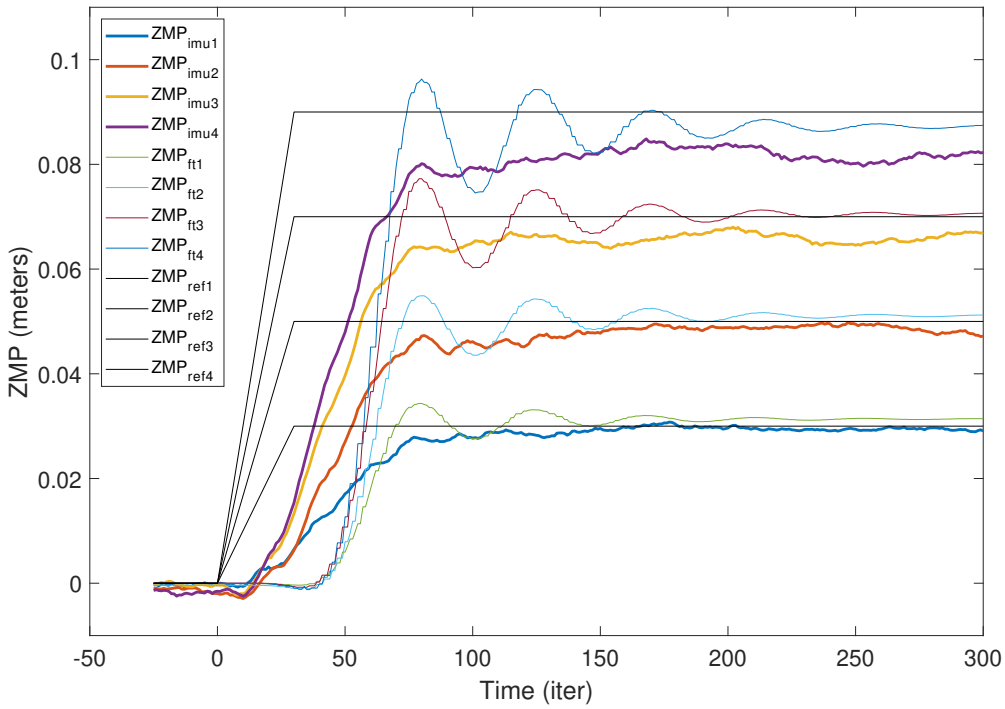

Figure 4.15: *Study of the error for the Cart-Table model.*

With the same purpose, this data set is the basis for developing a ZMP control without having to use parameter tuning in low-level controllers. In the next step, the goal is to analyse the inertial sensor behaviour against the different disturbances and compare the ZMP error.

4.5.3 Steady-State ZMP Error Evaluation

In this section, we have characterised the deviation of the ZMP for the inertial sensor. As in the DLIPM model, the controller can position the ankle correctly, but the ZMP measurement shows deviations. In other words, the ZMP value measured by the IMU has a deviation from the planned or expected value over an excellent angular control of the ankle joint. From the set of experimental data, we can determine the deviation from the ZMP.

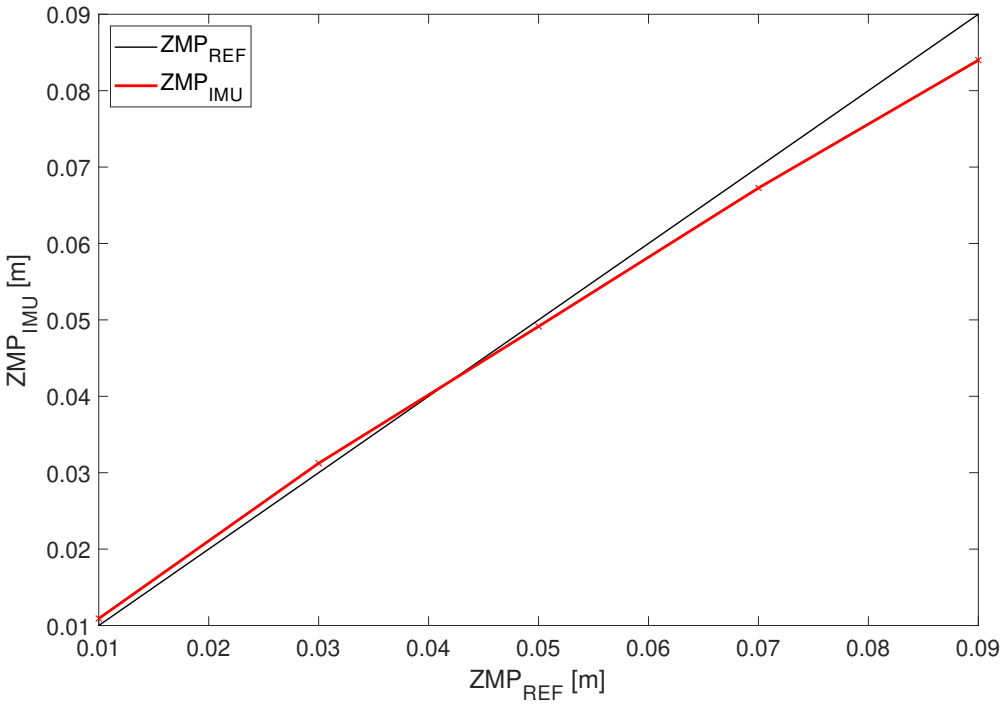

Figure 4.16: *Comparison of experimental $ZMP_{ref} - ZMP_{IMU}$ steady-state values.*

In this case, we do not fit each of the test points in an equation. The objective is not to model the error as in the previous study. Now, the objective is to study this trend of the ZMP error, which is quite linear, in order to find the best parametric adjustment to eliminate it.

4.5.4 Characterization of the Cart-Table Model

At the beginning of this study for the CT model, we indicated that the main requirement was that the values of both ZMP_{IMU} and ZMP_{FT} be equal. As the DLIPM model is correctly adjusted and contemplates the possible errors of the robot, we can use the ZMP_{FT} to improve the ZMP_{IMU} of the inertial sensor. For this, the most direct method is to match both ZMP's ($ZMP_{IMU} = ZMP_{FT}$) and adjust the parameters of the robot model for the cart-table.

If we match Equations 3.3 and 4.4 of the ZMP for each model in the plane (x-z), Equation 4.8 is obtained:

$$z_c = -\frac{g}{\ddot{x}} * ZMP_{FT} \tag{4.8}$$

where z_c is the distance to the CoM in the Z-axis, g is the gravity, $\ddot{x}$ is the linear acceleration in X-axis and ZMP_{FT} is the current measure of the ZMP with the F-T sensors using the DLIPM model.

In this case, the robot's mass disappears from Equation 4.8. Therefore, we can maintain the initial value of the mass ($m = 62.5kg$), and it is only necessary to tune the CoM height value in order to eliminate the ZMP error. Figure 4.17 shows the z_c values obtained for each of the tests, which depend on both the IMU linear acceleration and the ZMP of the DLIPM (blue line).

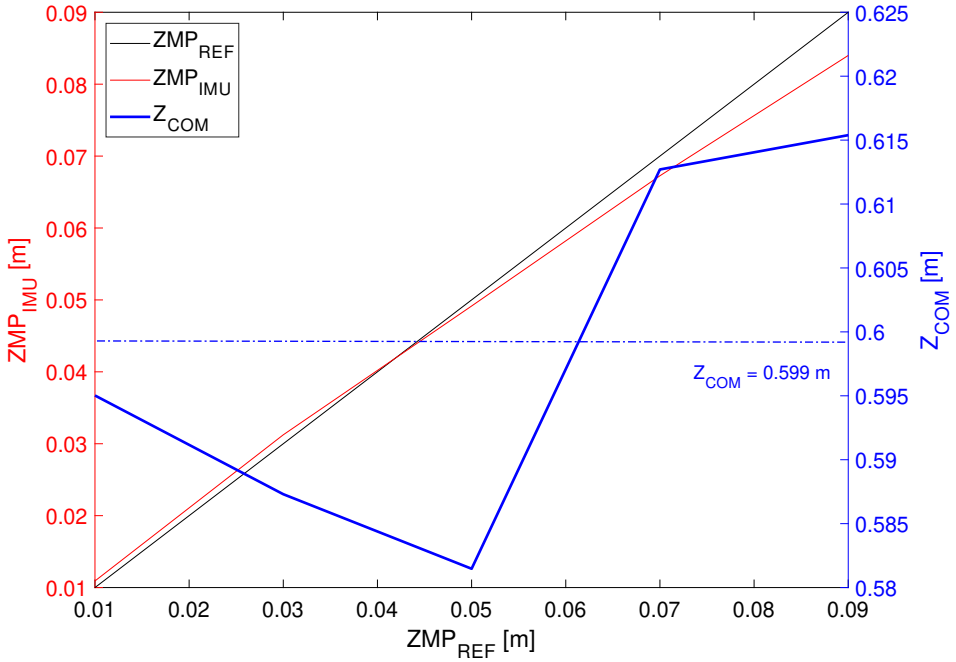

Figure 4.17: *Study of parametrisation of z_c for the Cart-Table model.*

The trend of z_c values is not very clear. Because we are working on a small working point of the ZMP [+/- 10 cm] and the trend of the ZMP error with the inertial sensor is quite linear, we have decided to average all the z_c values to a single constant value. The result obtained is $Zcom = 0.599m$.

4.5.5 ZMP Control using CT

With the new values of the CT model parameters, we must now validate that the error is corrected. For this, we have proposed a simple controller based on the classic control architecture shown in Figure 4.3. The main idea is to verify that the measured ZMP value of the inertial sensor corresponds to the reference when the robot is disturbed.

Figure 4.18 shows the architecture applied for the control of the ZMP using the CT. This system does not have any low-level controller (such as a PID) in which its parameters must be tuned. In this case, the system must correct the actuation output on the ankles of the robot (angle θ) commanded with the function $\theta = f(\tau)$, and use the CT model tuned with the new parameters to obtain τ from the Equation 3.5. Thus, when the inertial sensor reads the accelerations and computes the ZMPimu, this one becomes the same as the reference.

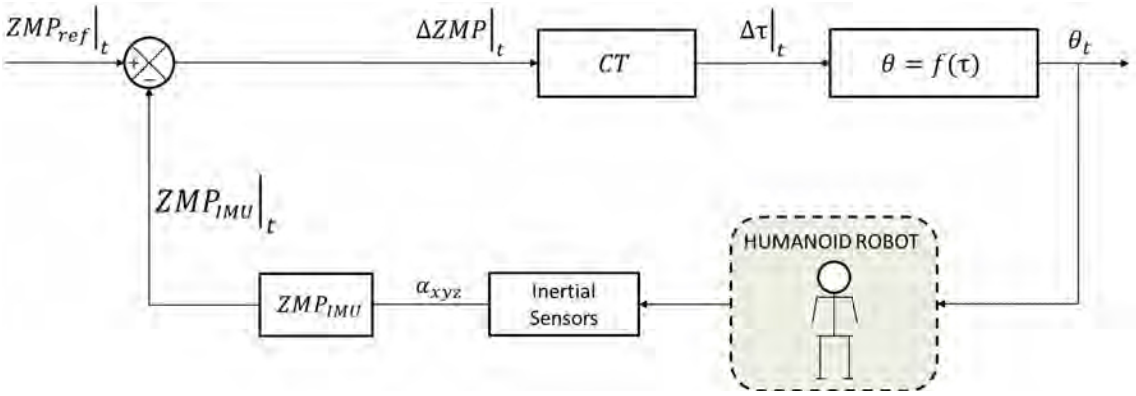

Figure 4.18: *Basic ZMP position controller using the CT model.*

The last part is associated with validating the tuning method of the CT model and checking the elimination of the stationary error. However, we have not studied and improved the transient response of the CT model because the inertial sensor itself has its low-pass filter. These filters make the response of the cart-table model more or less rapid. Nevertheless, this study does not fall within the objectives set with the improvement of this model.

4.6 Conclusion

Chapter 4 focuses on the stability of the robot and the knowledge of specific balance indicators. These parameters are materialised in mathematical models to simplify the humanoid body behaviour. However, the more simplified the model, the control performance will be less accurate. On the contrary, the computational complexity is then lower. Besides, the mechanics and electronics of the robot have inherent inaccuracies that are added to those of the model.

In this chapter, we have presented a method to propose a new humanoid robot model considering these inaccuracies and improve the balance control system. The experimental procedure, based on Push-Recovery trials, was used to determine the steady-state error and the dynamic response of the system. This procedure can be applied to any humanoid robot because it is independent of the system and can characterise any inaccuracy. Additionally, this methodology can be extrapolated to other models to unify and compare different balance indicators.

Chapter 5

Non-Grasping Object Balance

5.1 Introduction

In the last years, many researches have been focused on different aspects of robotic grasping. Their studies chase a vital objective: transport objects by robots. Many interesting investigations explain how to grab an object: the best way to do it (Ma and Dollar, 2011), the most efficient way (Okamura et al., 2011), or the ability to grasp different objects with different shapes (Lynch and Mason, 1999). The systems used in these researches have a high degree of computational complexity and use many sensory systems that produce a significant amount of data.

However, to transport objects without grabbing them simplifies, at first sight, the study of this task. The main reason is that it is not necessary to deal with the intrinsic requirements of gripping, such as the kinematic computation of each finger or the control of the forces exerted by the hand. Obviously, there are different methods of transporting object without grasping them. Specifically, this chapter presents a method to achieve a non-grasping transporting objects task. It avoids the complexity of grasping but, on the other hand, it requires the balance control of the transported object.

Consequently, because there is a lack of solid union, it is more difficult to ensure a proper transportation task while preventing the object from falling. There are many useful features that can be applied in object balance control, such as its inclination angle or ZMP value. The appropriate selection of features among all of them depends on the control methods and algorithms applied later on. Considering the object transported acting as a simple linear inverted pendulum over the tray, the most important piece of information will be the one related with its rotation and its range of stability. Therefore in this chapter, we introduce the evaluation of the object stability and the control architecture using/fusing the visual information from the camera and the dynamic data from the F-T sensor of the wrist.

The chapter is organized as follows. The section 5.2 introduces some preliminary work and research on non-grasping manipulation and computer vision. Section 5.3 explains in detail the problems associated with transport task and the perception systems used. Section 5.4 describes the stability evaluation process of the transported object based on the visual and F-T sensors. Section 5.5 presents the control architecture based on fusion sensor. The purpose is to keep the object balance using a decision making system. Finally, in the last section 5.7, some conclusions are summarised.

5.2 Related Works

When a robot is handling without grip, it could employ centrifugal, gravitational or Coriolis forces as virtual motors. The idea is to control an object with more DoFs. Additional freedoms of movement of the piece are displayed as rolling, sliding and flying freely. A good example of manipulation without gripping is to shoot a basketball: by free flight or rolling, the ball is thrown into the hoop. Due to accelerations of contact restrictions, the relative movement between the ball and the hand is induced by forces. However, depending on the manipulation way of the object, it can be more examples.

- **"Reorienting parts"**. By the use of a simulator considering dynamics and friction, we can compute the force applied on a flat surface to "lift" a block placed on top.

- **"Throwing"**. The ability to throw a ball can be improved through learning methods. Previous research reported that throwing a ball with a dynamic grip. We define a dynamic grasping as an acceleration of the manipulator. For example, the object attached to the robotic arm is kept by the dynamic load while the arm is working (Miyashita et al., 2009).

- **"Catching"**. Other works described three different "mirror laws" to juggle, catch and hit a ball with a flat surface. With the change of the juggling control laws to "catching", the robotic arm can go from "juggling" the object to "balancing" it over the surface. For example, the catching robot can use visual data to calculate the flight of a ball, matches the trajectory of the final effector with that of the ball and then grabs it (Deguchi et al., 2008).

- **"Pushing"**. There is a discovery of a simple rule to determine the direction of rotation for an object pushed. This one is related to the object's centre of friction. We can employ these results and improve it with new works. These can be the planning of routes between barries, building parts feeders or planning parallel jaw grasping (Hauser et al., 2010).

The method of graspless manipulation used in this thesis is **"Pivoting"**. In this kind of non-grasping, the robot's tray keeps the balance an object (the bottle) as if making it "walk" on the floor by using appropriate points as its virtual feet (Aiyama et al., 2013). In order words, the behaviour of the bottle will be similar to the walking behaviour of a humanoid robot.

For that reason, the LIPM and ZMP concepts are also introduced in this part of the thesis (and we can use their references again). Pivoting is frequently observed when a human moves a large or heavy object like a piece of furniture by raising it up on a vertex, sliding it, turning it, supporting it, pushing it, and so on.

5.3 Problem Statement

For the implementation of the object balance controller, it is necessary to take into account all related problems. In this case, we must consider the requirements for the transport of objects without grasping. For this, we must study: the effects of manipulation with or without grip, the advantages and disadvantages of bi-manipulation, the problems of the robot's own morphology, the adaptation of the FT sensor values for the task and the complications associated with the use of cameras or computer vision.

5.3.1 Grasping vs Non-Grasping

A non-prehensile or non-grasping manipulation is a common option for transporting objects task. In other words, it is a task in which the objects are not gripped. The opposite option is a grasping manipulation. In this one, the object is gripped. But grasping tasks can imply some problems. For example, if a robot has the ability of developing a large number of movements for different objects. One way is to use an enveloping grasp to affix the object to the tool on the arm. This enveloping grasp has to conform to the shape of the object, but the class of candidate object shapes is quite large. So how can a device exhibit such a wide range of forms? What is the maximum weight of the objects? Or how many objects can it grasp at the same time? These questions are a problem for grasp manipulation.

On the other hand, the option of non-grasping objects has a surprising advantage. Since the object is not rigidly attached to the effector, the object can exhibit a broader class of motions than the effector. Simpler arms can be used to transport more than one object by pushing, and sometimes regardless of their weights.

In robotics, several types of research have studied non-grasping manipulation. Pushing (Dogar and Srinivasa, 2010), tumbling, pivoting (Aiyama et al., 2013), hitting, throwing (Lynch and Mason, 1999), juggling and so forth. Moreover, non-grasping manipulation has other advantages like:

- **"New robot primitives"**. When a robotic arm has to handle a big or heavy object, picking it up or lifting, Non-Prehensile grasping can offer an opportunity.

- **"Simpler manipulators"**. By deleting the gripper, we can simplify the structure of a robotic arm.

- **"Flexibility"**. We usually design tools to grasp with the idea to grip objects with a specific size or form. However, we can manipulate objects, without grasping if the manipulator employs an acceleration on the object.

- **"Increased workspace size"**. The kinematic workspace for a TCP is generally described as the workspace for the robot. In more details, the workspace for the manipulator is the set of available positions to reach an object. If the robot can throw the object to locations outside its kinematic workspace, the area of manipulation for the robot grows efficiently, if the object is thrown to locations outside its kinematic workspace.

- **"Increased workspace dimensionality"**. We must consider at least the same number of degrees of freedom of the object in the robot when we move an object gripped. However, it is possible to handle more DoF than the robot itself, if the object moves around the robot arm. This one is underactuated manipulation.

Nevertheless, these advantages are obtained at the expense of higher complexity in control and planning. Non-grasping handling transforms part of the problems of a manipulator from hardware (grippers, actuators and joints) to control and to plan. In our case, this problem is divided into two parts. On the one hand, the calculation of the ZMP bottle. On the other hand, the actuation of the arm in the Cartesian space.

5.3.2 Uni-Manipulation vs Bi-Manipulation

If we want to compare Uni-manipulators and Dual-Arm manipulators, we can see that both types of robots have their advantages and disadvantages. In the case of Dual-Arm robots, they offer potential advantages compared to Mono-Arm robots, with higher operating speeds and accelerations, low inertia, greater accuracy and greater overall rigidity.

On the contrary, the disadvantages of these robots are related to more complex kinematics and control algorithms, intricate mechanical designs or reduced workspaces. For Dual-Arm manipulators, some different factors motivate the use of these robots (Taylor and Seward, 2010, Edsinger and Kemp, 2007, Fuchs et al., 2009):

- **"Similarity to operator"**. Bi-manual user capabilities are transferred to a remote location only when the slave system has two arms. Additionally, it is logical that a user wants to perform bi-manual tasks. Therefore, this is the reason why using bi-manipulators for teleoperation tasks.
- **"Flexibility and stiffness"**. The dexterity and flexibility of a serial link robotic arm could be mixed with the strength and stiffness of a dual-arm robot, considering the use of closed kinematic chains for two arms.
- **"Manipulability"**. The idea of being able to manipulate different parts of a task or objects is the motivation to use bi-manipulators. For complex tasks such as cooking, performance is optimized with the use of bi-manipulators. These considerably increase the workspace.
- **"Cognitive motivation"**. From an HRI point of view, it is more understandable for a human being the actions that a bi-manipulator robot can perform. This one is because bi-manual manipulation is easier and more intuitive in the daily tasks of humans. Therefore, they have investigated the relationship between cognition and human physical interaction, using dual-arm robotics configurations.
- **"Human form factor"**. The idea that bi-manipulated robots would work better if they had a human-like shape is being promoted. These are due to the advent of robots, working on scenarios prepared for human beings. However, performance could be significantly restricted by this condition of human similarity, especially in robustness and power.

(a) Uni-Manipulation. (b) Bi-Manipulation.

Figure 5.1: *Main goal of the manipulation task, keeping the balance of the bottle with the camera and the F-T sensor in the wrist. (a) Object transport task with ONE arm. And (b) Object transport task with TWO arms.*

It is really difficult to say which type of robot is better, Uni-manipulator or Bi-manipulator. A robot selection process is a very hard and complex activity. It depends on many different elements, such as the type of application (dangerous, repetitive and boring, accurate), task requirements (DoF, accuracy, speed, repeatability), workspace, load requirements, economic justification, time of programming, maintenance,...

Dual-arm manipulators are more successful in applications such as motion simulators, high-precision positioning devices, medical applications, microbots and ultra-fast and place robots. However, Uni-manipulators dominate almost every manufacturing application. These will probably change with the continuous resolution of the open problems in bi-manipulation robotics given in (Pandilov and Dukovski, 2011) or using hybrid structures. Hybrid structures are, in fact, a compromise between the advantages and disadvantages of Mono-arm and Dual-arm structures.

5.3.3 Morphology of the Manipulation

An important problem, that arises to calculate the equilibrium state of the bottle, is the robot's structure. As seen in Figure 5.1(a), this robot has both a hand and a tray. But it has been considered that it is necessary to place the TCP (Tool Centre Point) of the arm in the centre of the tray and not in the hand. The main reason is related to the control, which should be on the Cartesian space. By controlling the pose of the tray, it can be positioned and oriented according to the state of the bottle. And to facilitate this task, the axes of the TCP coordinate system of the tray (SoC_{tray}) have been equalled to the root coordinate system (SoC_{root}). In any case, the SoC_{tray} is not inertial with respect to the SoC_{root}, because the tray will describe an accelerated movement with respect to the SoC_{root} of the robot (Figure 5.2).

On the other hand, the TCP position makes the bottle rest in the centre of the tray. It can be proposed that the 3D-LIPM, which models the bottle, can pivot on the TCP of the tray. Therefore, all the forces and torques that are generated will be related to this pivot point (TCP). The problem arises because the sensor, which measures the forces and torques, is not located exactly in the TCP (or at least under the tray). The sensor is just after the front wrist joint and therefore there is a link connecting the sensor with the tray rigidly (Figure 5.2).

This mechanical arrangement causes that the coordinate system of the force-torque sensor (SoC_{FT}) is not the same as SoC_{tray}, because the origin of both systems is different. In this case, both systems are inertial, since they are rigidly joined and there can never be an accelerated movement between them. And therefore, the forces and torques read from the sensor are not equal to the force and torques applied to the 3D-LIPM model in the tray.

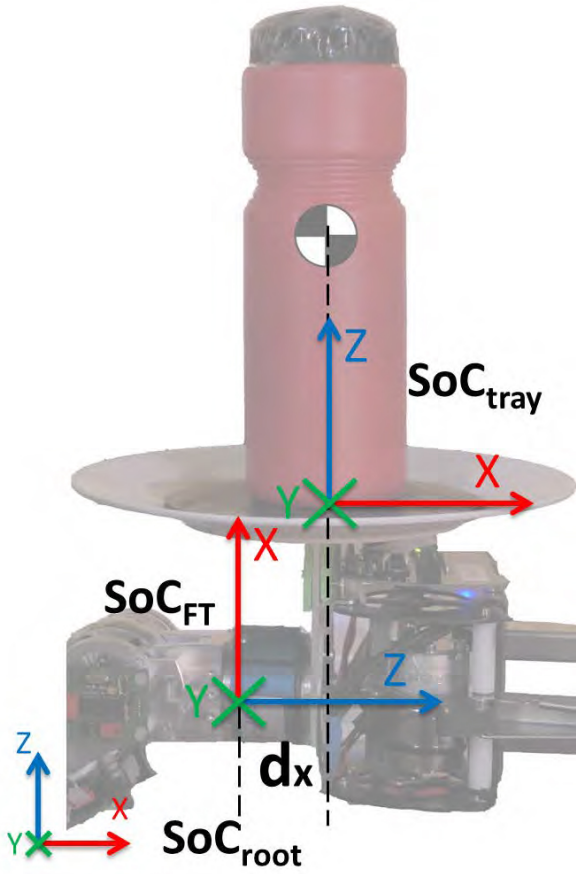

Figure 5.2: *Representation of SoCs involved in the computation of the object balance with an horizontal orientation of the tray.*

In addition, it must be added that SoC_{FT} is an *anti-clockwise* system. Unlike SoC_{root} and SoC_{tray} systems that are *clockwise*. This makes it difficult to interpret the forces and torques from the F-T sensor that will be necessary to calculate the stability of the bottle through the ZMP. In section 5.4.1 together with Figure 5.2, this problem will be thoroughly explained and solved.

5.3.4 Sensor Pose Estimation

There is another problem related to the computation of the ZMP and the sensor's pose. It depends on the position of the F-T sensor and the location of the CoM of each limb to be balanced (in our case, only the bottle). If the bottle is modelled as a 3D-LIPM model, the forces and torques needed to calculate the ZMP will be simpler. And therefore the ZMP calculation will be easier. There are two main reasons why this assumption can be performed.

The first reason is the possibility of using F-T sensors to measure all the forces and torques needed. The 3D-LIPM model relates forces and torques with the movement of the pendulum. Therefore, if the robot has an F-T sensor, it will be useful to apply the 3D-LIPM model.

The second reason is related to the material of the tray. The roughness of the tray has been created as high as possible. In this way, the object will have a very high friction coefficient and therefore the bottle will not slip (only pivot, like a 3D-LIPM). With this assumption and at the same time requirement, we make the bottle behave similarly to the 3D-LIPM model.

However, when the F-T sensor is used, a problem related to its orientation appears. To follow the ZMP equations presented in the section 3.7.1, the tray should always be aligned with the horizontal plane (coplanar system). In this way, all the forces and torques exerted by the bottle would be reflected correctly in the sensor (ignoring the first mechanical problem) and therefore, the ZMP equation could be applied.

However, the sensor and the tray will have different orientations during object balance control (Figure 5.1(a)). These orientations, related to the stable state of the bottle, generate readings in the sensor that cannot be applied in the model. To be able to use them, it is necessary to apply a transformation based on the *"3D Dynamic Slopes"* concept. This concept allows interpreting the data from the sensor correctly according to the estimation of the angle of the tray. It is applicable both in the frontal plane and in the sagittal plane.

5.3.5 Vision Perspective and Time Complexity

For the balance control of the bottle, the model input information (inclination angle, location of the object, etc.) can obtained by computer vision techniques. The visual data processing requires a high-level of computing effort and sequentially the application of different algorithms to obtain the proper data to be applied in a controller. These *classic* methods of visual data treatment are quite slow and constitutes an obstacle to improve balance controllers' performance.

The other important point to consider is the inherent errors enclosed in the images obtained by computer vision. They have to be corrected if real information obtained from a camera is used as these inputs. When describing the errors introduced in systems based on computer vision, a classification of two groups can be made: errors produced by the camera defects, which are directly related to the camera lenses and errors caused by the perspective in which the object is being observed.

The camera defects are related to the nature of the lenses that are being used. Due to this fact, different kinds of radial deformations in the image can be found, as seen in Figure 5.3.

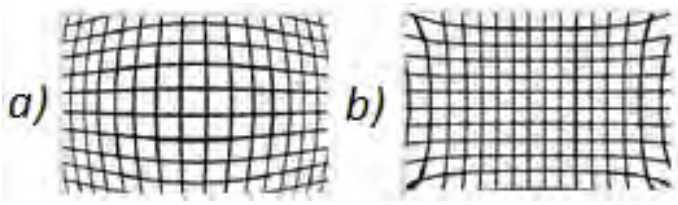

Figure 5.3: *Image deformation caused by the camera lenses. (a) barrel deformation. And (b) pincushion distortion.*

On one hand, if the focal length of the camera is short, the barrel deformation (a) will appear. In barrel distortion, image magnification decreases with distance from the optical axis. The apparent effect is that of an image which has been mapped around a sphere (or barrel). Whereas, on the other hand, if the focal length of the camera is long, a different deformation, named pincushion distortion (b), will appear. The image magnification increases with the distance from the optical axis. The visible effect is that lines that do not go through the centre of the image are bowed inwards, towards the centre of the image, like a cushion.

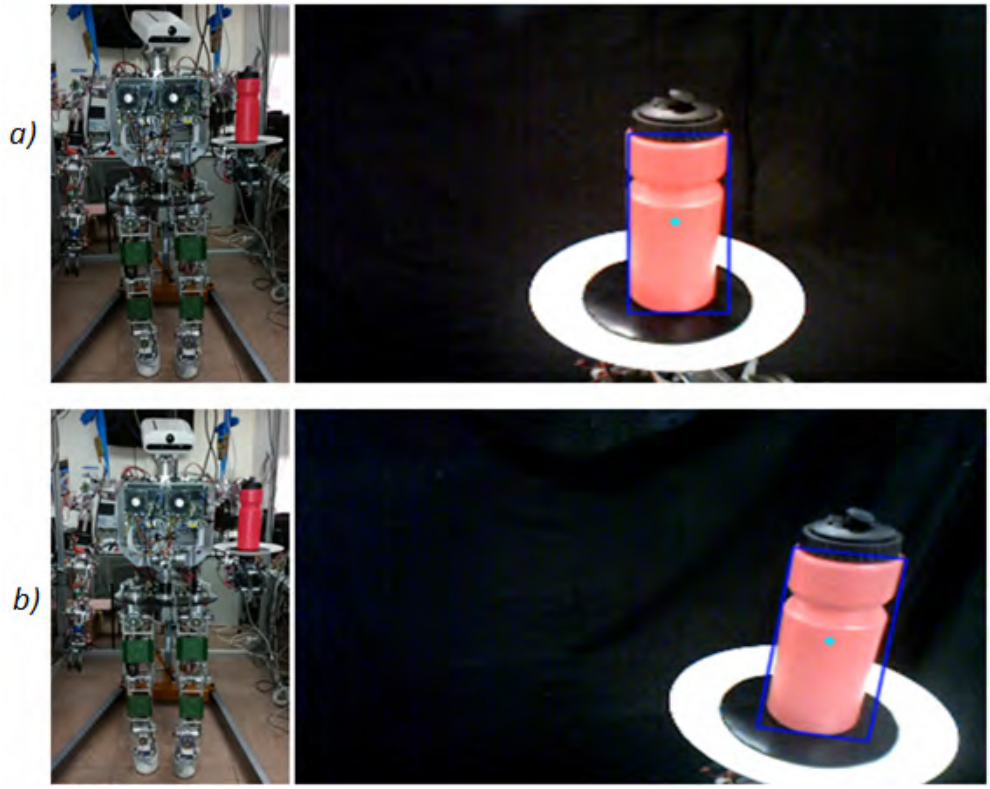

Figure 5.4: *Visualization of the perspective error for the same bottle angle. (a) Detected bottle angle* $= 90°$*. And (b) Detected bottle angle* $\neq 90°$*.*

As the defects introduced by the camera lenses in our system are so low, they have been disregarded. However, high errors are introduced by the perspective in which the bottle is being observed by the camera at each moment. To understand this error, in Figure 5.4, two images can be seen. In both of them, the tray and the bottle are maintained in the same pose. The only variation has been made in the orientation of the TEO's head.

As it can be observed, the image changes completely, considering the bottle to be fully straight in one image (a) and with an inclination angle in the other (b). Even though in both cases the relative position between tray and bottle is the same, if the real tilt angle is aimed to be obtained directly from these images without using any filter, the data acquired in the first one would be similar to the real angle, whereas the second one would be interpreted wrongly, obtaining an erroneous inclination angle.

A wide range of procedures is already available to correct the perspective error. For example, some of the techniques that we found implement a correction by comparing images obtained from different points of view (stereo-images) (Kumar et al., 2010), whereas, in others, the correction is achieved by adjusting images from uncalibrated cameras (Wu and Yu, 2005).

Another example is the research developed in (Jagannathan and Jawahar, 2005), in which the perspective error in different kinds of images is well corrected. However, in the above cases, the original image must be modified. These techniques were applied as a base for our first approach to obtain the real angle inclination of the bottle in the waiter application. However, different problems were found and the image rectification approach was discarded.

As mentioned previously, in the end, the real inclination angle of the bottle is needed to control its equilibrium. By using image rectification methods, the geometric image characteristics are modified. As a consequence, from this image, it is not possible to obtain any real information about the inclination angles without introducing errors, as shown in Figure 5.5 (top). Despite this, if the angle measurement error could be corrected, it would imply the use of other information provided by sensors other than the camera, such as kinematic estimations of the handling posture.

The other inconvenience is the time complexity of the algorithm. In many research papers (Prabhakar et al., 2014, Mukhopadhyay and Chaudhuri, 2015, Slembrouck et al., 2012), different Hough transformations and computer vision algorithms are presented. Depending the algorithm and the amount of data processed, the minimum time complexity that can be achieved with the Hough transformation is $O(N)^3$. The pseudo-code that represents the basic procedure for angle calculation based image transformation techniques is exposed in the Algorithm 1:

As it can be seen in this algorithm, to obtain the required values of the bottle by this procedure, the image is captured from the camera ($Binarize(Img)$). Then, a filter is applied to get the object of interest (in this case, the bottle) ($Object\_detected(Img)$). In the next step, the Hough lines transformation is used ($Set\_lines = Hough\_lines(Img)$) to obtain the lines of the bounding box of the bottle. This operation implies a time complexity of $O(N)^3$). Then, the angle of the lines is computed ($\theta = Pers\_Angle\_Estimation(Set\_lines)$) and the image is rotated this angle ($Img\_rect = Rot\_pers(img, \theta)$). This operation is not only applied to the object of interest but to the whole image, masking other useful information.

Algorithm 1 Data acquisition modifying the image nature. (Figure 5.5 top).

Input: Capture image

Output: Extract $CoG(X, Y), \beta$ values

Initialize: camera ON

1: Capture (Img)
2: Binarize (Img) //*Threshold of the object to be detected*
3: **if** (Object_detected (Img) == **true**) **then**
4: //*Image Pre-Processing*
5: Set_lines = Hough_lines(Img)
6: θ = Pers_Angle_Estimation(Set_lines) //*Calculation of perspective angle*
7: Img_rect = Rot_pers(img,θ) //*Image rotation*
8:
9: //*Parameter computation*
10: Bottle = Get_Blobs(Img_rect)
11: (X_{CoG}, Y_{CoG}) = Get_CoG(Bottle)
12: $\beta = \theta$
13: **end if**
14: **return** $(X_{CoG}, Y_{CoG}), \beta$

In the last part of this algorithm (parameter computation), the bottle area is extracted ($Bottle = Get\_Blobs(Img\_rect)$) to compute the CoG ($(X_{CoG}, Y_{CoG}) = Get\_CoG(Bottle)$). Finally, the inclination angle is equal to the angle obtained with the Hough transformation. ($\beta = \theta$). Using this transformation, the perspective errors in the image cannot be corrected. Because of this, the angle obtained has big distortion. In the sections 5.4.3, a new method to obtain the information is going to be presented in order to have a lower time complexity and lesser errors.

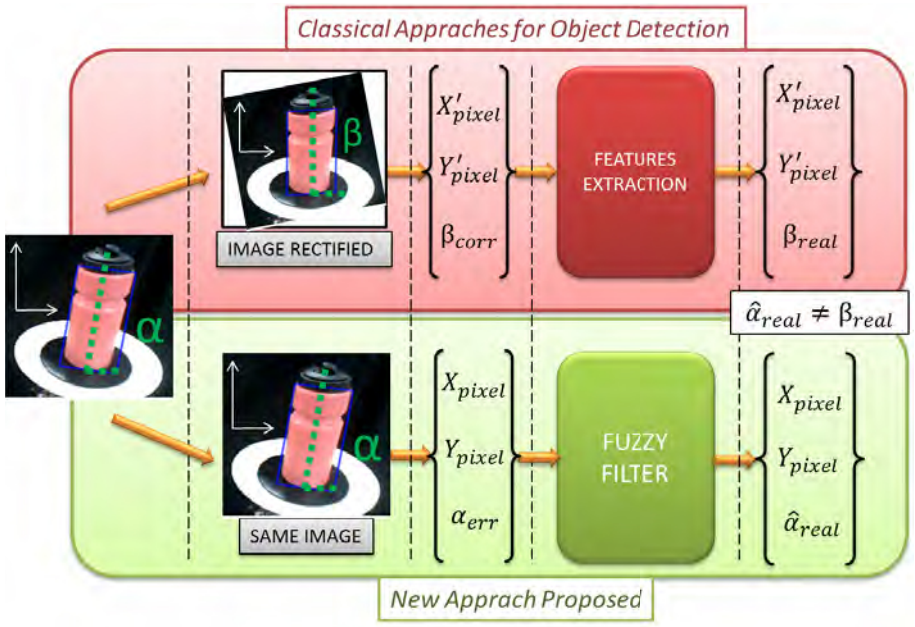

Figure 5.5: *Comparison between the classical and the proposed approaches.*

5.4 Object Stability Evaluation for Uni-Manipulation

The purpose of this section is to use the ZMP equations in the 3D-LIPM model of the bottle. For this, the goal is to obtain suitable F-T readings and accurate camera values. The solutions proposed below attempt to place virtually SoC_{FT} at the pivot point of the bottle and always on the axial plane (dynamic SoC''_{FT}).

5.4.1 Study of ZMP object

As it has been explained in the previous section, there are two basic problems related to the mechanical structure of the robot. These ones must be taken into account to make an effective calculation of the bottle's ZMP. For this purpose, the essential goal is to apply equation 3.14. And therefore, the necessary requirement to apply this equation is that the forces and torques used must be applied on the SoC_{tray}.

On the one hand, it is necessary to solve the problem related to the type of coordinate system of the F-T sensor. As a reminder, both SoC_{root} and SoC_{tray} are clockwise systems. By contrast, SoC_{FT} is an anti-clockwise system. Figure 5.2 depicts this trouble. It has been solved by applying two transformations. The first one is based on a reflection matrix. The second one is a rotational transformation. The reflection matrix is applied in the XY plane on SoC_{FT} and then the rotation matrix (90 degrees) is applied on the Y axis to align all the coordinate systems.

On the other hand, it is necessary to solve the problem related to the origin of SoC_{FT} and SoC_{tray} systems. As a reminder, both SoC_{FT} and SoC_{tray} have a different coordinate origin, and as a consequence, the forces and torques applied in both systems are not the same. In Figure 5.2, this problem is shown again. Now only one basic translation matrix has been used. The reason is that both systems are inertial. That is, both systems are linked through a link rigidly.

The translation matrix is applied to the vector that joins the SoC_{FT} and SoC_{tray} origin systems. In this way, the F-T sensor would be virtually placed in the TCP of the tray and the data from the F-T sensor will be able to associate with the inclination of the 3D-LIPM model or bottle as pretended. In the equation 5.1, the SoC calculation shows the SoC'_{FT} conversion from anti-clockwise to clockwise and the translation.

$$\begin{pmatrix} X'_{FT} \\ Y'_{FT} \\ Z'_{FT} \end{pmatrix} = I_{ref}(XY)Rot_Y(\frac{\pi}{2})Tras \begin{pmatrix} d_x \\ d_y \\ d_z \end{pmatrix} \begin{pmatrix} X_{FT} \\ Y_{FT} \\ Z_{FT} \end{pmatrix} \tag{5.1}$$

Finally, applying these corrections over the F-T values from the sensor, the new bottle ZMP is represented in equations 5.2 and 5.3. The equations consider subtracting the d value from all x_i and y_i. Where d_X is the distance on the X-axis between both SoC. d_Y is the distance on the Y-axis. And d_Z is the distance on the Z-axis. In our case, $d_Y = 0$ and d_Z has an imperceptible effect on ZMP equations. Moreover, the inertias of the bottle have not been considered.

$$X'_{zmp} = \frac{\sum_{i=1}^{n} m_i(\ddot{z}_i + g)(x_i - d_X) - \sum_{i=1}^{n} m_i \ddot{x}_i z_i}{\sum_{i=1}^{n} m_i(\ddot{z}_i + g)} \tag{5.2}$$

$$Y'_{zmp} = \frac{\sum_{i=1}^{n} m_i(\ddot{z}_i + g)(y_i - d_Y) - \sum_{i=1}^{n} m_i \ddot{y}_i z_i}{\sum_{i=1}^{n} m_i(\ddot{z}_i + g)} \tag{5.3}$$

5.4.2 3D Dynamical Slopes

If the tray is always placed in the axial plane, the problem of calculating the ZMP would be solved. However, during a possible control, there will be instants when the tray will be in another plane. The reason is associated with the control strategy. As there is no motor control over the bottle (non-grasping task), it is mandatory to move the tray to counteract the degree of instability of the bottle.

To do this, the tray must be tilted at an angle in the opposite direction to the bottle's movement. Therefore, that angle will be related to the value of the bottle ZMP. But before this angle can be obtained, it is necessary to know the value of this ZMP.

As mentioned above, the use of equations 5.2 and 5.3 is conditioned to the tray being horizontal, but there may be cases where this situation does not occur. Therefore, the concept of 3D Dynamic Slope has been applied to deal with the problem of the horizontality of the task, to achieve a virtual coplanar plane of the F-T sensor.

As explained in the previous section 5.4.1, it is necessary that the virtual pose of the F-T sensor is always in the TCP of the tray and also its orientation is always on the axial plane (SoC''_{FT}). Only in this way, the values read by the sensor can be applied to the ZMP equations.

For this, the solution of 3D Dynamic Slope consists of obtaining the angle of inclination of the tray θ and the rotation's axis $\vec{n}$. The $\vec{n}$ vector has to be perpendicular to the tilt axis of the bottle and go through the origin of SoC'_{FT}. Then, a θ rotational transformation on the axis of rotation $\vec{n}$ is applied over the SoC'_{FT} system to obtain SoC''_{FT}.

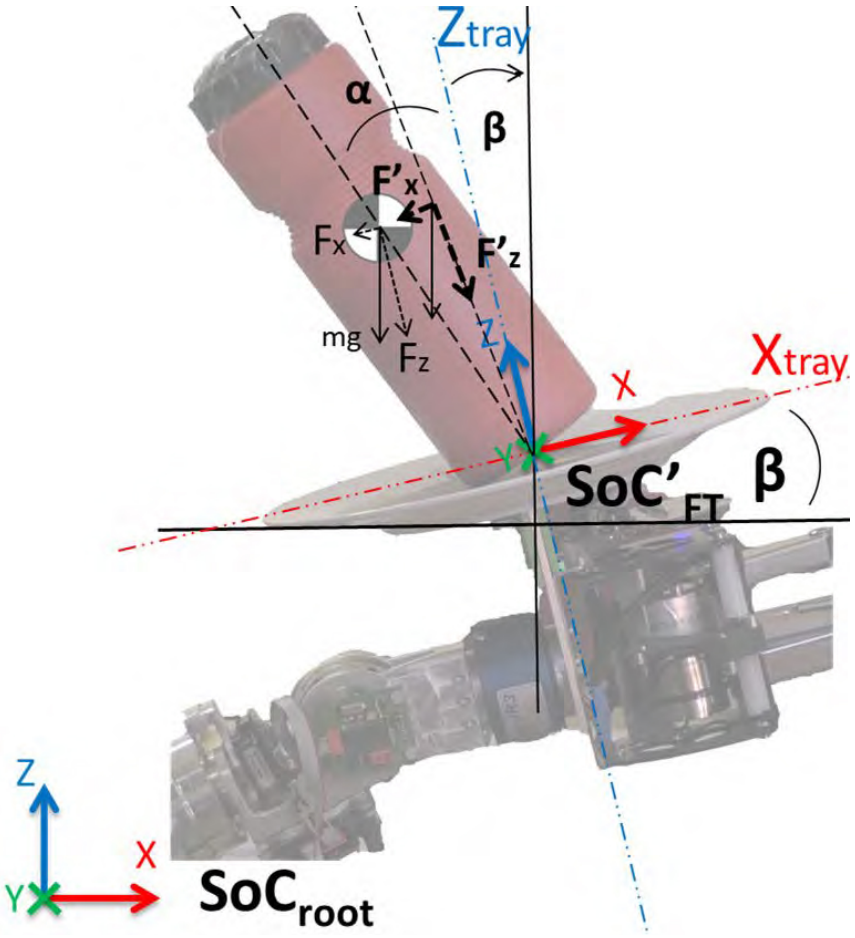

Figure 5.6: *Representation of the rotational transformation on the sensor's forces as a function of the angle of inclination (slope).*

In Figure 5.6, the process is shown. In this situation (frontal plane), both the bottle (α) and the tray (β) angles are inclined, and the F-T sensor is reading the forces F'_x and F'_z. But when the rotation transformation (θ) on the Y-axis is applied, the new virtual forces become F''_x and F''_z (Equation 5.4). The angle of the bottle (α) can be calculated geometrically with F''_x and F''_z, which is needed for a future control.

$$\begin{pmatrix} X''_{FT} \\ Y''_{FT} \\ Z''_{FT} \end{pmatrix} = Rot_{\vec{n}}(\theta) \begin{pmatrix} X'_{FT} \\ Y'_{FT} \\ Z'_{FT} \end{pmatrix} \tag{5.4}$$

Finally, applying these corrections over the F-T values from the sensor, the new bottle ZMP are represented in equations 5.5 and 5.6. The equations take into account subtracting the d values from all x_i and y_i. And also the inclination angle with respect to the ZMP calculation plane. Where β is the angle of inclination for the frontal plane. Analogously, it will be necessary to obtain and apply an angle β' for the sagittal plane. The geometric sum of β and β' is related to the angle of inclination θ of the tray.

$$X''_{zmp} = \frac{\sum_{i=1}^{n} m_i(\ddot{z}_i + g)(x_i - d_X) - \sum_{i=1}^{n} m_i \ddot{x}_i z_i}{\sum_{i=1}^{n} m_i(\ddot{z}_i + g) * cos(\beta)} \tag{5.5}$$

$$Y''_{zmp} = \frac{\sum_{i=1}^{n} m_i(\ddot{z}_i + g)(y_i - d_Y) - \sum_{i=1}^{n} m_i \ddot{y}_i z_i}{\sum_{i=1}^{n} m_i(\ddot{z}_i + g) * cos(\beta')} \tag{5.6}$$

5.4.3 Visual Correction based on Neuro-Fuzzy Learning

To obtain the information needed to make the visual corrections in the image and to remove the errors caused by the perspective deformation and the ones caused by the camera lenses, an experimental set-up has been defined. In this section, we explain the steps followed in this set-up and the way to obtain the information for the Fuzzy filter.

As it was said in section 5.3.5, in other existing techniques, irregardless of the real inclination or orientation, the operations used to correct the perspective error in the images modify the object nature in such a way that the bottle finally appears fully straight. This variation in the obtained information, as shown in the top part of Figure 5.5 named Classical Approaches for Object Detection, leads into a lack of knowledge of the real inclination angle of the bottle, making it unsuitable for our application. As a consequence, it is not possible to achieve arm control to maintain the bottle in equilibrium.

If it is this way, in order to obtain the real angle of the bottle, several trigonometric operations must be added to the operations previously performed over the bottle image. This would lead to an increase in the computational cost due to the high time complexity of the algorithms (Trenaman et al., 1996). As it was explained in the subsection of vision inside the background, the operations that are performed to modify the image have a computational cost with an order of $O(n)^3$. This makes these procedures infeasible for our proposes.

Therefore, instead of making a correction on the image based on trigonometric calculus, which takes too much time, an alternative to these classical methods is proposed in this paper, avoiding the complex image manipulation steps needed in the other procedures.

As seen in Figure 5.5 in the green section called New Approach Proposed, on the proposed approach, the image is not corrected, maintaining the wrong information in the image. However, we correct the perspective errors and the camera errors that have a previous knowledge of the real angle of the bottle. These reference data are recovered in datasets, by performing several experiments that are used later in a Neuro-Fuzzy learning system to model the error. Once the Fuzzy filter has been trained, the error introduced in each point of the image acquired by the camera is known.

The diagram shown in Figure 5.7 represents the procedure followed to develop the Fuzzy filter using ANFIS tool. First of all, the information needed to train the Fuzzy filter has been obtained. To acquire the data, several sweeps have been done, positioning the bottle in front of the robot camera and obtaining "n-IMAGES". These sweeps were done by configuring the bottle in controlled and known inclination angles. From the images obtained, the characteristics needed to close the control loop have been obtained "m-FEATURE" (position of the geometrical centre of the bottle (x,y), inclination angle of the bottle). As is known, those angle features are mixed with the camera errors.

However, as the data was recovered, knowing the real angle of the bottle, it is possible to have knowledge of the error, which is introduced in each position of the image. With all of this information, both a "TRAINING DATASET" and a "CHECKING DATASET" have been created.

On the one hand, in the training dataset, the behaviour of the error introduced in the inclination angle among the image space has been recovered in a table. With this data, the error has been modelled, and it contains information to correct it later. In contrast, in the second dataset, the information has been obtained from other different positions of the space in the image, adding knowledge about the whole vision field. In those datasets, the real inclination angles are well known, having a relation between the real angles and the angles obtained by vision. This information allows us to check if the Neuro-Fuzzy learning system is reliable.

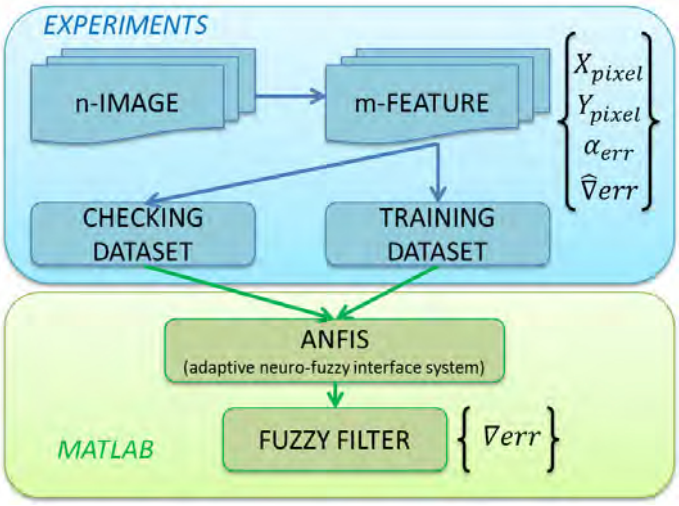

Figure 5.7: *Experimental set-up followed in the visual experiments performed.*

To develop a robust system, it it necessary to train it with different configurations. A total of 50 samplings in a wide range of positions have been made, acquiring more than 20,000 data points that have been introduced in the training and checking datasets. The number of iterations has been changed, starting with a low number and increasing it in the next tests in order to find the right number of iterations to train the system properly.

Once the Fuzzy filter has been trained with the information of the error regarding each of the positions set in the dataset, it is capable of doing a correction in the new information obtained with the camera. In this step, the program implemented in TEO is the Fuzzy filter obtained, the behaviour of which corresponds to the one shown in the Algorithm 2.

As it can be deduced from the pseudo-code presented, the image captured by the camera ($Capture(Img)$) is pre-processed ($Binarize(Img)$) to isolate the bottle ($Object\_detected(Img)$). With this image, the bottle area is computed ($Bottle = Get\_Blobs(Img)$), the CoG position is obtained ($X_{CoG}, Y_{CoG} = Get\_CoG(Bottle)$), and the inclination angle ($\alpha = Get\_Angle\_Inclination(Bottle)$) are extracted. However, this angle still has the intrinsic errors of the process of capturing the image. Thus, the trained Fuzzy filter is applied. The location of the bottle (CoG) and the inclination detected are the inputs to the Fuzzy filter.

This process allocates an error (ϵ) according to bottle location, as depicted in Figure 5.8. The output from the filter is the error of the angle ($Angle_{error}$) that must be subtracted from the previous inclination angle (α) to obtain the real one ($\hat{\alpha}_{real}$). In this case, the Fuzzy filter time complexity corresponds to linear time $O(n)$ (Kim et al., 2000), as far as it depends on the amount of data (n) that was previously included in the training dataset. The time complexity is lower than that of the "Classical approaches".

Algorithm 2 Data acquisition by using a Fuzzy filter. (Figure 5.5 bottom).

Input: capture image

Output: extract $\hat{\alpha}_{real}, CoG(X,Y)$ values

Initialize: camera ON

Capture (Img)
Binarize (Img) *//Threshold of the object to be detected*
if (Object_detected (Img) == **true**) **then**
    //Extraction values from the original frame
    Bottle = Get_Blobs(Img)
    (X_{CoG}, Y_{CoG}) = Get_CoG(Bottle)
    α = Get_Angle_Inclination(Bottle)
end if

//Applying of the Fuzzy filter previously trained
while $(i \text{ ¡ } n)$ **do**
    //Search of similarities within the dataset
    if $((Li_n < X_{CoG} < Ls_n)$ **and** $(Ri_n < Y_{CoG} < Rs_n)$ **and** $(Pi_n < \alpha < Ps_n))$ **then**
        $\hat{\alpha}_{real} = Angle_{error} - \alpha$
        return
    end if
    i++
end while
return $X_{CoG}, Y_{CoG}, \hat{\alpha}_{real}$ // $\hat{\alpha}_{real}$ *is the real inclination angle*

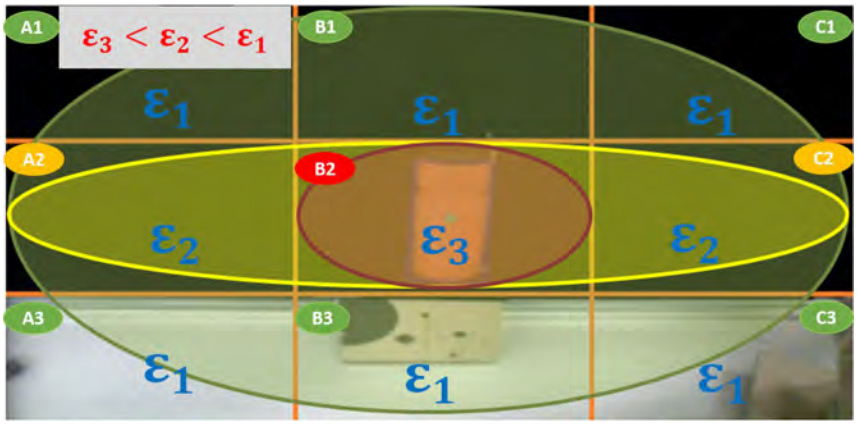

Figure 5.8: *Selection of the Error Priority in the different quadrants of the Image.*

5.5 Object Oriented Control for Uni-Manipulation

In this section, we describe the Object Oriented controller proposal for Uni-manipulation. This controller uses both visual and F-T information to compute the degree of stability of the bottle. With the ZMP value, the Fuzzy control generates the performance on the arm to maintain the stability of the object.

5.5.1 Controlling Sensory Inputs

Before explaining the control architecture, we want to present some details related to the sensors. These add-ons help to improve control taking into account specific conditions.

For the vision system case, during the data acquisition, we have established a priority in the information obtained. As we can see in Figure 5.8, we have divided the images into nine zones. This division will help to achieve a robust human-inspired balance control (Martínez et al., 2012) of a bottle on a tray. The main reason behind this division is: after having evaluated all the acquired information, a relationship has been shown. The further the bottle is from the centre of the image (Zone B2), the higher the distortion error is.

This relation also appears when the results are evaluated in the three different rows; the central one has the lower distortion. As a consequence, the TEO's head has been configured to move in such a way that the bottle is maintained most of the time in the centre of the image (Zone B2) or in the three central zones of the image (A2, B2, C2). Thus, it can be said that these nine different zones have been defined according to the accuracy in the correction required for each one of them. The head's control is a simple PD controller. It tries to match the centre of the image with the geometric centre of the bottle.

The quadrant division has been defined considering the main positions that the bottle occupies in the image. Because the head of the robot has been programmed in such a way that, when it moves, it tries to keep the bottle centred in the divisions A2, B2 and C2 seen in Figure 5.8, and the bottle is positioned most of the time in the three horizontal central quadrants. As those quadrants are occupied by the bottle most of the time, the accuracy in the error correction is higher inside them. As the central quadrant has the highest rate of cases in which the bottle is positioned, the error there must be the lowest in the image. This additional controller does not affect to the object balance control.

For the F-T system case, it is not necessary considering any kind of requirement or condition. With the 3D Dynamical Slopes, we have prepared all F-T data for the ZMP computation.

5.5.2 Control Architecture

Within our WBPC control architecture, in this section, we only explain the part of the UBC controller. At any time, any component of the Lower-Body Controller influences the study of object stability, and therefore we only focus on the control of the arm and the associated sensors (Figure 5.9).

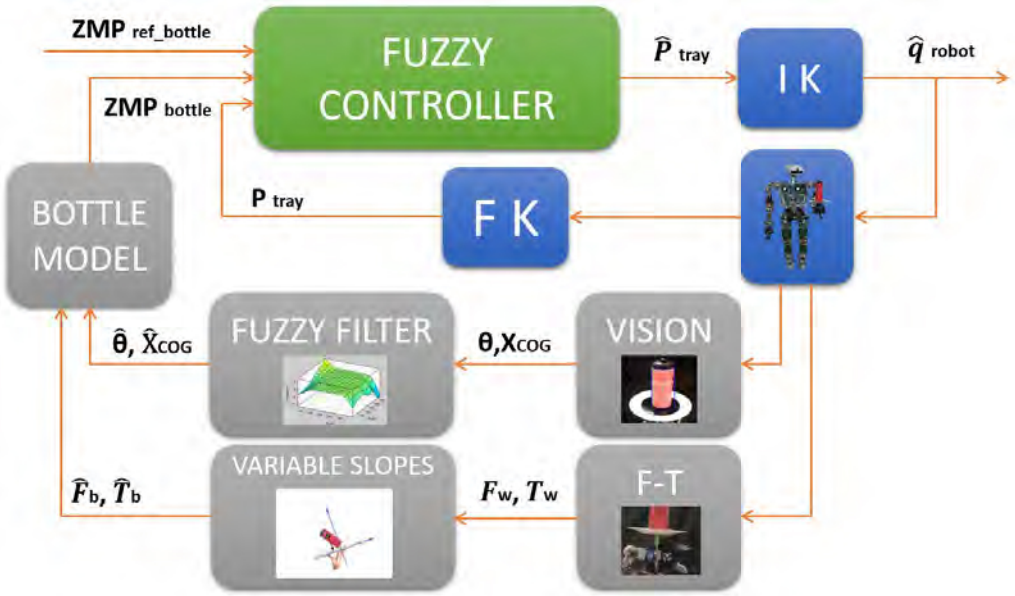

Figure 5.9: *Object Balance Control Architecture for Uni-Manipulation.*

For this case, the upper-body controller has three inputs (Figure 6.2 bottom). These inputs are the proprioceptive sensors of the arm, the F-T sensor on the wrist, and the vision system of the camera. Each input is associated with a specific information. For example, the proprioceptive sensors of the arm denote the joint angles (q_{arm}), The F-T sensor is the force and torque wrenches/vectors generate by the object and measure on the wrist (F_W, T_W) and the vision system computes the position of the geometric centre and the inclination angle of the bottle (θ, X_{CoG})

Therefore, the UBC controller receives and reads the information from these three sensory systems and processes it. On the one hand, visual information is filtered through the trained Fuzzy filter (we have explained this process in section 5.4.3). The result is an estimated angle closer to the real value ($\hat{\theta}$). On the other hand, the F-T information is transformed using the "3D Dynamical Slopes" method (we have presented this process in section 5.4.2). The result is a new forces and torques vector associated with a co-planar coordinate system ($\hat{F}_W, \hat{F}_W$). With this data, we can compute the bottle ZMP (ZMP_{bottle}). To do this, we use the 3D-LIPM model to define bottle behaviour.

Finally, the proprioceptive information of the joints is transformed into Cartesian space to obtain the pose of the tray (P_{tray}). Therefore, this pose and the object ZMP value are the inputs of the proposed Fuzzy controller. And the output is the new pose of the tray ($\hat{P}_{tray}$) to avoid the fall of the bottle. We apply the inverse kinematic to return to the joint space and obtain the final joint angles ($\hat{q}_{arm}$). We explain this predictive controller in detail in the next section.

5.5.3 Decision Making System

For quasi-static postures or movements with slow dynamics, the feedback controllers run perfectly. However, the control systems must be improved if the movements begin to accelerate, and the system is considerably disturbed. In humans, there is an anticipatory system within their postural control systems to be able to predict what state they will be in. Therefore, it is possible to adjust the properties of the controller through advanced information associated with fast movements using predictive control (Pollock et al., 2000).

Following Figure 5.9 (grey colour), we divide the sensory system into three perceptions (tray pose, stability and inclination value of the bottle). Robot sensations are produced by raw sensory information. In our case, proprioceptive, F-T and vision. Considering these perception systems, it is necessary to obtain relevant perceptions. Therefore, we must generate some thresholds for this purpose. By the use "sensory thresholds psychophysics concept", we can perform them (Nashner, 1970).

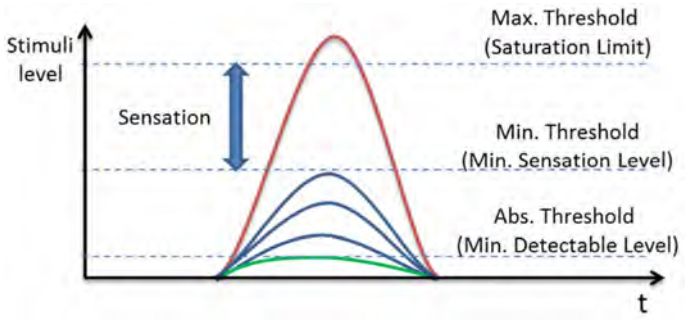

Figure 5.10: *Example of sensation threshold based on surprising events.*

Once the raw sensors' data compose the sensation, we have to filter, classify and evaluate this information and convert them into manageable data. Now, the difficulty is the application in object balance control this manageable data. We establish the method "surprising events" to evaluate the trigger reactions in the anticipatory controller. We could consider disturbances as unforeseen situations. And also, the surprise activation as the processing output (Ortony and Partridge, 1987). Finally, the system has to choose and mix information from the available perceptual sets.

In the transportation task case, the foundations for the "surprises events" are related to the characteristic of the application. The decision method begins evaluating the visual perception system ($\hat{\theta}$). Before starting a reaction, we must mix the visual "surprise event" value with the other "surprise events" (ZMP_{bottle}, P_{tray}). The idea is to describe the reaction for the robot. With two diverse goals, the maximum value among the sensory "surprise events" is used. Firstly, triggering or not the reaction ($\hat{\theta}$). Secondly, defining the reaction and its (ZMP_{bottle}, P_{tray}).

The numeric value ($\hat{P}_{tray}$) is the reaction of the decision-making system (Figure 5.9 - green colour). For the fulfilment of the pre-established handling synergies, we use this value. These synergies work as anticipated motor responses. The goal is to train a neuro-fuzzy system (like the vision Fuzzy filter with the ANFIS tool). So, from an experimental dataset, we must to obtain this numeric variable. Then, we infer the synergy parameter $\hat{P}_{tray}$ using this neuro-fuzzy system (Figure 5.11). The output of this evaluation system (evaluating vision, F-T and proprioceptive sensors) is this variable $\hat{P}_{tray}$, described by Equation 5.7.

$$\hat{P}_{tray} = f(\hat{\theta}, ZMP_{obj}, P_{tray}) \tag{5.7}$$

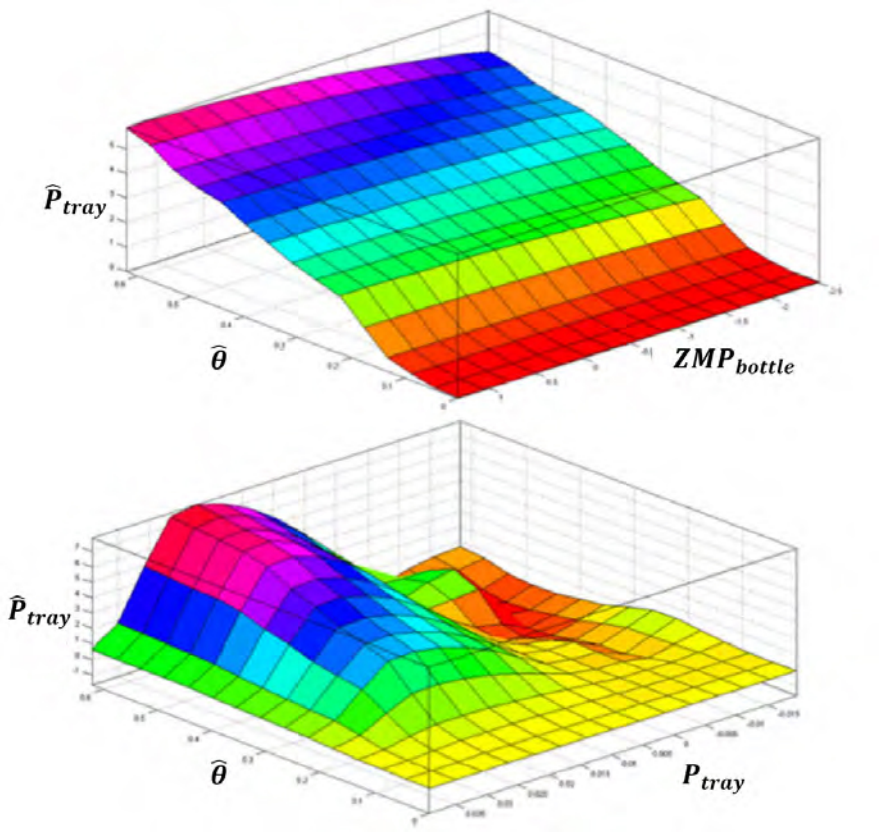

Figure 5.11: *$\hat{P}_{tray}$ Fuzzy Inference System.*

5.6 Alternative Object Object Controller for Bi-Manipulation

All this research on the transport of objects can be extrapolated to a bi-manipulator robot. In this case, we would again consider all the previously described problems, making emphasis on the use of two F-T sensors of both wrists. Newly, we should take into account two issues: the morphology of both sensors and their estimated orientation depending on the tray inclination.

For the implementation of a balance controller based on bi-manipulation, the first step would be to recalculate and evaluate the degree of stability. In the case of Dual-Arm manipulation, the robot holds the tray through two support points (right hand and left hand). And again, the bottle is resting on the tray, as shown in Figure 5.12. Additionally, each wrist has its F-T sensor installed, which read the forces and torques generated by the weight of the bottle. At no time, the position of the tray, the form of grip or the execution of the bi-manipulation task influence the performance of the vision system.

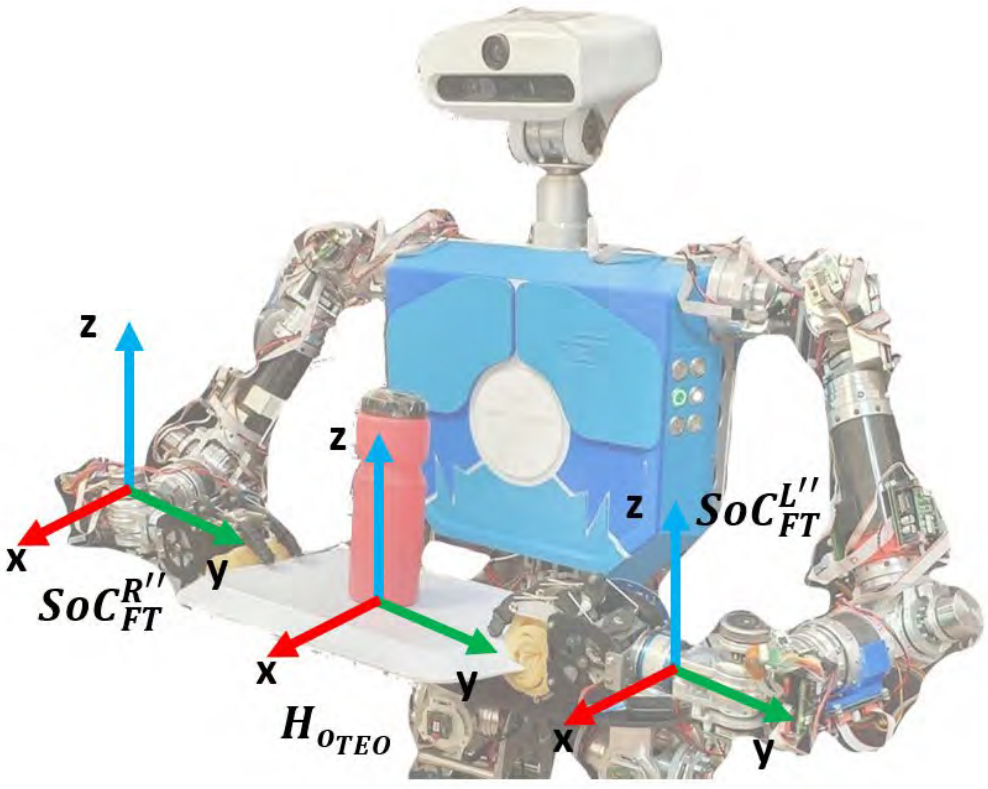

Figure 5.12: *Representation of the coplanar coordinate systems for bi-manipulation.*

If we take into account that the behaviour of the bottle is like an inverted pendulum again, we can say that the bi-manipulation task is similar to the stability control of the robot body. The assumption is simple. As explained in chapter 4, the body can be modelled with the 3D-LIPM model, and as explained in chapter 3.7.1, there is a relationship to calculate the global ZMP when there are two support points - ZMP left foot and ZMP right foot (as in the walk). Therefore, we can apply the same concept to the task of bi-manipulation. Now, the hands are the two footholds. And the tray is the floor where the hands rest.

5.6.1 Stability Evaluation for Bi-Manipulation

Therefore, the steps to follow for the ZMP computation of the bottle are the same. Firstly, it is necessary to take into account the robot morphology and the arrangement of the F-T sensors on the wrists. Both sensors have an anti-clockwise system. As a reminder, both the SoC_{root} root coordinate system (located in the CoM) and the SoC_{tray} tray coordinate system are clockwise systems. In particular, each arm has its own coordinate systems. SoC^L_{FT} and SoC^L_{tray} for the left arm, and SoC^R_{FT} and SoC^R_{tray} for the right arm. In any case, we must apply a reflection matrix to the SoC^L_{FT} and SoC^R_{FT} systems to change them to clockwise systems and then a rotation matrix (90 degrees) to match those axes with those of the systems SoC^L_{tray} and SoC^R_{tray} respectively.

After this, it is necessary to correct the problem related to the origins of SoC^L_{FT} with SoC^L_{tray}, and SoC^R_{FT} with SoC^R_{tray} respectively. To do this, a translation matrix is applied to the to displace and match both origins. By subtracting the offset vector $[d_x, d_y, d_z]$, the new virtual systems $SoC^{R'}_{FT}$ and $SoC^{L'}_{FT}$ match the hands systems SoC_{tray}. Since both arms are the same, so are the displacement vectors. Therefore, we can assume that the behaviour of both arms is identical at the mathematical level. So, the ZMP computation is the same as for a single arm. Then we can apply the Equation 5.1 to solve this problem. The only exception is that the angle of rotation for the SoC^R_{FT} system is opposite to the SoC^L_{FT} system. The result is to obtain $X^{R'}_{zmp}$ and $Y^{R'}_{zmp}$ for the right arm, and $X^{L'}_{zmp}$ and $Y^{L'}_{zmp}$ for the left arm.

With the same idea, we have the same problem of reorienting the tray, but we can also continue to apply the "3D Dynamical Slope" concept to each virtual system $SoC^{R'}_{FT}$ and $SoC^{L'}_{FT}$. Applying the rotation matrix corresponding to the angle of inclination of the tray, we obtain the coplanar systems $SoC^{R''}_{FT}$ and $SoC^{L''}_{FT}$. These systems correct the readings of the F-T sensors correctly and can calculate the ZMP of the bottle through the Equations 5.5 and 5.6. The result is to obtain $X^{R''}_{zmp}$ and $Y^{R''}_{zmp}$ for the right arm, and $X^{L'}_{zmp}$ and $Y^{L'}_{zmp}$ for the left arm.

The last step is to calculate the total bottle ZMP, considering the previous calculations of each of the arms. We adapt the Equation 3.16 of the double support to obtain the real ZMP of the bottle for the DA manipulation task.

$$X_{ZMP_{DS}} = -\frac{X_{ZMP}^{R''} \cdot F_z^{R''} + X_{ZMP}^{L''} \cdot F_z^{L''}}{F_z^{R''} + F_z^{L''}} \tag{5.8}$$

$$Y_{ZMP_{DS}} = -\frac{Y_{ZMP}^{R''} \cdot F_z^{R''} + Y_{ZMP}^{L''} \cdot F_z^{L''}}{F_z^{R''} + F_z^{L''}} \tag{5.9}$$

From this point on, the driver implementation would be very similar to the one proposed in section 5.5.2. We would apply 3D Dynamical slopes to both wrist F-T sensors and the Fuzzy filter to the vision system to obtain the ZMP value of the object. And then we would use a new predictive controller to maintain the stability of the bottle. However, even this last part has not yet been possible to test and validate. In this case, a first version based on the tray pose instead of the object ZMP has been started.

5.6.2 Control Architecture for Bi-Manipulation

For tray control based on a bi-manipulator, we have applied the same philosophy as the single manipulator controller. We have proposed similar control architecture. In this case, the new Fuzzy controller (based on section 5.5.3) must interpret the tray and object pose values, with the only difference that these values are now associated with two F-T sensors, as shown in Figure 5.13.

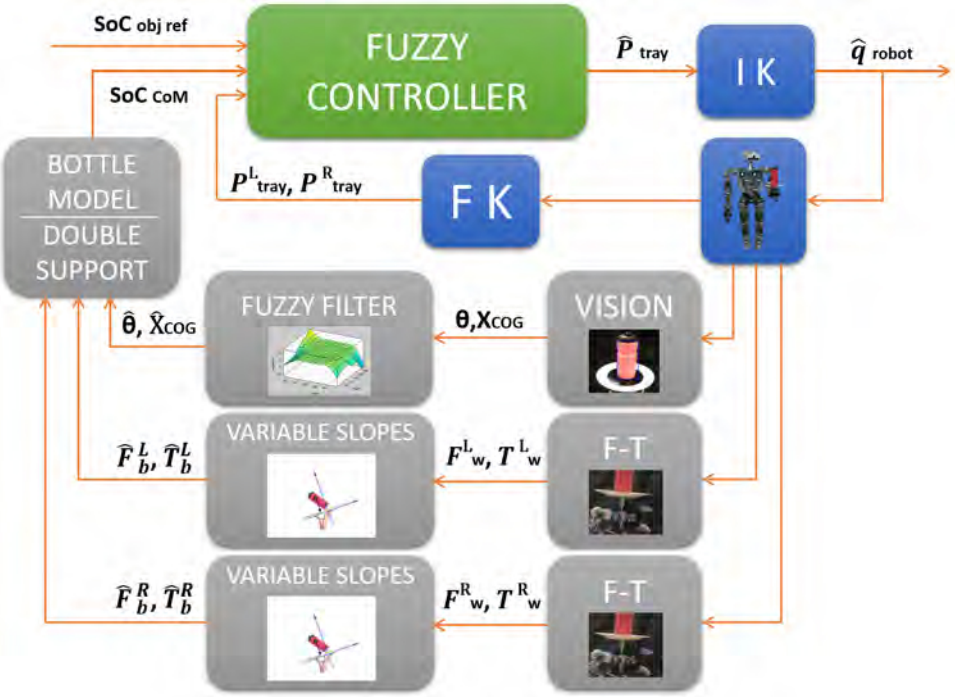

Figure 5.13: *Control Architecture for object transportation with Bi-Manipulation.*

Through the robot, we obtain the F-T values of the two wrists, the bottle angle with the camera and position of the joints involved in the task. On the one hand, the joint positions are transformed to the Cartesian space to obtain the pose of both hands. And we do the same for visual and F-T information (section 5.5.2). With the sensory information processed and filtered, we generate the Fuzzy controller inputs.

In our case of Dual-Arm manipulation (Figure 5.12), we have the condition of working with a closed chain in a robot that is rigid. Therefore, an essential requirement is that the F-T values of both hands are very similar during the control. But, we must consider two important ideas to implement the Fuzzy controller rules. Firstly, the behaviour of the object is related to the F-T values of both hands. And secondly, the planning of the tray pose depends on the transported object pose, and the possible mismatches between the FT values of both hands, such as it is shown in Equation 5.10.

$$H_{O_{TEO}} = f(H_{CoM_{obj}} = f(W_R, W_L)) \tag{5.10}$$

where $H_{O_{TEO}} \in \mathbb{R}^6$ represents the tray pose, $H_{CoM_{obj}} \in \mathbb{R}^6$ is CoM pose for the transported object. $W_R \in \mathbb{R}^6$ and $W_L \in \mathbb{R}^6$ (related to $SoC_{FT}^{R''}$ and $SoC_{FT}^{L''}$) denote the vector of forces and torques for each right and left wrists.

5.7 Conclusions

For Chapter 5, we introduce the problem of manipulation without grip. When we want to transport an object on a tray, numerous problems and conditions arise that must be taken into account. These drawbacks may be due to the influence of the robot's own stability, other external forces, the use of one or two hands, the sensory systems involved, the morphology of the robot or the simple fact that the object is not firmly hold.

In this chapter, we have detailed the need to improve control algorithms, especially in balance control, due to their rapid dynamics. The increase in the speed of data processing and the quality of the resulting information is a way to achieve adequate control. The task of transporting a bottle in a tray is a clear example of a balance control task. This task needs accurate sensor information and needs to get the information as quickly as possible.

For the vision system, the fuzzy filter-based visual correction method promises more accurate results and notably faster. The offline training method based on experimentally obtained data allows modelling the error quite accurately to be later eliminated through the fuzzy filter entered with the ANFIS tool. For the F-T system, the proposed mathematical method of pose estimation is effective. The system to obtain the ZMP adapts to the morphology of the robot and the current pose of the tray and can obtain more real values of the stability of the bottle.

Besides, with FIS systems, it is also possible to generate fuzzy filters for handling control by merging different sensory information, allowing us to predict instability and generate faster actions.

Finally, we have investigated the possibility of applying this task of controllers of both uni-manipulation and bi-manipulation. Because the TEO humanoid robot is rigid, the adaptation from one manipulation to another is almost direct. This condition only affects the computation of the object's ZMP, but not the control architecture and how to approach the problem.

Chapter 6

Whole-Body Object Balance

6.1 Introduction

Robotics research is growing more and more. Each time the robots are more efficient in developing various operations. Manipulate objects, climb stairs, run or jump. Nevertheless, in almost all circumstances, we address these works independently. This one forces limitation for integration into real environments of the robots. Although occasionally humans are overcome by robots in certain tasks; For the resolution of multiple complex tasks, these are not yet able to adjust and connect various behaviours. In the human sphere, this flexibility generates knowledge to face new tasks (never before done) and with a high degree of success. Therefore, the performance of multiple operations simultaneously is exposed to the investigation.

For this case, Whole-body control is the solution. This promising new field of research addresses the problems of multitasking. Whole-body control aims to determine a small set of low-dimensional, simple precepts that are enough to ensure the proper execution of any single task or of multiple simultaneous tasks. The idea is to be able to use floating-based, redundant robots and all their capabilities. And also, to be able to use them in any environment in a multi-contact interaction. Thus, a whole-body control system should necessarily be general enough to allow the execution of several (ideally any) tasks.

If we focus on the case of the TEO humanoid robot and the waiter application, we can understand this application is multitasking. In order to perform this task as a waiter, the humanoid robot must be able to maintain balance and transport the object simultaneously. In that way, the proposed Whole-Body Postural Control architecture is focused and implemented with this WB ideal, and can even be adapted to uni-manipulation or bi-manipulation tasks.

On the other side, after the bi-manipulation extension, we also try to apply part of our dual-arm manipulation concept to the humanoid robot TORO. In the second part of the chapter, we combine the passivity-based whole-body controller from (Henze et al., 2016b) with a dual-arm task in order to allow for bi-manipulation of an object while balancing the robot. For this purpose, the feedforward terms are adapted to preserve a good performance and robustness in the case of following a dynamic trajectory with the transported object. The final control architecture shows the structure of a PD+ controller. This one ensuring the stability and passivity for the controller.

As a result, we have developed a controller capable of performing balance and bi-manipulation tasks. This new system is equipped with various skills: First, the bi-manipulation task-oriented feedforward control allows making robust and efficient tracking in the movement of the transported object. Second, we have added the ability to distribute the load on the manipulator's arms according to the situation. We can decide which one holds the whole load or if the weight is distributed evenly, like in a collaborative task. Thus, the framework is able to solve the wrench distribution problem for the bi-manipulation and the balancing task. Third, we have provided the ability to readjust the bi-manipulation model according to the object to be grasped. And finally, the compliance controller allows continuing absorbing external disturbances.

The chapter is organized as follows. The section 6.2 introduces some preliminary work and research on dual-arm manipulation and whole-body control. Section 6.3 explains in detail the problems associated with whole-body transport task in TEO and the interaction among the subtasks. Section 6.4 describes the bi-manipulation problem and the integration process to use bi-manipulation in a compliance robot. Finally, in the last section 6.5, some conclusions are summarised.

6.2 Related Works

The essential behaviour of a humanoid robot must have the capacity to keep stability and also walk (compliantly) with the application of possible external perturbations. By using joint torque sensing and control, we could achieve sensitive compliance or impedance control (Ott et al., 2008). We can apply torque-sensing in some humanoid robots like Valikyrie (Radford et al., 2015), in which its joint architecture eliminates the additional noise in both position and torque sensing to improve the control. At the Institute of Robotics and Mechatronics of DLR, the humanoid robot TORO has been developed using the joint technology of the KUKA Light-Weight Robot. This would be operated in torque or position (Ott et al., 2010).

Figure 6.1: *The humanoid robot TORO transporting objects on a tray.*

More complex methodologies are implemented when using a whole-body control approach. For instance, a whole-body nonlinear model predictive control approach for rigid body systems subject to contacts is presented in (Neunert et al., 2018). By the use of a contact model as part of the whole-dynamic system, the approach is able to optimize the location, sequence, and timings of the contacts efficiently.

Because passivity theory can guarantee robustness during interaction with the environment, this has been proven and integrated with whole-body control in others works. S. Fahmi et al. in (Fahmi et al., 2019) presents a passive whole-body control method for quadruped robots that succeeds in dynamic locomotion while compliantly balancing the robot. The motion tracking takes into account the full-robot rigid body dynamics. A humanoid robot controller based on passivity was presented in (Henze et al., 2016b), which incorporates feedforward terms for following dynamic trajectories. The framework was combined in (Henze et al., 2016a) with methods from the field of hierarchical multi-objective control to achieve a prioritization of tasks. The combined framework was adapted in (Henze et al., 2017) for operating humanoid robots in confined spaces, such as they occur in aircraft manufacturing.

On the other hand, in many robotic applications using manipulators, the desired Cartesian impedance behaviour is typically chosen as a system similar to a mass-spring-damper. Some works are related to the design and application (Caccavale et al., 1999, Natale, 2003). Also, there are works focused on the problem of implementing a dual-arm manipulation controller or even object oriented control (Zacharias et al., 2010, Vahrenkamp et al., 2009, Garcia-Haro et al., 2018d, T. Wimböck, C. Ott, and G. Hirzinger, 2007). Note that the field of dual-arm manipulation as well as balance control of legged robots suffers from the same challenge as pointed out in (Ott et al., 2011). In both cases, the closed-kinematic chain arising from the multiple contacts of the feet with the floor or of the hands with the object causes a redundancy in the space of the contact wrenches.

6.3 Waiter WB Manipulation for the case of Uni-Manipulation

In the previous chapters, the locomotion and manipulation systems have been studied separately. Both systems deal with different problems related to mechanical problems and the complexity of the task. In any case, the proposed solutions have been verified individually, obtaining quite acceptable results.

In the case of locomotion, the LBC dynamically adjusts itself depending on its stability status. But this LBC takes the physics of the body into consideration only as if it was a rigid solid (LIPM model). The effect of arm movement is not contemplated at any time. In the case of manipulation, the UBC adapts dynamically the state of the bottle and the tray. But in the same way, this controller only contemplates the movement of the object. In this case, it is not considered how the stability of body control affects the balance of the bottle on the tray.

But it is obvious that, in a human being or a humanoid robot, the movements of the upper-lower limbs affect on each other. On the one hand, if a human carries a weight on his outstretched arms, his body will swing forward. On the other hand, if he starts or stops walking, the acceleration or deceleration will affect the bottle on the tray. And the effect is greater because the bottle is not physically attached. For these reasons, the waiter application (shown in Figure 3.6) is proposed. In this application, both upper-body and lower-body controllers continue controlling the balance of the stability of the body and the object respectively. But now, both controllers are influenced each other due to arm and body movements.

For this purpose, the waiter application is divided into three levels. At the low level, all robot devices that interact directly with the outside are located. On the one hand, the robot takes advantage of the information from the F-T and inertial sensors (inputs). And on the other hand, the robot acts on the drivers of each joint (motors), both for the upper- and lower-body.

At the middle level, there are two types of processes. There are processes that take advantage of the postural information of the robot and the sensors, and there are processes that modify the posture of the robot. For this application, four processes have been developed altogether. The OBP (Object Balance Perception) process is responsible for discerning the equilibrium state of the transported object. The BBP (Body Balance Perception) process has the objective of calculating the equilibrium state of the body. The OBE process (Object Balance Execution) generates the corresponding action on each of the joints of the arm. Finally, the BBE process (Body Balance Execution) controls the joints of both legs.

At the high level, there is the Whole-Body Postural Control (WBPC). This one is made up of two processes. The UBC process (Upper-Body Controller) decides the action to follow in the arms according to OBP and BBP. The LBC process (Lower-Body Controller) chooses the work to do in the legs depending also on OBP and BBP.

6.3.1 Control Architecture

For a better understanding of the development of this waiter application, the WBPC architecture is explained in more detail in Figure 6.2, in which the evaluation of multiple ZMP (object and body) is performed. Starting from the architecture scheme (Figure 3.7), the WBPC architecture is based on executing the upper-body and the lower-body controllers in parallel. These two controllers are based on systems type FIS (Fuzzy Inference System).

The reason for using this type of system is bio-inspiration. By using a humanoid robot and also imitating an application of human beings, it is interesting to use a system similar to the way human beings think. In fact, FIS systems can model the qualitative aspects of human knowledge and reasoning processes. The use of Fuzzy systems presents multiple advantages. Some of these advantages are the use of real information of the system to be controlled, its good resistance to the noise, or the low computation effort. In addition, the capability of the Fuzzy filters to come up against nonlinear systems is useful. So, it can fit very well with the behaviour of a humanoid robot (Hernandez-Vicen et al., 2018).

As a small reminder of (Jang, 1993), to train the FIS systems for the controllers, we use the ANFIS tool from Matlab. "The architecture and learning procedure underlying ANFIS is given as a fuzzy inference system implemented in the framework of adaptive networks. By using a hybrid learning procedure, the suggested ANFIS can create an input-output mapping based on both stipulated input-output data pairs and human knowledge (in the form of fuzzy *if-then* rules). This tool produces a single-output Sugeno FIS and tunes the system parameters using the defined input/output training data. The FIS structure is automatically created using grid partitioning. The training algorithm utilises a combination of *backpropagation gradient descent and the least-squares* methods to model the training data set".

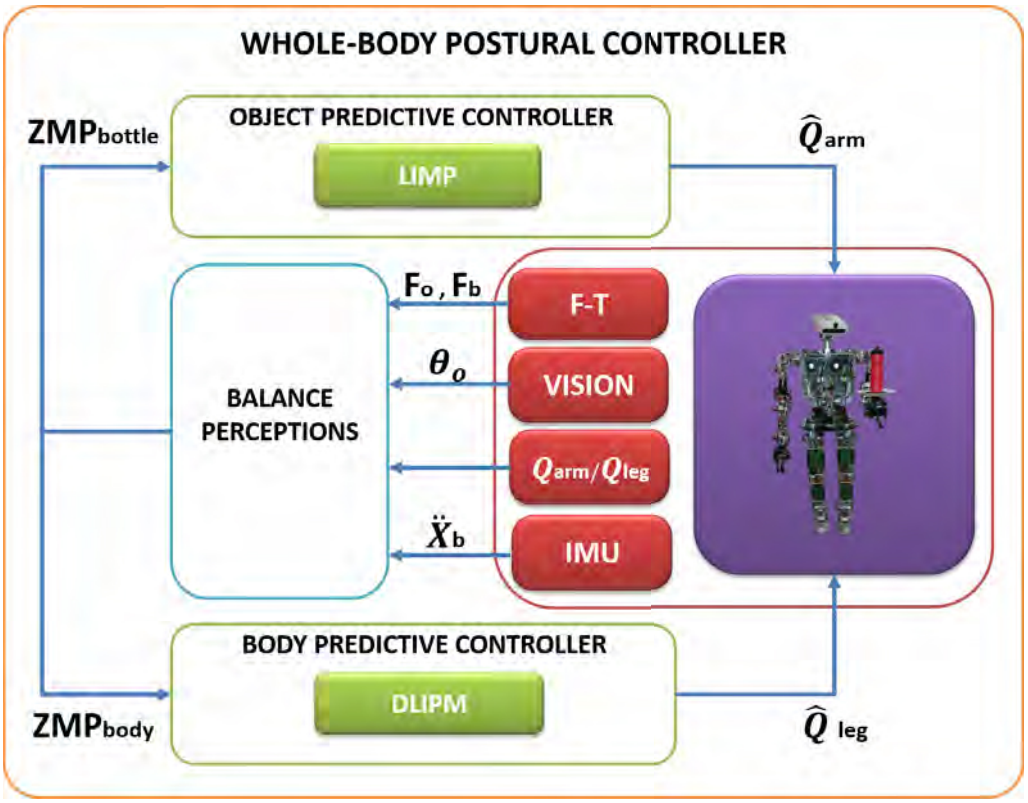

Figure 6.2: *Whole-Body Postural Controller.*

The lower-body controller has three inputs (Figure 6.2 top). These three inputs are the proprioceptive sensors of the legs (Q_{leg}), the two F-T sensors on the ankles (F_b), and the inertial sensor ($\ddot{X}_b$) located very close to the CoM. The fusion of the three inputs serves to calculate the body's ZMP (ZMP_{body}) and predict its stability range. In this case, the position of the arm (Q_{arm}) produces an almost negligible effect on the body's ZMP. The reason is due to the fact that the difference between the mass of the arm and the body is significant. Even so, it has been decided to include this value for a more precise body control.

The upper-body controller also has three inputs (Figure 6.2 bottom). These three inputs are the proprioceptive sensors of the arm (Q_{arm}), the F-T sensor on the wrist (F_o), the vision sensor (θ_o) of the camera. The calculation of the object's ZMP (ZMP_{bottle}) still considers the inclination of the bottle, the forces and torques, and the pose of the tray. But now, the performance of the body balance control affects the value of the object's ZMP. Due to the mass difference, the object balance control will be influenced to a greater extent by the body movement. Depending on whether we use the DLIPM model or not, the effect will be better or worse.

6.4 Waiter Whole-Body Manipulation for the case of Bi-Manipulation

As we said in section 5.6, all this research on the transport of objects can be extrapolated to a bi-manipulator robot. In our case of Bi-Manipulation, we have the requirement of working with a closed chain in a robot that is rigid again. Therefore, an essential condition is that the behaviour of the F-T sensors for both hands is the same as in uni-manipulation. Nevertheless, we have to take into account the same two ideas to implement bi-manipulation control. Firstly, the behaviour of the object is related to the F-T values of both hands. And secondly, the planning of the tray pose depends on the transported object pose, and the possible mismatches between the FT values of both hands, as we mentioned in Equation 5.10.

This requirement for bi-manipulation is very important. However, it does not have a visible effect on the proposed WBPC architecture. The process of implementing the UBC controller is obviously affected by the use of two F-T sensors at the low-level. The planning of the tray pose depends on the bottle state, and this depends on the F-T vectors/wrench of the hands. However, the command output to the robot remains the same: the new tray pose. And at any time, the LBC controller is influenced by this extension of the manipulation.

6.4.1 Adaption for Compliance BiManipulation

For the problem of bi-manipulation and closed chains in a rigid robot, we have proposed a predictive controller, which is properly integrated into our WBPC architecture. However, if we use a compliance robot like the TORO humanoid robot, we must adapt certain aspects in order to integrate the bi-manipulation task into a passivity-based whole-body controller.

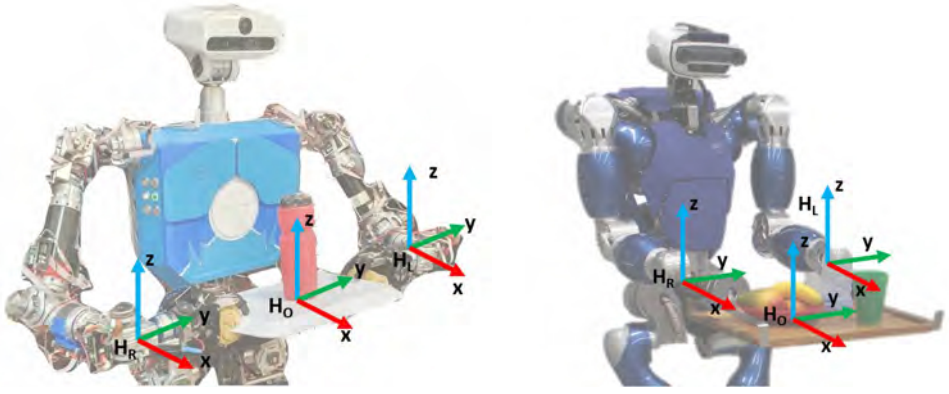

(a) TEO. (b) TORO.

Figure 6.3: *Comparison between TEO and TORO for the bi-manipulation task.*

The main idea is to be able to apply the same concept of TEO bi-manipulation on the TORO robot. To do this, we have extracted the properties of the TORO robot, to adapt the concept of bi-manipulation to a new one that can be implemented and integrated. The TORO robot is a torque-controlled humanoid robot. Its balancing and posture controller is able to compute the desired contact vectors/wrenches based on the equilibrium position of the robot's CoM. In other words, the controller computes the forces and torques of the legs' and arms' TCPs to keep in balance using the complete body (Figure 6.3).

Because the TORO robot computes hand wrenches, we can approximate them to the behaviour of F-T sensors in TEO. Therefore, in order to use the TORO arms for bi-manipulation, we take advantage of the Equation 5.10. The only difference we have adapted is the way to plan the pose of the bi-manipulated object. In the case of TEO, $H_{O_{TEO}}$ depends on the object transported state on the tray, which depends on the forces and torques of the hands. In the case of TORO, $H_{O_{TORO}}$ depends on the planning of the robot's CoM, which partly depends on the forces and torques of the hands. Equation 6.1 defines the relationship between robots and the possibility of applying the same concept for bi-manipulation.

$$f(H_{CoM_{obj}} = f(W_R, W_L)) = H_{O_{TEO}} = H_{O_{TORO}} = f(H_{CoM_{robot}} = f(W_R, W_L)) \tag{6.1}$$

Next, the integration process of the bi-manipulation task over the passivity-based balancing controller in the TORO compliance robot is presented step by step.

6.4.2 Modelling

For the robot TORO, the dynamic model is described in this subsection. We employ this model in the following subsection 6.4.3 to implement the dynamic model for the balance controller, which will be used to implement the bi-manipulation and balance controller in turn in subsections 6.4.4 and 6.4.5. The controller has the goal to use the end-effectors more specifically. On the one hand, the feet's end-effectors will be in contact with the ground to control the stability of the robot. And, on the other hand, the hands' end-effectors will be in contact with the bi-manipulated object, which will be influenced by the stability and the CoM of the robot. In this way, we can implement tasks where a humanoid robot would be able to transport large objects compliantly without the robot falling.

For the whole-body humanoid robots, it is popular the use of floating bases in dynamic models. The reason is related to the flexibility respect to contact changes. Models with fixed base are less flexible than models with floating base. Typically, a base link is chosen as a central body. This one is within the kinematic robot structure (like the hip or the trunk or the hip). Since the CoM depicts a fundamental measure for balancing, some researches also use the CoM as a central base.

Here, we have followed the notation of (Henze et al., 2016b) by defining: "a CoM frame $\mathcal{C}$, which is located at the CoM and has the same orientation of the hip. Let $\boldsymbol{x}_c \in \mathbb{R}^3$ and $\boldsymbol{R}_c \in \mathcal{SO}(3)$ denote the position and orientation of the frame $\mathcal{C}$ with respect to the world frame $\mathcal{W}$. The corresponding translational and rotational velocities are $\dot{\boldsymbol{x}}_c$ and $\boldsymbol{\omega}_c$, respectively. Based on the n joint angles $\boldsymbol{q} \in \mathbb{R}^n$ and $\boldsymbol{v}_c = (\dot{\boldsymbol{x}}_c^T, \boldsymbol{\omega}_c^T)^T$, the dynamics of the humanoid robot is given by":

$$\boldsymbol{M}\begin{pmatrix}\dot{\boldsymbol{v}}_c\\ \ddot{\boldsymbol{q}}\end{pmatrix} + \boldsymbol{C}\begin{pmatrix}\boldsymbol{v}_c\\ \dot{\boldsymbol{q}}\end{pmatrix} + \underbrace{\begin{pmatrix}m\boldsymbol{g}_0\\ \boldsymbol{0}\end{pmatrix}}_{\boldsymbol{g}} = \begin{pmatrix}\boldsymbol{0}\\ \boldsymbol{\tau}\end{pmatrix} + \boldsymbol{\tau}_{\text{ext}}. \tag{6.2}$$

where "$\boldsymbol{M} \in \mathbb{R}^{(6+n)\times(6+n)}$ and $\boldsymbol{C} \in \mathbb{R}^{(6+n)\times(6+n)}$ denote the inertia and Coriolis matrix, respectively. The gravitational torques are expressed by $\boldsymbol{g} \in \mathbb{R}^{6+n}$ with m denoting the overall mass of the robot and $\boldsymbol{g}_0 \in \mathbb{R}^6$ the gravitational acceleration. In this case, $\boldsymbol{g}_0$ is six-dimensional by also containing the rotational DoFs. The joint torques are described by $\boldsymbol{\tau} \in \mathbb{R}^n$. The influence of external wrenches on the robot is taken into account by the generalized torque vector $\boldsymbol{\tau}_{\text{ext}} \in \mathbb{R}^{6+n}$".

"We separate the ψ end-effectors into two subgroups, the first one is referred to as *balancing end-effector* (*bal*) and contains the ψ_{bal} end-effectors that are used by the robot to support itself (usually the feet). The remaining $\psi_{\text{int}} = \psi - \psi_{\text{bal}}$ end-effectors are called *interaction end-effectors* (*int*), as they are still free to be used in a manipulation or interaction task (usually the hands). So, following this definition, the Cartesian velocities of the end-effectors $\boldsymbol{v} \in \mathbb{R}^{6\psi}$ are given by":

$$\boldsymbol{v} = \begin{pmatrix}\boldsymbol{v}_{\text{bal}}\\ \boldsymbol{v}_{\text{int}}\end{pmatrix} = \underbrace{\begin{bmatrix}\boldsymbol{Ad}_{\text{bal}} & \boldsymbol{J}_{\text{bal}}\\ \boldsymbol{Ad}_{\text{int}} & \boldsymbol{J}_{\text{int}}\end{bmatrix}}_{\begin{bmatrix}\boldsymbol{Ad} & \boldsymbol{J}\end{bmatrix}} \begin{pmatrix}\boldsymbol{v}_c\\ \dot{\boldsymbol{q}}\end{pmatrix} \tag{6.3}$$

with $\boldsymbol{v}_{\text{bal}} \in \mathbb{R}^{6\psi_{\text{bal}}}$ and $\boldsymbol{v}_{\text{int}} \in \mathbb{R}^{6\psi_{\text{int}}}$. The Adjoint matrix $\boldsymbol{Ad} \in \mathbb{R}^{6\psi\times 6}$ maps the movement of the CoM to the TCPs. Meanwhile, the Jacobian matrix $\boldsymbol{J} \in \mathbb{R}^{6\psi\times n}$ accounts for a motion of the joints. particularly, $\boldsymbol{\tau}_{\text{ext}}$ is simplified to $\boldsymbol{\tau}_{\text{ext}} = \boldsymbol{J}^T\boldsymbol{F}_{\text{ext}}$ due to all external perturbance works only at the TCPs.

6.4.3 Balancing

In (Henze et al., 2016b), a balancing control based on passivity was presented. It is used as a basis for the bi-manual control for torque-controlled humanoid robots in the next subsection.

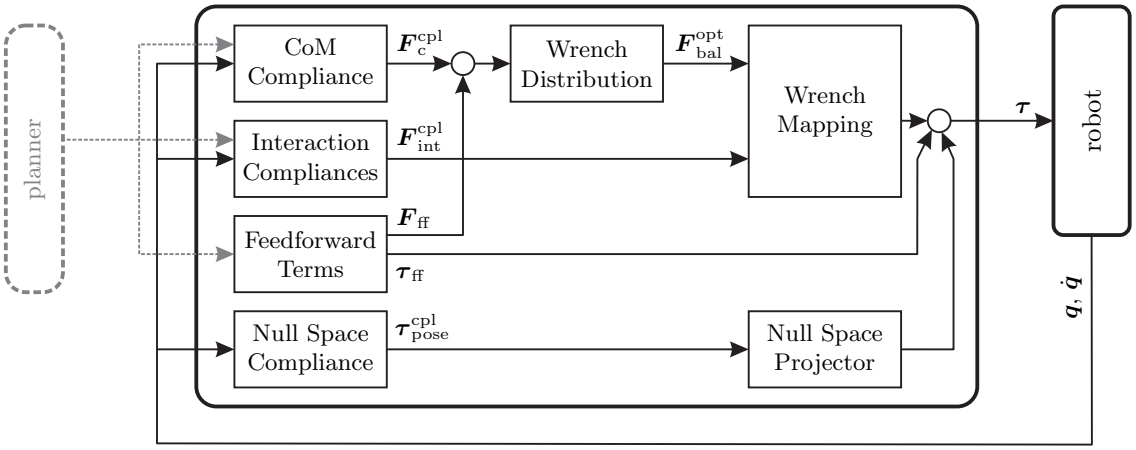

Figure 6.4: *Structure of the passivity-based balancing control from (Henze et al., 2016b).*

The balancing controller from (Henze et al., 2016b) features several Cartesian compliances for stabilizing the centre of mass frame $\mathcal{C}$ and the interaction end-effectors. An overview of the control approach is given in Figure 6.4. Note that the controller can utilize multiple contacts to support the robot, which creates a closed-kinematic chain involving the balancing end-effectors. The resulting redundancy in the space of the contact or balancing wrenches $\boldsymbol{F}_{\text{bal}}$ is also known as the Wrench Distribution Problem (WDP). In order to resolve the redundancy, the controller distributes the compliance wrench $\boldsymbol{F}_c^{\text{cpl}}$ (including gravity compensation $\boldsymbol{g}$) to the balancing end-effectors by solving a constrained quadratic optimization. Finally, the end-effector wrenches $\boldsymbol{F}_{\text{bal}}^{\text{opt}}$ and $\boldsymbol{F}_{\text{int}}^{\text{cpl}}$ are mapped to the control torques $\boldsymbol{\tau}$.

For the improvement of the tracking behaviour, the feedback loop adds the feedforward control. The controller, similar to PD+, is the result of this combination. This one permits to test passivity and balance in a closed-loop system (Paden and Panja, 1988, Whitcomb et al., 1993).

In order to derive the controller, a coordinate transformation is defined in (Henze et al., 2016b). In this transformation, the Cartesian coordinates of the TCPs replace the joint velocities in the dynamic model (6.3). Excluding singular configurations and redundant robots from our considerations, the transformation matrix $\boldsymbol{T}$ is defined by:

$$\begin{pmatrix} \boldsymbol{v}_c \\ \dot{\boldsymbol{q}} \end{pmatrix} = \underbrace{\begin{bmatrix} \boldsymbol{I} & \boldsymbol{0} \\ -\boldsymbol{J}^{-1}\,\boldsymbol{Ad} & \boldsymbol{J}^{-1} \end{bmatrix}}_{\boldsymbol{T}^{-1}} \begin{pmatrix} \boldsymbol{v}_c \\ \boldsymbol{v} \end{pmatrix}. \tag{6.4}$$

Applying (6.4) to (6.2) leads to the transformed model

$$\boldsymbol{\Lambda} \begin{pmatrix} \dot{\boldsymbol{v}}_c \\ \dot{\boldsymbol{v}} \end{pmatrix} + \boldsymbol{\mu} \begin{pmatrix} \boldsymbol{v}_c \\ \boldsymbol{v} \end{pmatrix} + \boldsymbol{g} = \begin{bmatrix} -\boldsymbol{Ad}^T \\ \boldsymbol{I} \end{bmatrix} \boldsymbol{J}^{-T}\boldsymbol{\tau} + \boldsymbol{T}^{-T}\boldsymbol{\tau}_{\text{ext}} \tag{6.5}$$

with $\boldsymbol{\Lambda} = \boldsymbol{T}^{-T}\boldsymbol{M}\boldsymbol{T}^{-1}$, $\boldsymbol{\mu} = \boldsymbol{T}^{-T}\boldsymbol{C}\boldsymbol{T}^{-1} + \boldsymbol{T}^{-T}\boldsymbol{M}\dot{\boldsymbol{T}}^{-1}$. The transformed model is reused in Section 6.4.5 for integrating the bi-manipulation task.

However, this controller lacks to ability to manipulate a common object with both hands. In theory, the trajectories for both hands can be designed such that they stay in formation while moving the common object, but designing such a trajectory is rather cumbersome. Furthermore, the resulting stiffness and damping of the object can only be parametrized indirectly via the individual hand compliances. The same holds for the load distribution between the hands in case the robot is carrying a heavy object.

For this reason, a new controller has been developed that is capable of performing dual-arm manipulation by defining a Cartesian compliance for the common object instead of the individual hand compliance. the resulting object wrench is distributed to both hands by solving the closed kinematic chain of the upper body as detailed in the next section.

6.4.4 Dual-Arm Manipulation

We aim at integrating customized impedance control laws for dual arm manipulation into the whole-body controller from (Henze et al., 2016b). Based on the concept (T. Wimböck, C. Ott, and G. Hirzinger, 2007), we have developed a control system with abilities of balance and manipulation with two arms.

As shown in Figure 6.5, our approach is based on using two spring-dampers. This type of stiffness implementations allows adding the potential function, which is associated with the spatial spring. This characteristic, in turn, is closely related to the concepts of stability and passivity in closed-loop systems. Additionally, this impedance structure allows two different behaviours to be implemented. On the one hand, one behaviour defines the frame of the virtual object H_O, which depends on the end-effectors frames of the right H_R and left H_L arms (Natale, 2003). This virtual object is connected through the spring-damper K_o to the virtual equilibrium position frame H_D, which depends on the CoM frames. In this way, we can control the movement of the grabbed object considering the impedance behaviour of the CoM. On the other hand, we can control the relative motion between the two arms (H_R, H_L) by adding the damper coupling K_c. In this way, we can control the distance between hands when the robot has to go to grasp an object or directly keeping the grip distance. Therefore, with K_o and K_c, we have defined an impedance behaviour which is useful for grabbing large objects with two hands.

In Figure 6.5, the potential function for these two-arm impedance behaviours is defined by the Equation (6.6).

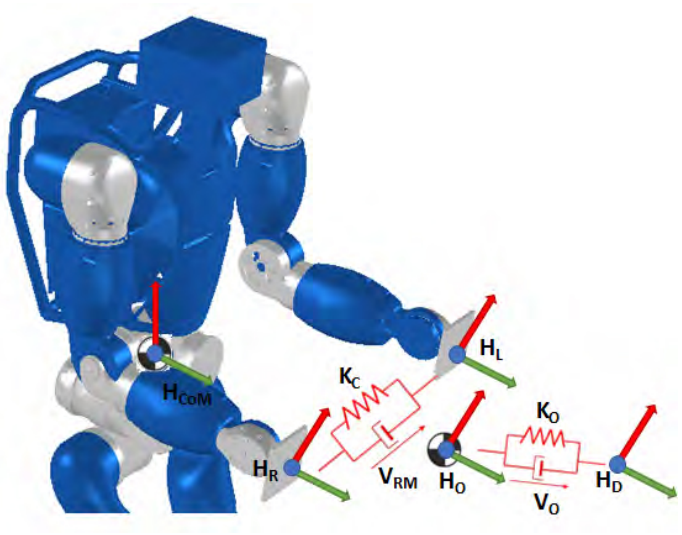

Figure 6.5: *Object and coupling compliance for dual-arm manipulation.*

$$V(\theta) = V_S(H_O(H_R(\theta), H_L(\theta)), H_D(H_{CoM}(\theta)), K_o) + V_S(H_R(\theta), H_L(\theta), K_c) \quad (6.6)$$

The movement of the object can be obtained by the derivation of the Equation (6.6), as shown in (T. Wimböck, C. Ott, and G. Hirzinger, 2007). This movement is represented by the object velocity wrench ($\boldsymbol{v}_o$ and $\boldsymbol{v}_{RM}$) and their relation to the hands' end-effectors velocity wrenches ($\boldsymbol{v}_R$ and $\boldsymbol{v}_L$) for the integration in the controller. In this case, we have defined the relationship between velocities through the transformation matrix $\tilde{\boldsymbol{T}}$. The corresponding transformation $\tilde{\boldsymbol{T}}$ is defined by:

$$\underbrace{\begin{pmatrix} \boldsymbol{v}_c \\ \boldsymbol{v}_{\text{bal}} \\ \boldsymbol{v}_o \\ \boldsymbol{v}_{\text{RM}} \end{pmatrix}}_{\begin{pmatrix} \tilde{\boldsymbol{v}}_c \\ \tilde{\boldsymbol{v}} \end{pmatrix}} = \underbrace{\begin{bmatrix} \boldsymbol{I} & \boldsymbol{0} & \boldsymbol{0} & \boldsymbol{0} \\ \boldsymbol{0} & \boldsymbol{I} & \boldsymbol{0} & \boldsymbol{0} \\ \boldsymbol{0} & \boldsymbol{0} & \gamma\, \boldsymbol{Ad}_{RO} & (1-\gamma)\, \boldsymbol{Ad}_{LO} \\ \boldsymbol{0} & \boldsymbol{0} & \boldsymbol{Ad}_{RO} & -\boldsymbol{Ad}_{LO} \end{bmatrix}}_{\tilde{\boldsymbol{T}}} \underbrace{\begin{pmatrix} \boldsymbol{v}_c \\ \boldsymbol{v}_{bal} \\ \boldsymbol{v}_R \\ \boldsymbol{v}_L \end{pmatrix}}_{\begin{pmatrix} \boldsymbol{v}_c \\ \boldsymbol{v} \end{pmatrix}} \quad (6.7)$$

where $\boldsymbol{v}_o \in \mathbb{R}^6$ is the velocity of the virtual object, $\boldsymbol{v}_{RM} \in \mathbb{R}^6$ is the relative speed between the end-effectors of the hands, $\boldsymbol{v}_R \in \mathbb{R}^6$ is the right hand velocity, $\boldsymbol{v}_L \in \mathbb{R}^6$ is the left hand velocity and $\gamma \in [0; 1]$ is the load distribution factor. $\boldsymbol{Ad}_{RO} \in \mathbb{R}^{6\times6}$ and $\boldsymbol{Ad}_{LO} \in \mathbb{R}^{6\times6}$ are the Adjoint matrices between the right hand and the object and between the left hand and the object respectively.

As explained above, the final goal of the new controller is to achieve bi-manipulation and balance compliance for a humanoid robot, ensuring the passivity and using multi-contacts. The implementation of the balance is maintained as in the previous version and has not been modified ($\boldsymbol{F}_{\text{bal}}^{\text{opt}}$). However, now the rest of the end-effectors act according to the new described behaviour in Figure 6.5.

For this, the bi-manipulation and balancing multi-contact controller is presented in two parts. Firstly, to describe the novel bi-manipulation and balancing behaviour, we change the model in Equation (6.5) into the task space. In order to obtain a representative new dynamic model, the Cartesian coordinates of the interaction end-effectors are replaced with the new task coordinates (in this case the grasped object $\boldsymbol{v}_o$ and $\boldsymbol{v}_{RM}$) through the transformation $\tilde{\boldsymbol{T}}$. Secondly, by employing the definition of the resulting equation for the new model, we derive the controller to compute the torque control $\boldsymbol{\tau}$.

With this model, the bi-manipulation part of the controller will be able to have various skills. Through K_o, the robot can control the object pose for handling tasks. Through K_c, the robot can perform tasks of approaching the hands towards the object and vice versa. The gamma parameter will allow distributing the object load in different ways between the arms. If the load is not uniform or ideally is not at the same distance from the hands' end-effector, the gamma factor can also help to compensate for this inequality.

Moreover, the compliance behaviour helps to absorb external disturbances on the robot. Finally, the model readjustment admits to achieving different tasks. For example, if the virtual object frame is inside of the hands, the task will be focused on transport. If the virtual object frame is outside of the hands, the task will be focused on sweeping.

6.4.5 Integration into Whole-Body Controller

The bi-manipulation and balancing controller should be able of stabilising a fixed equilibrium CoM point. But also, following a given CoM and object trajectories at the same time. Now, the new control architecture is shown in Figure 6.6 and the controller requires the following information from the planner: the desired position $\boldsymbol{x}_c^d \in \mathbb{R}^3$ and orientation of the CoM frame $\mathcal{C}$. Also, it is necessary the desired position $\boldsymbol{x}_o^d \in \mathbb{R}^3$ and orientation $\boldsymbol{R}_o^d \in \mathcal{SO}(3)$ of the object and, of course, the desired position $\boldsymbol{x}_{RM}^d \in \mathbb{R}^3$ and orientation $\boldsymbol{R}_{RM}^d \in \mathcal{SO}(3)$ of the relative motion between the hands.

This controller is divided in two wrench distribution. The first one, the balance wrench distribution ($\boldsymbol{F}_{\text{bal}}^{\text{opt}}$) is computed by the force wrench of the CoM ($\boldsymbol{F}_c^{\text{cpl}}$) (through the CoM compliance) and the feedforward wrench ($\boldsymbol{F}_{ff}$) (through the Feedforward Terms). This feedforward wrench has been adapted to the new dynamic model.

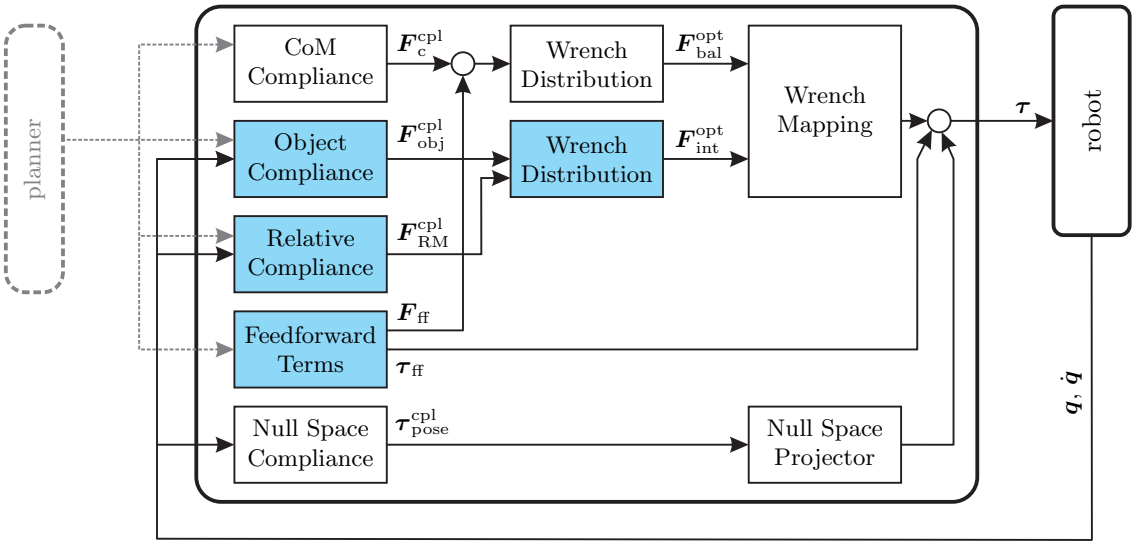

Figure 6.6: *Control architecture with the new wrench distribution system related to the dual-arm manipulation.*

The second one, the object interaction wrench distribution ($\boldsymbol{F}_{\text{int}}^{\text{opt}}$) is calculated with the force wrench of the object ($\boldsymbol{F}_{o}^{\text{cpl}}$) (through the Object compliance) and the the force wrench of the relative motion ($\boldsymbol{F}_{RM}^{\text{cpl}}$) (through the Relative compliance). The last part is a null space control (Null Space Compliance and Projector) and it is the same as the previous version.

Finally, the joint torques applied to the robot is a sum of three parts. a) The wrench mapping transforms the balance and object interaction wrenches ($\boldsymbol{F}_{\text{bal}}^{\text{opt}}$ and $\boldsymbol{F}_{\text{int}}^{\text{opt}}$) into torques. b) The Feedforward control also compute another part of the torques. And c) the Null Space control generates the third part of the torques (τ_{ff}). However, to understand the calculation of the joint torques to apply on the robot, firstly, we must obtain the dynamic model of the robot by applying the transformed model on the previous model (6.5) with matrix $\tilde{\boldsymbol{T}}$ in the new task space:

$$\tilde{\boldsymbol{\Lambda}} \begin{pmatrix} \dot{\tilde{\boldsymbol{v}}}_c \\ \dot{\tilde{\boldsymbol{v}}} \end{pmatrix} + \tilde{\boldsymbol{\mu}} \begin{pmatrix} \tilde{\boldsymbol{v}}_c \\ \tilde{\boldsymbol{v}} \end{pmatrix} + \tilde{\boldsymbol{T}}^{-T} \boldsymbol{g} = \tilde{\boldsymbol{T}}^{-T} \begin{bmatrix} -\boldsymbol{A}\boldsymbol{d}^T \\ \boldsymbol{I} \end{bmatrix} \boldsymbol{J}^{-T} \boldsymbol{\tau} + \tilde{\boldsymbol{\tau}}_{\text{ext}} \tag{6.8}$$

where $\tilde{\boldsymbol{\Lambda}} = \tilde{\boldsymbol{T}}^{-T} \boldsymbol{\Lambda} \tilde{\boldsymbol{T}}^{-1}$ and $\tilde{\boldsymbol{\mu}} = \tilde{\boldsymbol{T}}^{-T} \boldsymbol{\mu} \tilde{\boldsymbol{T}}^{-1} + \tilde{\boldsymbol{T}}^{-T} \boldsymbol{\Lambda} \frac{d}{dt} (\tilde{\boldsymbol{T}}^{-1})$. The generalised external forces are given by $\tilde{\boldsymbol{\tau}}_{\text{ext}} \in \mathbb{R}^{6+n}$. And $\boldsymbol{Ad}$ is the rotated grasp matrix, providing a mapping between the set of end-effectors wrenches and the total wrench at the CoM.

From a predefined trajectory and taking in considerations deviations in orientation, position and velocity, we chose the behaviour of the desired closed-loop system:

$$\tilde{\boldsymbol{\Lambda}} \begin{pmatrix} \Delta\dot{\boldsymbol{v}}_c \\ \Delta\dot{\boldsymbol{v}}_{\text{bal}} \\ \Delta\dot{\boldsymbol{v}}_o \\ \Delta\dot{\boldsymbol{v}}_{\text{RM}} \end{pmatrix} + \tilde{\boldsymbol{\mu}} \begin{pmatrix} \Delta\boldsymbol{v}_c \\ \Delta\boldsymbol{v}_{\text{bal}} \\ \Delta\boldsymbol{v}_o \\ \Delta\boldsymbol{v}_{\text{RM}} \end{pmatrix} = \tilde{\boldsymbol{\tau}}_{\text{ext}} - \begin{pmatrix} \boldsymbol{F}_c^{\text{cpl}} \\ \boldsymbol{F}_{\text{bal}}^{\text{opt}} \\ \boldsymbol{F}_o^{\text{cpl}} \\ \boldsymbol{F}_{\text{RM}}^{\text{cpl}} \end{pmatrix} \tag{6.9}$$

If we compare Equation (6.9) with Equation (6.8), the identification of the required control law for the torques $\boldsymbol{\tau}$ is:

$$\tilde{\boldsymbol{T}}^{-T} \begin{bmatrix} -\boldsymbol{A}\boldsymbol{d}^T \\ \boldsymbol{I} \end{bmatrix} \boldsymbol{J}^{-T}\boldsymbol{\tau} = \tilde{\boldsymbol{\Lambda}} \begin{pmatrix} \dot{\boldsymbol{v}}_c^d \\ \dot{\boldsymbol{v}}_{\text{bal}}^d \\ \dot{\boldsymbol{v}}_o^d \\ \dot{\boldsymbol{v}}_{\text{RM}}^d \end{pmatrix} + \tilde{\boldsymbol{\mu}} \begin{pmatrix} \boldsymbol{v}_c^d \\ \boldsymbol{v}_{\text{bal}}^d \\ \boldsymbol{v}_o^d \\ \boldsymbol{v}_{\text{RM}}^d \end{pmatrix} + \boldsymbol{g} - \begin{pmatrix} \boldsymbol{F}_c^{\text{cpl}} \\ \boldsymbol{F}_{\text{bal}}^{\text{opt}} \\ \boldsymbol{F}_o^{\text{cpl}} \\ \boldsymbol{F}_{\text{RM}}^{\text{cpl}} \end{pmatrix} \tag{6.10}$$

Considering that $\boldsymbol{F}_{\text{bal}}^{\text{opt}}$ and $\boldsymbol{\tau}$ are the rest of the free variables in Equation (6.10), they can be determined in two steps using this equation. Firstly, the characterisation of the external load calculate the task wrenches $\boldsymbol{F}_c^{\text{cpl}}$, $\boldsymbol{F}_{\text{bal}}^{\text{opt}}$, $\boldsymbol{F}_o^{\text{cpl}}$. Secondly, the representation of the internal load calculate the control torque $\boldsymbol{\tau}$

So, dividing Equation (6.10) in two parts:

$$-\ \tilde{\boldsymbol{T}}^{-T}\,\boldsymbol{A}\boldsymbol{d}^T(\boldsymbol{J}^{-T}\boldsymbol{\tau}) \ = \ \tilde{\boldsymbol{\Lambda}}_1 \begin{pmatrix} \dot{\boldsymbol{v}}_c^d \\ \dot{\boldsymbol{v}}_{\text{bal}}^d \\ \dot{\boldsymbol{v}}_o^d \\ \dot{\boldsymbol{v}}_{\text{RM}}^d \end{pmatrix} \ + \ \tilde{\boldsymbol{\mu}}_1 \begin{pmatrix} \boldsymbol{v}_c^d \\ \boldsymbol{v}_{\text{bal}}^d \\ \boldsymbol{v}_o^d \\ \boldsymbol{v}_{\text{RM}}^d \end{pmatrix} \ + \ m\boldsymbol{g}_0 \ - \ \boldsymbol{F}_c^{\text{cpl}} \tag{6.11}$$

$$\tilde{\boldsymbol{T}}^{-T}(\boldsymbol{J}^{-T}\boldsymbol{\tau}) \quad = \quad \tilde{\boldsymbol{\Lambda}}_2 \begin{pmatrix} \dot{\boldsymbol{v}}_c^d \\ \dot{\boldsymbol{v}}_{\text{bal}}^d \\ \dot{\boldsymbol{v}}_o^d \\ \dot{\boldsymbol{v}}_{\text{RM}}^d \end{pmatrix} \ + \ \tilde{\boldsymbol{\mu}}_2 \begin{pmatrix} \boldsymbol{v}_c^d \\ \boldsymbol{v}_{\text{bal}}^d \\ \boldsymbol{v}_o^d \\ \boldsymbol{v}_{\text{RM}}^d \end{pmatrix} \ - \ \begin{pmatrix} \boldsymbol{F}_{\text{bal}}^{\text{opt}} \\ \boldsymbol{F}_o^{\text{cpl}} \\ \boldsymbol{F}_{\text{RM}}^{\text{cpl}} \end{pmatrix} \tag{6.12}$$

where we can describe $\tilde{\boldsymbol{\Lambda}} = [\tilde{\boldsymbol{\Lambda}}_1^T \tilde{\boldsymbol{\Lambda}}_2^T]^T$ and $\tilde{\boldsymbol{\mu}} = [\tilde{\boldsymbol{\mu}}_1^T \tilde{\boldsymbol{\mu}}_2^T]^T$ with $\tilde{\boldsymbol{\Lambda}}_1, \tilde{\boldsymbol{\mu}}_1 \in \mathbb{R}^{6\times 6+6\psi}$ and $\tilde{\boldsymbol{\Lambda}}_2, \tilde{\boldsymbol{\mu}}_2 \in \mathbb{R}^{6\psi\times 6+6\psi}$. Therefore, based on this new variables and comparing (10) and (11) without the common variable $\boldsymbol{J}^{-T}\boldsymbol{\tau}$ yields to:

$$\tilde{\boldsymbol{Ad}}^T \begin{pmatrix} \boldsymbol{F}_{\text{bal}}^{\text{opt}} \\ \boldsymbol{F}_{o}^{\text{cpl}} \\ \boldsymbol{F}_{\text{RM}}^{\text{cpl}} \end{pmatrix} = \underbrace{(\tilde{\boldsymbol{\Lambda}}_1 + \tilde{\boldsymbol{Ad}}^T \tilde{\boldsymbol{\Lambda}}_2) \begin{pmatrix} \dot{\boldsymbol{v}}_c^d \\ \dot{\boldsymbol{v}}_{\text{bal}}^d \\ \dot{\boldsymbol{v}}_o^d \\ \dot{\boldsymbol{v}}_{\text{RM}}^d \end{pmatrix} + (\tilde{\boldsymbol{\mu}}_1 + \tilde{\boldsymbol{Ad}}^T \tilde{\boldsymbol{\mu}}_2) \begin{pmatrix} \boldsymbol{v}_c^d \\ \boldsymbol{v}_{\text{bal}}^d \\ \boldsymbol{v}_o^d \\ \boldsymbol{v}_{\text{RM}}^d \end{pmatrix}}_{\text{feedforward}=\boldsymbol{F}_{ff}} + \underbrace{m\boldsymbol{g}_0}_{\text{gravity compensation}} - \underbrace{\boldsymbol{F}_c^{\text{cpl}}}_{\text{feedback}} \tag{6.13}$$

with $\tilde{\boldsymbol{Ad}} = \tilde{\boldsymbol{T}}\, \boldsymbol{Ad}\, \tilde{\boldsymbol{T}}^{-1}$. On the one side, the right side of the Equation (6.13) can be interpreted as the general wrench in the CoM. The controller has to create this wrench for the stability task of the robot. As in PD+ control, the feedforward component, the gravity compensation and the feedback part compose this wrench (Paden and Panja, 1988). On the other side, the wrenches of the TCPs gives the left side of the equation. The desired wrench in the CoM has to be added to these wrenches.

However, there is an important detail. The transformed Adjoint matrix $\tilde{\boldsymbol{Ad}}$ in Equation (6.13) has 6 lines and $\boldsymbol{F}_{\text{bal}}^{\text{opt}}$ has a size of $6\psi_{\text{bal}}$. Therefore, if the robot is using for balancing more than one end-effector ($\psi_{\text{bal}} > 1$), it is not possible to compute $\boldsymbol{F}_{\text{bal}}^{\text{opt}}$ directly. To solve this issue, we apply the constrained quadratic optimization problem, like in (Henze et al., 2016b). With this method, we can avoid the redundancy in $\tilde{\boldsymbol{Ad}}$ and its force distribution problem.

After determining the wrench distribution $\boldsymbol{F}_{\text{bal}}^{\text{opt}}$ for the balancing end-effectors, the torque mapping can be calculated, employing Equation (6.12):

$$\boldsymbol{\tau} = \underbrace{\boldsymbol{J}^T \tilde{\boldsymbol{T}}^T \left(\tilde{\boldsymbol{\Lambda}}_2 \begin{pmatrix} \dot{\boldsymbol{v}}_c^d \\ \dot{\boldsymbol{v}}_{\text{bal}}^d \\ \dot{\boldsymbol{v}}_o^d \\ \dot{\boldsymbol{v}}_{\text{RM}}^d \end{pmatrix} + \tilde{\boldsymbol{\mu}}_2 \begin{pmatrix} \boldsymbol{v}_c^d \\ \boldsymbol{v}_{\text{bal}}^d \\ \boldsymbol{v}_o^d \\ \boldsymbol{v}_{\text{RM}}^d \end{pmatrix} \right)}_{\text{feedforward}=\boldsymbol{\tau}_{ff}} - \boldsymbol{J}^T \begin{pmatrix} \boldsymbol{F}_{\text{bal}}^{\text{opt}} \\ \boldsymbol{F}_{\text{int}}^{\text{opt}} \end{pmatrix} \tag{6.14}$$

Note that the wrench distribution for the hands is given by

$$\boldsymbol{F}_{\text{int}}^{\text{opt}} = \begin{bmatrix} \gamma\, \boldsymbol{Ad}_{RO}^T & \boldsymbol{Ad}_{RO}^T \\ (1-\gamma)\, \boldsymbol{Ad}_{LO}^T & -\boldsymbol{Ad}_{LO}^T \end{bmatrix} \begin{pmatrix} \boldsymbol{F}_{o}^{\text{cpl}} \\ \boldsymbol{F}_{\text{RM}}^{\text{cpl}} \end{pmatrix} \tag{6.15}$$

based on Equation (6.7). The parameter $\gamma \in [0, 1]$ determines the portion of $\boldsymbol{F}_o^{\text{cpl}}$ that is mapped to the right and the left hand, respectively.

6.5 Conclusions

Chapter 6 has focused on the integration of all previous threads. For the integration of body and object controllers, the WBPC architecture has been used. This architecture is based on the multiple ZMP evaluation and the stability interrelation between the object and the robot. In this way, the exposed methods for the calculation of the stability consider the influences between them obtaining promising results. Also, we can extrapolate this architecture to bi-manipulation tasks for the same reason explained in the previous paragraph.

This achievement has also allowed us to verify the adaptation of our bi-manipulation system in another totally different robotic platform. In this case, the TORO humanoid robot is not rigid, but compliance. However, the process of planning the movement of the tray is identical in both cases (TEO and TORO). In both, we use the forces and torque of the hands to compute the performance of the tray. To verify this condition, we developed a new dynamic WB control model adding the handling capacity to the TORO robot. The results after applying our manipulation on the compliance system have been very satisfactory.

Part III

Experimentation and Conclusions

Chapter 7

Experiments and Results

7.1 Introduction

All the experiments carried out for this thesis are explained in this chapter 7. The purpose of this organisation is to visualise the progress we have made to get a waiter robot. The evolution of these experiments is written from less to more complex.

This chapter of experiments is ordered as follows. Sections 7.2 and 7.3 focus on testing the stability individually the behaviour of the body and the object. Section 7.4 are divided into three important parts. Subsection 7.4.1 validate the integration the two previous controllers of the body and the object in a Whole-Body task. Subsection 7.4.2 verifies the extension of bi-manipulation with a rigid robot. And subsection 7.4.3 the integrated bi-manipulated system on the compliance robot TORO is tested. Finally, in the last section 7.5, some conclusions are summarised.

7.2 Testing the Body Balance based on Models

In chapter 4, we have studied the problems related to the stability of a humanoid robot. On the one hand, the use of ZMP controllers based on simplified models generated errors based on linearisation. On the other hand, with the use of such simplified models, other errors appeared mainly based on the mechanics of the robot and the electronics of the sensors. All these errors made it difficult to implement a stability controller. Therefore, we have investigated the readjustment of simplified models. On the one hand, we have modelled and integrated these errors on the LIPM model (obtaining the DLIPM model). On the other hand, starting from the DLIPM model, we have tuned the robot parameters in the CT model, to adapt it to a more realistic behaviour.

7.2.1 Study the Force-Torque System in the DLIPM.

The purpose of this experiment is to validate the DLIPM model. In more detail, this experiment shows how the new simplified model dynamically adapts without modifying anything of the robot's mechatronic system (the F-T perception system and the robot's mechanical structure)

Set Up - 1° Experiment

To validate the usefulness of the new proposed model, we have tested experimentally by performing a set of trials for evaluating the response of the control system against a change on the ZMP target. The DLIPM state-space model has been customised with the parameters for each ZMP target, following the step pattern. Then, the outputs of the model have been the customised angle commands following the ZMP planning.

Results - 1° Experiment

Table 7.1 shows numeric results of the ZMP locations, comparing the values obtained from the classical approach and the DLIPM approach. It can be observed that the static error is reduced in each working point. Even in the most critical ZMP location ($ZMP = 10cm$), the error was reduced by more than 80% when comparing the obtained ZMP measurements using the classical LIPM and the compensated model proposed in this dissertation.

ZMP_{REF} (m)	$ZMP_{F\ T}$ (m)			
	LIPM Model	% Error	DLIPM Model	% Error
0.00	5×10^{-5}	0.0	2×10^{-7}	0.0
0.01	0.0092	0.8	0.0100	0.0
0.02	0.0211	1.1	0.0201	0.1
0.03	0.0306	0.6	0.0310	1.0
0.04	0.0419	1.9	0.0412	1.2
0.05	0.0547	4.7	0.0512	1.2
0.06	0.0641	4.1	0.0620	2.0
0.07	0.0756	5.6	0.0714	1.4
0.08	0.0841	4.1	0.0816	1.6
0.09	0.0958	5.8	0.0898	0.2
0.10	0.1116	11.6	0.1020	2.0

Table 7.1: *ZMP comparison using the LIPM and DLIPM.*

Data from Table 7.1 have been depicted in Figure 7.1. We can observe that the error in the classical system is higher when the ZMP location is further from the initial zero position (ZMP_{LIPM}). Furthermore, the DLIPM curve (ZMP_{DLIPM}) is better adjusted to the desired linear response (ZMP_{LIN}).

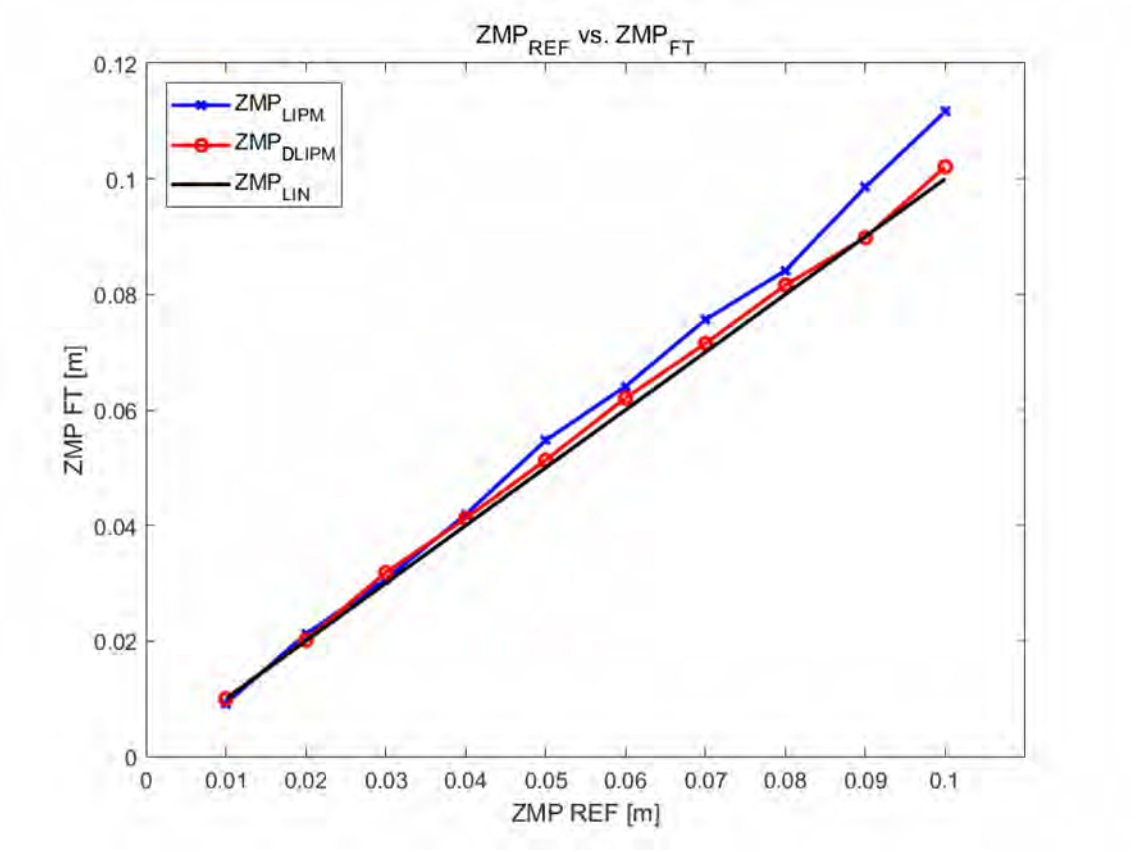

Figure 7.1: *ZMP comparison using the LIPM and DLIMP.*

Concerning the dynamic response of the system, Figure 7.2 depicts the results of all the trials performed. Comparing this figure with Figure 4.8, it is easy to observe that the level and the duration of oscillations have been reduced. While the overshooting has similar levels in some experiments, the state of the robot is stabilised in general earlier than the classical architecture.

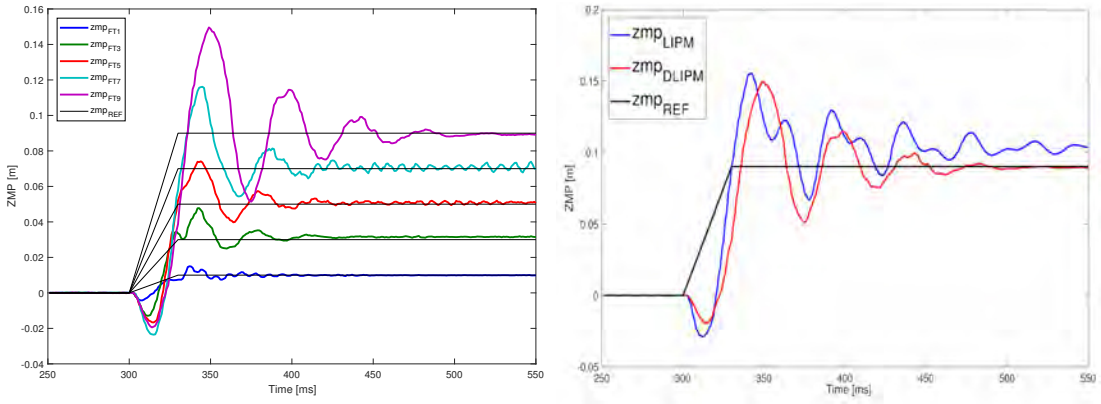

(a) (b)

Figure 7.2: *Comparison of ZMP step responses. (**a**) Step response experiments on DLIPM; (**b**) Comparison between the LIPM and DLIPM for ZMP = 9 cm.*

7.2.2 Experiments with the Inertial System for the Cart-Table

The goal of this experiment is to verify the parametric adjustment for the CT model. In more detail, this experiment shows how the new values for the parameters of the robot with the cart-table model reduce the ZMP error. In this case and again, we have not modified anything of the robot's mechatronic system (the inertial perception system and the robot's mechanical structure)

Set Up - 2º Experiment

The validation of the new robot parameters on the CT model has been performed in the same way as with the DLIPM model. We have tested a set of tests to evaluate the response of the control system against a change in the ZMP objective. In this case, the robot parameters are not dynamically adjusted but remain constant. Finally, we have commanded custom angles again following the ZMP planning based on the results of the tuned CT model.

Results - 2º Experiment

Table 7.2 summarises the results of the ZMP locations, comparing the values obtained from the tuned and unprocessed CT model and also concerning the DLIPM model. We can see that the static error has been reduced again at each work point. Even with the most critical ZMP ($ZMP = 9cm$), the error has been reduced again by more than 80 % when comparing the ZMP measurements obtained using the classic LIPM and the compensated model proposed in this thesis.

ZMP_{REF} (m)	ZMP_{IMU} (m)			
	pre-CT Model	% Error	Adj-CT Model	% Error
0.01	0.0109	0.9	0.0105	0.5
0.03	0.0312	1.2	0.0305	0.5
0.05	0.0491	0.9	0.0510	1.0
0.07	0.0672	2.8	0.0697	0.3
0.09	0.0839	6.1	0.0889	1.1

Table 7.2: *ZMP comparison using the LIPM and DLIPM.*

Data from Table 7.2 have been depicted in Figure 7.3. In this case with the CT model, we can appreciate that the error with the real robot parameters values of the robot ($ZMP_{CT}(after)$) is higher when the ZMP location is further from the initial zero position (ZMP_{REF}). Furthermore, the tuned CT model curve ($ZMP_{CT}(before)$) is better adjusted to the desired linear response (ZMP_{REF}).

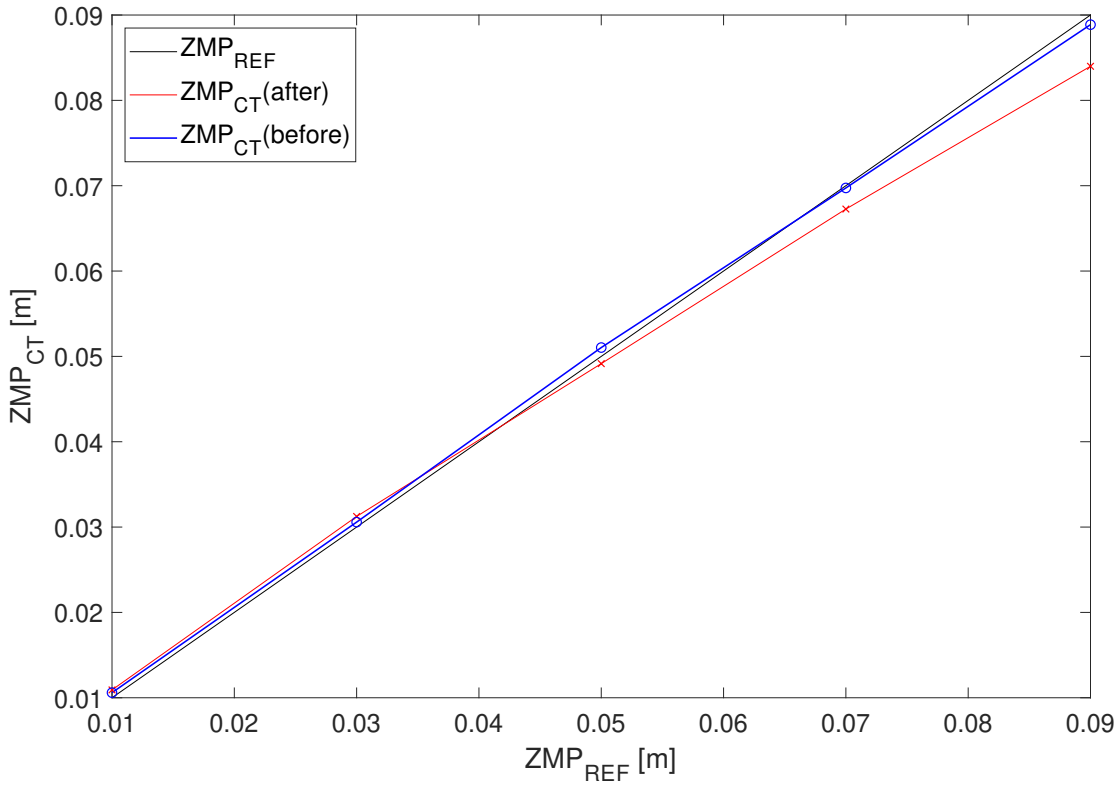

Figure 7.3: *ZMP comparison after/before the adjustment of the CT.*

Concerning the dynamic response of the system, Figure 7.2 depicts the results from all the trials performed with the CT model. Comparing this figure with Figure 4.15, we can conclude that there is no representative improvement. The transient response of the tuned CT model is very similar because the modification of the parameters does not influence its behaviour. For this case, if we want the response to be faster, we should change the frequency of the low-pass filters of the inertial sensor. However, we have not contemplated this particular case in this thesis.

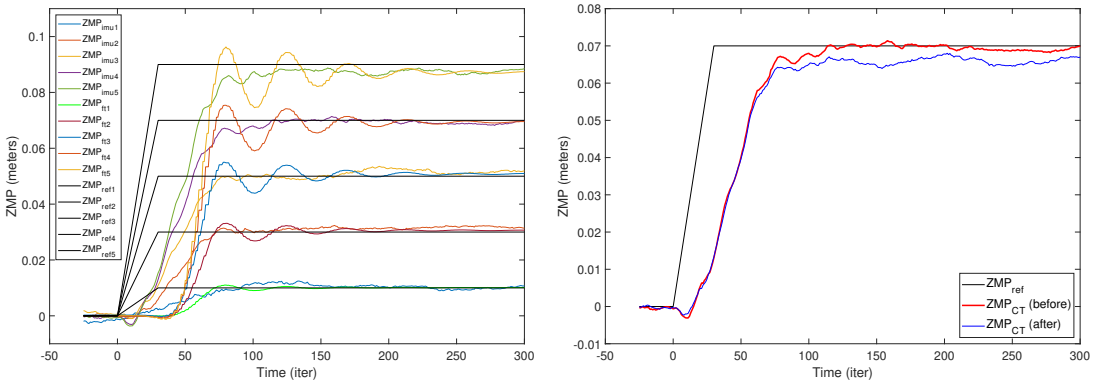

(a) (b)

Figure 7.4: *Comparison of ZMP step responses in CT. (a) Step response experiments on DLIPM and CT; (b) Comparison of the adjustment in the CT for ZMP = 7 cm.*

For both the DLIPM model and the parametric adjustment of the CT model, we have obtained excellent results. In the case of the DLIPM model, we have laid the foundations to be able to implement a model-based balance controller. This controller is designed to operate at multiple work points, minimising the error in each of them. In this way, we are fulfilling two crucial aspects with the DLIPM: the progression of the ZMP between two consecutive positions and the level of error in each ZMP. In the first case, a smoother trajectory between the locations has been achieved, with the decrease in the number of unwanted oscillations, especially in critical locations of ZMP. In the second case, the error between the desired ZMP location and the measured ZMP has been reduced.

In the case of the tuned CT model, we can conclude that the parametric adjustment method based on other models also works well. The error level of the ZMP has been considerably reduced, obtaining very similar values between the desired ZMP location and the ZMP measured by the inertial sensor. Additionally, the most important of this research in both models is the methodology based on experimental (not theoretical) adjustments with the robot. This one has allowed modelling the unknown behaviour of a robot and adjusting it only through push-recovery experiments, which are replicable in any humanoid robot.

7.3 Object Balance Control with Fusion Sensor

7.3.1 Experiments with the Visual Correction System

In this section, we describe the experiments related to the Fuzzy filter to validate its performance against different situations. The standard procedure followed during the experiments consists of positioning the bottles in the different areas depicted in Figure 7.5. Then, the camera captures the image of the bottle, and the Fuzzy algorithm proposed is applied to obtain the bottle angle. We have performed two different experiments.

Set Up - 3º Experiment

In this first experiment, the main goal is to evaluate the visual correction algorithm in the central visual area for a constant bottle angle. Several sweeps in the central horizontal row have been done, as shown in Figure 7.5. During these sweeps, the bottle has been maintained entirely straight, with an angle of 90 degrees in relation to the horizontal plane, keeping the bottle straight and keeping the axis of the pixel coordinate Y constant.

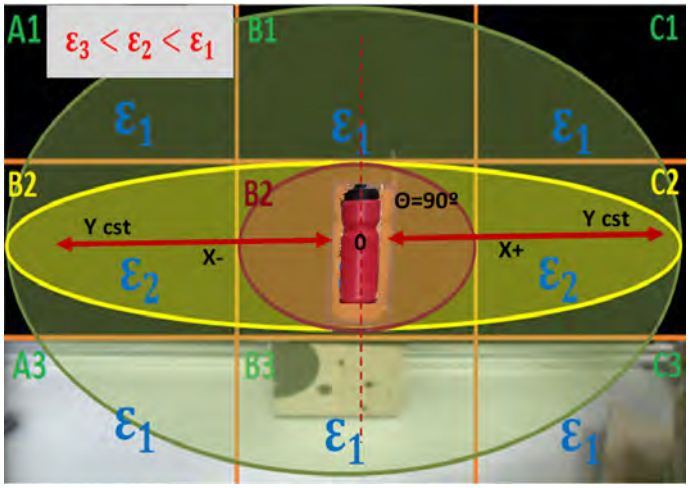

Figure 7.5: *First evaluation set up sweeping the central horizontal row.*

The images obtained with the robot camera have been post-processed (following the steps in 5.4.3), and the information extracted from those images has been stored in a cluster be processed by the Fuzzy filter. This cluster is made up by the position of the geometrical centre of the bottle in the pixel X and pixel Y, and the inclination angle perceived by the camera. After having processed this information through the Fuzzy filter, the estimated real tilt angle of the bottle has been obtained.

Results - 3º Experiment

In Figure 7.6, the *Y-Axis* represents the inclination angles, whereas the *X-Axis* represents the different existing pixels in the *X-Axis* of the image. In this graphic, two different lines can be seen. The blue one represents the angle perceived by the humanoid robot in the different positions of the pixel coordinate *X*. It can be seen that, when the bottle is next to the lateral limits of the image, the error that is introduced increases. The real angle of the bottle in the experiment was kept constant (90 degrees). However, while the bottle is next to the centre of the image, this error disappears, and some correction is needed. Due to the explanation related to Figure 7.5, the behaviour of the information acts as expected. Considering that the obtained images have about 283 pixels in the *X-Axis*, if we divide it into three quadrants, the number of pixels per quadrant would be about 95. Therefore, it can be seen in the graphic that the error is higher in the lateral ones. Additionally, this blue signal is also very noisy. The origin of this instability is caused by the error introduced in the vision systems by the illumination conditions, which can affect the recognition of the bottle.

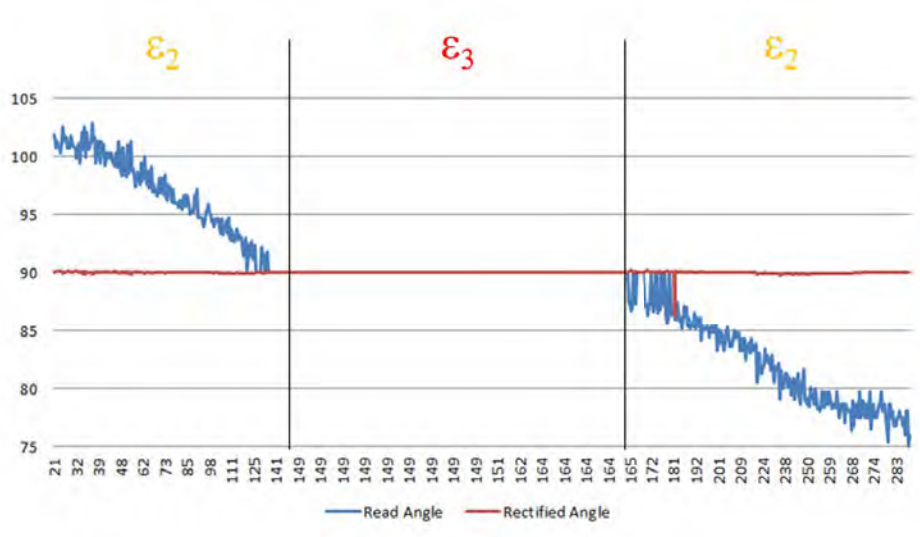

Figure 7.6: *Results from the first experiment.*

After having post-processed the information with the Fuzzy filter, the error was corrected, and the obtained angle has been 90 degrees. The red line shows this corrected information. As can be seen in the graph, this red line is close to 90 degrees. Knowing that the experiment has been performed with a real angle of the bottle equal to 90 degrees, we have evaluated the higher value of the red line and the calculated error of the system for this experiment is not higher than 0.0172 degrees. This error completely fulfils our established requirement of obtaining an angle with an error below 0.5 degrees.

Set Up - 4º Experiment

Once we have demonstrated the reliability of the Fuzzy filter in a controlled situation, such as a horizontal scan, we have performed a second more complicated experiment. In this case, we have placed the bottle in the tray attached to the robot. So, the arm makes sweeps the bottle, locating it in the different quadrants in which the image has been divided.

This second experiment has been carried out by placing the bottle on different inclinations. These inclinations are measured manually and known before the experiment. In this case, the objective of this second experiment is to verify the ability to properly rectify the visual data with the Fuzzy filter outside its training zone. For this, we have studied different bottle inclination angles in different quadrants where the bottle is located at that time.

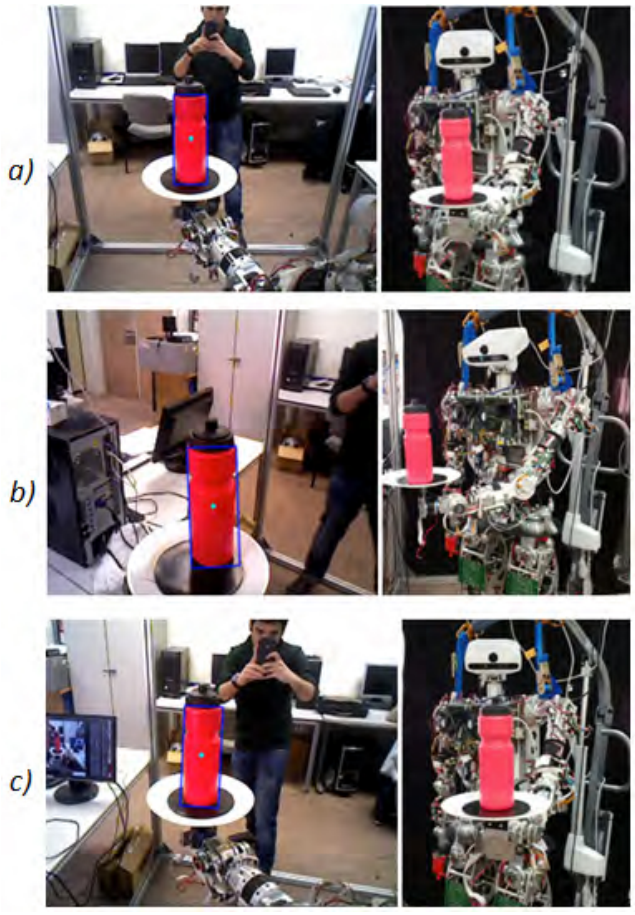

Figure 7.7: *Positioning the bottle in different inclination angles and quadrants. (a) Bottle at robot left side (inclination 87 degrees); (b) Bottle at the front of the robot (inclination 90 degrees) and (c) Bottle at robot left side (inclination 90degrees).*

We have divided this experiment into two phases. In the first part, the bottle has been placed in the tray that holds the robot, and the robot arm has moved it throughout the room (Figure 7.7). The robot camera has recorded all those movements of the bottle. From these movements, the information related to the position in the image coordinate in pixels (pixel X and pixel Y), and the angle of inclination detected ($\alpha_{measured}$) are stored in another cluster time. In summary, in Table 7.3, some of the values obtained and more significant are shown. It is important to note that the angle of inclination detected ($\alpha_{measured}$) is different from the real angle (α_{real}).

In the second part (and the most important), the information stored in this cluster has been processed by the Fuzzy filter, which applies the corresponding correction in the angle of inclination detected for the bottle using the filter created by the ANFIS tool. After applying the corresponding angular correction on the error surface ($\Delta F_{Correction}$), the new corrected angles ($\alpha_{corrected}$) are saved again for later comparison. This processed information must correspond to the original inclination angle (α_{real}) of the bottle at all times.

Results - 4º Experiment

Table 7.3 shows the results of the first phase. Through the different arm sweeps of the humanoid robot, we have saved all the data in the cluster. At first glance, we can already see the effect of perspective and others on the detected angle ($\alpha_{measured}$).

Table 7.3: *Angle measured by computer vision knowing the real angle previously.*

Point	**Pixel X/Y**	$\boldsymbol{\alpha_{real}}$ **(deg)**	$\boldsymbol{\alpha_{measured}}$ **(deg)**
P1	270/157	81	68.159
P2	26/62	81	93.0146
P3	294/149	99	83.405
P4	44/66	99	107.354
P5	282/152	87	74.0545
P6	43/69	87	98.7461
P7	286/148	93	76.7594
P8	35/62	93	103.3924
P9	131/67	90	91.1691

Then in Table 7.4, the results of the second phase are shown. Now, all the data previously saved in the cluster (shown in table 7.3) is processed by the Fuzzy filter, applying the Fuzzy correction ($\Delta F_{Correction}$) and obtaining the new corrected angles ($\alpha_{corrected}$).

Table 7.4: *Angle corrected by the Fuzzy filter related to the saved cluster.*

Point	$\Delta F_{Correction}$ (deg)	$\alpha_{corrected}$ (deg)
P1	−18.5025	86.6615
P2	8.6881	84.3265
P3	−6.3794	89.7844
P4	20.4483	86.9057
P5	−13.3798	87.4343
P6	9.0118	89.7343
P7	−13.2984	90.0578
P8	12.816	90.5764
P9	0.9414	90.2277

As we can see in the results shown in Table 7.5, the angle detected ($\alpha_{measured}$) by the camera differs from the real one (α_{real}). However, after processing the cluster, the results between the corrected angle ($\alpha_{corrected}$) and the real angles (α_{real}) of the bottle are quite similar. It is true that, in some cases, there is still a high error rate. This effect means that we must increase the training dataset to improve the Fuzzy filter response. Even with the most critical angles ($\alpha_{real} = [81^o, 99^o]$), the error has been reduced by more than 40% when comparing the error of the angle detected ($\%Error_{Camera}$) and the error of the angle corrected ($\%Error_{Fuzzy}$).

Table 7.5: *Comparison of the angles obtained using the Fuzzy filter.*

α_{real} (deg)	$\alpha_{measured}$ (deg)	% Error Camera	$\alpha_{corrected}$ (deg)	% Error Fuzzy
81	68.159	15.83	86.6615	6.9
81	93.0146	14.83	84.3265	4.1
99	83.405	15.75	89.7844	9.3
99	107.354	8.43	86.9057	12.2
87	74.0545	14.87	87.4343	0.5
87	98.7461	13.50	89.7343	3.1
93	76.7594	17.46	90.0578	3.2
93	103.3924	11.17	90.5764	2.6
90	91.1691	1.29	90.2277	0.2

Therefore, we can validate the behaviour of the Fuzzy filter for the reduction of visual errors. Moreover, since this method is totally experimental and does not consider the characteristics of the camera, we can apply it to any vision system.

7.3.2 Study the Force-Torque System in the Tray. Part 2.

In this section, the results of the proposed 3D Dynamic Slope method for ZMP calculations are discussed in four parts. The tests have been carried out on TEO humanoid robot using the YARP middleware platform.

Set Up - 5º Experiment

For this set-up experiment, four tests have been carried. All tests try to verify the 3D dynamic slope concept, applying four different slopes. For this purpose, the tray will be reoriented in the Cartesian space, rotating on a fixed point (the origin of the SoC_{tray}) to change the slope (the inclination of the tray).

In all the figures in this section, three variables are shown. $Ang_{ref-tray}$ is the orientation angle (slope) applied to the tray. β and β' are the calculation of the theoretical angle that the tray is having for the X-axis and the Y-axis, respectively. These values are calculated from transformed forces $F''x$, $F''y$ and $F''z$. And X_{zmp} and Y_{zmp} are the values of stability of the bottle according to the equations 5.5 and 5.6 and to the $Ang_{ref-tray}$ angle.

The first two experiments evaluate the ZMP for **positive** slopes. The range of slope values is [0,9] degrees. In Figure 7.8, the slope of the tray changes with positive values and rotates respect to the X-axis of SoC_{tray}. In Figure 7.9, the slope of the tray changes with positive values too and rotates respect to the Y-axis of SoC_{tray}.

The other two experiments are very similar. They evaluate the ZMP for **negative** slopes. The range of inclination values is [-9,0] degrees. In Figure 7.10, the slope of the tray changes with negative values and rotates respect to the X-axis of SoC_{tray}. In Figure 7.11, the slope of the tray changes with negative values too and rotates respect to the Y-axis of SoC_{tray}.

Results - 5º Experiment

In Figures 7.8 and 7.9, for positive slopes, the β and β' angles are reasonably close to the reference. The error does not exceed 5%. And there is no notable difference in the rotation between the X-axis and the Y-axis. Also, the ZMP values are consistent with the $Ang_{ref-tray}$ angle; the same value of ZMP is obtained in both axes.

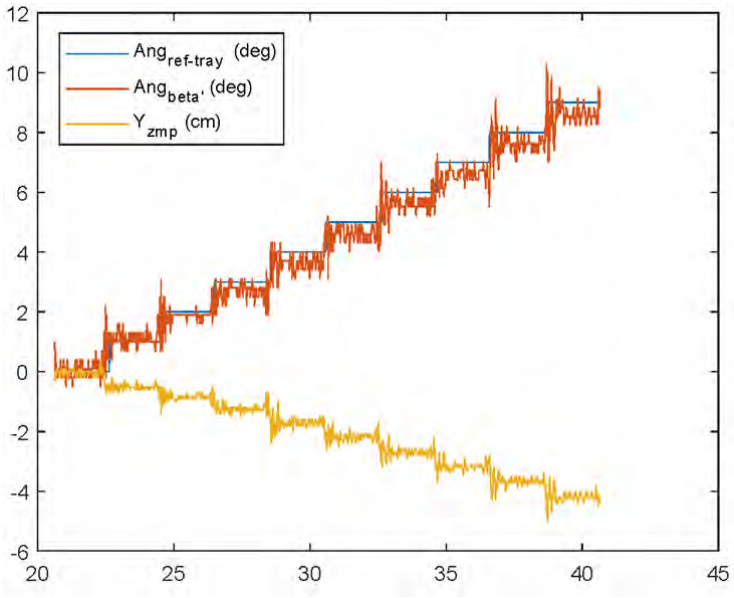

Figure 7.8: *Evaluation of positive slopes in the X-axis.*

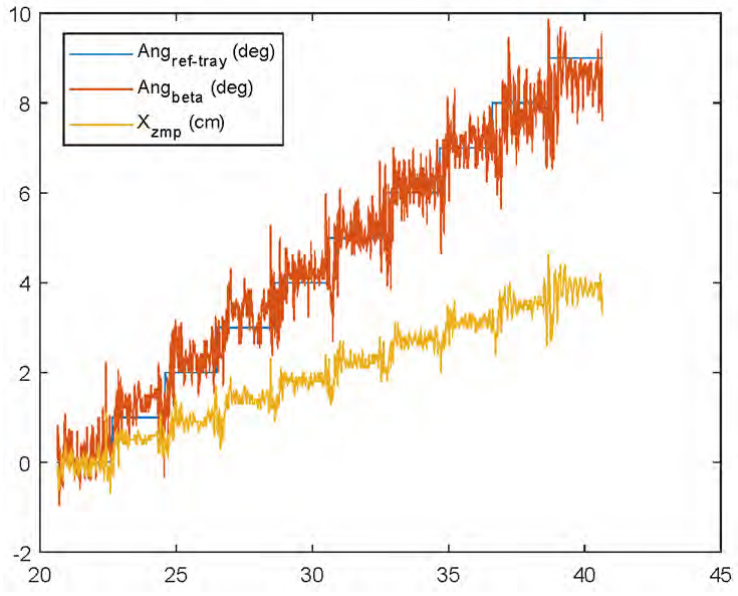

Figure 7.9: *Evaluation of positive slopes in the Y-axis.*

The same argument is valid for negative slopes in Figures 7.10 and 7.11. Both β and β' angles coincide with the reference $Ang_{ref-tray}$. The error continues to be less than 5%. Also, the ZMP behaviour is good. In fact, also in these experiments, both X_{zmp} and Y_{zmp} have the same value for the same $Ang_{ref-tray}$ reference.

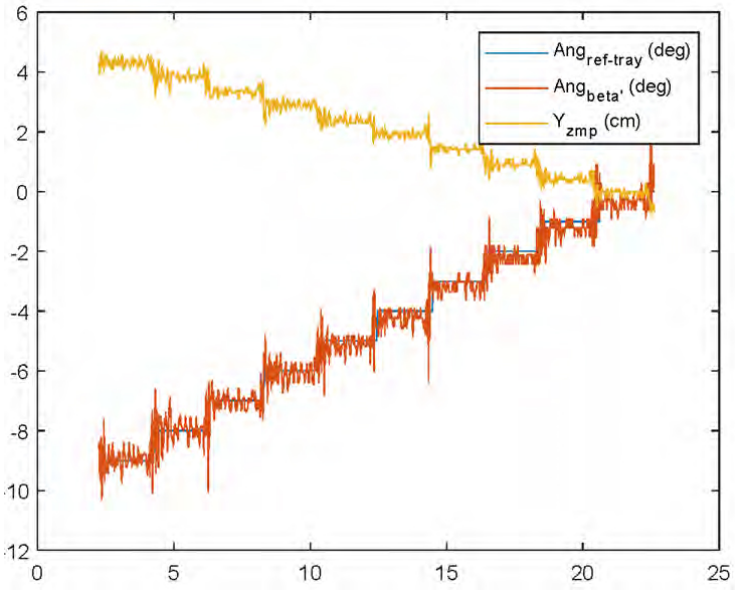

Figure 7.10: *Evaluation of negative slopes in the X-axis.*

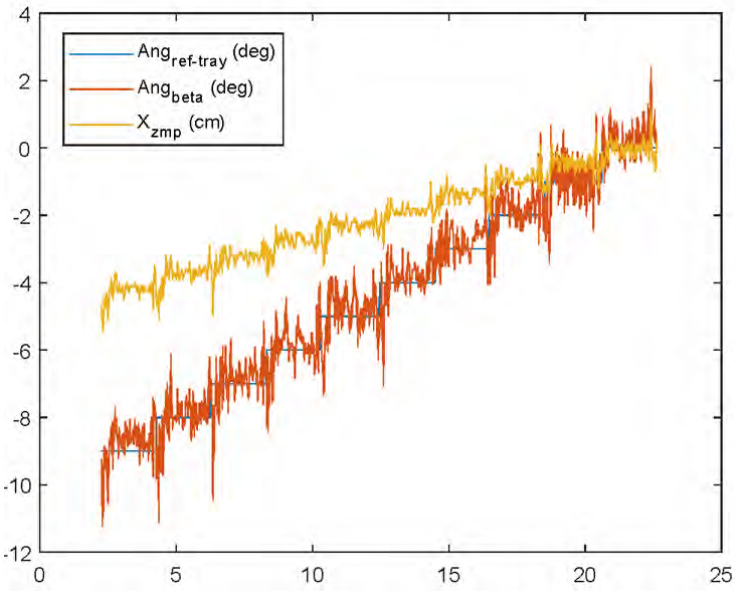

Figure 7.11: *Evaluation of negative slopes in the Y-axis.*

Therefore, with these experiments, this mathematical method can calculate a practical calculation of ZMP regardless of the value of the slope and the inclination vector. Dynamically, we can compute the corresponding ZMP while the tray changes its pose.

7.3.3 Object Balance Control.

In this section, we have unified the two previously validated perception systems. Both the Fuzzy filter and the 3D Dynamical Slopes method allow us to adjust the sensory information to test the object balance control. Now, the decision-making system is evaluated, checking the fusion of the sensory systems.

Set Up - 6º Experiment

The experiment focuses on control of the left arm through the decision-making system. This predictive controller evaluates the visual, F-T and proprioceptive information of the arm to generate the appropriate reaction on the tray (Figure 7.12). As a first evaluation, we have introduced perturbations (step inputs), checking the response of the controller to different "surprise events".

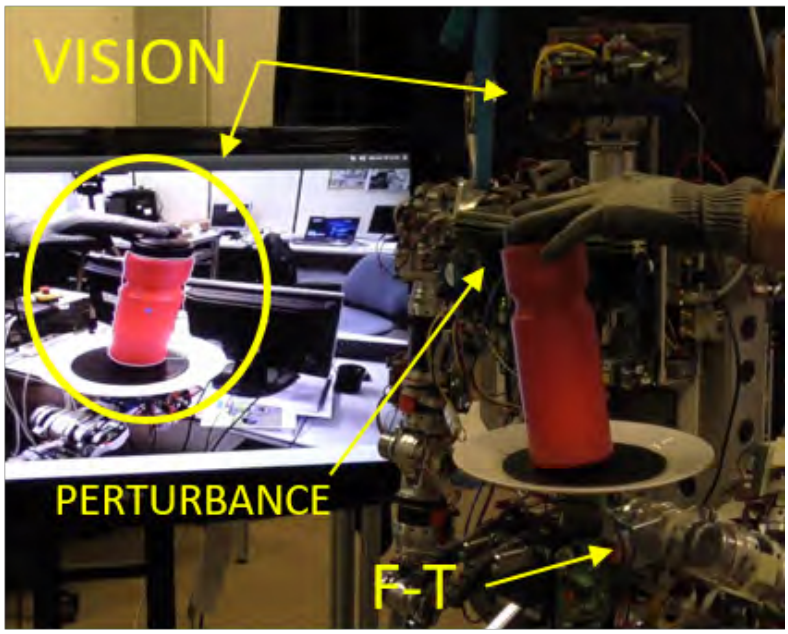

Figure 7.12: *Experimental Set-Up for the object balance control fusing sensory data.*

Results - 6º Experiment

The decision-making system behaves reasonably well (Figure 7.13). The system reacts to a dangerous inclination of the bottle (through the vision system). When this limit is exceeded, the controller computes the movement of the tray considering the object's ZMP and the tray's pose (F-T and proprioceptive sensors). The system proves to have potential, but it is necessary to improve neuro-fuzzy training to improve the robustness of the controller.

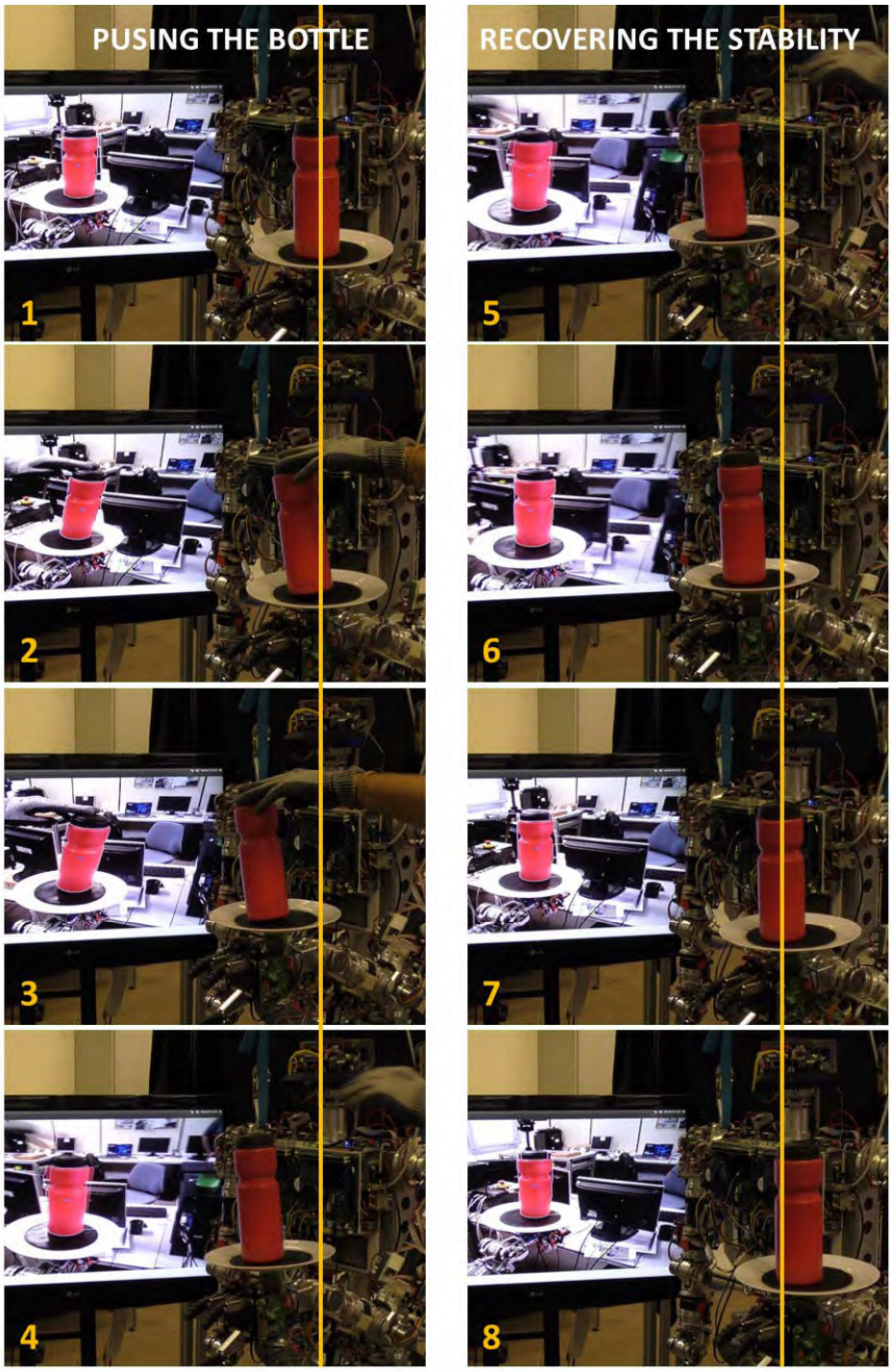

Figure 7.13: *From top to bottom, from left to right. The sequence of the object stability control merging visual and F-T sensory information.*

7.4 Waiter Whole-Body Manipulation

This section is divided into three parts. These are focused on the experimentation and validation of the waiter task for both Uni-Manipulation and Bi-Manipulation using the humanoid robots TEO and TORO.

7.4.1 Case of Whole-Body Uni-Manipulation.

To check the feasibility of the proposed system, the WBPC including the DLIPM model, is compared experimentally with the same WBPC but including the LIPM. In the trials, the response of both ZMP_{obj} and ZMP_{body} is captured against external forces applied to the robot.

Set Up - 7º Experiment

The trials applied to both cases consist of applying an external perturbation to the humanoid robot and compute the stability parameters. In the case of using the LIPM, the model is fixed, and the response of the system depends on it. The control effort and its effectiveness relies on the accuracy of the model.

However, in the case of using the DLIPM, the model is adapted to the conditions of stability (ZMP_{body}). It means that the model is re-configured in each control step. Thus, the control effort relies on a more accurate model, and its response improves the performance of the balance. In both cases, the output of the model is the posture command according to the ZMP planning.

Results - 7º Experiment

The WBPC controls the upper-body and the ZMP_{obj} using the 3D dynamical slope method. This control is improved thanks to the application of the DLIPM because it modifies the dynamics of the task and reduces the impact of any kind of perturbation over the object.

Figure 7.14 shows the performance of stability control for the upper-body controller (ZMP_{obj}) and the lower-body controller(ZMP_{body}). In these tests, the robot is pushed to verify its response. In the first case with the LIPM, both controllers fulfil the objective of maintaining stability.

However, the controllers overshoot in excess and have a large stabilisation time (Figure 7.14 top). The model totally determines the dynamics of the balance, and it is not possible to modify it. Thus, the upper-body controller must deal as well with the perturbations not eliminated by the lower-body controller.

For the case of the WBPC using the DLIPM, the response is better in different aspects. The overshoots of the body's ZMP are smaller and less intense. The time response is four times smaller. Additionally, the object's ZMP stabilises faster. The reason is that the DLIPM can absorb so external as internal disturbances (due to its dynamic adjustment). In such a way, the effects of the body movement caused to the arm are minimized, and the upper-body controller performs better (Figure 7.14 bottom).

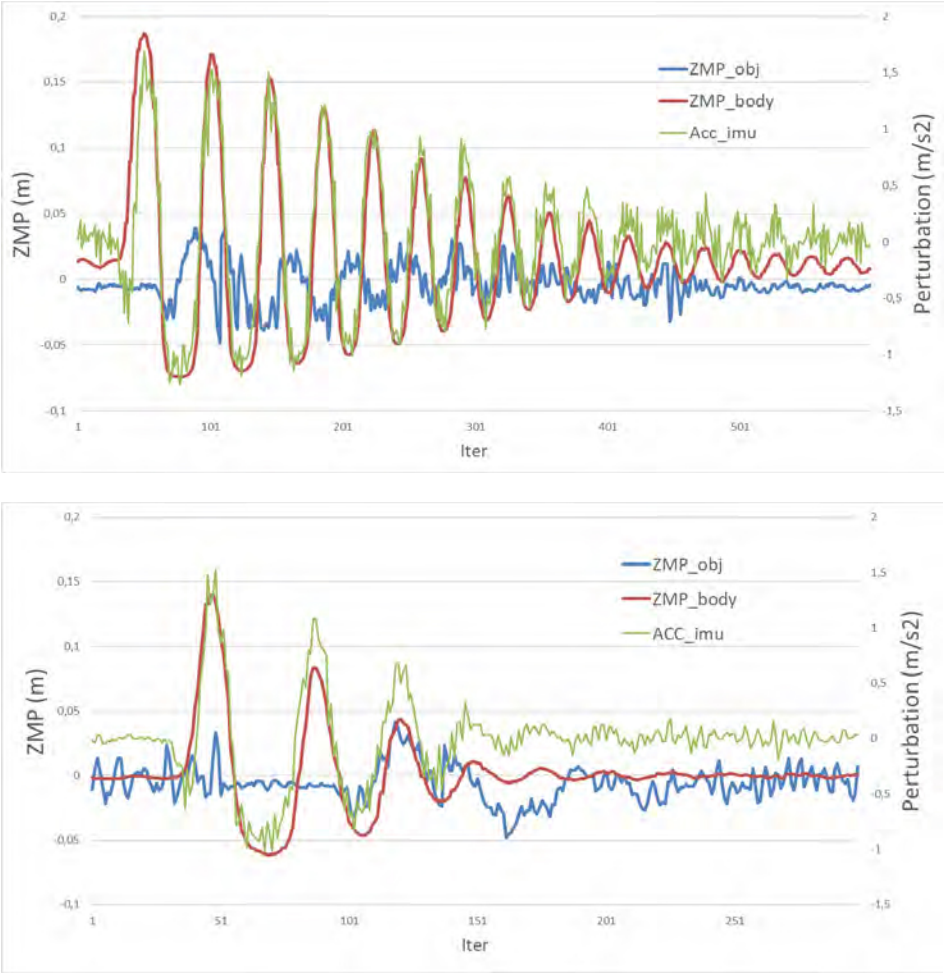

Figure 7.14: *Time evolution of the body's ZMP and the bottle's ZMP based on an external disturbance (push). The first graph is related to a WB system without DLIPM. The second graph with the proposed WB waiter system, including the DLIPM.*

In Figure 7.14, the acceleration of an inertial sensor is also represented. It has two purposes. The first one is to catch the event of pushing the robot (first oscillation). The second one is to check how the system responds globally corroborating the results of the ZMP values.

7.4.2 Study of the Bi-Manipulation in TEO.

In this section, we have extended the task of objects' transporting to a Dual-Arm manipulation. For this purpose, we have two F-T sensors in each hand that show the behaviour of the tray grasped. Now, we have to take into account and study the problems of closed chain and the use of a rigid robot.

Set Up - 8º Experiment

Manipulation with a rigid robot is a complicated situation because the movement is also rigid. If one arm moves more than the other arm, problems such as breaking the object or simply not achieving the goal of bi-manipulating an object could arise. In this experiment, a very basic movement of the tray is proposed.

In this case, the tray is rotated +/- 5 degrees with respect to its geometric centre on the *X-axis* (Figure 7.15). Although the value of ZMP has not been calculated, in this case, we also take the opportunity to study the application of 3D Dynamical Slopes method for bi-manipulation.

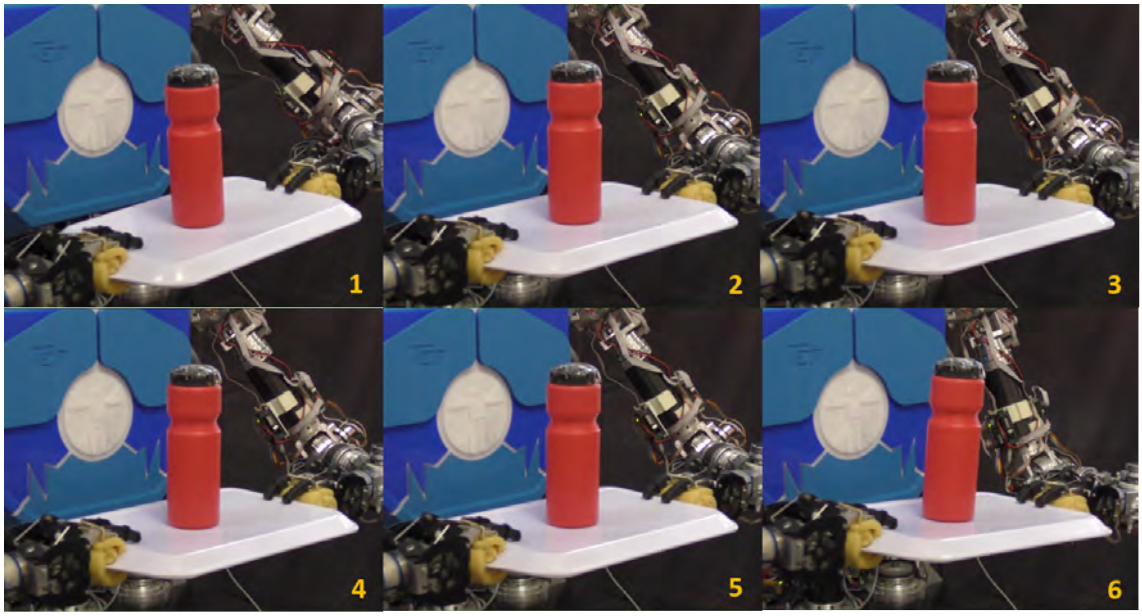

Figure 7.15: *From left to right, from top to bottom. The sequence of the bi-manipulation rotating the tray.*

Results - 8º Experiment

In this first bi-manipulation version, the results obtained in this experiment are satisfactory. Firstly, the force and torque values are adjusted to the behaviour of the 1Kg bottle on the tray. Both the behaviours of the forces (Figure 7.16(a) and Figure7.16(b)) and the torques (Figure 7.17(a) and Figure7.17(b)), the values are very similar. This is precisely the performance what we are looking for, where both arms move together for a particular trajectory. Additionally, the 3D Dynamical Slopes application still works correctly. We can observe how the values of F_z and M_x are adjusted during the trajectory.

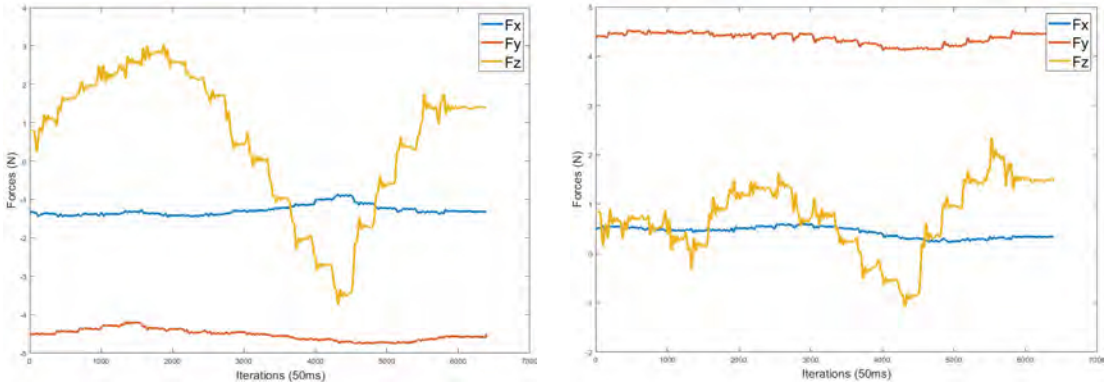

(a) Left TCP. (b) Right TCP.

Figure 7.16: *Evaluation of the TCP forces for bi-manipulation.*

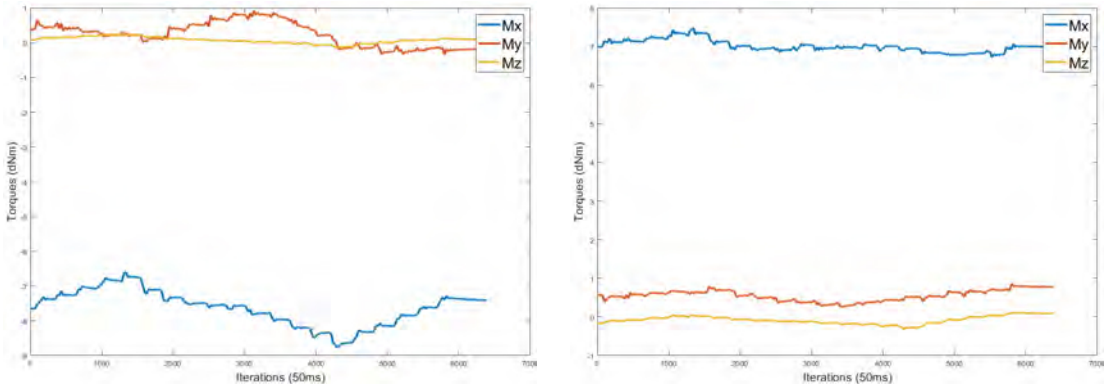

(a) Left TCP. (b) Right TCP.

Figure 7.17: *Evaluation of the TCP torques for bi-manipulation.*

7.4.3 Study of the Bi-Manipulation in TORO.

We performed experiments on various situations with the torque-controlled humanoid robot TORO (Englsberger et al., 2014). The different experiments in this sub-section validate the compliance behaviour of the Dual-Arm and Balance Whole-Body controller of TORO. The three presented experiments are the most appropriated to validate the new bi-manipulation and balance controller.

TORO is a whole-body humanoid robot. Its weight is 76.4 kg, and its height is 174 cm. This humanoid robot has 25 torque-controllable joints (six in each limb, and one for vertical torso rotation), 2 position-controlled joints in the neck, and is equipped with multiple sensors: position and torque sensors in each joint, an inertial measurement unit in the torso, force-torque sensors at the feet, and stereo and depth-perception cameras in the head. We have implemented the controller in Matlab/Simulink.

Set Up - 9º Experiment

The first set of experiments is focused on the performance of the bi-manipulation-oriented feedforward part of the controller. By varying the speed of the virtual object frame on the z-axis, it has been possible to verify the importance of this system within the controller and how tracking improves by adding the feedforward control.

The most demanding experiment performed is shown in Figure 7.18, where the displacement of the virtual object frame of 25 cm in 0.5 seg has been interpolated. In the upper graph, the feedforward control is deactivated.

By contrast, in the lower graph, the system is activated. The black line represents the desired position of the object, the dashed red line represents the measured position of the object, and the blue line represents the tracking error.

Results - 9º Experiment

In the lower part of Figure 7.18, with the feedforward system activated in the controller, both tracking and position error improve by around 40%. The control compliance allows redistributing the forces. In this case, the CoM moves in the opposite direction to absorb the inertia of the movement and help in tracking. Therefore, we can validate the proposed bi-manipulation model and all the developed mathematics.

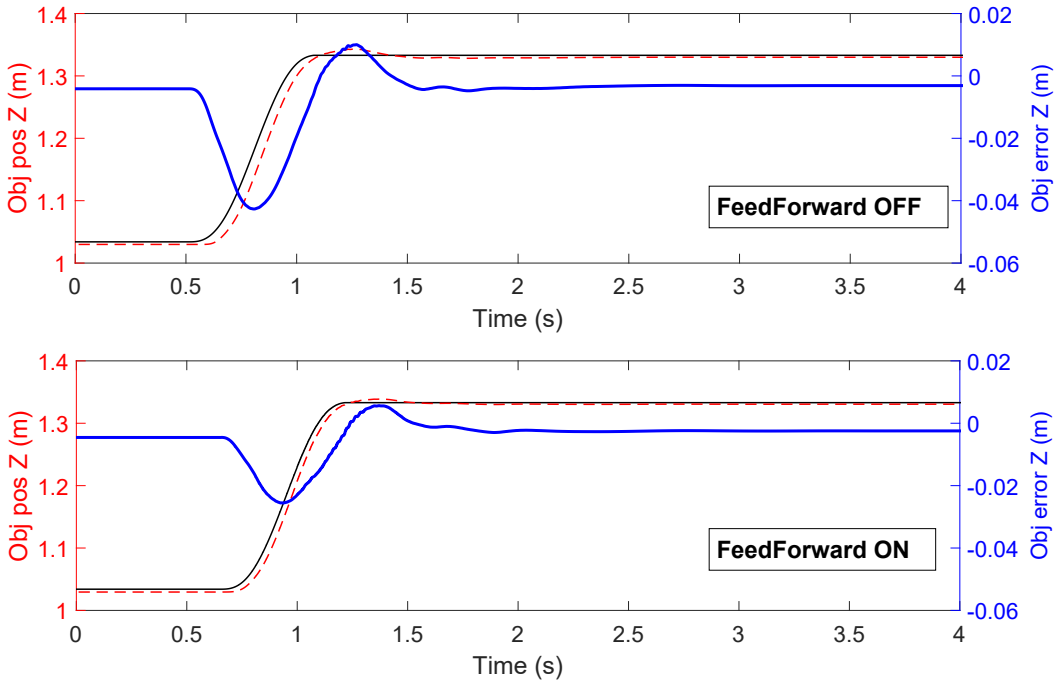

Figure 7.18: *Comparison of the object tracking error. Upper graph - FFWD deactivated. Lower graph - FFWD activated*

Set Up - 10º Experiment

The second set of experiments is focused on the operation of the gamma factor. In this case, a load of 4 kg has been placed on a bar that the robot grabs with both hands. The gamma parameter has taken these values [0.5 - 0.25 - 0.5 - 0.75] to verify the load distribution, while the position of the virtual object frame is kept. Changes in the gamma factor have been applied as a step response. Therefore, a significant oscillation in the phases of change is shown in the graph. The continuous red line represents the force wrench of the right arm, the discontinuous red line represents the force wrench of the left arm, and the blue line represents the measured object position.

Results - 10º Experiment

Figure 7.19 shows a correct and satisfactory force distribution on each of the hands end-effectors. When the gamma value is 25%, the highest force is made by the left arm. When the gamma value is 75%, the highest force is made by the right arm. At all times, the controller continues working to keep the object position. There is never an error bigger than 0.5 cm.

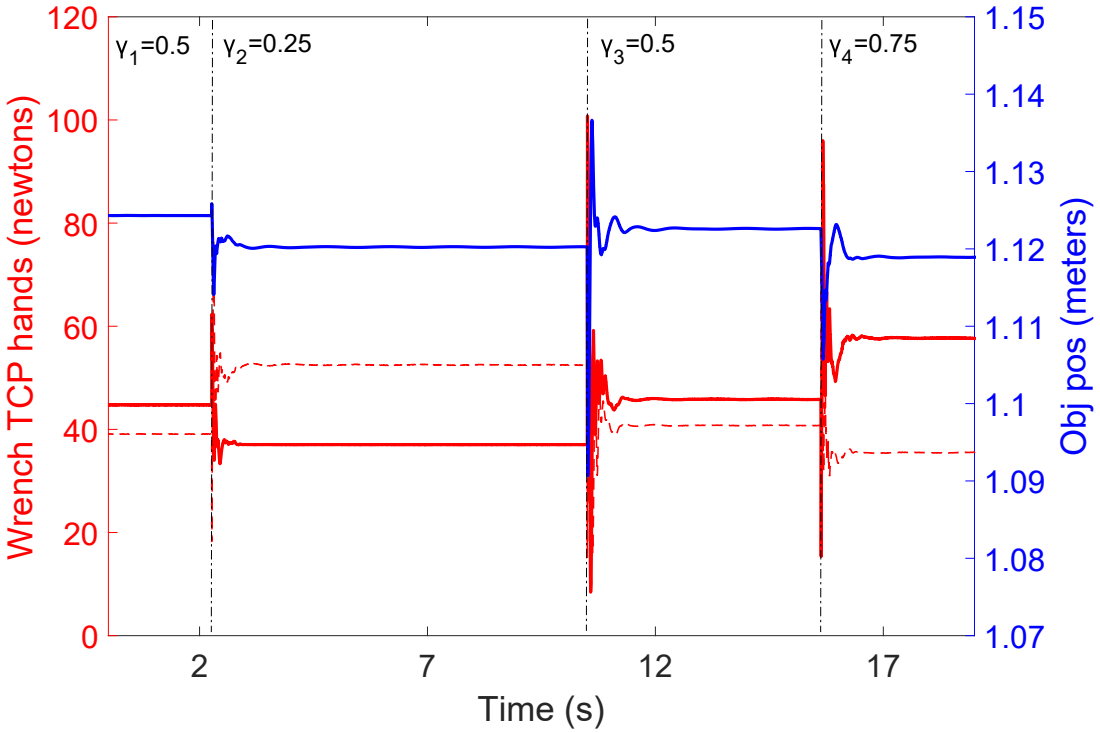

Figure 7.19: *TCP Force wrenches distribution.* $\gamma = 0.5$ *in* $t = 0s$, $\gamma = 0.25$ *in* $t = 2s$, $\gamma = 0.5$ *in* $t = 10.5s$, $\gamma = 0.75$ *in* $t = 15.5s$.

Set Up - 11º Experiment

The third set of experiments is focused on the behaviour of the controller against external disturbances. In this case, we want to verify the behaviour of the bi-manipulation system in two different ways. During the first part of the test, the computation of Vo is associated with CoM value. If the CoM moves due to external perturbations, the object will follow the same trajectory.

During the second phase (after the second 12.5), the computation of Vo is associated with the value of the World frame. In this case, the World frame remains static at all times and therefore also the virtual object frame, independently of the external perturbations observed in the CoM. Figure 7.20 shows the evolution of the three axes. The black line represents the desired object position, the discontinuous red line represents the measured object position, and the blue line represents the measured CoM position.

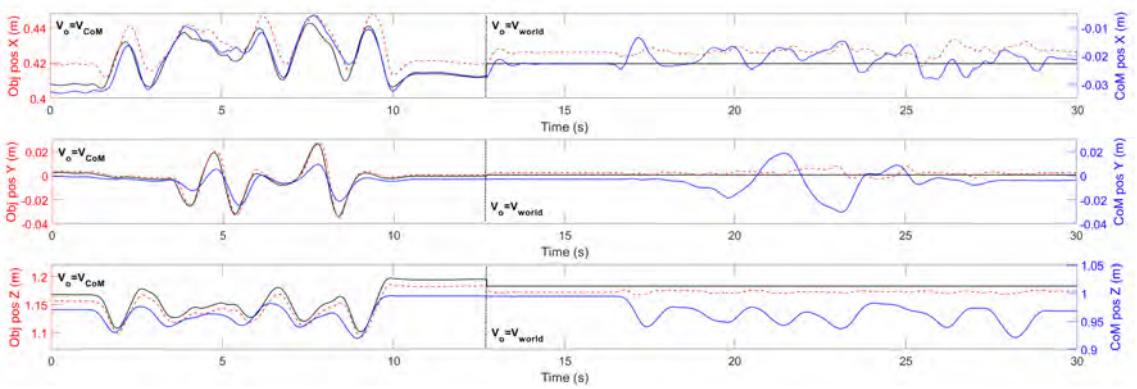

Figure 7.20: *Application of external perturbations in the CoM to validate the compliance control of the new dynamic model.*

Results - 11º Experiment

Figure 7.20 shows the behaviour of two essential parts of the bi-manipulation and balance controller. The first part checks if the controller is capable of performing proper object tracking. And the second part analyses if the controller absorbs disturbances in a compliant manner and then keep the balance. When $V_o = V_{CoM}$, the tracking of the virtual object frame is very robust, having errors below 2 cm. When $V_o = V_{world}$, the tracking is even better (below 1 cm). This type of test has also been proven by introducing trajectories of the CoM (walk) instead of disturbance. The obtained results have been very similar.

Other Experiments

In addition to these experiments, we have carried out other tests where the efficiency and robustness of the new controller for trajectories of both V_o and V_{RM} have been verified while running the CoM trajectory at the same time.

One of the tests is related to the relative movement between the hands while maintaining the pose of the object frame. As seen in Figure 7.21, we have planned three movements consecutively: an increase of 5 cm in the second 1 on the Y-axis, an increase of 5 cm in the second 4 on the X-axis and an increase of 5 cm in the second 7.5 on the Z-axis. The blue line is the position of the left-hand frame, and the yellow line is the position of the right-hand frame. The mirror movement is correctly observed in all three cases, being able to validate its ability to adapt the bi-manipulation to different sizes of objects.

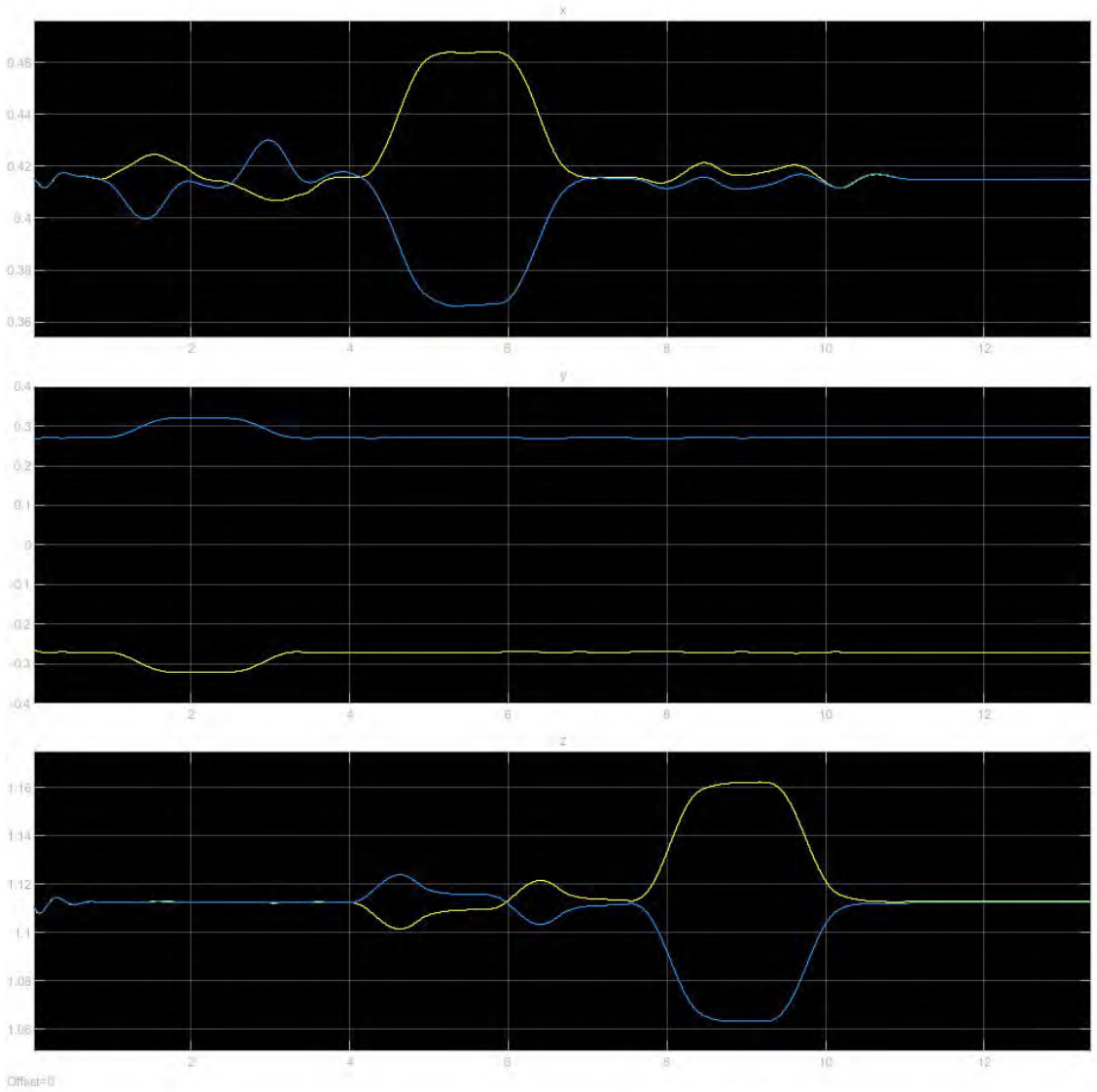

Figure 7.21: *Trajectories of the Arm's TCP validating the mirror movement in the three axes.*

Another test is related to the adaptation of the relative object frame position with respect to the hand frames. In Figures 7.22(a) and 7.22(b), two snapshots are shown where a 10-degree turn is applied. In Figure 7.22(a), the object frame is between the two hands at the same distance. However, in Figure 7.22(b), the object frame is +27 cm from the frame of the right hand. This ability allows bi-manipulation to be adapted to tasks such as sweeping the ground (Figure 7.22(c)).

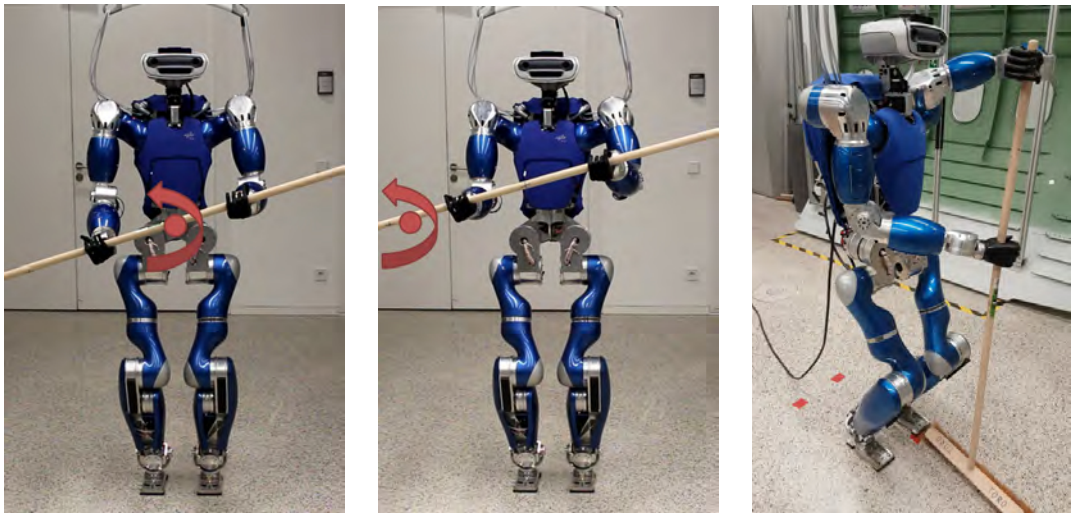

(a) Inside (b) Outside (c) Final purpose

Figure 7.22: *Relative motion between Object frame and Hands frame. (a) Between the hands' frame. (b) Furthest from the right-hand frame. and (c) Final application*

The last test is related to the ability to absorb external disturbances while the robot walks and maintains the position of the object frame (Figure 7.23). In this case, we get good results. The robot continues walking without falling and recovers the reference position of the object frame.

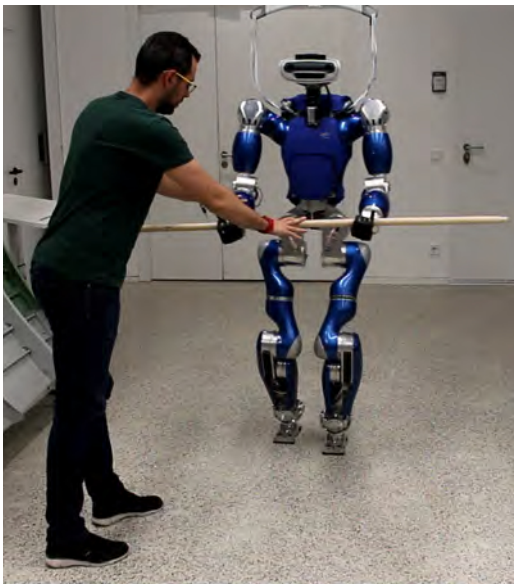

Figure 7.23: *Application of external perturbation in a Whole-Body task.*

7.5 Conclusions

In Chapter 7, we have shown all the experiments that have been carried out throughout this doctoral thesis. We have been able to validate our proposal of a waiter robot transporting objects through different experiments from less to higher complexity. The results obtained can certify the research carried out with this doctoral thesis.

Chapter 8

Conclusions

8.1 Final Conclusions

The main conclusion of this thesis is the implementation of Whole-Body Postural Control of the humanoid robot, focused on the task of transporting non-grasping objects. We have completed the study of a waiter humanoid robot behaviour and its requirements related to the manipulation of a bottle over a tray, performed with one or two arms. The waiter humanoid robot has been able to control both arms to guarantee the transport of the object while the robot is maintaining its own balance. Also, we have validated the task in two different humanoid robots, TEO and TORO.

Nevertheless, we have not solved the issues of whole-body postural performance in humanoids so far. The scientific community is addressing it with great interest. The reason is that advances in control and learning methods are attracting other scientific fields to robotics, making this matter of significant importance. If the next generation of humanoid robots should share the same scenarios with us, they should have skills to interact with human beings, be independent, walk carefully, or even interpret orders. In particular, for waiter robots, the humanoid platforms should be able to do similar tasks. In the evolution towards a humanoid waiter robot, we have contributed a new step in each chapter. Therefore, we present the final conclusions of this dissertation.

Chapter 2 described the state of the art of service robots. We explained the economic progress of this sector and classified the robots according to their application. In both professional and personal robots, there is a great variety. The explanation of this great diversity is due to the need to automate processes. Therefore, it is logical that new types of robot or classifications arise. This one is the case of catering robots (robochefs and waiterbots). These new service robots move away from housework and focus on more professional sectors, such as restaurants.

Nowadays, the current waiter robots are basic or perform straightforward tasks, but in summary, these service robots must have reasonable performance, within an acceptable time frame and without limitations by the environment. For achieving these features, a waiter service robot must have different skills, such as classification, human-robot interaction, detection and tracking of human being, planning, object detection and grasping. Nevertheless, all these skills are interdisciplinary and active investigation areas by themselves.

In Chapter 3, we introduced the specific objective of the waiter robot for this thesis. We explained that the waiter robot must be able to do a Whole-Body Postural Control while transporting objects. To do this, firstly, the TEO humanoid platform has been described, detailing the tools available both hardware and software, and explaining the requirements to generate the tasks proposed in Chapter 2.

Secondly, we presented the approach of the waiter robot, explaining in detail the task of transporting objects without grip them. In our case, a bottle on a tray. The application focuses on controlling the stabilities of the robot and the bottle at the same time. Therefore, we have defined a WBPC architecture that allows generating sub-tasks (such as manipulation without grip, bi-manipulation, body control) or the main task as the situation requires. Finally, we introduced the concepts, methods and tools necessary to explain and understand the rest of the chapters.

Chapter 4 focuses on the stability of the robot. The humanoid balance control is based on the knowledge of specific balance indicators. These parameters are materialised in mathematical models that represent simplifications of the humanoid body behaviour. However, the more simplified the model, the less precise the control performance will be. By contrast, the computational complexity is then lower. If we particularise for simplified classic models (such as LIPM or CT), they have a high level of simplification. Although they can model behaviour and balance while walking, they can also introduce several errors. Besides, the electromechanics of the robot has inherent inaccuracies that are added to those of the model.

In this chapter, we presented a method that proposes a new humanoid robot model considering these inaccuracies and improve the balance control system. The experimental procedure, based on Push-Recovery trials, was used to determine the steady-state error and the dynamic response of the system. This procedure can be applied to any humanoid robot because it is independent of the system and can characterise any inaccuracy. Additionally, this methodology can be extrapolated to other models to unify and compare different balance indicators.

For chapter 5, we introduced the problem of manipulation without grasping. When we want to transport an object on a tray, numerous problems and conditions arise that we have to take into account. These drawbacks are related to the influence of the robot's own stability issues, other external forces, the use of one or two hands, the sensory systems involved, the morphology of the robot or the simple fact that the object is not firmly gripped.

In this chapter, we detailed the need to improve control algorithms, especially in balance control, due to their fast dynamics. The increase in the speed of data processing and the quality of the resulting information is a way to achieve adequate control. The task of transporting a bottle in a tray is a clear example of a balance control task. This task needs accurate sensor information and needs to get the information as quickly as possible.

For the sensor information related to the vision system, the Fuzzy-filter-based visual correction method promises more accurate results and notably faster. The offline training method is based on the data acquisition experimentally. This procedure allows modelling the error accurately to be later eliminated through the trained Fuzzy filter. For the F-T system, the proposed mathematical method of pose estimation is effective. The system to obtain the ZMP adapts to the posture of the robot and the current pose of the tray and can obtain more real values of the stability of the bottle. Besides, with FIS systems, it is also possible to generate fuzzy filters for manipulation control by merging different sensory information, allowing us to predict instability and generate the appropriate corrections.

Finally, we investigated the possibility of applying this task of controllers of both uni-manipulation and bi-manipulation. Because the TEO humanoid robot is rigid, the adaptation from one manipulation to another is almost direct. This condition only affects the computation of the object's ZMP, but not the control architecture and how to approach the problem.

Chapter 6 has focused on the integration of all previous threads. For the integration of body and object controllers, the WBPC architecture has been used. This architecture is based on the multiple ZMP evaluation and the stability interrelation between the object and the robot. In this way, the exposed methods for the calculation of the stability consider the influences among them obtaining promising results. Also, we can extrapolate this architecture to bi-manipulation tasks for the same reason explained in the previous paragraph.

This achievement has also allowed us to verify the adaptation of our bi-manipulation system in another totally different robotic platform. In this case, the TORO humanoid robot is not rigid, but compliance. However, the process of planning the movement of the tray is identical in both cases (TEO and TORO). In both, we use the forces and torque of the hands to compute the performance of the tray. To verify this condition, we developed a new dynamic Whole-Body control model adding the Dual-Arm manipulation capacity to the TORO robot. The results after applying our manipulation on the compliance system have been very satisfactory.

In chapter 7, we have shown all the experiments that have been carried out throughout this doctoral thesis. We have been able to validate our proposal of robot waiter transporting object through different experiments from less to higher complexity. The results obtained can certify the research carried out with this doctoral thesis.

8.2 Key Contributions

The main contributions of this dissertation are summarised as follow:

"Regarding Waiter Humanoid Robots" We implemented a controller that provides a robot with the capacities of a waiter to transport non-grasping objects. For this purpose, we introduced two approaches:

- The first approach focused on implementing a whole-body modular architecture that was able to adapt to different phases during the transport of objects or other conditions. This architecture initially focused on the bio-inspiration of human waiters, observing what requirements we should contemplate in our architecture. In this way, one of the characteristics to take into account was the use of different sources of sensory information that never was mixed, force and vision. Using these two sensors is one of the novelties of this thesis and is inspired in real waiter's skills.

- The second approach was to take advantage of this sensory modularity to implement different ways of transporting objects. In our case, first, we were able to extrapolate the problem of balance control of objects to both uni-manipulation and bi-manipulation without any need to alter such architecture. Afterwards, we were able to apply our bi-manipulation concept to other robotic platforms, readjusting the dynamic model of the new platform to be able to bi-manipulate while the robot was walking.

"Regarding Dynamic – Linear Inverted Pendulum Model" Here, we contributed in two different manners:

- We studied the intrinsic problems for the stability control of humanoid robots. We realised that there were several problems that, added together, made it impossible to control the robot's balance. In the beginning, these problems arose from using simplified models such as LIPM. But problems also arose due to mechanical clearances, flexibility, and inaccurate sensory readings.

- We proposed a method to overcome these problems based on dynamic adaptation models. Instead of correcting all the problems that the robot had one by one, we implemented a simplified mathematical model of the robot that contemplated both its own behaviour and that of the associated errors. This model was implemented experimentally for different work points guaranteeing the dynamic adjustment based on "Gain Scheduling". Therefore, this methodology could be applied to other robots.

"Regarding 3D Dynamical Slopes" For the non-grasping manipulation task, we presented two different contributions:

- Starting from studies of humanoid robots' stability, particularly for cases of irregular or unknown terrain, we were able to study the case of the balance control of an object where the support varied in position and orientation. This condition meant that the ZMP stability criterion could not be applied, as long as the tray plane was not coplanar to the floor plane. On the other hand, given the numerous possibilities that could arise from the control of a bottle on a tray, we say that we use materials that only allow the bottle to pivot as an inverted pendulum.

- We implemented a method that was able to adapt, in the first place, to the morphology of the robot. The unique condition was to be able to obtain the forces and torques of the manipulator's TCP (or the TCPs in case of bi-manipulation). And secondly, the method applied the necessary transformation in the TCP to obtain a virtual coordinate system that was coplanar and obtain the correct readings of the object's ZMP. Moreover, this method could be extended to a dual-arm application considering the two supports of the hands as if they were the double support of the walk.

"Regarding Vision correction based on FIS systems" This research has presented two main contributions:

- After studying the behaviour of the TEO humanoid robot's vision system and its problems related to perspective, lens deformation, and speed computation, we considered the application of a filter as a good option. The capacities offered by the ANFIS tool to implement a Fuzzy filter were acceptable, and we took advantage of it to deal with all these computer vision problems.

- Besides, this Fuzzy filter laid the foundations of being able to implement other filters. Thanks to the possibility of using different information from the same sensor for a single purpose, we realised that we could merge other sensors at the same time for other objectives at a higher level or even to implement controllers.

8.3 Future Works

"Waiter Humanoid Robots V2.0" Our business leaves other paths open for investigation:

- First, our WBPC controller has only been able to be tested on tasks related to stability with the TEO humanoid robot, but we have never been able to experience the balance control of the bottle while the robot walks. It would be interesting to implement a walk planner or even a dynamic planner that could recalculate trajectories before PR trials.

- Second, another essential possibility to consider is the transformation of TEO. We could go from having a rigid robot to compliance. In this way, we could verify how our controller works against disturbances/perturbations or investigate the interactions between the body and the object during transport.

- Other future work would be related to the transport of objects. For this thesis, we have always been working with a bottle with a weight of 1Kg. However, we could expand our control, transporting different objects of different sizes and weight. One possibility would be to implement an adaptive controller based on fractional control.

- Finally, we could investigate new hardware and software systems to improve the low-level operation of the TEO robot. For example, with the problem of lens distortion, there are cameras that by default already contemplate and correct it. Another option would be to search for cameras with faster resolutions and computing speeds. In the case of F-T sensors, this system has a filter that improves sensory information but not enough.

"Dynamic – Linear Inverted Pendulum Model" Almost all future tasks for the in-hand DLIPM Model are related to improvements in the stability control of the robot. The most exciting future work in this area can be:

- In this thesis, we have experimentally adjusted both the DLIPM and the CT model for the robot. In both models, the value of the ZMP is robust and also unique. Therefore, we could use them to unify the information of the F-T and inertial sensors to implement a predictive controller.

- On the other hand, it would be interesting to implement a controller that is capable of adapting to different intensities of external disturbances. This option could be related to the previous paragraph. Although the main idea would be the development of more complex PR strategies such as "Hip" or "Step".

"Adaptive 3D Dynamical Slopes" Regarding our 3D Dynamical Slopes method, some future works are still open:

- Since in this investigation, we merge sensory information, an intuitive idea would be to integrate also the inertial sensor into the object control system. This information would allow more dynamic and predictive control to obtain information from the robot's body and thus generate better action strategies to impede instabilities on the object.
- On the other side, based on real experiences of people or waiter transporting objects on a tray, there is a reasonably important condition. Usually, objects resting on the tray can slide, instead of pivoting. Therefore, a possible job would be to modify the surface type of the tray and investigate the behaviour, physics of movement and other boundary conditions for this new case.

"3D Vision correction based on FIS systems" Regarding the visual correction based on FIS systems, some works may be worth pursuing. Among them, the two most attractive could be:

- Firstly, for the computer vision system, the angle-obtaining algorithm is only enabled for the 2D plane. However, the TEO humanoid robot has a camera with depth vision. Therefore, the next step would be to extend our visual correction system using Fuzzy filter to three-dimensional space.
- Additionally, we could also investigate the use of databases. With more extensive training databases, an improved and more robust Fuzzy filter could be generated, further reducing the visual distortion error.

8.4 Publications

8.4.1 Journals

This last part introduces a list of journals that have been published during this dissertation. The five publications are indexed in the Journal Citation Reports (JCR), being two in the first quartile (Q1), one in the second quartile (Q2), one in the first quartile (Q3) and one in the fourth quartile (Q4).

1. **Garcia-Haro, J.M.**, Martinez, S., Monje, C.A. & Balaguer, C. Development of Applications for Humanoid Robots using Multiple Platforms, Tools, and Cloud Data Sharing. *International Journal of Humanoid Robotics (IJHR).* 2019 (Q4). [accepted, pending publication]

2. Oña, E.D., **Garcia-Haro, J.M.**, Jardón, A., & Balaguer, C. Robotics in Health Care: Perspectives of Robot-Aided Interventions in Clinical Practice for Rehabilitation of Upper Limbs. *Appled Sciences*. 2019, 9, 2586. (Q2). [Oña et al., 2019]

3. Martinez, S., **Garcia-Haro, J.M.**, Victores, J., Jardon, A., & Balaguer, C. (2018). Experimental Robot Model Adjustments Based on Force-Torque Sensor Information. *Sensors*, 18(3), 836. (Q1). [Martinez et al., 2018]

4. Hernandez-Vicen, J., Martinez, S., **Garcia-Haro, J.M.**, & Balaguer, C. (2018). Correction of Visual Perception Based on Neuro-Fuzzy Learning for the Humanoid Robot TEO. *Sensors*, 18(4), 972. (Q1). [Hernandez-Vicen et al., 2018]

5. Pérula-Martínez, R., **Garcia-Haro, J.M.**, Balaguer, C., & Salichs, M.A. (2016). Developing Educational Printable Robots to Motivate University Students Using Open Source Technologies. *Journal of Intelligent & Robotic Systems*, 81(1), 25–39. (Q2). [Pérula-Martínez et al., 2016]

8.4.2 Conferences

1. **J.M. Garcia-Haro**, E. D. Oña, S. Martinez, J. G. Victores, C. Balaguer. Whole-Body Postural Control Approach Based on Multiple ZMP Evaluation in Humanoid Robots. 2019 IEEE/RSJ International Conference on Intelligent Robots and Systems (IROS). 2019-11-5, Macau, China. [accepted, pending publication]

2. **J.M. Garcia-Haro**, B. Henze, G. Mesesan, S. Martinez, C. Ott. Integration of Dual-Arm Manipulation in a Passivity Based Whole-Body Controller for Torque-Controlled Humanoid Robots. In Humanoid robots, 2019 IEEE-RAS International Conference on. IEEE. 2019-10-15, Toronto, Canada. 2019. [accepted, pending publication]

3. **J.M. Garcia-Haro**, S. Martinez, C. Balaguer. Balance Computation of Objects Transported on a Tray by a Humanoid Robot Based on 3D Dynamic Slopes. In Humanoid robots, 2018 IEEE-RAS International Conference on. IEEE. 2018-11-06, Beijing, China. 2018. [Garcia-Haro et al., 2018d]

4. **J.M. Garcia-Haro**, E. D. Oña, S. Martinez, J. Hernandez-Vicen, C. Balaguer. Waiter Robot Application: Balance Control for Transporting Objects. 2018 IEEE/RSJ International Conference on Intelligent Robots and Systems (IROS). 2018-10-5, Madrid, Spain. [Garcia-Haro et al., 2018a]

5. **J.M. Garcia-Haro**, S. Martinez, C. Balaguer. Detección de la Orientación mediante Visión Artificial para el Control de Equilibrio en Robots Humanoides. XXXIX Jornadas de Automática. ISBN: 978-84-09-04460-3, pages: 951-957, CEA-IFAC. 2018-09-05, Badajoz, Spain. 2018. [Garcia-Haro et al., 2018b]

6. **J.M. Garcia-Haro**, S. Martinez, C. Balaguer. Humanoid Balance Control based on Force/Torque and Visual Information. Jornadas Nacionales de Robótica 2018. Jornadas Nacionales de Robótica 2018, Actas de las Jornadas Nacionales de Robótica 2018, ISBN: 978-84-09-02877-1, CEA-IFAC. 2018-06-14, Valladolid, Spain. 2018. [Garcia-Haro et al., 2018c]

7. **J.M. Garcia-Haro**, S. Martinez, M. Pinel, C. Balaguer. Experimental Error Compensation of the Linear Inverted Pendulum Model for humanoid robot TEO. 2017 IEEE/RSJ International Conference on Intelligent Robots and Systems (IROS). ISBN: 9781538626818, page: 5489, IEEE. 2017-09-24, Vancouver, BC, Canada. 2017. [Garcia-Haro et al., 2017]

8. J. Hernandez-Vicen, **J.M. Garcia-Haro**, S. Martinez, C. Balaguer. Control of Robotic Arm for Transporting Objects based on Neuro-Fuzzy Learning Visual Information. XXXVIII Jornadas de Automática, ISBN: 978-84-16664-74-0, pages: 760-765, CEA-IFAC. 2017-09-06, Oviedo, Spain. 2017. [Hernandez-Vicen et al., 2017]

9. J. Lorente, **J.M. Garcia-Haro**, S. Martinez, J. Hernández, C. Balaguer. Waiter Robot : Advances in Humanoid Robot Research at UC3M. RoboCity16 Open Conference on Future Trends in Robotics. RoboCity16 Open Conference on Future Trends in Robotics, ISBN: 978-84-608-8452-1, pages: 195-202, CSIC. 2016-05-26, Madrid, Spain. 2016. [Lorente et al., 2016]

10. J. Hernández, **J.M. Garcia-Haro**, S. Martinez, J. Lorente, C. Balaguer. Manipulation Balance Control System by Computer Vision Tools. RoboCity16 Open Conference on Future Trends in Robotics. RoboCity16 Open Conference on Future Trends in Robotics, ISBN: 978-84-608-8452-1, pages: 203-210, CSIC. 2016-05-26, Madrid, Spain. 2016. [Hernandez-Vicen et al., 2016]

References

L. Acosta, E. González, J. Rodríguez, A. Hamilton, J. Méndez, S. Herneández, M. Sigut, and G. Marichal. Design and Implementation of a Service Robot for a Restaurant. *International Journal of Robotics and Automation*, 21(4):273–281, 2006. ISSN 1925-7090. doi: 10.2316/journal.206.2006.4.206-2909.

Y. Aiyama, M. Inaba, and H. Inoue. Pivoting: A new method of graspless manipulation of object by robot fingers. In *Proceedings of 1993 IEEE/RSJ International Conference on Intelligent Robots and Systems (IROS '93)*, volume 1, pages 136–143. IEEE, 2013. ISBN 0-7803-0823-9. doi: 10.1109/IROS.1993.583091.

A. Albu-Schäffer, S. Haddadin, C. Ott, A. Stemmer, T. Wimböck, and G. Hirzinger. The DLR lightweight robot: Design and control concepts for robots in human environments. *Industrial Robot*, 34(5):376–385, 2007. ISSN 0143991X. doi: 10.1108/01439910710774386.

F. Alonso-Martín, V. Gonzalez-Pacheco, Á. Castro-González, A. A. Ramey, M. Yébenes, and M. A. Salichs. Using a Social Robot as a Gaming Platform. *International Conference on Social Robotics*, pages 30–39, nov 2010. doi: 10.1007/978-3-642-17248-9_4.

R. D. Andrea and P. Wurman. Future Challenges of Coordinating Hundreds of Autonomous Vehicles in Distribution Facilities. *Technologies for Practical Robot Applications, 2008. TePRA 2008. IEEE International Conference on*, pages 80–83, 2008. doi: 10.1109/TEPRA.2008.4686677.

M. Arbulu and C. Balaguer. Real-Time gait planning for Rh-1 humanoid robot, using Local Axis Gait algorithm. *International Journal of Humanoid Robotics*, 6 (1):71–91, 2009. ISSN 0219-8436. doi: 10.1142/S0219843609001681.

M. Arbulú, J. M. Pardos, L. Cabas, P. Staroverov, D. Kaynov, C. Pérez, M. Rodriguez, and C. Balaguer. Rh-0 humanoid full size robot's control strategy based on the Lie logic technique. In *Proceedings of 2005 5th IEEE-RAS International Conference on Humanoid Robots*, pages 271–276. IEEE, 2005. ISBN 0780393201. doi: 10.1109/ICHR.2005.1573579.

S. H. Asenador. La tecnología se cuela en el menú de los restaurantes del futuro. *Expansión*, 2016. [Accessed Jan-2018].

T. Asfour, K. Regenstein, P. Azad, J. Schröder, A. Bierbaum, N. Vahrenkamp, and R. Dillmann. ARMAR-III: An integrated humanoid platform for sensory-motor control. *Proceedings of the 2006 6th IEEE-RAS International Conference on Humanoid Robots, HUMANOIDS*, pages 169–175, 2006. ISSN 2164-0572. doi: 10.1109/ICHR.2006.321380.

M. Asif, M. Sabeel, and K. Mujeeb-ur Rahman. Waiter robot-solution to restaurant automation. In *Proceedings of the 1st student multi disciplinary research conference (MDSRC), At Wah, Pakistan*, pages 14–15, 2015.

T. M. Assman. *Humanoid push recovery stepping in experiments and simulations*. MSc Thesis, Technische Universiteit Eindhoven, Eindhoven, Holland, 2012.

K. Barrett. Weaver Dairy's well thought-out modernization. *DairyBusiness East*, pages 28–29, 2014.

M. Beetz, D. Jain, L. Msenlechner, and M. Tenorth. Towards performing everyday manipulation activities. *Robotics and Autonomous Systems*, 58(9):1085–1095, 2010. ISSN 09218890. doi: 10.1016/j.robot.2010.05.007.

B. J. Benda, P. O. Riley, and D. E. Krebs. Biomechanical Relationship Between Center of Gravity and Center of Pressure During Standing. *IEEE Transactions on Rehabilitation Engineering*, 2(1):3–10, 1994. ISSN 10636528. doi: 10.1109/86.296348.

S. Bodiroža, H. I. Stern, and Y. Edan. Dynamic gesture vocabulary design for intuitive human-robot dialog. *Proceedings of the seventh annual ACM/IEEE international conference on Human-Robot Interaction - HRI '12*, page 111, 2012. ISSN 21672121. doi: 10.1145/2157689.2157710.

S. Bodiroža, G. Doisy, and V. V. Hafner. Position-invariant, real-time gesture recognition based on dynamic time warping. In *ACM/IEEE International Conference on Human-Robot Interaction*, pages 87–88. IEEE, mar 2013. ISBN 9781467330558. doi: 10.1109/HRI.2013.6483514.

J. Bohren, R. B. Rusu, E. G. Jones, E. Marder-Eppstein, C. Pantofaru, M. Wise, L. Mösenlechner, W. Meeussen, and S. Holzer. Towards autonomous robotic butlers: Lessons learned with the PR2. In *Proceedings - IEEE International Conference on Robotics and Automation*, pages 5568–5575, 2011. ISBN 9781612843865. doi: 10.1109/ICRA.2011.5980058.

W. Budiharto, J. Moniaga, M. Aulia, and A. Aulia. A framework for obstacles avoidance of humanoid robot using stereo vision. *International Journal of Advanced Robotic Systems*, 10(4):204, 2013. ISSN 1729-8806. doi: 10.5772/55608.

T. Buschmann, S. Lohmeier, and H. Ulbrich. Humanoid robot Lola: Design and walking control. *Journal of Physiology Paris*, 103(3-5):141–148, 2009. ISSN 09284257. doi: 10.1016/j.jphysparis.2009.07.008.

F. Caccavale, C. Natale, B. Siciliano, and L. Villani. Six-dof impedance control based on angle/axis representations. *IEEE Transactions on Robotics and Automation*, 15(2):289–300, 1999.

J. C. Castillo, J. Serrano-Cuerda, and A. Fernández-Caballero. Robust people segmentation by static infrared surveillance camera. *Lecture Notes in Computer Science (including subseries Lecture Notes in Artificial Intelligence and Lecture Notes in Bioinformatics)*, 6096 LNAI(PART 1):348–357, 2010. ISSN 03029743. doi: 10.1007/978-3-642-13022-9_35.

A. Castro-González, H. Admoni, and B. Scassellati. Effects of form and motion on judgments of social robots' animacy, likability, trustworthiness and unpleasantness. *International Journal of Human Computer Studies*, 90:27–38, 2016. ISSN 10959300. doi: 10.1016/j.ijhcs.2016.02.004.

C. Chen, Q. Gao, Z. Song, O. Liping, and X. Wu. Catering service robot. In *Proceedings of the World Congress on Intelligent Control and Automation (WCICA)*, pages 599–604. IEEE, jul 2010. ISBN 9781424467129. doi: 10.1109/WCICA.2010.5553843.

S. Choi, G. F. Rossano, G. Zhang, and T. Fuhlbrigge. Service Robots : An Industrial Perspective. *Technologies for Practical Robot Applications (TePRA), 2015 IEEE International Conference on*, 2015. doi: 10.1109/TePRA.2015.7219679.

S. A. Cholewiak, R. W. Fleming, and M. Singh. Visual perception of the physical stability of asymmetric three-dimensional objects. *Journal of Vision*, 13(4):12–12, 2013. doi: 10.1167/13.4.12.

V. Ciupe and I. Maniu. New trends in service robotics. In *New trends in medical and service robots*, pages 57–74. Springer, 2014.

F. Coffrini. Restaurantes de China despiden a sus camareros robot por su ineficacia. *elPeriodico*, 2016. [Accessed Jan-2018].

S. Curtis. Pizza Hut hires ROBOT waiters to take orders and process payments at its fast-food restaurants. *Mirror Online*, 2016. [Accessed Jan-2018].

P. Deegan, B. J. Thibodeau, and R. Grupen. Designing a self-stabilizing robot for dynamic mobile manipulation. Technical report, University of Massachusetts, Department of Computer Science, 2006.

K. Deguchi, H. Sakurai, and S. Ushida. A goal oriented just-in-time visual servoing for ball catching robot arm. In *2008 IEEE/RSJ International conference on intelligent Robots and Systems*, pages 3034–3039. IEEE, 2008.

D. Derlukiewicz and M. Cieślak. Study of the causes of boom elements cracking of electric demolition machine with use of experimental and numerical methods. *Lecture Notes in Mechanical Engineering*, Part F10:109–119, 2017. ISSN 21954364. doi: 10.1007/978-3-319-50938-9_12.

DigitalFoodLab. NYMBLE LABS - The smart kitchen appliance, 2010. [Accessed Apr-2019].

M. R. Dogar and S. S. Srinivasa. Push-grasping with dexterous hands: Mechanics and a method. In *IEEE/RSJ 2010 International Conference on Intelligent Robots and Systems, IROS 2010 - Conference Proceedings*, pages 2123–2130, 2010. ISBN 9781424466757. doi: 10.1109/IROS.2010.5652970.

C. Eckes, K. Biatov, F. Hülsken, J. Köhler, P. Breuer, P. Branco, and L. M. Encarnacao. Towards Sociable Virtual Humans: Multimodal Recognition of Human Input and Behavior. *International Journal*, 6(4):21–30, 2007.

A. Edsinger and C. C. Kemp. Manipulation in human environments. *Proceedings of the 2006 6th IEEE-RAS International Conference on Humanoid Robots, HUMANOIDS*, pages 102–109, 2006. ISSN 2164-0572. doi: 10.1109/ICHR.2006.321370.

A. Edsinger and C. C. Kemp. Two arms are better than one: A behavior based control system for assistive bimanual manipulation. In *Recent progress in robotics: Viable robotic service to human*, pages 345–355. Springer, 2007.

P. Elinas, J. Hoey, D. Lahey, J. Montgomery, D. Murray, S. Se, and J. Little. Waiting with Jose, a vision-based mobile robot. *Proceedings 2002 IEEE International Conference on Robotics and Automation (Cat. No.02CH37292)*, 4:3698–3705, 2003. doi: 10.1109/robot.2002.1014284.

J. Englsberger, A. Werner, C. Ott, B. Henze, M. A. Roa, G. Garofalo, R. Burger, A. Beyer, O. Eiberger, K. Schmid, et al. Overview of the torque-controlled humanoid robot toro. In *2014 IEEE-RAS International Conference on Humanoid Robots*, pages 916–923. IEEE, 2014.

J. Englsberger, A. Werner, C. Ott, B. Henze, M. A. Roa, G. Garofalo, R. Burger, A. Beyer, O. Eiberger, K. Schmid, and A. Albu-Schäffer. Overview of the torque-controlled humanoid robot TORO. In *IEEE-RAS International Conference on Humanoid Robots*, volume 2015-Febru, pages 916–923, 2015. ISBN 9781479971749. doi: 10.1109/HUMANOIDS.2014.7041473.

H. Enotiades, F. Makedon, S. Phan, and P. McMurrough, Christopher Shiakolas. Talos – Assistive Robotic Platform Harris. In ACM, editor, *Proceedings of the 7th International Conference on PErvasive Technologies Related to Assistive Environments*, page 69, 2014. ISBN 978-1-4503-2746-6. doi: 10.1093/nq/s8-X.255.397-c.

D. Estevez, J. G. Victores, R. Fernandez-Fernandez, and C. Balaguer. Robotic ironing with 3D perception and force/torque feedback in household environments. In *2017 IEEE/RSJ International Conference on Intelligent Robots and Systems (IROS)*, pages 6484–6489. IEEE, sep 2017. ISBN 978-1-5386-2682-5. doi: 10.1109/IROS.2017.8206556.

EuRobotics. 1st SciRoc Challenge. *ERL Consumer Service Robots*, 2019. [Accessed Oct-2019].

S. Fahmi, C. Mastalli, M. Focchi, and C. Semini. Passive whole-body control for quadruped robots: Experimental validation over challenging terrain. *IEEE Robotics and Automation Letters*, 4(3):2553–2560, 2019.

S. Feng and Z. Sun. Biped robot walking using three-mass linear inverted pendulum model. In *International Conference on Intelligent Robotics and Applications*, pages 371–380. Springer, oct 2008. ISBN 3540885129. doi: 10.1007/978-3-540-88513-9-40.

A. Fernández-Caballero, M. V. Sokolova, J. Serrano-Cuerda, J. C. Castillo, V. Moreno, R. Castiñeira, and L. Redondo. HOLDS: Efficient fall detection through accelerometers and computer vision. *Proceedings - 8th International Conference on Intelligent Environments, IE 2012*, pages 367–370, 2012. doi: 10.1109/IE.2012.11.

R. Fernandez-Fernandez, J. Victores, D. Estevez, and C. Balaguer. Real Evaluations Tractability using Continuous Goal-Directed Actions in Smart City Applications. *Sensors*, 18(11):3818, nov 2018. ISSN 1424-8220. doi: 10.3390/s18113818.

F. Ferro and L. Marchionni. REEM: A Humanoid Service Robot. *ROBOT2013: First Iberian Robotics Conference*, 252:521–525, 2014. doi: 10.1007/978-3-319-03413-3_38.

Flyppy. Miso Robotics, 2017. [Accessed Jan-2018].

K. Fregene. Unmanned aerial vehicles and control: Lockheed Martin Advanced Technology Laboratories. *IEEE Control Systems*, 32(5):32–34, 2012. ISSN 1066033X. doi: 10.1109/MCS.2012.2205474.

M. Fuchs, C. Borst, P. R. Giordano, A. Baumann, E. Kraemer, J. Langwald, R. Gruber, N. Seitz, G. Plank, K. Kunze, et al. Rollin'justin-design considerations and realization of a mobile platform for a humanoid upper body. In *2009 IEEE International Conference on Robotics and Automation*, pages 4131–4137. IEEE, 2009.

J. M. Garcia-Haro, S. Martinez, M. D. Pinel, and C. Balaguer. Experimental Error Compensation of the Linear Inverted Pendulum Model for humanoid robot TEO. In IEEE, editor, *2017 IEEE/RSJ International Conference on Intelligent Robots and Systems (IROS)*, page 5489, 2017. ISBN 9781538626818.

J. M. Garcia-Haro, E. Daniel Ona, S. Martinez, J. Hernandez-Vicen, and C. Balaguer. Waiter Robot Application: Balance Control for Transporting Objects. In *2018 IEEE/RSJ International Conference on Intelligent Robots and Systems (IROS)*, page 5036, Madrid, Spain, 2018a. IEEE. ISBN 9781538680933. doi: 10.1109/iros.2018.8593760.

J. M. Garcia-Haro, S. Martinez, and C. Balaguer. Detección de la Orientación mediante Visión Artificial para el Control de Equilibrio en Robots Humanoides. In U. de Extremadura, editor, *XXXIX Jornadas de Automática, Actas de las XXXIX Jornadas de Automática*, pages 951–957. CEA-IFAC, Badajoz, Spain, 2018b. ISBN 978-84-09-04460-3.

J. M. Garcia-Haro, S. Martinez, and C. Balaguer. Humanoid Balance Control based on Force/Torque and Visual Information. In U. de Valladolid, editor, *Jornadas Nacionales de Robótica 2018*. CEA-IFAC, Valladolid, Spain, 2018c. ISBN 978-84-09-02877-1.

J. M. Garcia-Haro, S. Martinez, and C. Balaguer. Balance Computation of Objects Transported on a Tray by a Humanoid Robot Based on 3D Dynamic Slopes. In *2018 IEEE-RAS 18th International Conference on Humanoid Robots (Humanoids)*, pages 704–709. IEEE, nov 2018d. ISBN 978-1-5386-7283-9. doi: 10.1109/HUMANOIDS.2018.8624920.

S. Garrido, L. Moreno, and D. Blanco. Exploration of a cluttered environment using Voronoi Transform and Fast Marching. *Robotics and Autonomous Systems*, 56(12):1069–1081, 2008. ISSN 09218890. doi: 10.1016/j.robot.2008.02.003.

E. Gat. Integrating reaction and planning in a heterogeneous asynchronous architecture for mobile robot navigation. *ACM SIGART Bulletin*, 2(4):70–74, 2007. ISSN 01635719. doi: 10.1145/122344.122357.

M. Ghallab, D. Nau, and P. Traverso. *Automated Planning: Theory and Practice*. Morgan Kaufmann, 2004. ISBN 9781558608566. doi: 10.1016/B978-1-55860-856-6.X5000-5.

M. Gienger, H. Janßen, and C. Goerick. Task-oriented whole body motion for humanoid robots. In *Proceedings of 2005 5th IEEE-RAS International Conference on Humanoid Robots*, volume 2005, pages 238–244, 2005. ISBN 0780393201. doi: 10.1109/ICHR.2005.1573574.

E. Gómez Vargas, N. Obregón Neira, and V. Socarras Quintero. Application of neuro-fuzzy anfis model vs neural network, to the predictive monthly mean flow problem in the bogotá river in villapinzón. *Tecnura*, 14(27):18–29, 2010.

M. González-Fierro, C. Monje, and C. Balaguer. Fractional Control of a Humanoid Robot Reduced Model with Model Disturbances. *Cybernetics and Systems*, 47(6), 2016. ISSN 10876553. doi: 10.1080/01969722.2016.1187031.

P. D. Groves. Principles of GNSS, inertial, and multisensor integrated navigation systems. *IEEE Aerospace and Electronic Systems Magazine*, 30(2):26–27, 2015. ISSN 0885-8985. doi: 10.1109/maes.2014.14110.

R. Gualotuña and E. LLinín. *Implementación de un algoritmo de búsqueda informada en el robot móvil Robotino de Festo para la obtención de la trayectoria mas óptima en tiempo real dentro de un entorno controlado.* PhD thesis, Universidad Politécnica Salesiana, 2011.

S. Gurav, P. Khot, D. Potadar, S. Shelke, and P. B. Chougula. Remote controlled Waiter Robot for Restaurant Automation. *International Journal of Application or Innovation in Engineering & Management (IJAIEM)*, 6(5):156–160, 2017.

T. C. Hain and J. O. Helminski. Anatomy and physiology of the normal vestibular system. *Vestibular rehabilitation*, 1(1):2, 2007.

S. Hart, S. Ou, J. Sweeney, and R. Grupen. A framework for learning declarative structure. Technical report, University of Massachusetts, Department of Computer Science, 2006.

K. Hauser, V. Ng-Thow-Hing, and H. Gonzalez-Baños. Multi-modal motion planning for a humanoid robot manipulation task. In *Robotics Research*, pages 307–317. Springer, 2010.

B. Henze, A. Dietrich, and C. Ott. An approach to combine balancing with hierarchical whole-body control for legged humanoid robots. *IEEE Robotics and Automation Letters*, 1(2):700 – 707, 2016a.

B. Henze, M. A. Roa, and C. Ott. Passivity-based whole-body balancing for torque-controlled humanoid robots in multi-contact scenarios. *The International Journal of Robotics Research*, 35(12):1522–1543, 2016b.

B. Henze, A. Dietrich, M. A. Roa, and C. Ott. Multi-contact balancing of humanoid robots in confined spaces: Utilizing knee contacts. In *2017 IEEE/RSJ International Conference on Intelligent Robots and Systems (IROS)*, pages 697–704. IEEE, 2017. ISBN 978-1-5386-2682-5. doi: 10.1109/IROS.2017.8202227.

J. Hernandez-Vicen, J. M. Garcia-Haro, S. Martinez, J. Lorente, and C. Balaguer. Manipulation Balance Control System by Computer Vision Tools. In R. E. Fernández and H. Montes, editors, *RoboCity16 Open Conference on Future Trends in Robotics*, chapter 25, pages 203–210. CSIC, 2016. ISBN 978-84-608-8452-1.

J. Hernandez-Vicen, J. M. Garcia-Haro, S. Martinez, and C. Balaguer. Control of Robotic Arm for Transporting Objects based on Neuro-Fuzzy Learning Visual Information. In U. de Oviedo, editor, *XXXVIII Jornadas de Automática, Actas de las XXXVIII Jornadas de Automática*, pages 760–765. CEA-IFAC, Oviedo, Spain, 2017. ISBN 978-84-16664-74-0.

J. Hernandez-Vicen, S. Martinez, J. M. Garcia-Haro, and C. Balaguer. Correction of Visual Perception Based on Neuro-Fuzzy Learning for the Humanoid Robot TEO. *Sensors*, 18(4):972, 2018. doi: 10.3390/s18040972.

J. Hertzberg, J. Zhang, L. Zhang, S. Rockel, B. Neumann, J. Lehmann, K. S. Dubba, A. G. Cohn, A. Saffiotti, F. Pecora, et al. The race project. *KI - Künstliche Intelligenz*, 28(4):297–304, 2014.

A. G. Hofmann. *Robust execution of bipedal walking tasks from biomechanical principles*. PhD Thesis, Massachusetts Institute of Technology, Boston, MA, USA, 2006.

International Organization for Standardization. ISO 8373:2012 - Robots and robotic devices - Vocabulary, 2012. [Accessed Mar-2018].

S. H. Ivanov, C. Webster, and K. Berezina. Adoption of Robots and Service Automation by Tourism and Hospitality Companies. *Revista Turismo & Desenvolvimento*, 27(28):1501–1517, may 2017.

L. Jagannathan and C. Jawahar. Perspective Correction Methods for Camera Based Document Analysis. *Proceedings of First International Workshop on Camera-based Document Analysis and Recognition*, pages 148–154, 2005.

J.-S. Jang. Anfis: adaptive-network-based fuzzy inference system. *IEEE transactions on systems, man, and cybernetics*, 23(3):665–685, 1993.

A. Jardón, A. Giménez, R. Correal, S. Martinez, and C. Balaguers. Asibot: Robot portátil de asistencia a discapacitados. concepto, arquitectura de control y evaluación clínica. *Revista Iberoamericana de Automática e Informática Industrial RIAI*, 5(2):48–59, 2008a. ISSN 16977912. doi: 10.1016/S1697-7912(08)70144-4.

A. Jardón, P. Zafra, S. Martínez, and A. Giménez. CEABOT: Nationalwide Little humanoid robots competition; rules, experiences and new challenges. In *Intl. Conf. on Simulation, Modeling and Programming for Autonomous Robots*, Venice, Italy, 2008b. ISBN 9788895872018.

A. Jevtic, E. Lucet, A. Kozlov, and J. Gancet. INTRO: A multidisciplinary approach to intelligent Human-Robot Interaction. *World Automation Congress (WAC), 2012*, pages 1–6, 2012. ISSN 21544824.

R. Kahn, M. Swain, P. Prokopowicz, and R. Firby. Gesture recognition using the Perseus architecture. *Computer Vision and Pattern Recognition, 1996. Proceedings CVPR'96*, pages 734–741, 2002. doi: 10.1109/cvpr.1996.517154.

S. Kajita, F. Kanehiro, K. Kaneko, K. Fujiwara, K. Harada, K. Yokoi, and H. Hirukawa. Biped Walking Pattern Generation by using Preview Control of Zero-Moment Point. In *2003 IEEE International Conference on Robotics and Automation (Cat. No.03CH37422)*, pages 1620–1626. IEEE, 2003. ISBN 0-7803-7736-2. doi: 10.1109/ROBOT.2003.1241826.

S. Kajita, H. Hirukawa, K. Harada, and K. Yokoi. Introduction to Humanoid Robotics. *Springer Tracts in Advanced Robotics*, 101, 2014. ISSN 1610742X. doi: 10.1007/978-3-642-54536-8.

K. Kaneko, H. Kaminaga, T. Sakaguchi, S. Kajita, M. Morisawa, I. Kumagai, and F. Kanehiro. Humanoid Robot HRP-5P: An Electrically Actuated Humanoid Robot With High-Power and Wide-Range Joints. *IEEE Robotics and Automation Letters*, 4(2):1431–1438, 2019. ISSN 2377-3766. doi: 10.1109/LRA.2019.2896465.

D. Katz, E. Horrell, Y. Yang, and B. Burns. The umass mobile manipulator uman: An experimental platform for autonomous mobile manipulation. *Workshop on manipulation in human environments at robotics: science and systems. Citeseer.*, 2006. doi: citeulike-article-id:10043893.

D. Kaynov, P. Souères, P. Pierro, and C. Balaguer. A practical decoupled stabilizer for joint-position controlled humanoid robots. In *2009 IEEE/RSJ International Conference on Intelligent Robots and Systems, IROS 2009*, pages 3392–3397, St. Louis, USA, 2009. IEEE. ISBN 9781424438044. doi: 10.1109/IROS.2009.5354431.

J. C. Keller. Engineer / Entrepreneur Inspired by R2-D2. *IEEE Women in Engineering Magazine (Volume: 2, Issue: 1, Summer 2008)*, 2(1):28–30, 2008. doi: 10.1109/MWIE.2008.925800.

C. C. Kemp, A. Edsinger, and E. Torres-Jara. Challenges for robot manipulation in human environments [Grand challenges of robotics]. *IEEE Robotics and Automation Magazine*, 14(1):20–29, 2007. ISSN 10709932. doi: 10.1109/MRA.2007.339604.

W. Kilby, J. R. Dooley, G. Kuduvalli, S. Sayeh, and C. R. Maurer. The CyberKnife® robotic radiosurgery system in 2010. *Technology in Cancer Research and Treatment*, 9(5):433–452, 2010. ISSN 15330346. doi: 10.1177/153303461000900502.

J.-H. Kim and J.-H. Oh. Walking control of the humanoid platform KHR-1 based on torque feedback control. *IEEE International Conference on Robotics and Automation, 2004. Proceedings. ICRA '04. 2004*, 1(April):623–628, 2004. ISSN 1050-4729. doi: 10.1109/ROBOT.2004.1307218.

Y. H. Kim, S. C. Ahn, and W. H. Kwon. Computational complexity of general fuzzy logic control and its simplification for a loop controller. *Fuzzy Sets and Systems*, 111(2):215–224, 2000. ISSN 01650114. doi: 10.1016/S0165-0114(97)00409-0.

E. Kljuno and R. L. Williams. Humanoid Walking Robot: Modeling, Inverse Dynamics, and Gain Scheduling Control. *Journal of Robotics*, 2010, 2010. ISSN 1687-9600. doi: 10.1155/2010/278597.

A. Kumar, D. Kumar, and S. K. Jarial. A Hybrid Clustering Method Based on Improved Artificial Bee Colony and Fuzzy C-Means Algorithm. *International Journal of Artificial Intelligence*, 15(2):40–60, 2017.

S. Kumar, C. Micheloni, C. Piciarelli, and G. L. Foresti. Stereo rectification of uncalibrated and heterogeneous images. *Pattern Recognition Letters*, 31(11):1445–1452, 2010. ISSN 01678655. doi: 10.1016/j.patrec.2010.03.019.

V. Kumar, M. Efran, and J. P. Ostrowski. Motion Planning and Control of Robots. *Handbook of Industrial Robotics*, pages 295–315, 2007. doi: 10.1002/9780470172506.ch15.

S. M. LaValle. *Planning algorithms*. Cambridge University Press, 1st ed edition, 2006. ISBN 9780511546877. doi: 10.1017/CBO9780511546877.

S. H. Lee and A. Goswami. The reaction mass pendulum (RMP) model for humanoid robot gait and balance control. In B. Choi, editor, *Humanoid Robots*, volume 71, pages 169–186. InTech, first edition, 2009. ISBN ISBN 978-953-7619-44-2.

J. Lehmann, B. Neumann, W. Bohlken, and L. Hotz. A Robot Waiter that Predicts Events by High-level Scene Interpretation. *Proceedings of the 6th International Conference on Agents and Artificial Intelligence*, pages 469–476, 2014. doi: 10.5220/0004819704690476.

G. Litzenberger. Service Robots. *International Federation of Robotics*, 2018. [Accessed Mar-2018].

J. Lorente, J. M. Garcia-Haro, S. Martinez, J. Hernandez-Vicen, and C. Balaguer. Waiter Robot : Advances in Humanoid Robot Research at UC3M. In R. E. Fernández and H. Montes, editors, *RoboCity16 Open Conference on Future Trends in Robotics*, chapter 24, pages 195–202. CSIC, 2016. ISBN 978-84-608-8452-1.

K. M. Lynch and M. T. Mason. Dynamic Nonprehensile Manipulation: Controllability, Planning, and Experiments. *The International Journal of Robotics Research*, 18(1):64–92, jan 1999. ISSN 0278-3649. doi: 10.1177/027836499901800105.

R. R. Ma and A. M. Dollar. On dexterity and dexterous manipulation. In *IEEE 15th International Conference on Advanced Robotics: New Boundaries for Robotics, ICAR 2011*, pages 1–7, 2011. ISBN 9781457711589. doi: 10.1109/ICAR.2011.6088576.

S. Martínez, C. A. Monje, A. Jardón, P. Pierro, C. Balaguer, and D. Muñoz. TEO: Full-Size Humanoid Robot Design Powered by a Fuel Cell System. *Cybernetics and Systems*, 43(3):163–180, 2012. ISSN 0196-9722. doi: 10.1080/01969722.2012.659977.

S. Martínez, C. A. Monje, A. Jardón, P. Pierro, C. Balaguer, and D. Munoz. Teo: Full-size humanoid robot design powered by a fuel cell system. *Cybernetics and Systems*, 43(3):163–180, 2012.

S. Martinez, J. M. Garcia-Haro, J. G. Victores, A. Jardon, and C. Balaguer. Experimental robot model adjustments based on force–torque sensor information. *Sensors*, 18(3):836, 2018.

S. Martínez de la Casa Díaz. *Human inspired humanoid robot control architecture*. PhD thesis, University Carlos III of Madrid, 2012.

G. Martinic. The proliferation, diversity and utility of ground-based robotic technologies. *Canadian Military Journal*, 14(4):52, 2014.

B. A. Maxwell, L. A. Meeden, N. Addo, L. Brown, P. Dickson, J. Ng, S. Olshfski, E. Silk, and J. Wales. Alfred: The Robot Waiter Who Remembers You. In AAAI Press, editor, *Proceedings of AAAI Workshop on Robotics*, pages 1–12, 1999.

S. G. McGill, Y. Zhang, L. Vadakedathu, A. Sreekumar, S.-J. Yi, and D. D. Lee. Comparison of obstacle avoidance behaviors for a humanoid robot in real and simulated environments. In *Proceedings of the 2012 IEEE International Conference on Humanoid Robots, Osaka, Japan*, volume 29, 2012.

W. Meeussen, M. Wise, S. Glaser, S. Chitta, C. McGann, P. Mihelich, E. Marder-Eppstein, M. Muja, V. Eruhimov, T. Foote, J. Hsu, R. B. Rusu, B. Marthi, G. Bradski, K. Konolige, B. Gerkey, and E. Berger. Autonomous door opening and plugging in with a personal robot. In *Proceedings - IEEE International Conference on Robotics and Automation*, pages 729–736. IEEE, 2010. ISBN 9781424450381. doi: 10.1109/ROBOT.2010.5509556.

H. Miyashita, T. Yamawaki, and M. Yashima. Control for throwing manipulation by one joint robot. In *2009 IEEE International Conference on Robotics and Automation*, pages 1273–1278. IEEE, 2009.

Moley Robotics. MK1 – The world's first robotic kitchen, 2015. [Accessed Apr-2019].

M. Morisawa, N. Kita, S. Nakaoka, K. Kaneko, S. Kajita, and F. Kanehiro. Biped locomotion control for uneven terrain with narrow support region. In *2014 IEEE/SICE International Symposium on System Integration*, pages 34–39. IEEE, 2014. doi: 10.1109/SII.2014.7028007.

P. Mukhopadhyay and B. B. Chaudhuri. A survey of Hough Transform. *Pattern Recognition*, 48(3):993–1010, 2015. ISSN 00313203. doi: 10.1016/j.patcog.2014.08.027.

G. R. Murthy and R. S. Jadon. Hand gesture recognition using neural networks. *2010 IEEE 2nd International Advance Computing Conference, IACC 2010*, pages 134–138, 2010. doi: 10.1109/IADCC.2010.5423024.

L. M. Nashner. *Sensory feedback in human posture control.* PhD thesis, Massachusetts Institute of Technology, 1970.

C. Natale. *Interaction control of robot manipulators: six degrees-of-freedom tasks*, volume 3. Springer Science & Business Media, 2003.

L. Natale and E. Torres-Jara. A sensitive approach to grasping. In *Proceedings of the sixth international workshop on epigenetic robotics*, pages 87–94, 2006.

N. Neckel, W. Wisman, and J. Hidler. Limb alignment and kinematics inside a lokomat robotic orthosis. *Annual International Conference of the IEEE Engineering in Medicine and Biology - Proceedings*, pages 2698–2701, 2006. ISSN 05891019. doi: 10.1109/IEMBS.2006.259970.

B. Neumann, L. Hotz, P. Rost, and J. Lehmann. A robot waiter learning from experiences. In *Lecture Notes in Computer Science (including subseries Lecture Notes in Artificial Intelligence and Lecture Notes in Bioinformatics)*, volume 8556 LNAI, pages 285–299, 2014. ISBN 9783319089782. doi: 10.1007/978-3-319-08979-9_22.

M. Neunert, M. Stäuble, M. Giftthaler, C. D. Bellicoso, J. Carius, C. Gehring, M. Hutter, and J. Buchli. Whole-body nonlinear model predictive control through contacts for quadrupeds. *IEEE Robotics and Automation Letters*, 3(3):1458–1465, 2018.

C. Nguyen. Chinese restaurants are replacing waiters with robots. *Tech Insider*, 2016. [Accessed Jan-2018].

K. Nishiwaki, Y. Murakami, S. Kagami, Y. Kuniyoshi, M. Inaba, and H. Inoue. A six-axis force sensor with parallel support mechanism to measure the ground reaction force of humanoid robot. In *Proceedings 2002 IEEE International Conference on Robotics and Automation (Cat. No.02CH37292)*, pages 2277–2282, 2003. doi: 10.1109/robot.2002.1013571.

M. Z. Noor, A. A. Rahman, M. F. Saaid, M. S. Ali, and M. Zolkapli. The development of Self-Service Restaurant Ordering System (SROS). In *Proceedings - 2012 IEEE Control and System Graduate Research Colloquium, ICSGRC 2012*, pages 348–353. IEEE, jul 2012. ISBN 9781467320368. doi: 10.1109/ICSGRC.2012.6287190.

K. Ogata. *Modern control engineering*. Prentice Hall Upper Saddle River, NJ, 2009. ISBN 0-13-615673-8.

A. Okamura, N. Smaby, and M. Cutkosky. An overview of dexterous manipulation. In *Proceedings 2000 ICRA. Millennium Conference. IEEE International Conference on Robotics and Automation. Symposia Proceedings (Cat. No.00CH37065)*, volume 1, pages 255–262. IEEE, 2011. ISBN 0-7803-5886-4. doi: 10.1109/ROBOT.2000.844067.

E. D. Oña, J. M. Garcia-Haro, A. Jardón, and C. Balaguer. Robotics in Health Care: Perspectives of Robot-Aided Interventions in Clinical Practice for Rehabilitation of Upper Limbs. *Applied Sciences*, 9(13):2586, jun 2019. ISSN 2076-3417. doi: 10.3390/app9132586.

A. Ortony and D. Partridge. Surprisingness and expectation failure: what's the difference? In *IJCAI*, pages 106–108, 1987.

C. Ott, A. Albu-Schaffer, A. Kugi, and G. Hirzinger. On the passivity-based impedance control of flexible joint robots. *IEEE Transactions on Robotics*, 24 (2):416–429, 2008.

C. Ott, C. Baumgärtner, J. Mayr, M. Fuchs, R. Burger, D. Lee, O. Eiberger, A. Albu-Schäffer, M. Grebenstein, and G. Hirzinger. Development of a biped robot with torque controlled joints. In *2010 10th IEEE-RAS International Conference on Humanoid Robots*, pages 167–173. IEEE, 2010.

C. Ott, M. A. Roa, and G. Hirzinger. Posture and balance control for biped robots based on contact force optimization. In *IEEE-RAS Int. Conf. on Humanoid Robots*, pages 26 – 33, 2011.

B. Paden and R. Panja. Globally asymptotically stable 'PD+' controller for robot manipulators. *Int. J. of Control*, 47(6):1697 – 1712, 1988.

Z. Pandilov and V. Dukovski. Several open problems in parallel robotics. *Acta Technica Corviniensis-Bulletin of Engineering*, 4(3):77, 2011.

J. Pardos and C. Balaguer. Humanoid Robot Kinematics Modeling Using Lie Groups. In *Climbing and Walking Robots*, pages 569–575. Springer Berlin Heidelberg, Berlin, Heidelberg, 2005. doi: 10.1007/3-540-29461-9_56.

R. Pérula-Martínez, J. M. Garcia-Haro, C. Balaguer, and M. A. Salichs. Developing Educational Printable Robots to Motivate University Students Using Open Source Technologies. *Journal of Intelligent & Robotic Systems*, 81(1):25–39, 2016. ISSN 15730409. doi: 10.1007/s10846-015-0205-3.

S. Pieskä, M. Luimula, J. Jauhiainen, and V. Spiz. Social service robots in public and private environments. *Recent Researches in Circuits, Systems, Multimedia and Automatic Control*, pages 190–196, 2012.

S. Pieskä, M. Luimula, J. Jauhiainen, and V. Spiz. Social Service Robots in Wellness and Restaurant Applications. *Journal of Communication and Computer*, 10(1):116–123, 2016. ISSN 1875-4791. doi: http://dx.doi.org/10.1177/1938965511434112.

P.-G. Plöger, K. Pervölz, C. Mies, P. Eyerich, M. Brenner, and B. Nebel. The DESIRE Service Robotics Initiative. *KI Zeitschrift*, 22(4):29–32, 2008. ISSN 0933-1875.

A. S. Pollock, B. R. Durward, P. J. Rowe, and J. P. Paul. What is balance? *Clinical rehabilitation*, 14(4):402–406, 2000.

D. Pontaza. Estas robots ofrecen servicio de camareras en una pizzería. *TecReview*, 2017. [Accessed Jan-2018].

M. B. Popovic, A. Goswami, and H. Herr. Ground reference points in legged locomotion: Definitions, biological trajectories and control implications. *International Journal of Robotics Research*, 24(12):1013–1032, 2005. ISSN 02783649. doi: 10.1177/0278364905058363.

P. Prabhakar, P. Anupama, and S. R. Resmi. Automatic vehicle number plate detection and recognition. In *International Conference on Control, Instrumentation, Communication and Computational Technologies (ICCICCT)*, pages 185–190. IEEE, jul 2014. ISBN 978-1-4799-4190-2. doi: 10.1109/ICCICCT.2014.6992954.

R. Prado, F. Hoffmann, S. García-Galán, J. Muñoz Expósito, and T. Bertram. On Providing Quality of Service in Grid Computing through Multi-objective Swarm-Based Knowledge Acquisition in Fuzzy Schedulers. *International Journal of Approximate Reasoning*, 53(2):228–247, 2012. ISSN 0888-613X. doi: 10.1016/J.IJAR.2011.10.005.

R.-E. Precup, S. Preitl, and G. Faur. PI predictive fuzzy controllers for electrical drive speed control: methods and software for stable development. *Computers in Industry*, 52(3):253–270, 2003. ISSN 0166-3615. doi: 10.1016/S0166-3615(03)00130-1.

K. Puerto. Un equipo de robots camarero del MIT sirve la cerveza de forma eficiente. *Xataka*, 2015. [Accessed Jan-2018].

P. Qi, C. Liu, A. Ataka, H. K. Lam, and K. Althoefer. Kinematic Control of Continuum Manipulators Using a Fuzzy-Model-Based Approach. *IEEE Transactions on Industrial Electronics*, 63(8):5022–5035, 2016. ISSN 0278-0046. doi: 10.1109/TIE.2016.2554078.

Y. Qing-Xiao, Y. Can, F. Zhuang, and Z. Yan-Zheng. Research of the localization of restaurant service robot. *International Journal of Advanced Robotic Systems*, 7(3):227–238, 2010. ISSN 17298806. doi: 10.5772/9706.

N. A. Radford, P. Strawser, K. Hambuchen, J. S. Mehling, W. K. Verdeyen, A. S. Donnan, J. Holley, J. Sanchez, V. Nguyen, L. Bridgwater, et al. Valkyrie: Nasa's first bipedal humanoid robot. *Journal of Field Robotics*, 32(3):397–419, 2015.

C. Ray, F. Mondada, and R. Siegwart. What do people expect from robots? In *2008 IEEE/RSJ International Conference on Intelligent Robots and Systems, IROS*, pages 3816–3821. IEEE, 2008. ISBN 9781424420582. doi: 10.1109/IROS.2008.4650714.

U. Reiser, C. Connette, J. Fischer, J. Kubacki, A. Bubeck, F. Weisshardt, T. Jacobs, C. Parlitz, M. Hagele, and A. Verl. Care-O-bot® 3 - Creating a product vision for service robot applications by integrating design and technology. In *2009 IEEE/RSJ International Conference on Intelligent Robots and Systems, IROS 2009*, pages 1992–1998. IEEE, oct 2009. ISBN 9781424438044. doi: 10.1109/IROS.2009.5354526.

Rob Price. Two restaurants close down due to terrible robot waiters - Business Insider. *Business Insider*, 2016. [Accessed Jan-2018].

W. Robotics. Executive Summary World Robotics 2017 Industrial Robots. *World Robotic Report - International Federation of Robotics*, pages 15–24, 2017. [Accessed Jan-2018].

S. Russel and P. Norvig. *Artificial intelligence—a modern approach 3rd Edition*. PEARSON, 3rd edition, 2012. ISBN 0136042597. doi: 10.1017/S0269888900007724.

A. Safiotti. Fuzzy logic in autonomous robotics: behavior coordination. *Proceedings of 6th International Fuzzy Systems Conference*, 1(july):573–578, 1997. ISSN 05333164. doi: 10.1109/FUZZY.1997.616430.

J. Salichs, A. Castro-González, and M. A. Salichs. Infrared Remote Control with a Social Robot. *In FIRA RoboWorld congress*, 44:86–95, 2009. doi: 10.1007/978-3-642-03986-7_10.

M. A. Salichs, I. P. Encinar, E. Salichs, Á. Castro-González, and M. Malfaz. Study of Scenarios and Technical Requirements of a Social Assistive Robot for Alzheimer's Disease Patients and Their Caregivers. *International Journal of Social Robotics*, 8(1):85–102, jan 2016. ISSN 1875-4791. doi: 10.1007/s12369-015-0319-6.

P. Sardain and G. Bessonnet. Forces acting on a biped robot. Center of pressure - Zero moment point. *IEEE Transactions on Systems, Man, and Cybernetics - Part A: Systems and Humans*, 34(5):630–637, 2004.

M. Scheutz, P. Schermerhorn, C. Middendorff, J. Kramer, D. Anderson, and A. Dingler. Toward Affective Cognitive Robots for Human-Robot Interaction Affective Architectures for Complex Robots. *AAAI 2005 Robot Workshop*, pages 61–66, 2005.

C. Shen, L. Hang, J. Wang, W. Qin, Y. Huangfu, X. Huang, and Y. Wang. Modeling and Analysis on Position and Gesture of End-Effector of Cleaning Robot Based on Monorail Bogie for Solar Panels. *In International Conference on Intelligent Robotics and Applications*, pages 122–133, aug 2016. doi: 10.1007/978-3-319-43506-0_11.

N. E. Sian, T. Sakaguchi, K. Yokoi, Y. Kawai, and K. Maruyama. Operating humanoid robots in human environments. In *Workshop on Manipulation for Human Environments, Robotics: Science and Systems*, 2006.

E. Sirin, B. Parsia, B. C. Grau, A. Kalyanpur, and Y. Katz. Pellet: A practical OWL-DL reasoner. *Web Semantics*, 5(2):51–53, 2007. ISSN 15708268. doi: 10.1016/j.websem.2007.03.004.

M. Slembrouck, M. Heyvaert, D. Van Cauwelaert, D. Van Hamme, P. Veelaert, and W. Philips. Time complexity of traditional vision algorithms on a block-based image processor (blip). In *2012 Sixth International Conference on Distributed Smart Cameras (ICDSC)*, pages 1–6. IEEE, 2012.

Spyce. Culinary excellence elevated by technology., 2018. [Accessed Apr-2019].

S. S. Srinivasa, D. Ferguson, C. J. Helfrich, D. Berenson, A. Collet, R. Diankov, G. Gallagher, G. Hollinger, J. Kuffner, and M. V. Weghe. HERB: A home exploring robotic butler. *Autonomous Robots*, 28(1):5–20, 2010. ISSN 09295593. doi: 10.1007/s10514-009-9160-9.

P. Staroverov, R. Martinez, D. Kaynov, M. Arbulu, L. Cabas, and C. Balaguer. Detecting Sound Source with the Humanoid Robot RH-1. In *Advances in Climbing and Walking Robots*, pages 615–622. World Scientific, jul 2007. ISBN 978-981-270-815-1. doi: 10.1142/9789812770189_0071.

B. Stephens. Humanoid push recovery. In *Proceedings of the 2007 7th IEEE-RAS International Conference on Humanoid Robots, HUMANOIDS 2007*, pages 589–595, 2008. ISBN 9781424418626. doi: 10.1109/ICHR.2007.4813931.

B. Stephens. *Push recovery control for force-controlled humanoid robots*. PhD thesis, Carnegie Mellon University, The Robotics Institute, 2011.

B. J. Stephens and C. G. Atkeson. Push recovery by stepping for humanoid robots with force controlled joints. In *2010 10th IEEE-RAS International Conference on Humanoid Robots, Humanoids 2010*, pages 52–59, 2010. ISBN 9781424486885. doi: 10.1109/ICHR.2010.5686288.

T. Wimböck, C. Ott, and G. Hirzinger. Impedance behaviors for two-handed manipulation: Design and experiments. In *IEEE Int. Conf. on Robotics and Automation*, pages 4182 – 4189, 2007.

T. Takagi and M. Sugeno. Fuzzy identification of systems and its applications to modeling and control. *IEEE Transactions On Systems Man And Cybernetics*, 15 (1):116–132, 1985. ISSN 00189472.

T. H. Tan, C. S. Chang, and Y. F. Chen. Developing an intelligent e-restaurant with a menu recommender for customer-centric service. *IEEE Transactions on Systems, Man and Cybernetics Part C: Applications and Reviews*, 42(5):775–787, 2012. ISSN 10946977. doi: 10.1109/TSMCC.2011.2168560.

C. J. Taylor and D. Seward. Control of a dual-arm robotic manipulator. *Nuclear Engineering International*, 55(673):24–26, 2010.

B. Thuilot, P. Martinet, L. Cordesses, and J. Gallice. Position based visual servoing: Keeping the object in the field of vision. *Proceedings - IEEE International Conference on Robotics and Automation*, 2:1624–1629, 2002. ISSN 10504729. doi: 10.1109/ROBOT.2002.1014775.

A. Trenaman, D. Barry, and D. Vernon. An analysis of strategies to reduce computational complexity and processing time in industrial optical data processing and analysis. *Proceedings of OEPE*, 96, 1996.

J. H. Tzou and K. L. Su. The development of the restaurant service mobile robot with a laser positioning system. *Proceedings of the 27th Chinese Control Conference, CCC*, 14(2):252–256, 2009. doi: 10.1109/CHICC.2008.4605839.

United States of America. Bureau of Labor Statistics, 2017. [Accessed Jan-2018].

P. Vadakkepat and D. Goswami. Biped Locomotion: Stability, Analysis and Control. *International Journal on Smart Sensing and Intelligent Systems*, 1:187–207, 2008.

N. Vahrenkamp, D. Berenson, T. Asfour, J. Kuffner, and R. Dillmann. Humanoid motion planning for dual-arm manipulation and re-grasping tasks. In *2009 IEEE/RSJ International Conference on Intelligent Robots and Systems*, pages 2464–2470. IEEE, 2009.

P. H. Veltink, H. J. Luinge, B. J. Kooi, C. T. Baten, P. Slycke, W. Olthuis, and P. Bergveld. The artificial vestibular system-design of a tri-axial inertial sensor system and its application in the study of human movement. *Control of Posture and Gait, Proceedings of the International Society for Postural and Gait Research ISPG*, 2001.

M. M. Vermeulen and M. Wisse. Maximum allowable manipulator mass based on cycle time, impact safety and pinching safety. *Industrial Robot*, 35(5):410–420, 2008. ISSN 0143991X. doi: 10.1108/01439910810893581.

M. Vukobratović and B. Borovac. Zero-moment point—thirty five years of its life. *International journal of humanoid robotics*, 1(01):157–173, 2004.

Weimin Zhang, Qiang Huang, Peng Du, Jianxi Li, and Kejie Li. Compliance control of a humanoid arm based on force feedback. In *2005 IEEE International Conference on Information Acquisition*, pages 528–531, 2006. doi: 10.1109/icia.2005.1635145.

L. L. Whitcomb, A. A. Rizzi, and D. E. Koditschek. Comparative experiments with a new adaptive controller for robot arms. *IEEE Trans. Robotics and Automation*, 9(1):59 – 70, 1993.

H. H. P. Wu and Y. H. Yu. Projective rectification with reduced geometric distortion for stereo vision and stereoscopic video. *Journal of Intelligent and Robotic Systems: Theory and Applications*, 42(1):71–94, 2005. ISSN 09210296. doi: 10.1007/s10846-004-3023-6.

Z. Xia, L. Liu, J. Xiong, Q. Yi, and K. Chen. Design aspects and development of humanoid robot THBIP-2. *Robotica*, 26(1):109–116, jan 2008. ISSN 02635747. doi: 10.1017/S0263574707003645.

Y. Xu, Y. Ohmoto, K. Ueda, T. Komatsu, T. Okadome, K. Kamei, S. Okada, Y. Sumi, and T. Nishida. A platform system for developing a collaborative mutually adaptive agent. In *Lecture Notes in Computer Science (including subseries Lecture Notes in Artificial Intelligence and Lecture Notes in Bioinformatics)*, volume 5579 LNAI, pages 576–585, 2009. ISBN 3642025676. doi: 10.1007/978-3-642-02568-6_58.

N. Yap. This Kuching restaurant has robot waiters to serve you. *TheHypedGeek*, 2016. [Accessed Jan-2018].

C. Yin. Walking Stability of a Humanoid Robot Based on Fictitious Zero-Moment Point. *Power Engineering*, pages 1–6, 2006.

S.-k. Yun, A. Goswami, and Y. Sakagami. Safe fall: Humanoid robot fall direction change through intelligent stepping and inertia shaping. In *2009 IEEE International Conference on Robotics and Automation*, pages 781–787. IEEE, 2009. ISBN 978-1-4244-2788-8. doi: 10.1109/ROBOT.2009.5152755.

F. Zacharias, D. Leidner, F. Schmidt, C. Borst, and G. Hirzinger. Exploiting structure in two-armed manipulation tasks for humanoid robots. In *2010 IEEE/RSJ International Conference on Intelligent Robots and Systems*, pages 5446–5452. IEEE, 2010.

T. Zhang, Q. Li, C.-S. Zhang, H.-W. Liang, P. Li, T.-M. Wang, S. Li, Y.-L. Zhu, and C. Wu. Current trends in the development of intelligent unmanned autonomous systems. *Front Inform Technol Electron Eng*, 18(1):68–85, 2017. ISSN 20959230. doi: 10.1631/FITEE.1601650.

M. Zinn, B. Roth, O. Khatib, and J. K. Salisbury. A new actuation approach for human friendly robot design. *International Journal of Robotics Research*, 23(4-5): 379–398, 2004. ISSN 02783649. doi: 10.1177/0278364904042193.